

AD-758 431

**CRYOGENIC SYSTEMS AND SUPERCONDUCTIVE  
POWER**

B.D. Hatch, et al

General Electric Company

Prepared for:

Advanced Research Projects Agency

20 December 1972

DISTRIBUTED BY:

**NTIS**

**National Technical Information Service  
U. S. DEPARTMENT OF COMMERCE  
5285 Port Royal Road, Springfield Va. 22151**

# DISCLAIMER NOTICE

THIS DOCUMENT IS THE BEST  
QUALITY AVAILABLE.

COPY FURNISHED CONTAINED  
A SIGNIFICANT NUMBER OF  
PAGES WHICH DO NOT  
REPRODUCE LEGIBLY.

AD 758431

# **CRYOGENIC SYSTEMS AND SUPERCONDUCTIVE POWER**

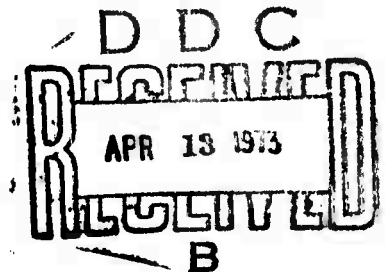
FIRST SEMIANNUAL TECHNICAL REPORT

20 December 1972

Prepared for  
DEPARTMENT OF DEFENSE  
ADVANCED RESEARCH PROJECTS AGENCY  
WASHINGTON, D. C. 20301

Prepared Under  
Contract No. DAHC-15-72-C-0235, ARPA Order No. 2200

Prepared by  
Cryogenics Branch  
Mechanical Engineering Laboratory  
Research and Development Center  
General Electric Company  
Schenectady, New York 12301



Approved for public release - distribution unlimited.  
The views and conclusions contained in this document  
are of the authors and should not be interpreted as  
necessarily representing the official policies, either  
expressed or implied, of the Advanced Research Pro-  
jects Agency or the U. S. Government.

Reproduced by  
NATIONAL TECHNICAL  
INFORMATION SERVICE  
U S Department of Commerce  
Springfield VA 22151

SRD-73-022

Short Title of Work	CRYOGENIC SYSTEMS AND SUPERCONDUCTIVE POWER
Contract No.	DAHC-15-72-C-0235
ARPA Order No.	2200
Contractor	Cryogenics Branch Mechanical Engineering Laboratory Research and Development Center General Electric Company Schenectady, New York 12301
Principal Investigator	B. D. Hatch Telephone: 518*374-2211, Ext. 5-5969
Project Scientists	R. B. Fleming Telephone: 518*374-2211, Ext. 5-3836  D. W. Jones Telephone: 518*374-2211, Ext. 5-4280  D. L. Kerr Telephone: 518*374-2211, Ext. 5-5968  S. H. Minnich Telephone: 518*374-2211, Ext. 5-4540
Effective Date of Contract	1 June 1972
Contract Expiration Date	31 July 1973
Amount of Contract	\$563, 997

*ib*

## FOREWORD

This first semiannual technical report was prepared by the Research and Development Center of the General Electric Company in Schenectady, New York, under Advanced Research Projects Agency Contract No. DAHC-15-72-C-0235, "Cryogenic Systems and Superconductive Power," ARPA Order No. 2200. This contract is administered by the General Electric Research and Development Center for the Department of Defense, Advanced Research Projects Agency, Washington, D. C.

The engineering development work reported covers the period from 1 June 1972 to 30 November 1972. This work is under the direction of Mr. B. D. Hatch, Principal Investigator.

## **ABSTRACT**

Cryogenic refrigeration is a common requirement of all superconductivity applications. For this reason, dominant emphasis is being given to this portion of the program. Its specific application to an integrated superconductive ship propulsion system with the extreme environments involved will assure that particular attention is given to each factor affecting reliability, maintainability, safety, and availability of the cryogenic system components.

The specific objectives of this program are to:

- Conduct a limited but broad application survey of multiple applications in which the use of cryogenic and superconductive systems and components offer substantial advantages through improvements in the performance of propulsion, communication, detection, or weapons systems.
- Define, investigate, and experimentally evaluate the key elements of a representative cryogenic turborefrigerator subsystem suitable for providing reliable long-lived cryogenic refrigeration for a superconductive ship propulsion system.
- Provide a sound technical basis for subsequent applications of superconductive power in the area of ship propulsion. Other applications, and their requirements, will be reviewed and evaluated, in order to form a preliminary evaluation of those applications that might deserve more detailed study.

Unclassified

Security Classification

DOCUMENT CONTROL DATA - R & D

(Security classification of title, body of abstract and indexing annotation must be entered when the overall report is classified)

1. ORIGINATING ACTIVITY (Corporate author)

Research and Development Center  
General Electric Company  
Schenectady, New York 12301

2a. REPORT SECURITY CLASSIFICATION  
Unclassified

2b. GROUP

3. REPORT TITLE

CRYOGENIC SYSTEMS AND SUPERCONDUCTIVE POWER

4. DESCRIPTIVE NOTES (Type of report and inclusive dates)

First Semiannual Technical Report, 1 June 1972 through 30 November 1972

5. AUTHOR(S) (First name, middle initial, last name)

B.D. Hatch, R.B. Fleming, D.W. Jones, S.H. Minnich, and D.L. Kerr

6. REPORT DATE

20 December 1972

7a. TOTAL NO. OF PAGES

278

7b. NO. OF REFS

12

8a. CONTRACT OR GRANT NO.

DAHC-15-72-C-0235

9a. ORIGINATOR'S REPORT NUMBER(S)

SRD-73-022

8b. PROJECT NO.

ARPA Order No. 2200

9b. OTHER REPORT NO(S) (Any other numbers that may be assigned this report)

10. DISTRIBUTION STATEMENT

Approved for Public Release - Distribution Unlimited

11. SUPPLEMENTARY NOTES

12. SPONSORING MILITARY ACTIVITY

Department of Defense  
Advanced Research Projects Agency  
Washington, D. C. 20301

Cryogenic refrigeration is a common requirement of all superconductivity applications. For this reason, dominant emphasis is being given to this portion of the program. Its specific application to an integrated superconductive ship propulsion system with the extreme environments involved will assure that particular attention is given to each factor affecting reliability, maintainability, safety, and availability of the cryogenic system components. The specific objectives of this program are to:

- Conduct a limited but broad application survey of multiple applications in which the use of cryogenic and superconductive systems and components offer substantial advantages through improvements in the performance of propulsion, communication, detection, or weapons systems.
- Define, investigate, and experimentally evaluate the key elements of a representative cryogenic turborefrigerator subsystem suitable for providing reliable long-lived cryogenic refrigeration for a superconductive ship propulsion system,
- Provide a sound technical basis for subsequent applications of superconductive power in the area of ship propulsion. Other applications, and their requirements will be reviewed and evaluated, in order to form a preliminary evaluation of those applications that might deserve more detailed study.

14

## KEY WORDS

## LINK A

## LINK B

## LINK C

ROLE

WT

ROLE

WT

ROLE

WT

Cryogenic

Refrigeration

Superconductive

Turborefrigerator

Liquid metal

Propulsion

Electrical

Machinery

ia

## TABLE OF CONTENTS

<u>Section</u>		<u>Page</u>
1	SUMMARY . . . . .	1
	Technical Problem . . . . .	1
	Methodology . . . . .	1
	Technical Results . . . . .	4
	Department of Defense Implications . . . . .	6
	Implications for Further Research . . . . .	7
2	CRYOGENIC TURBOREFRIGERATOR. . . . .	9
	Refrigerator Applications Study . . . . .	9
	Refrigerator Systems and Components . . . . .	9
	Refrigerator Systems . . . . .	9
	Compressor . . . . .	11
	Compressor Requirements . . . . .	11
	Compressor Description. . . . .	12
	Compressor Design Basis . . . . .	16
	Turboalternator . . . . .	25
	Turboalternator Requirements . . . . .	26
	Turboalternator Description . . . . .	27
	Turboalternator Design Basis . . . . .	41
	Cryogenic Heat Exchanger. . . . .	46
	Metal-Plastic Laminate Heat Exchanger . . . . .	47
	Computer Program . . . . .	51
	Elements and Components . . . . .	53
	Cycle Program Organization. . . . .	59
	Refrigerator System Design . . . . .	60
	Design Requirements and Trade-Offs . . . . .	60
	A-C Generator . . . . .	62
	Refrigeration System for A-C Generator . . . . .	62
	Turboalternators for A-C Generators. . . . .	67
	Compressors for A-C Generator . . . . .	89
	D-C Generator . . . . .	97
	Refrigeration System for D-C Generator . . . . .	97
	Turboalternators for D-C Generator . . . . .	102
	Compressors for D-C Generator . . . . .	102
	D-C Motor. . . . .	115
	Refrigeration System for D-C Motor . . . . .	115
	Turboalternators for D-C Motor . . . . .	119
	Compressors for D-C Motor. . . . .	120
	Summary of System Designs . . . . .	132
	Compressor Subsystem Weight and Size. . . . .	133
	Refrigeration System Arrangements . . . . .	134

**Preceding page blank**

## TABLE OF CONTENTS (Cont'd)

<u>Section</u>	<u>Page</u>
2	CRYOGENIC TURBOREFRIGERATOR (Cont'd)
	Comparison of Refrigeration Turbomachinery . . . 135
	Off-Design Performance Study (Task R-30) . . . 137
	Conceptual Model System . . . 140
	Reference Model . . . 142
	Heat Exchanger Model . . . 144
	Computational and Transient Considerations . . . 145
3	SUPERCONDUCTIVE POWER SYSTEMS . . . 147
	Superconductive Power Applications Study . . . 147
	Ship Propulsion . . . 148
	Superconductive Alternators . . . 150
	MHD Power Generation . . . 152
	Pulse Energy Storage . . . 152
	Refrigeration Requirements . . . 157
	Potential for Advanced Superconductors . . . 158
	Ship Propulsion System Requirements and Criteria . . 160
	System Requirements . . . 160
	System Description and Potential
	Advantages . . . 160
	Potential Naval Applications . . . 162
	Investigation of Specific Ships . . . 164
	Selection of System Rating and Type of Ship . . 164
	System Requirements . . . 165
	Refrigeration Requirements . . . 167
	Comparison Criteria . . . 176
	Comparative Performance and Recommended
	Approach . . . 177
	Scope . . . 177
	Summary and Conclusions . . . 178
	Performance Comparisons . . . 181
	Recommendations . . . 190
	Analysis . . . 191
	Fuel Economy and Operating Time
	of Prime Movers . . . 191
	A-C Generator . . . 204
	D-C Generator . . . 207
	D-C Motor . . . 211
	A-C/D-C Transformers and Rectifiers . . . 217
	D-C/D-C System . . . 218
	Refrigeration . . . 229
	Model System . . . 229

## TABLE OF CONTENTS (Cont'd)

<u>Section</u>	<u>Page</u>
3	SUPERCONDUCTIVE POWER SYSTEMS (Cont'd)
	Materials and Process Evaluations . . . . . 230
	Liquid-Metal Current Collection . . . . . 230
	Sodium Potassium Metals and Alloys . . . . . 231
	Gallium Metal and Alloys . . . . . 233
	Other Liquid Metals and Alloys . . . . . 236
	Superconductive Coil Technology . . . . . 237
 <u>Appendix</u>	
I	IDEAL HEAT EXCHANGER MODEL . . . . . 239
	Assumptions . . . . . 239
	Analysis . . . . . 241
II	SYSTEM REQUIREMENTS FOR SUPERCONDUCTING NAVAL SHIP PROPULSION SYSTEM . . . . . 245
	Scope . . . . . 245
	Applicable Documents . . . . . 245
	System Definition . . . . . 245
	Performance Requirements . . . . . 246
	Motor Rating . . . . . 246
	Main Generator Rating . . . . . 246
	Main Gas Turbine Rating . . . . . 247
	Cruise Turbine/Generator Unit . . . . . 247
	Efficiency . . . . . 247
	Weight . . . . . 247
	Size . . . . . 247
	Cross-Connect Capability . . . . . 248
	Cross-Connect Switching Time . . . . . 248
	Cooldown . . . . . 248
	Generator Starting Time . . . . . 248
	Motor Starting Time . . . . . 248
	Crash Reversal . . . . . 248
	Warmup . . . . . 249
	Overspeed . . . . . 249
	Short Circuit . . . . . 249
	Loss of Superconductivity . . . . . 249
	Resonant Frequencies . . . . . 249
	Operational Requirements . . . . . 249
	Duty Cycle . . . . . 249
	Life . . . . . 250
	Reliability . . . . . 250
	Maintainability . . . . . 250

## TABLE OF CONTENTS (Cont'd)

<u>Appendix</u>	<u>Page</u>
II	<b>SYSTEM REQUIREMENTS FOR SUPERCONDUCTING NAVAL SHIP PROPULSION SYSTEM (Cont'd)</b>
	Noise and Electromagnetic Interference . . . . . 251 Safety . . . . . 251 Vulnerability to Accident or Enemy Action . . . . . 251 Environmental Requirements . . . . . 251 Shock . . . . . 251 Vibration . . . . . 252 Magnetic Field Strength . . . . . 252 Inclination . . . . . 252 Surface Temperature . . . . . 252 Temperature Rise . . . . . 252 Ambient Temperature . . . . . 252 Coolant . . . . . 252 Humidity . . . . . 253 Salt . . . . . 253 Grounding . . . . . 253
III	<b>CALCULATION OF D-C GENERATOR CONDUCTION AND RADIATION HEAT LEAKS TO SUPERCONDUCTING FIELD COIL . . . . .</b>
	255 Coil Weight . . . . . 255 Coil Enclosure Weight. . . . . 255 Thickness of Support Tubes . . . . . 255 Heat Transfer by Conduction. . . . . 256 Heat Transfer by Radiation . . . . . 257
IV	<b>TRANSIENT REFRIGERATION LOADS DUE TO RAMPING</b>
	259 Losses Due to Induced Currents in Support Structure . 259 Ramping Loss in Superconductor . . . . . 260
V	<b>AN INVESTIGATION OF GALLIUM LIQUID METAL CURRENT COLLECTORS FOR SPACE APPLICATIONS. .</b>
	263 Introduction . . . . . 263 Contamination . . . . . 265 Background . . . . . 265 Gallium Contamination Studies . . . . . 266 Immobilization . . . . . 269 Analysis. . . . . 269 Oxide Characteristics of Liquid Metals . . . . 272

## TABLE OF CONTENTS (Cont'd)

<u>Appendix</u>		<u>Page</u>
V	AN INVESTIGATION OF GALLIUM LIQUID METAL CURRENT COLLECTORS FOR SPACE APPLICATIONS (Cont'd)	
	Gallium Cleaning . . . . .	273
	General Comments . . . . .	273
	Electrolytic Cleaning . . . . .	273
	Filtering . . . . .	274
	REFERENCES . . . . .	277

## LIST OF ILLUSTRATIONS

<u>Figure</u>		
1	Program Work Schedule . . . . .	2
2	Major Milestones for Phases I and II . . . . .	3
3	Cycles Suitable for Turbomachinery . . . . .	9
4	U. S. Army Single-Stage Compressor Rotor . . . . .	14
5	Disassembled U. S. Army Single-Stage Compressor . . . . .	14
6	Gas Bearing, Single-Stage, Helium Gas Circulator . . . . .	15
7	Rotor for Gas Bearing Compressor (23, 000-Rpm, 150-Hp, 14-In-Diameter Impeller) . . . . .	15
8	Two-Stage Compressor Module of U. S. Air Force Cryogenic Refrigerator . . . . .	17
9	Helium Compressor Impellers (91, 000 Rpm). . . . .	17
10	Compressor System in Sealed Outer Casing . . . . .	18
11	Speed and System Pressure Ratio Versus Flow Rate . . . . .	22
12	Overall Efficiency Versus Flow Rate . . . . .	22
13	Wheel Efficiency and Specific Speed Versus Flow Rate . . . . .	23
14	Typical Dimensions Versus Flow Rate . . . . .	23
15	Compressor Performance Comparison . . . . .	24
16	Partial-Admission, Radial Impulse Turbine, 1.1-Inch Diameter . . . . .	27
17	Radial Impulse Turbine Wheel (0.625-Inch-Diameter) Mounted on 0.261-Inch-Diameter Alternator Shaft . . . . .	28

## LIST OF ILLUSTRATIONS (Cont'd)

<u>Figure</u>		<u>Page</u>
18	Three-Inch-Diameter, Full-Admission, Radial Reaction Turbine . . . . .	29
19	Turbine Wheel (1.90-Inch-Diameter) with 12 Blades . . .	29
20	Cryogenic Turboalternator (Cutaway) . . . . .	30
21	Full-Scale Model of Cryogenic Turboalternator . . . . .	31
22	Turboalternator Test Stand . . . . .	31
23	Two-Stage Cryogenic Turboalternator. . . . .	32
24	Turboalternator Parts for U. S. Air Force Cryogenic Refrigerator . . . . .	32
25	Single-Stage Big Bertha Cryogenic Turboalternator (0.50-Inch-Diameter Shaft) . . . . .	35
26	Single-Stage Grizzly Giant Cryogenic Turboalternator (1.0-Inch-Diameter Shaft) . . . . .	36
27	Surface Features of Self-Acting Bearings . . . . .	38
28	Tilting-Pad Journal Bearing for Big Bertha Turboalternator . . . . .	39
29	Inward-Pumping Spiral-Groove Thrust Bearing for Big Bertha . . . . .	40
30	Turbine Aerodynamic Performance. . . . .	42
31	Approximate Cryogenic Alternator Power Characteristics. . . . .	43
32	Principle of Perforated-Plate Heat Exchanger . . . . .	47
33	Cutaway View of Perforated-Plate Heat Exchanger. . . . .	49
34	Perforated-Plate Heat Exchanger in Cryogenic Test Apparatus . . . . .	50
35	Cross Section of Wire Mesh Heat Exchanger . . . . .	50
36	Four-Load Reversed Brayton Cycle. . . . .	52
37	Cryogenic Refrigeration-Cycle Elements . . . . .	54
38	Temperature Entropy Diagrams for Cryogenic Refrigeration-Cycle Elements . . . . .	55
39	One-Load Reversed Brayton Cycle . . . . .	56
40	Two-Load Reversed Brayton Cycle . . . . .	57

## LIST OF ILLUSTRATIONS (Cont'd)

<u>Figure</u>		<u>Page</u>
41	Three-Load Claude Cycle . . . . .	58
42	Cycle Design Program Organization . . . . .	59
43	Computer Results for A-C Generator (Run 6310) . . . . .	64
44	Turboalternator Partial-Admission Radial Impulse Design Point Computer Output (Design Case 630601006) . . . . .	70
45	Turboalternator Partial-Admission Radial Impulse Design Point Computer Output (Design Case 630602001) . . . . .	73
46	Turboalternator Partial-Admission Radial Impulse Design Point Computer Output (Design Case 630603005) . . . . .	76
47	Turboalternator Full-Admission Radial Reaction Design Point Computer Output ( Design Case 630601007). . . . .	84
48	Compressor System Arrangement . . . . .	91
49	Centrifugal Compressor Design Point Computer Output (Case No. 6310001) . . . . .	92
50	Computer Results for D-C Generator (Run 20205) . . . . .	99
51	Turboalternator Partial-Admission Radial Impulse Design Point Computer Output (Design Case 102010103) . . . . .	104
52	Turboalternator Partial-Admission Radial Impulse Design Point Computer Output (Design Case 102010202) . . . . .	107
53	Centrifugal Compressor Design Point Computer Output (Case No. 10204001) . . . . .	111
54	Computer Results for D-C Motor (Run 9206). . . . .	117
55	Turboalternator Partial-Admission Radial Impulse Design Point Computer Output (Design Case 920301006) . . . . .	122
56	Turboalternator Partial-Admission Radial Impulse Design Point Computer Output (Design Case 920302006) . . . . .	125
57	Centrifugal Compressor Design Point Computer Output (Case No. 9206001) . . . . .	129
58	Cryosection with Circular Heat Exchanger. . . . .	134
59	Cryosection with Y-Shaped Heat Exchanger . . . . .	135
60	Conceptual Model System . . . . .	141
61	Reference Model Block Diagram . . . . .	142
62	Reference Model . . . . .	143

## LIST OF ILLUSTRATIONS (Cont'd)

<u>Figure</u>		<u>Page</u>
63	Heat Exchanger Outputs . . . . .	144
64	Schematic Diagram of Basic System . . . . .	160
65	Cross-Connection Capability . . . . .	161
66	Potential Naval Applications . . . . .	163
67	Schematic of A-C Generator Rotor . . . . .	170
68	Acyclic Generator -- Dewar Construction . . . . .	173
69	Conventional Gear Propulsion System . . . . .	186
70	D-C/D-C Propulsion System . . . . .	187
71	A-C/D-C Propulsion System . . . . .	187
72	LM2500 Estimated Engine Performance (Subject to 5% Production Variation) . . . . .	192
73	Variation of Fuel Consumption with Horsepower and Speed (59°F Inlet Temperature, Fuel LHV=18,500 Btu/Lb) . . . .	193
74	Horsepower SFC Speed Characteristic GTPF990 . . . . .	194
75	Typical Minimum Specific Fuel Consumption of Marine Gas Turbine (~20,000 Hp) . . . . .	194
76	Typical Performance of 20,000-Hp Gas Turbine . . . . .	196
77	Typical Performance of 5000-Hp Gas Turbine . . . . .	197
78	Specific Fuel Consumption for Various Gas Turbine Combinations . . . . .	198
79	Typical Fuel Flow for 20,000-Hp Gas Turbine . . . . .	199
80	Typical Fuel Flow for 5000-Hp Gas Turbine . . . . .	199
81	Acyclic Generator Parametric Study (24,000 Hp, 3600 Rpm, 100V) . . . . .	208
82	Acyclic Motor Parametric Study, Diameter Versus Flux Density (40,000 Hp, 200 Rpm, 200V) . . . . .	212
83	Acyclic Motor Parametric Study, Losses Versus Flux Density (40,000 Hp, 200 Rpm, 200V) . . . . .	213
84	Generator/Motor Connections . . . . .	220
85	Circuit Interconnections and Switching at Zero Current (Cruise Condition) . . . . .	221

## LIST OF ILLUSTRATIONS (Cont'd)

<u>Figure</u>		<u>Page</u>
86	Circuit Interconnections and Switching at Zero Current (One Cruise Generator) . . . . .	222
87	Location of Equipment for Twin-Screw Destroyer (80,000 Hp) . . . . .	226
88	Effect of D-C/D-C Bus Losses on System Weight for Twin-Screw Ship (80,000 Total Hp) . . . . .	226
89	Effect of D-C/D-C Bus Losses on System Volume for Twin-Screw Ship (80,000 Total Hp) . . . . .	227
90	Effect of Bus Material and Generator Voltage on System Weight . . . . .	227
91	Effect of Bus Material and Generator Voltage on System Volume . . . . .	228
92	Output Temperatures as Functions of T and m . . . . .	239
93	Two Streams Separated by Large-Area, Thin Conducting Wall . . . . .	240
94	Basic System Schematic . . . . .	246
95	Distance from High-Temperature End of Member to Point Where $T = 25^\circ\text{K}$ . . . . .	257
96	Field Strength on Inner Coil Surface . . . . .	261

## LIST OF TABLES

<u>Table</u>		
1	Gas Bearing Compressor Comparison. . . . .	19
2	Comparison of Characteristics. . . . .	25
3	Refrigeration Loads Used for Refrigerator Designs . . .	61
4	Computer Results -- Refrigerator for A-C Generator . .	63
5	Turboalternator Requirements . . . . .	67
6	Turboalternator Design Summary for A-C Generator Refrigerator . . . . .	68
7	Comparison of Partial- and Full-Admission Turbo- alternators . . . . .	82

## LIST OF TABLES (Cont'd)

<u>Table</u>		<u>Page</u>
8	A-C Generator Refrigerator Turbocompressor Design Summary . . . . .	90
9	Computer Results -- Refrigerator for D-C Generator. . .	98
10	Turboalternator Requirements (Run 10204) . . . . .	102
11	Turboalternator Design Summary for D-C Generator Refrigerator . . . . .	103
12	D-C Generator Refrigerator Turbocompressor Design Summary . . . . .	110
13	Computer Results -- Refrigerator for D-C Motor . . . .	116
14	Turboalternator Requirements . . . . .	120
15	Turboalternator Design Summary for D-C Motor Refrigerator . . . . .	121
16	D-C Motor Refrigerator Turbocompressor Design Summary . . . . .	128
17	Summary of Refrigeration Systems . . . . .	133
18	Comparison of All Refrigerator Turboalternators . . . .	138
19	Comparison of All Refrigerator Turbocompressors. . . .	139
20	High-Power Programs . . . . .	149
21	Comparison of Power Requirements . . . . .	164
22	Summary of Steady-State Refrigeration Requirements. . .	168
23	Transient Refrigeration Loads . . . . .	169
24	Weight and Volume of Major Components . . . . .	182
25	Summary of Weight for Twin-Screw Ship . . . . .	183
26	Summary of Volume for Twin-Screw Ship . . . . .	184
27	Summary of System Weight for Twin-Screw Ship . . . . .	184
28	Summary of System Volume for Twin-Screw Ship. . . . .	185
29	System Losses . . . . .	188
30	Typical Mission Profile . . . . .	192
31	Mission Profile, Single-Screw Ship -- 40,000 Hp . . . .	200
32	Mission Profile for Twin-Screw Ship -- 80,000 Hp . . . .	200

## LIST OF TABLES (Cont'd)

<u>Table</u>		<u>Page</u>
33	Fuel Requirements for Single-Screw Ship . . . . .	201
34	Fuel Requirements for Twin-Screw Ship . . . . .	201
35	Comparison of Total Fuel Consumption for Various Propulsion-Combination Single-Screw Ship . . . . .	202
36	Comparison of Total Fuel Consumption for Various Propulsion-Combination Twin-Screw Ship . . . . .	202
37	Comparison of Typical Losses . . . . .	203
38	Relative Fuel Consumption. . . . .	204
39	Comparison of Turbine Operating Times Per Mission for Single-Screw Ship . . . . .	205
40	Comparison of Turbine Operating Times per Mission for Twin-Screw Ship . . . . .	205
41	Relative Operating Time . . . . .	205
42	D-C Acyclic Generator Parameters . . . . .	210
43	D-C Acyclic Motor Parameters . . . . .	216
44	Transformer and Rectifier Weights and Dimensions . . .	218
45	Copper Bus Parameters . . . . .	225
46	Physical Properties of Gallium . . . . .	235
47	Maximum Envelope Dimensions . . . . .	247
48	Typical Mission Profile . . . . .	250
49	Characteristics of Low-Melting-Temperature Metals. . .	270
50	Investigation Observations. . . . .	273

## **Section 1**

### **SUMMARY**

#### **TECHNICAL PROBLEM**

The specific objectives of this program are to:

- Conduct a limited but broad application survey of multiple applications in which the use of cryogenic and superconductive systems and components offer substantial advantages through improvements in the performance of propulsion, communication, detection, or weapons systems.
- Define, investigate, and experimentally evaluate the key elements of a representative cryogenic turborefrigerator subsystem suitable for providing reliable long-lived cryogenic refrigeration for a superconductive ship propulsion system.
- Provide a sound technical basis for subsequent applications of superconductive power in the area of ship propulsion. Other applications, and their requirements, will be reviewed and evaluated, in order to form a preliminary evaluation of those applications that might deserve more detailed study.

Cryogenic refrigeration is a common requirement of all superconductivity applications. For this reason, dominant emphasis is being given to this portion of the program. Its specific application to an integrated superconductive ship propulsion system with the extreme environments involved will assure that particular attention is given to each factor affecting reliability, maintainability, safety, and availability of the cryogenic system components.

#### **METHODOLOGY**

The program presented provided that the work would be divided into three phases:

- Phase I -- Cryogenic Application Studies
- Phase II -- Systems Technology Evaluations
- Phase III -- Key Component Development

The work in each phase was divided into various major tasks and was scheduled as shown in Figure 1. Major milestones were established, as illustrated in Figure 2, for the first two phases. All of the tasks necessary to fulfill the program were described in the statement of work. To assure direction and clarity, these tasks were divided into two groups: cryogenic turborefrigerators and superconductive power systems. The conduct of the broad but limited application surveys was independent of the more equip-

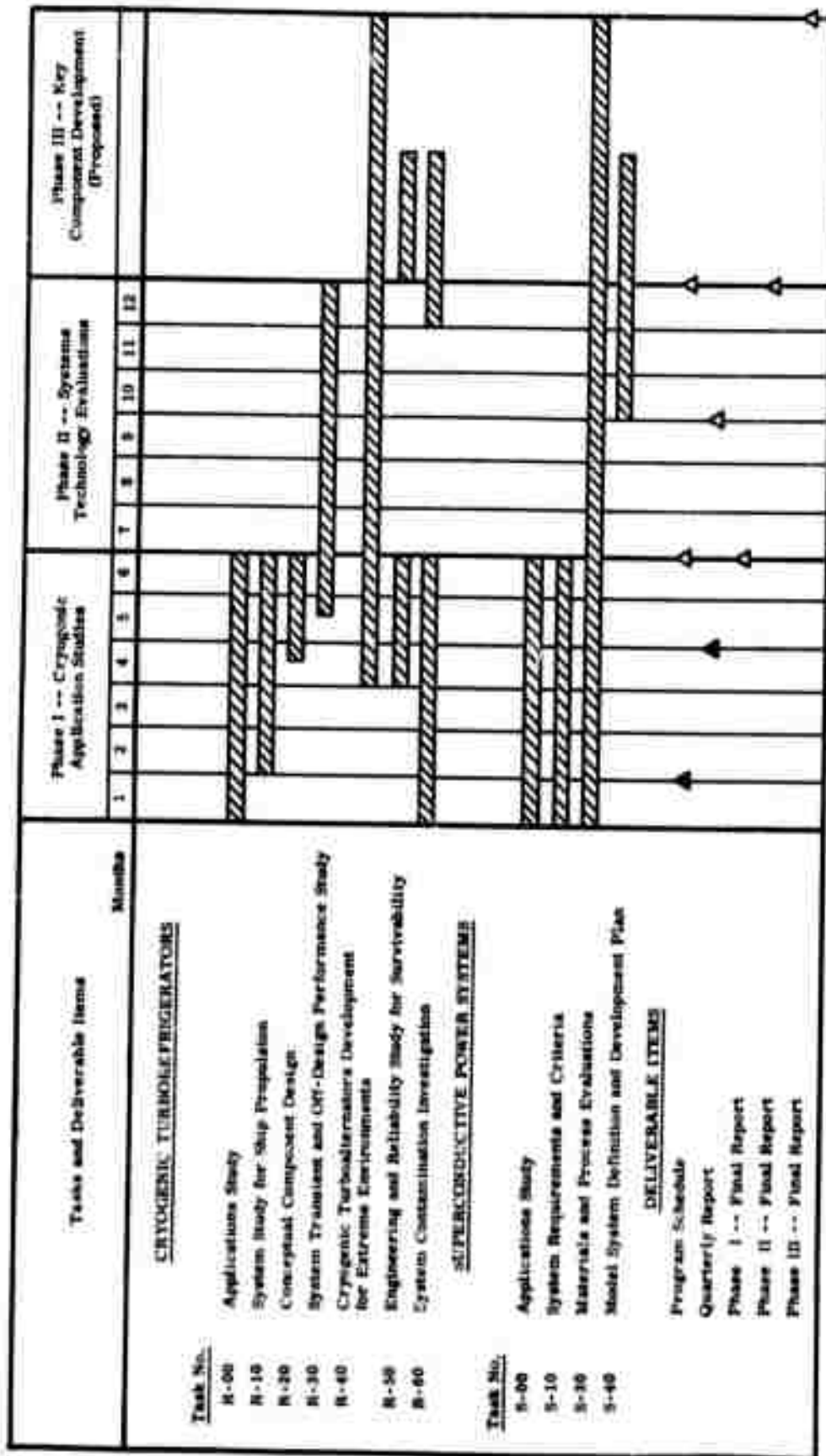


Figure 1. Program Work Schedule

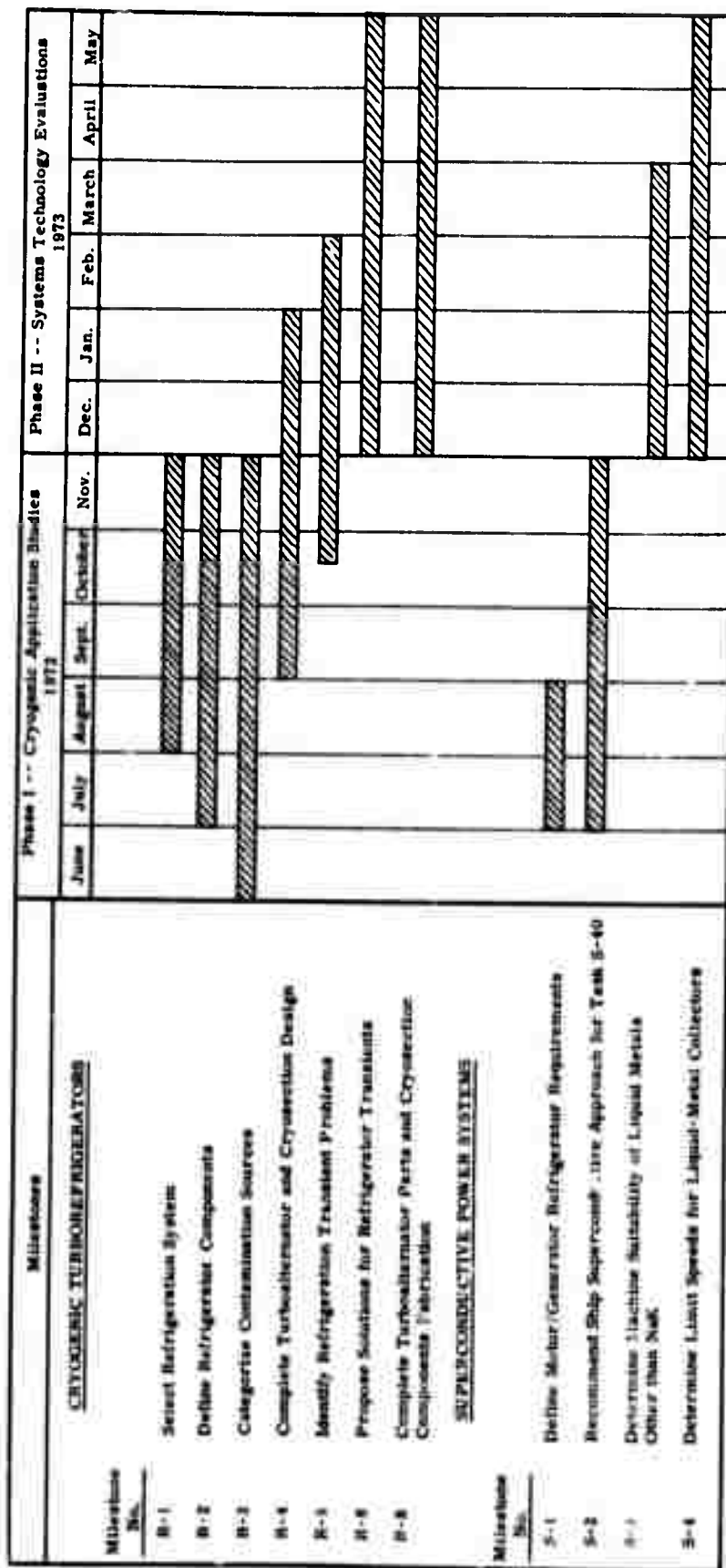


Figure 2. Major Milestones for Phases I and II

ment-oriented tasks. This report is structured to reflect performance under each of the planned tasks areas.

While work progressed in parallel in each of the two phases, a concentrated effort was made to provide an initial decision in Task S-10, "Ship Propulsion System Requirements and Criteria," because these inputs were necessary for the cryogenic refrigeration tasks.

The objectives of concentrated effort were to establish:

- Overall system requirements that superconductive ship propulsion must meet.
- Comparison criteria to be used in comparing various approaches to superconductive ship propulsion in order to arrive at the preferred concept, as well as to compare the resulting superconducting approach with the conventional propulsion approach for a given application.
- Requirements for the refrigeration subsystem consistent with the overall system requirements.
- Comparison of two kinds of superconductive ship propulsion systems with each other and with conventional propulsion.

## **TECHNICAL RESULTS**

Studies into the application of cryogenic turborefrigerators to Department of Defense uses and of the requirements pertinent to these uses have developed an extensive bibliography of source material concerning a wide range of possibilities, from magnetic sensors to lasers. In many instances the electrical power requirements are so small as to have no significance in regard to any application of superconductive power. In others, where large power requirements may exist, the definition of specific requirements is limited. It is recommended that these portions of the report be read directly by those interested rather than that a briefer summary be made here.

In Task R-00, the application of cryogenic turborefrigerators to Department of Defense requirements other than ship propulsion has been surveyed. Because of military classification, the report covering the work of this task has been submitted as a separate document. This document will also contain extracted portions, as necessary, of the report for Task S-00, "Applications of Superconductive Power."

In Section 2, "Cryogenic Turborefrigerator," the Claude cycle used in all refrigerators considered in this report is described. Also, the three major refrigerator components (compressor, turboalternator, and heat exchanger) are discussed in some detail, and the computer program used to design turborefrigerators is described briefly.

In Section 2, designs of three refrigeration systems (for a-c generators, d-c generators, and d-c motors) are summarized (Table 17), and detailed designs of all turboalternators and compressors are presented. It is significant that of all turboalternators designed for the three refrigeration systems, only two different frame sizes are required. Also, for all compressors designed, only one frame size is required; differences in flow rates and pressures are accommodated by changes in only the centrifugal impellers and compressor scrolls.

Most applications require the use of partial-admission turbines. However, in the turbine analysis, comparisons were made between partial-admission impulse turbines and full-admission reaction turbines. (The results are summarized in Table 7.) In the one comparison presented, the turbine efficiency could potentially be increased from 48 percent for the partial-admission turbine to 70 percent for the full-admission unit.

Heat exchanger designs showed that the plastic-laminate heat exchanger was typically less than half the volume and less than two-thirds the weight of the conventional plate-fin heat exchanger.

As described in Section 3 under "Comparative Performance and Recommended Approach" (and in other portions of this report), the application of superconductive power to the selected, representative ship resulted in a 17- to 22-percent saving in fuel and in a reduction in the average operating time of the prime movers of 47 percent (even greater reduction is obtained for a twin-screw ship in which a cruise unit is used.)

The size, weight, and power requirements for cryogenic turborefrigeration for either a-c or d-c generators are so similar that the refrigeration system, in itself, should not be a significant factor in system selection. Refrigeration system weight for the generators is about 5 percent of the generator weight, although refrigeration volume is approximately 75 percent of the generator volume.

The size and weight of the cryogenic refrigeration system for the 200-rpm d-c motor are very small relative to the motor. Weight is less than 1 percent. Cryosection volume (the portion that should be located near the motor) is less than 1 percent, and the total refrigeration volume is less than 10 percent of the motor volume.

The weight, volume, and area of d-c system buswork, though large compared to conventional higher voltage buses, are quite reasonable in relation to the rest of the equipment. It is about 1/3 the weight and about 1/100 the volume of the gas turbine inlet and exhaust ducts in a conventional gear drive. Thus the flexibility that the superconductive system provides in the location of the prime movers permits much shorter inlet and exhaust ducts to be used with corresponding savings in weight and volume. This bus volume, using copper, is about 4 percent of the volume of the reduction gearing for a con-

ventional gear drive of the same rating. The area of copper bus per 40,000-hp motor is 10 by 12 inches, including a 35-percent area allowance for cooling. This size was established by considering and minimizing overall system weight (including fuel).

The studies to date indicate that the transformer and rectifier sizes (applicable to the required a-c/d-c power conditioning between the generators and motor of an a-c/d-c system) are significantly larger than the size of the d-c motor itself and are perhaps 15 or more times as large and approximately 2 times as heavy as the d-c, copper buswork. The electrical losses in the transformers and rectifiers are very nearly the same as the losses in the d-c copper buswork of the size previously noted.

For the twin-screw destroyer mission profile used in this study, the superconductive systems (both a-c/d-c and d-c/d-c) have a total system volume about 30 percent less than that of a conventional gear drive.

For the same ship and mission profile, all three systems are very nearly equal in overall weight. It should be noted that in these comparisons, an increment of approximately 370,000 pounds is involved in the magnetic shields of the two d-c motors. This is about 14 percent of the total system weight, and the motor diameter and length could be reduced about 40 percent and 20 percent, respectively, if the motor shielding requirement, by reason of its location in the ship, could be eliminated. Where such reductions in weight or diameter are of value, further consideration should be given to this requirement (e. g., fully shielded at patrol speeds but only partially shielded at flank speeds).

Superconductive d-c machinery is indicated by this study to be preferable for ship propulsion service whenever such a decision is based solely upon the performance, reliability, cost, and simplicity for the propulsion system itself.

All d-c machines considered by this study employ liquid-metal current collectors. The materials and processes portion of the study includes major tasks in this area. It is significant to note that liquid-metal collectors using mercury and those using sodium potassium have been used successfully by the General Electric Company for many years. Collectors using sodium potassium have been provided and are currently offered for commercial, non-superconductive, acyclic, d-c generators by the General Electric Large D-C Motor Product Section. Very recently in developmental tests on a 10-inch-diameter experimental collector at 3600 rpm, liquid gallium has been successfully operated for more than 150 hours. This was made possible by a Company-funded development application in the General Electric Space Systems Products Division of a cleaning and reclamation circuit for the liquid gallium. Sodium potassium and gallium are considered to be best candidate liquid metals for superconductive machine service.

In Task R-40, "Cryogenic Turboalternators Development for Extreme Environments," turboalternator designs have been initiated. The major work of this task will be performed during Phases II and III of this program.

Task R-50, "Engineering and Reliability Study for Survivability," and Task R-60, "System Contamination Investigation," will also be performed during Phases II and III.

## **DEPARTMENT OF DEFENSE IMPLICATIONS**

The small size and weight of the turborefrigeration system for the superconductive machines studied on this program are such that these, in themselves, are of minor impact on applications such as hydrofoil ships, where it is desired to locate the motor and its cryogenic refrigeration equipment in pods where volume is at a premium.

The flexibility of component location and instrumentation and the ease and practicability of automation are of particular significance to the Department of Defense, because they offer real opportunities to reduce manning requirements and to simplify operational manpower qualifications. This advantage is felt to be very significant not only for military ships but for large supply and support ships.

The reduced size and weight, and particularly the possibilities for reducing the diameters of high-power motors for pod mounting or propellor shaft length reduction, are of value to the Department of Defense in all the new categories of ships studied.

This study is not yet complete; however, at this point there appears to be reasonable expectation that the cryogenic refrigeration and the other technologies applicable to superconductive power can produce highly reliable equipment with very little maintenance required.

## **IMPLICATIONS FOR FURTHER RESEARCH**

Based upon the work to date, in Phase I of this study, the following recommendations are made for future work, in addition to the completion of Phases II and III previously proposed:

- Perform experimental performance evaluation of gas bearing turboalternators in the 12°K to 15°K temperature range, which is the operating temperature of the Claude-cycle systems studied.
- Investigate further the application of full-admission reaction turbines in the larger refrigerator sizes, for a significant improvement in refrigerator efficiency.
- Conduct further experimental evaluation of the metal-plastic laminate heat exchanger, from the standpoints of structural integrity over a long period of time and outgassing characteristics.

- Conduct investigations of contamination-free helium compressor systems that may be attractive alternates to the very long-life, direct-motor-driven, gas bearing, centrifugal compressors included in this study.
- Make a more complete study of the weights, sizes, performance losses, and costs of the transformer/rectifier power-conditioning system, and its alternatives, for the a-c/d-c system. Make a more complete comparison and arrive at a conclusion regarding a-c/d-c versus d-c/d-c systems for various specific applications.
- Make a system study of superconductive propulsion equipment for hydrofoil and surface effect ship applications to determine the incentive for such use.
- Perform the following studies for displacement-type ships, including swath, destroyer, and supply/support categories:

Assess the effect of the capability for locating the prime mover at or near deck level for maintenance, overhauling, replacement of units, and manning requirements.

Assess the effect on overall mission life and the cost of reduced average operating time of the prime mover when using superconductive propulsion.

Assess the effect of utilizing contrarotating propellers and motors on the potential advantages of superconductive propulsion.

Assess the real advantage of volume savings when using a superconductive propulsion system, compared to a gear drive.

From the preceding studies, make a recommendation as to the incentive for applying superconductive propulsion to conventional destroyer-type ships as well as swath-type ships.

## Section 2

### CRYOGENIC TURBOREFRIGERATOR

#### REFRIGERATOR APPLICATIONS STUDY

A survey has been conducted of Department of Defense applications that might be suitable for cryogenic turborefrigerators. Because many of these applications are classified, the applications survey has been submitted as a separate, classified document.

#### REFRIGERATOR SYSTEMS AND COMPONENTS

##### REFRIGERATOR SYSTEMS

Under this contract, the type of refrigerator being considered is a turbo-refrigeration system that has all rotating components suspended on self-acting, gas-lubricated bearings. The elimination of sliding contact during steady operation avoids the wear-out failure mode, providing the potential for maintenance-free, long-life operation.

Turbomachinery is adaptable to either the reversed Brayton cycle or the Claude cycle (Figure 3). The principal components are:

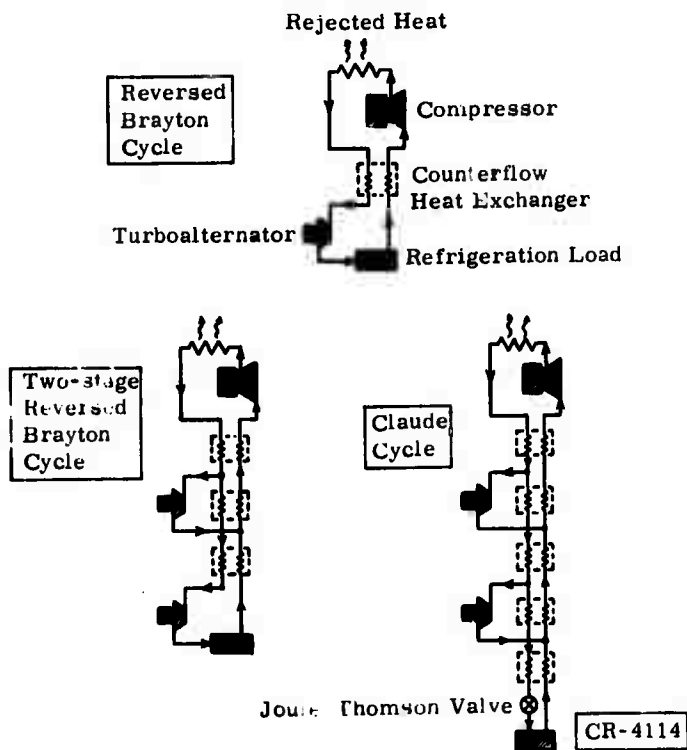


Figure 3. Cycles Suitable for Turbomachinery

- Motor-compressor at ambient temperature.
- Cryogenic heat exchangers.
- Cryogenic turboalternators.

Energy is added to the system by compressing gas at ambient temperature and removing the heat of compression from the refrigerant gas in the after-cooler. The gas is then cooled to cryogenic temperature in the cryogenic counterflow heat exchangers. Energy is removed from the refrigerant by the cryogenic turbines, cooling the gas and dropping its pressure. The turbine mechanical energy is converted to electrical energy by the cryogenic alternator, and this electrical energy is used or dissipated at ambient temperature. The low-pressure cooled gas is then available for removing heat from the refrigeration load and, finally, for removing heat from the high-pressure, incoming gas stream in the cryogenic heat exchangers.

As shown in Figure 3, the Claude cycle differs from the reversed Brayton cycle only in the addition of a Joule-Thomson valve and heat exchanger. Cooling through a Joule-Thomson valve to produce liquid is possible only at temperatures close to the refrigerant critical temperature, where the Joule-Thomson coefficient is above zero.

In all refrigerators considered in this report, the Claude cycle is used -- either a two-turbine machine, as shown in Figure 3, or a three-turbine unit, formed by the addition of one more turbine stage and two more cryogenic heat exchangers. A modification to the Claude cycle is also utilized; part of the helium liquid formed downstream of the Joule-Thomson valve is used for cooling, and the vapor evolved does not pass back through the heat exchanger system, as shown in Figure 3. Instead, the cold vapor is withdrawn from the refrigerator and is passed along electrical leads or structural supports, withdrawing heat from the leads or supports. After accomplishing this cooling job, the helium vapor is near room temperature, and the vapor reenters the refrigeration system at the compressor suction. In this way, a refrigerator is modified to perform with the principal characteristic of a liquefier; the low-pressure return flow through the cryogenic heat exchangers is less than the high-pressure flow rate on the other side of the same heat exchangers.

Characteristics of gas bearing turborefrigerators are summarized as follows:

- Gas bearings avoid sliding contact, providing potential for long life.
- Components are separable (the compressor or refrigeration station can be remotely located).
- There is essentially no vibration at the position of the refrigeration load.
- Input power is conditioned electrical power or shaft power from a mechanical energy source.

- Refrigeration load cooling is by means of a flowing gas or liquid stream.
- Temperatures of 4°K or lower can be attained.
- Refrigeration can be provided at more than one location and at more than one temperature simultaneously.
- Thermal time constants are large, and cold sections are well isolated thermally from warm sections (hence slow cooldown and slow warmup).

## COMPRESSOR

Different types of machinery have been used for compressors, in an effort to build refrigerators for a variety of applications. The compressor system lubrication plays a key role in the design of a cryogenic refrigerator. Oil-lubricated, positive displacement machinery will operate for extended periods of time, but the lubricant contaminates the cold section of the refrigerator and the system performance deteriorates eventually. Solid-lubricated, reciprocating machinery delays but does not avoid the contamination problem, and the wear rate is such that long-life operation is not attained. Efforts directed at nonlubricated, reciprocating compressor designs have led to the use of diaphragm compressors, bellows compressors, labyrinth-seal piston compressors, and helical rotor compressors.

The first two have very short lives because of fatigue. The labyrinth seal has obtained a modest success for a life of about 8000 hours but requires a vibration-free and shock-free environment to prevent contact between the piston and the cylinder walls. The helical rotor compressor potentially has the longest life of all positive displacement compressors, but suitable means to assure oil-free operation have not as yet been established.

High-speed dynamic compressors have the desirable long-life and non-contaminating characteristics required in a cryogenic system. Lubrication in the working space is not required because these compressors have no rubbing surfaces; rotating elements are suspended on gas fluid-film bearings. Therefore these compressors have the potential for very long life while supplying contaminant-free gas to the refrigerator.

As a consequence of these considerations, all of the cycle studies performed under this contract have incorporated gas bearing turbocompressors only.

## Compressor Requirements

The turbocompressor system provides the high-pressure gas to the refrigerator. Almost all of the power requirements of the refrigerator system are needed to drive the turbocompressors. Desirable requirements and features of the refrigerator compressor include:

- Long life.
- Assured contamination-free compressed gas.
- Reliable, continuous operation.
- Long intervals between service and maintenance.
- Capability of operating at momentary high g-loads.
- Low input power to the compressor as a consequence of:
  - High aerodynamic efficiency.
  - High motor electromagnetic efficiency.
  - Low bearing and windage parasitic losses.
- Minimum number of stages for low cost and high reliability.
- Compact arrangement to reduce weight and size.
- Convenient design arrangement for ease of assembly and disassembly.
- Compressor stages in series operation, with sufficient surge margins.
- Low rotating assembly weight for high critical speed.
- Low-weight impellers to reduce the overhung mass for high critical speed.
- Stationary impeller outer shroud to minimize the impeller stress level.
- Minimum axial thrust for low total bearing losses.
- Material selections compatible with low contamination requirements of refrigeration system.
- Gas bearings capable of stable operation within full ranges of speeds, pressures, and temperatures.
- High-speed motor stresses compatible with long life and compact rotor design.
- Adequate motor cooling.
- Capability of many start-stop cycles.
- Minimum development effort.
- Low seal leakages
- Reasonable manufacturing costs.

### Compressor Description

The General Electric Company has accumulated extensive experience with dynamic compressors that operate on fluid film bearings. Gas bearing turbocompressors have been developed in the sizes required by small turbo-refrigerators of a few horsepower, as well as in the 150-hp size range.

Both regenerative and centrifugal compressors have been applied to cryogenic refrigeration systems. Both types have similar motor, gas bearing, and rotor-dynamic requirements, but only the centrifugal compressor can be applied to the refrigerator requirements of this contract.

Regenerative Compressors. The General Electric Company has been active in the development of long-life, maintenance-free, noncontaminating compressors of the regenerative type. Regenerative compressors have a low specific speed characteristic that is compatible with the attainment of the high head/flow requirements of very small refrigerators with helium as the working fluid. Two multistage, regenerative compressors have been developed.

The first of these units was developed using General Electric Company funds. It consists of four stages of regenerative compression driven at 47,500 rpm by an integral 4-hp induction motor. The rotor is suspended on tilting-pad journal bearings and Raleigh step thrust bearings.

The second compressor was developed under contract to the U. S. Air Force. It is an advanced model of the first unit, in which the thrust bearing location has been changed and the speed has been increased to 100,000 rpm. This compressor delivers 1.1 grams per second of helium at 38 psia, which corresponds to a pressure ratio of 2.5. The induction motor power input was 3.5 hp.

A third regenerative compressor was developed under U. S. Army Mobility Equipment Research and Development Center sponsorship. This unit is a single-stage compressor that discharges 3.3 grams per second of helium at 42 psia and is designed for a pressure ratio of 1.4. This compressor's rotor is shown in Figure 4. The rotor is suspended on tilting-pad journal bearings and spiral-groove thrust bearings. The compressor is driven by a 4.4-hp, 90,000-rpm, brushless d-c motor, which is centrally mounted between the journal bearings. Figure 5 shows the disassembled compressor. Development has been completed, and the compressor has been operated up to design speed.

Centrifugal Compressors. The General Electric Company has been active in centrifugal compressor technology. The Company has conducted several programs aimed at the development of high-performance centrifugal compressors for small gas turbine applications. Recently the General Electric Company has been involved in the development of a small centrifugal stage for a turbo-shaft engine. This unit has achieved a pressure ratio of 3.0 and an efficiency of 0.81.

The Company has also been active in the design and development of gas bearing centrifugal compressors. A gas bearing, single-stage, helium gas circulator for a test reactor loop was developed. The arrangement is as shown in Figure 6. The rotor, which is shown in Figure 7, is supported by



**Figure 4. U. S. Army Single-Stage Compressor Rotor**

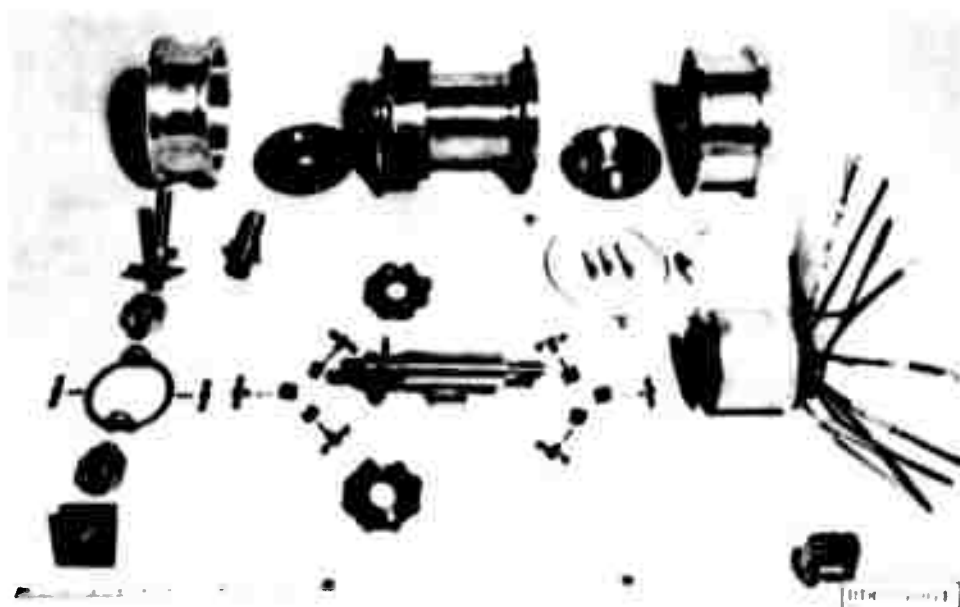


**Figure 5. Disassembled U. S. Army Single-Stage Compressor**



tilting-pad gas journal and thrust bearings. It is driven at 23,800 rpm by an integral, 150-hp induction motor. Four of these units were built and delivered.

Currently under development is a four-stage centrifugal compressor for use in a U.S. Air Force cryogenic refrigerator. This compressor consists of two two-stage modules, as shown in Figure 8. Each module is driven at 91,000 rpm by a 2.5-hp integral induction motor. The compressor delivers 2.3 grams per second of helium at 0.66 atmosphere, and the four stages in series will operate at an overall pressure ratio of two. Two impeller wheels are shown in Figure 9. Figure 10 shows the arrangement of the compressor system in a sealed outer casing.

Compressor Motors. Figures 6 and 7 show an induction motor integral with a single-stage centrifugal compressor.

The compressor drive motor is a two-pole, three-phase induction motor. Its nominal rating is 152 hp, 300 volts, 400 hertz operating at 24,000 rpm, 0.842 power factor, and 84.2-percent efficiency. Its rotor is solid steel with a cage of round aluminum bars. The overall outside diameter of the stator core is 13.5 inches, and the stack length is 5.5 inches.

High-speed induction motors have been developed by the General Electric Research and Development Center for the multistage regenerative compressors, and two 91,000-rpm, high-speed induction motors are currently under development for the U.S. Air Force centrifugal compressor. The compressor drive motor is supplied with six-phase power. Harmonic losses, core loss, and double ( $I^2R$ ) losses were reduced to the bare minimum to attain an electromagnetic efficiency of 94 percent. The stator is a two-pole design, rated 83 volts at 1525 hertz. The stack is 1.70 inches long and the rotor is 1.85 inches in diameter. The rotor is solid steel, and the cage is round bar aluminum.

A recent development included the design of a 4-hp, 90,000-rpm, gas-bearing-supported, motor-driven, single-stage, regenerative compressor and the design, construction, and testing of an advanced, brushless, d-c, permanent magnet, breadboard motor. During the first phase, the full-torque, 12,000-rpm, breadboard motor was built to operate from a d-c source without the use of brushes. An optoelectronic commutator and its associated power electronics energized the motor. The 90,000-rpm prototype motor has been tested at design speed and has been delivered to the U.S. Army Mobility Equipment Research and Development Center.

### Compressor Design Basis

The design of dynamic compressors for turborefrigerator cycle studies was based on the design accomplishments achieved at the General Electric Research and Development Center. Hence all designs from these studies will result in turbocompressors that could be designed, built, and operated.

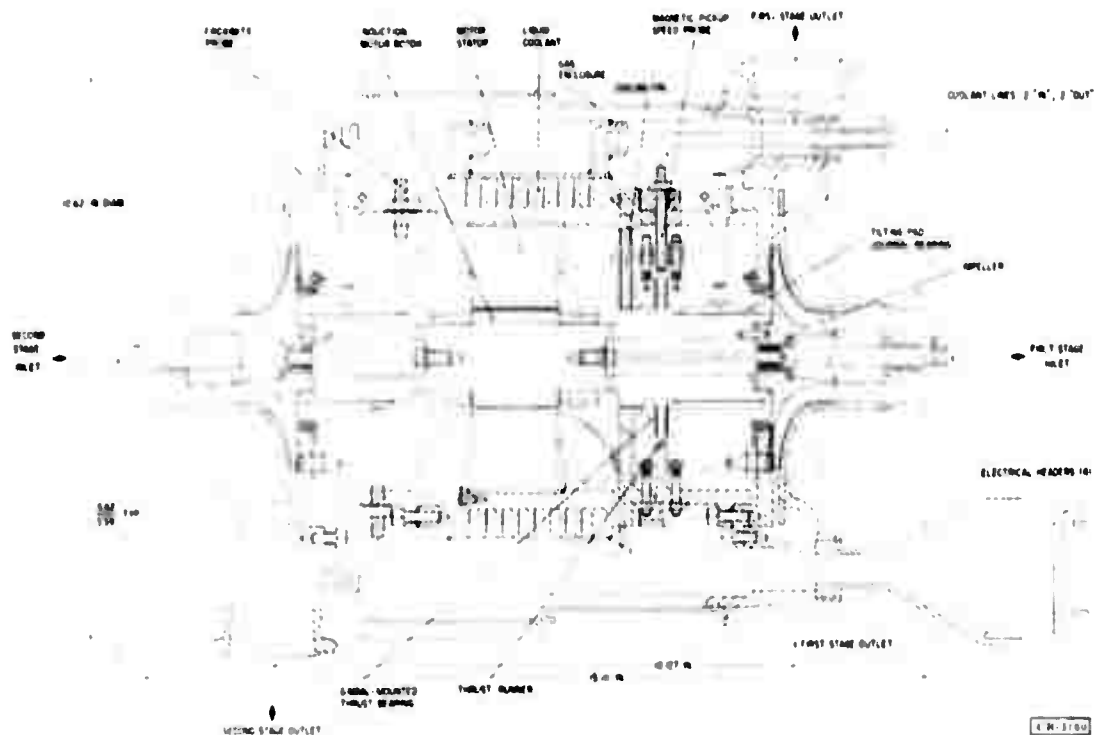
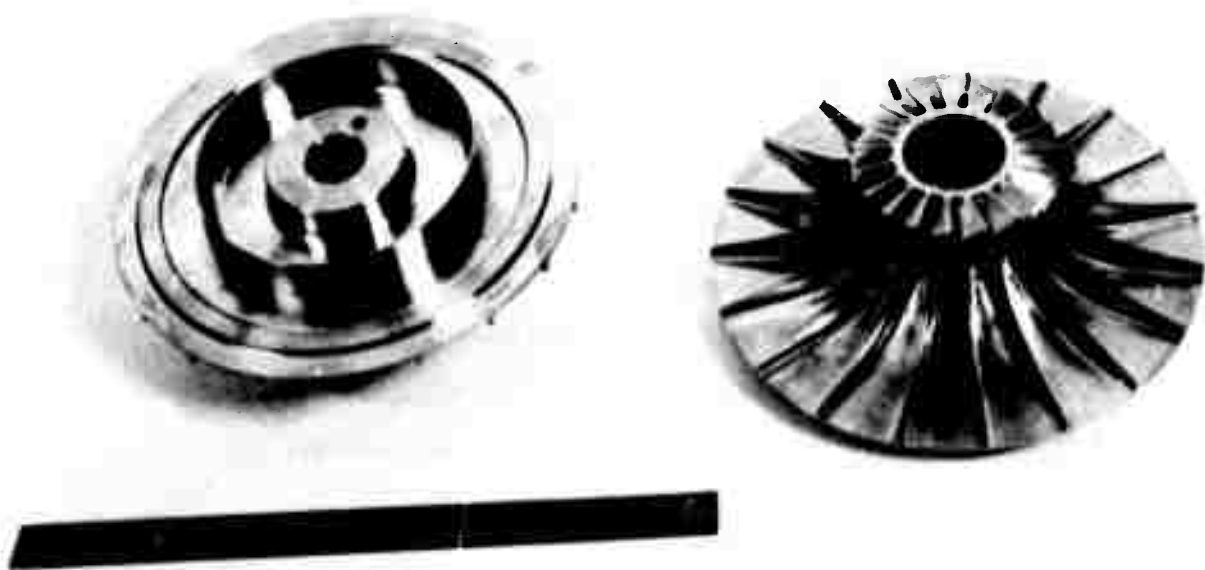
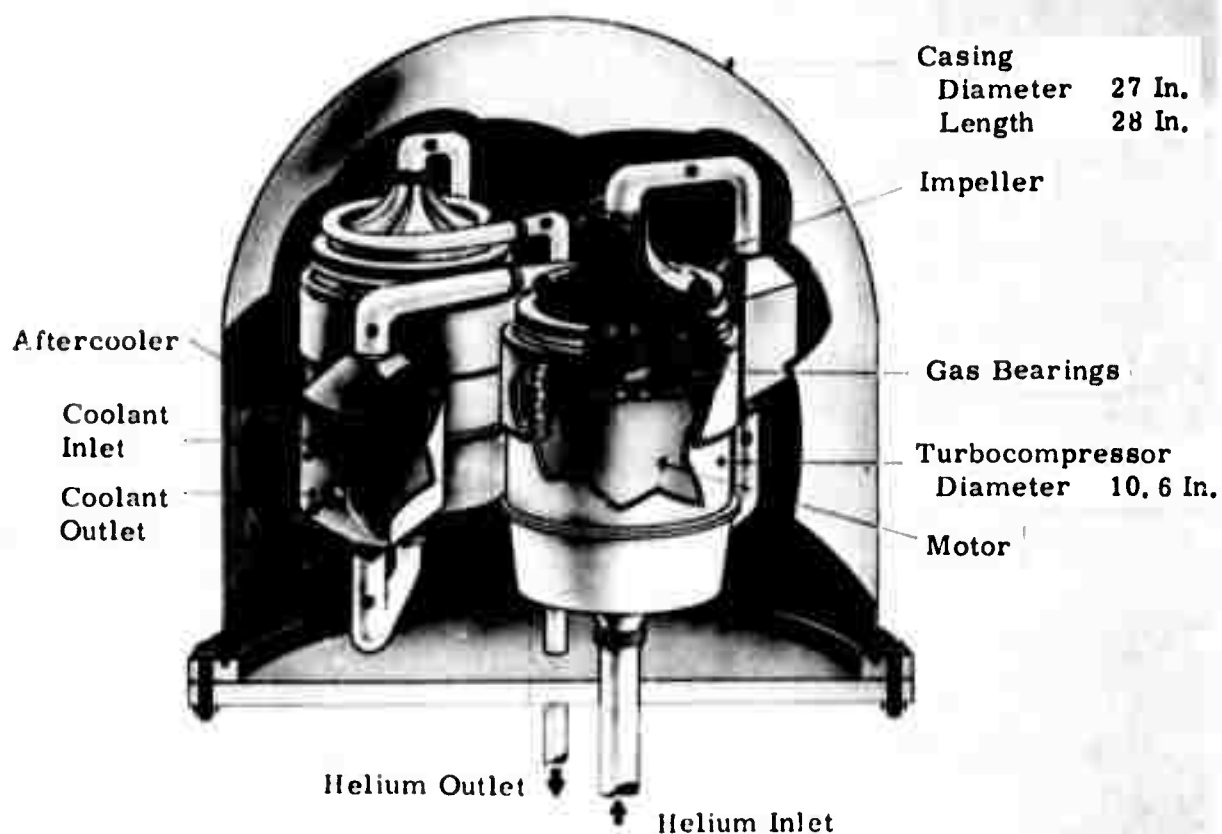


**Figure 8. Two-Stage Compressor Module of U. S. Air Force Cryogenic Refrigerator**



RDC 19304-1

**Figure 9. Helium Compressor Impellers (91,000 Rpm)**



RDC 18177

**Figure 10. Compressor System in Sealed Outer Casing**

The salient features of the turbocompressors include:

- Very long life potential.
- Proven design features.
- Design motor-driven impeller.
- Rotor supported on self-acting gas bearings.
- Minimum contamination problems.
- Rational development for extended life operation.

The design approaches to be taken to satisfy the overall requirements include:

- Minimum number of stages for low cost and high reliability.
- Material selections compatible with refrigerator low contamination requirements.

- Gas bearings capable of operating within complete ranges of speeds, pressures, and temperatures.
- High-speed motor stresses compatible with long life and compact rotor design.
- Compressor surge margins compatible with control needs.
- Low temperatures and stress levels for long creep-limited life.
- Short rotating assembly for high critical speed.
- Low input power to compressor:

High aerodynamic efficiency.

High motor electromagnetic efficiency.

Low bearing and windage parasitic losses.

Actually, except for the aerodynamic design, all of the turbocompressors to be considered fit between the design extremes of the Wright-Patterson Air Force Base Refrigerator B unit and the advanced test reactor (ATR) compressor described previously. Table 1 lists most of the principal dimensions of these two machines.

Table 1

GAS BEARING COMPRESSOR COMPARISON

Principal Dimensions	Refrigerator B (91,000 rpm, 2.50 hp, 1.87 kw)	ATR Circulator (24,000 rpm, 150.0 hp, 112.0 kw)
Impeller tip diameter (in.)	4.200	13.85
Journal diameter (in.)	1.650	4.47, 3.00
Thrust runner diameter (in.)	3.30	6.00
Motor diameter (in.)	1.85	5.84
Stator stack outside diameter (in.)	5.00	13.00
Journal pad length (in.)	1.500	6.00, 3.00
Distance between journals (in.)	7.25	15.375
Motor and stack length (in.)	1.700	5.280
End ring length (in.)	0.789	1.500
Motor rotor gap (in.)	0.030	0.080
Shaft length (in.)	9.235	21.813
Housing outside diameter (in.)	10.750	26.125
Overall assembled length (in.)	15.986	38.250
Rotating assembly weight (lb)	6.427	115.0

CR-3330

**Motor Design Basis.** The size of the compressor drive motor is determined by the horsepower and rotating speed. The rotor diameter is limited by the physical properties of its component parts. The length of the machine must be compatible with the stiffness requirements of the shaft. For this reason, there is a maximum horsepower that can be built for any specific rotating speed. When this maximum is exceeded, a new compressor design, which will result in a lower speed and larger diameter impeller, is needed. These factors result in a unique relationship for motor power as a function of speed, for the desired motor design proportions.

**Aerodynamic Design.** The computer program for impeller and diffuser aerodynamic design is based on the relationship of specific speed to centrifugal compressor stage efficiency for wheels operating in the regime of Reynolds numbers of  $10^5$  and above. The efficiency-versus-specific-speed relationship employed in the computer program is based on centrifugal compressor investigations in the 0.04 to 0.20 dimensionless specific speed range conducted at the General Electric Company and based on reported work by others in the 0.02 to 0.04 specific speed range. Because the efficiency is based on experimental data, it includes the losses of disk friction and leakage flow. A postulation has been made that impeller seal diametral clearances will be able to be maintained to prevent leakage flow from exceeding 5 percent of the total flow of the stage.

In addition to efficiency, the impeller entrance outside diameter and tip blade angle setting have been scheduled as a function of specific speed, based on a multitude of centrifugal compressor experimental and design data.

An accelerating impeller velocity schedule that is essential to good compressor performance, has been incorporated. The impeller tip axial width is determined from this schedule.

The computer program is structured so that the performance of each stage is printed out separately. The desired combined pressure ratio of the stages is made to converge within 0.7 percent. A list of output variables of each individual stage is presented.

The program contains two tip speed adjustment factors that are input values. One input designates the number of modules that will be maintained at a constant tip speed. The second factor is a fraction by which the tip speed may be reduced for the following stages. Thus the best efficiency for each stage may be obtained.

To maintain practical impeller shaft diameters, the program has a built-in limit of minimum impeller hub diameter. The program is also predicated on the assumption that impeller axial tip widths below a minimum value are beyond the manufacturing capability of impellers.

For the aerodynamic design of all impellers, the program has been designed to conduct a series of checks before proceeding to the stage-by-stage

calculations. These checks are made to prevent the generation of unusable data as a result of inputs that exceed either design limits or the limits of the program.

The gas bearing design approach used for the turbocompressors is the same as that used for the turboalternators, which is discussed below.

Centrifugal Compressor Performance Survey. As a guide for refrigeration system cycle studies, a centrifugal compressor study was conducted to examine refrigerators for 12°K temperature refrigeration applications. This examination was carried out under a U. S. Government contract. Above-atmospheric operation was assumed with heat rejection temperatures just above normal ambient conditions. Electrical component efficiencies were fixed:

- Conditioner controller efficiency 0.92 (fraction)
- Motor electromagnetic efficiency 0.93 (fraction)

The impeller tip speed was fixed at 1600 fps for all stages, which is typical for long-life operation with a good impeller structural design. This constant tip speed penalizes low specific speed units, because the best efficiency can be obtained by decreasing the tip speed with succeeding stages.

Bearing geometries and motor dimensions consistent with current design approaches were selected. These geometric values are expected to be approximately in the proper range, but many detailed design considerations would have to be made before final selections are made. These considerations include: overspeed margin, thrust load, acceleration loads, and the actual design life target.

The results of the centrifugal compressor performance survey are shown in Figures 11 through 14. Figure 11 shows the shaft rotational speed versus the compressor mass flow rate, along with the overall compressor system pressure ratio, as a function of the number of stages. Figure 12 shows the overall isentropic efficiency of the complete compressor system, with inter-stage cooling, as a function of the mass flow rate to the compressor. The reason for the increasing efficiency with the number of stages is a result of the intercooling between stages.

Figure 13 shows the individual aerodynamic wheel efficiencies for the first and last stages for compressor systems consisting of four, six, and eight stages operating in a series. The decrease in aerodynamic wheel efficiency with decreasing flow rate is a consequence of the lower specific speed, as shown on the lower part of Figure 13. Typical dimensions for the compressors, resulting from the survey, are shown in Figure 14 where both the shaft length and the tip diameter are shown. This is the shaft length of each of the modules and the impeller diameter for each one of the centrifugal compressor impellers.

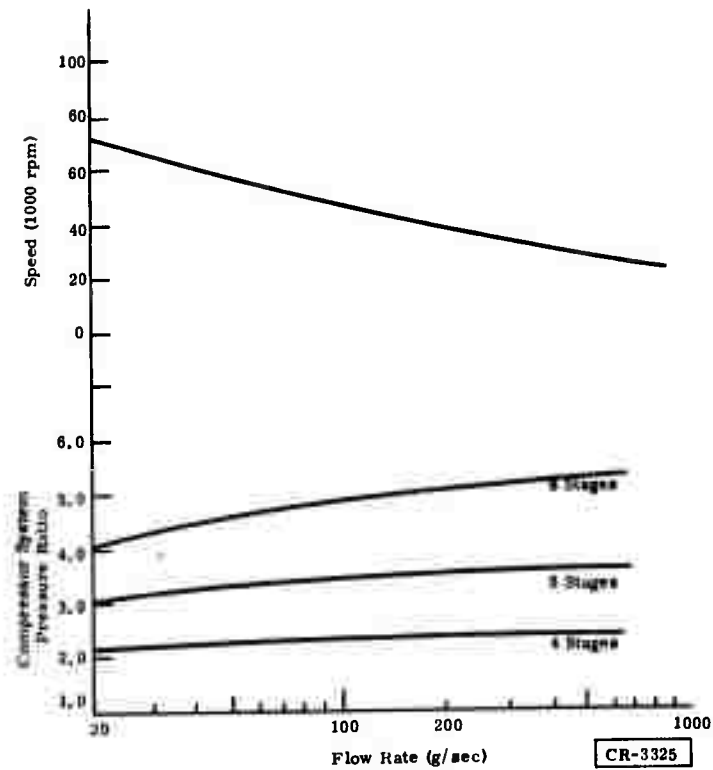


Figure 11. Speed and System Pressure Ratio Versus Flow Rate

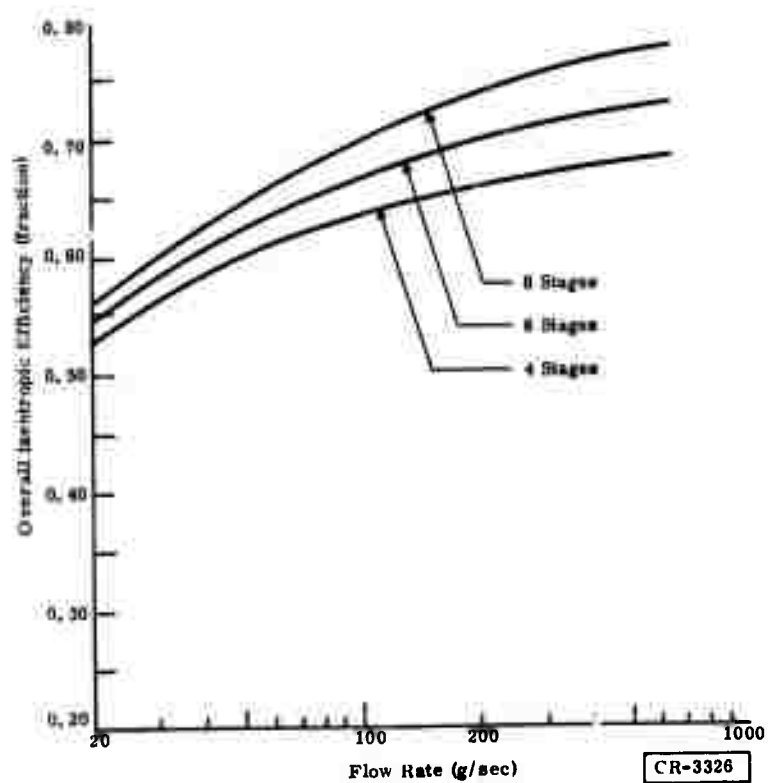


Figure 12. Overall Efficiency Versus Flow Rate

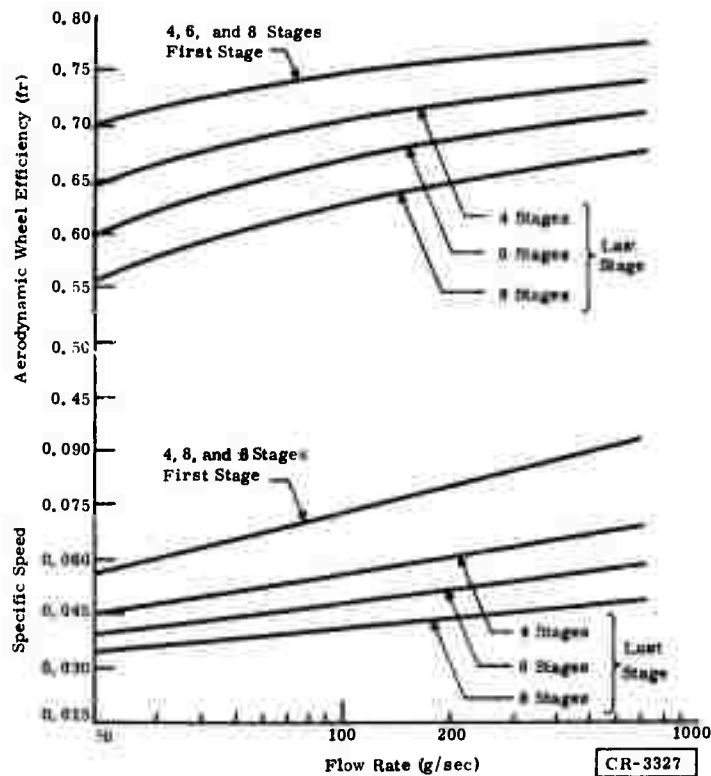


Figure 13. Wheel Efficiency and Specific Speed Versus Flow Rate

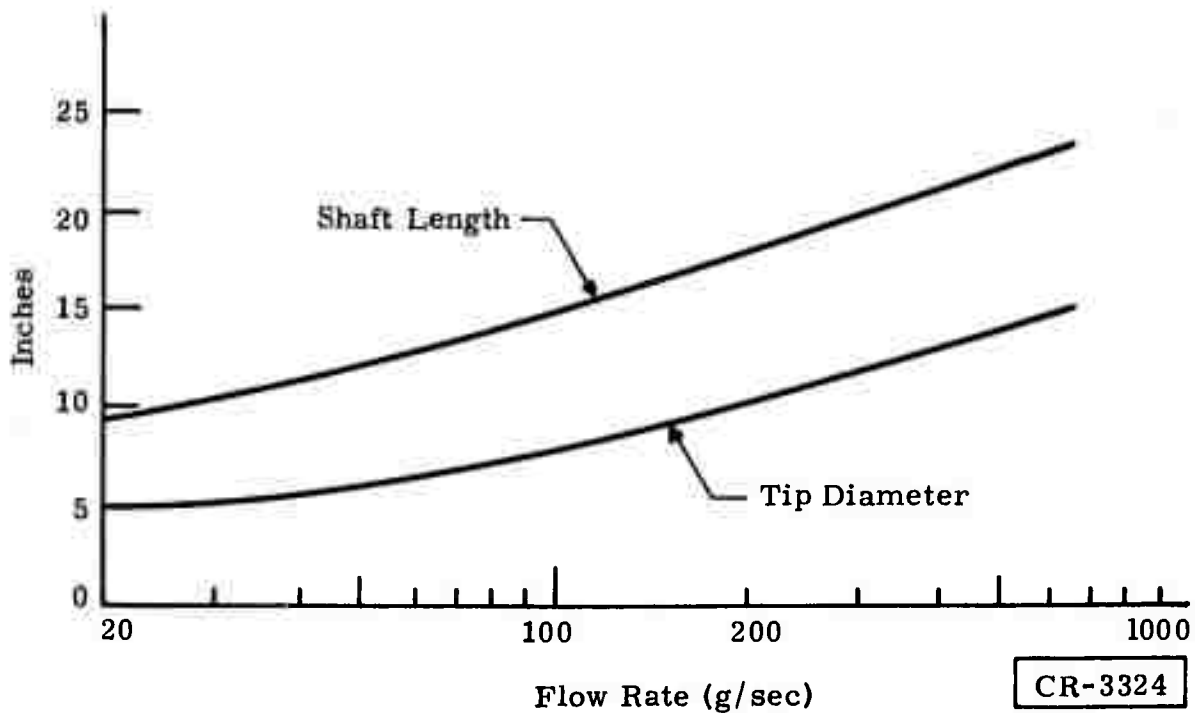


Figure 14. Typical Dimensions Versus Flow Rate

An interesting extension of the centrifugal compressor survey can be provided from work completed under the U. S. Army SAFEGUARD contract mentioned above. A comparison of positive displacement compressors for cryogenic refrigerators, along with dynamic compressors, has been made, and the overall efficiencies are shown in Figure 15.

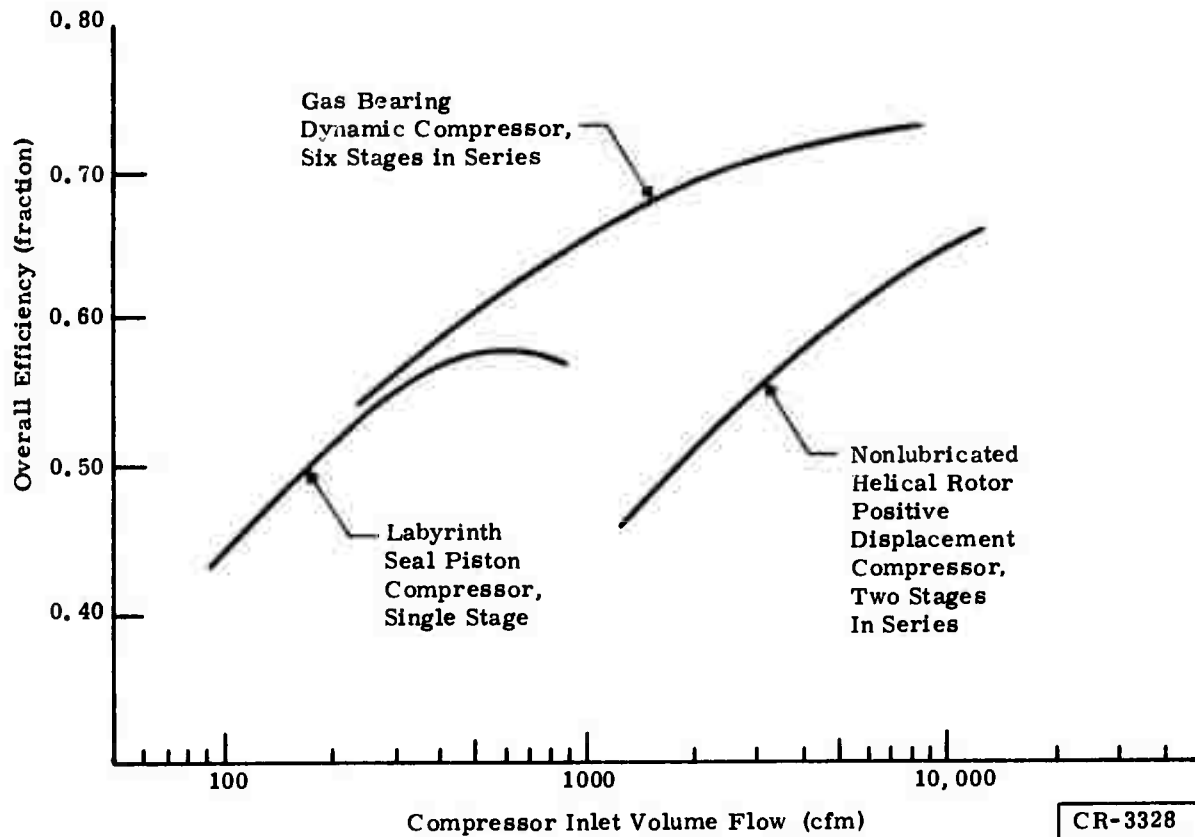


Figure 15. Compressor Performance Comparison

The centrifugal compressor performance is that for a six-stage arrangement, where the pressure ratios vary from 3.1 to 3.6. The labyrinth seal piston compressor is a single-stage unit, which has a pressure ratio of around four, made by Sulzer Brothers in Switzerland. The unit is nominally a dry operating compressor, but does have some inherent contamination potential.

For larger refrigeration systems, the nonlubricated, helical rotor, positive displacement compressor is shown with two stages in series, where the pressure ratio for these two stages is above four. This compressor arrangement has no contamination in the gas passages, but the helium-gas-to-oil seals do provide a serious contamination source.

Consideration was given to whether one or two stages should be used on each module. A relative comparison of characteristics is given in Table 2. From this appraisal, it can be seen that there is no clear-cut generalization that can be made a priori, because the key elements in making any decision

Table 2  
COMPARISON OF CHARACTERISTICS

Characteristic	One Stage per Module	Two Stages per Module
Development effort	Less	More
Machine complexity	Less	More
System compactness	Less	More
Aerodynamic efficiency	More	Less
Interstage leakage	None	Some
Overall efficiency	Similar	Similar
Thrust load	Large	Almost zero
Total development cost	Less	More
Total production cost	More	Less

would be relative to development effort and cost, as compared to total production cost. The other items listed can be handled adequately on an engineering basis, and there are no overriding considerations apparent.

The only tentative trend that may be postulated is that for a single bread-board refrigerator, one stage per module would probably involve less total cost. Conversely, it may be postulated that for large production quantities, two stages per module would result in the lowest total cost.

For the study reported here, it was postulated that the high-production-rate approach is warranted; hence all compressor modules include two impellers on a single motor-driven shaft. The specific design criteria used in the computer programs included:

- First-stage inlet pressure: above 1.0 atmosphere
- Pressure ratio: 2.5 to 3.5
- Speed: 1600-fps maximum impeller tip speed and motor diameter
- Arrangement: Two centrifugal stages per module
- Gas bearings: Tilting-pad journal; spiral-groove thrust
- Motor: Induction

### TURBOALTERNATOR

A variety of different expansion engine approaches has been used for the cryogenic expansion duty required in a closed-cycle cryogenic refrigeration system. These approaches include reciprocating devices with oil-lubricated,

solid-lubricated, and gas-lubricated pistons. Reciprocating expansion engines have also been built with diaphragms and bellows, and high-speed cryogenic turbines with oil- and gas-lubricated bearings have been employed.

Most of these expansion devices have a relatively short life and/or the possibility of contaminating the helium refrigerant fluid. The only exceptions are the gas bearing machinery. The positive displacement, gas-bearing, reciprocating expander is in an early development stage and has not been proven.

High-speed gas bearing turboalternators, however, have been successfully developed, have achieved the desired performance goals, and have provided the potential for the long operating life desired.

Hence all the detailed cycle studies conducted under this contract have incorporated gas bearing turboalternators only.

### Turboalternator Requirements

The refrigerator turboexpander is the means for extracting energy at low temperatures, thereby providing useful net refrigeration for the refrigeration load. Necessary and desirable features for cryogenic turboexpanders are:

- Long life.
- Reliable continuous operation.
- Long intervals between service and maintenance.
- High output power from the alternator as a consequence of:
  - High aerodynamic efficiency.
  - High alternator electromagnetic efficiency.
  - Low bearing and windage parasitic losses.
- Minimum number of stages for low cost and high reliability.
- Compact arrangement to reduce weight and size.
- Convenient design arrangement for ease of assembly and disassembly.
- Low rotating assembly weight for high critical speed.
- Low-weight wheels to reduce the overhung mass for high critical speed.
- Stationary wheel outer shroud to minimize the wheel stress level.
- Minimum axial thrust for low total bearing losses.
- Low stress levels to use high-strength aluminum wheels.
- Capability of operation at any attitude for specified g loads.
- Capability of normal operation after experiencing specified g loads, not operating.

- Low electrical load lead wire Joule and conductivity losses to ambient temperature.
- Minimum heat leak to the turbine wheel.
- No external gas supply to the bearings.
- High reliability.
- Material selections compatible with low contamination requirements of refrigeration system.
- Gas bearings capable of stable operation within complete ranges of speeds, pressures, and temperatures.
- Adequate alternator cooling.
- Capability of many start-stop cycles.
- Minimum development effort.
- Low seal leakages.
- Reasonable manufacturing costs.

#### Turboalternator Description

Two basic types of turbine are of interest for the turboexpander: impulse and reaction turbines. The partial-admission impulse turbine operates at a lower speed and is more adaptable to very small flow rates (Figures 16 and 17).

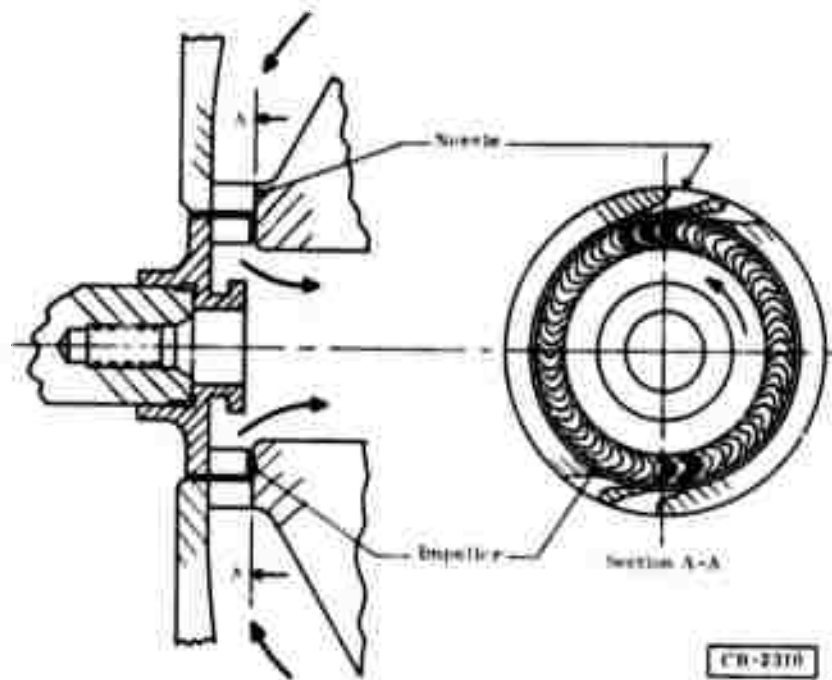


Figure 16. Partial-Admission, Radial Impulse Turbine,  
1.1-Inch Diameter



**Figure 17. Radial Impulse Turbine Wheel (0.625-Inch-Diameter)  
Mounted on 0.261-Inch-Diameter Alternator Shaft**

The reaction turbine is generally used for higher flow rates and is not attractive for partial admission (Figures 18 and 19).

In most cryogenic refrigeration applications at the General Electric Research and Development Center, the impulse turbine has been used because of the low flow requirements. Both radial and axial versions have been designed. The radial inflow reaction turbines have not found application in General Electric designs beyond the parametric studies for large cryogenic refrigerators.

Cryogenic turbine expansion provides a critical performance function in long-life refrigerators. Therefore, considerable research and development effort at the General Electric Company has gone into providing long-life turboalternators for cryogenic refrigeration systems.

Six turboalternators developed by the General Electric Company to date are:

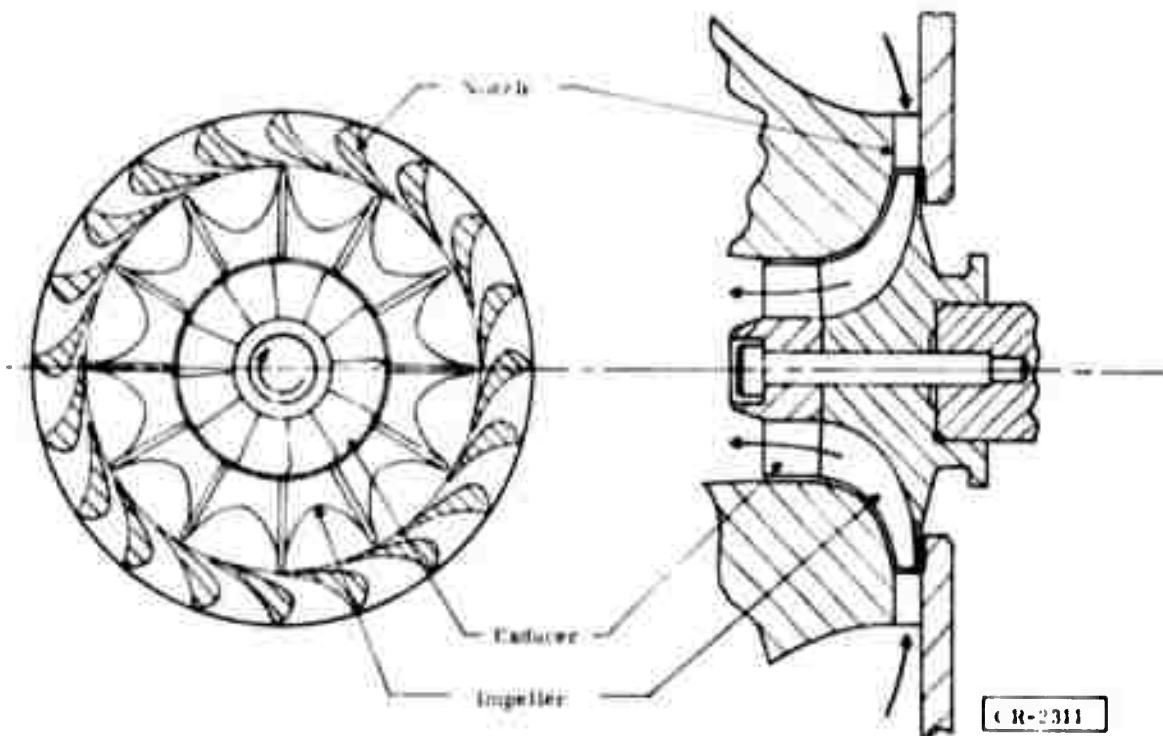


Figure 18. Three-Inch-Diameter, Full-Admission, Radial Reaction Turbine

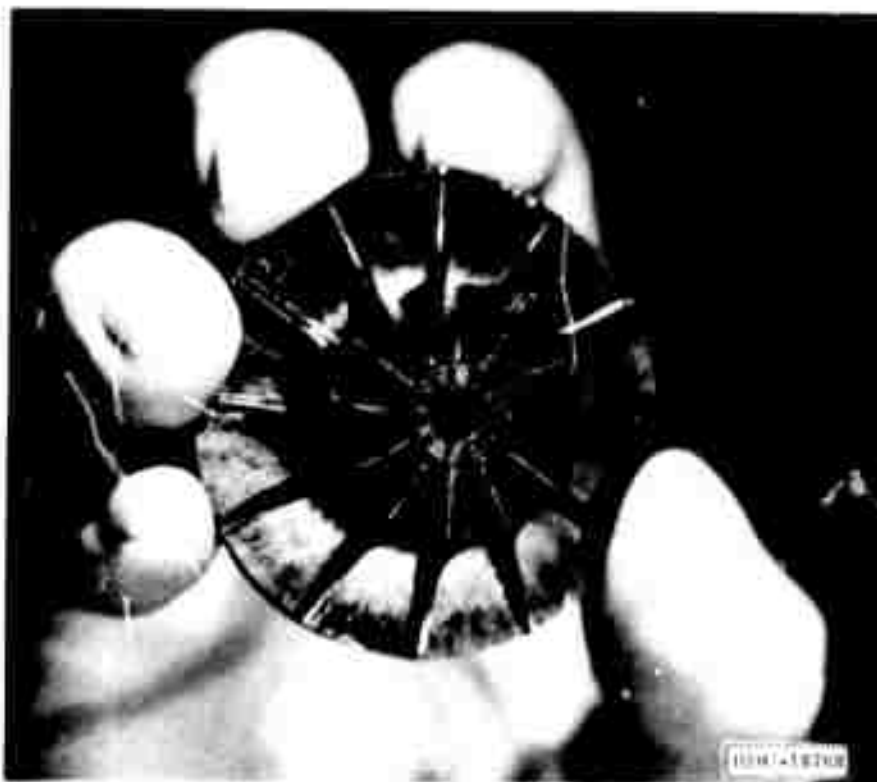


Figure 19. Turbine Wheel (1.90-Inch-Diameter) with 12 Blades

- Two for the U. S. Air Force for a liquid-helium-temperature refrigerator.
- One for a General Electric 80°K refrigerator.
- One for the U. S. Army, with a 60-watt output at 180,000 rpm.
- Two for the General Electric liquid-helium-temperature refrigerator.

All of these turboalternators have been of the partial-admission, radial inflow, impulse configuration, with a single expansion stage. Figure 20 shows

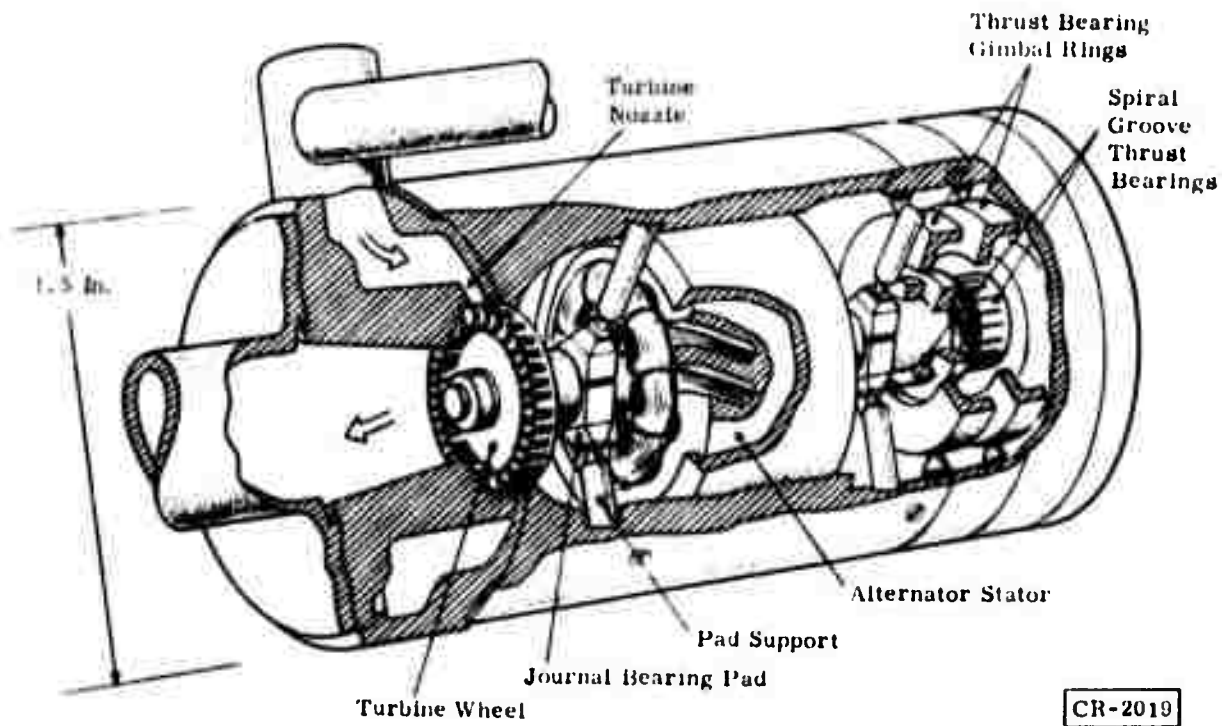


Figure 20. Cryogenic Turboalternator (Cutaway)

the arrangement of the single-stage turboalternator pictured in Figure 21. Figure 22 shows the turboalternator under test.

Current work at the General Electric Research and Development Center is aimed at developing units with longer life and higher efficiency than previously obtained. Two different two-stage turboalternators have been designed and built for the U. S. Air Force. Their configuration is shown in Figure 23. These turboalternators will be capable of operating effectively under low flow conditions. One of these turboalternators has been assembled and is being tested. Figure 24 shows all the parts for this machine.

The design for two single-stage turboalternators for a U. S. Army Mobility Equipment Research and Development Center 4.2°K refrigerator has been initiated.

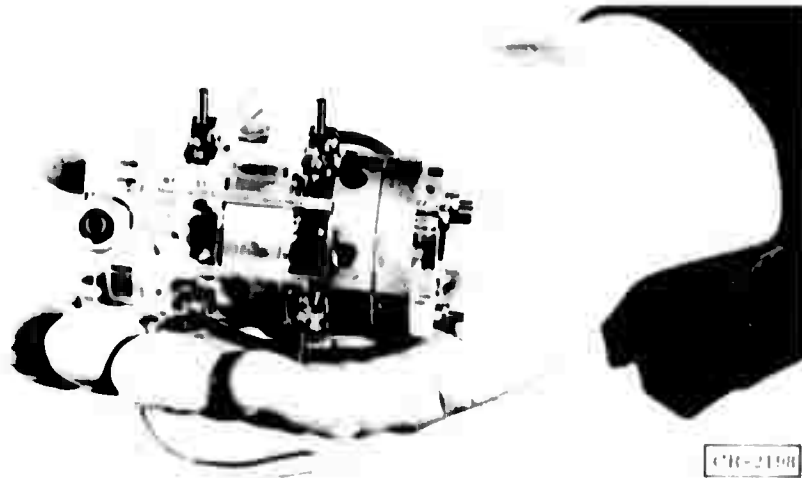
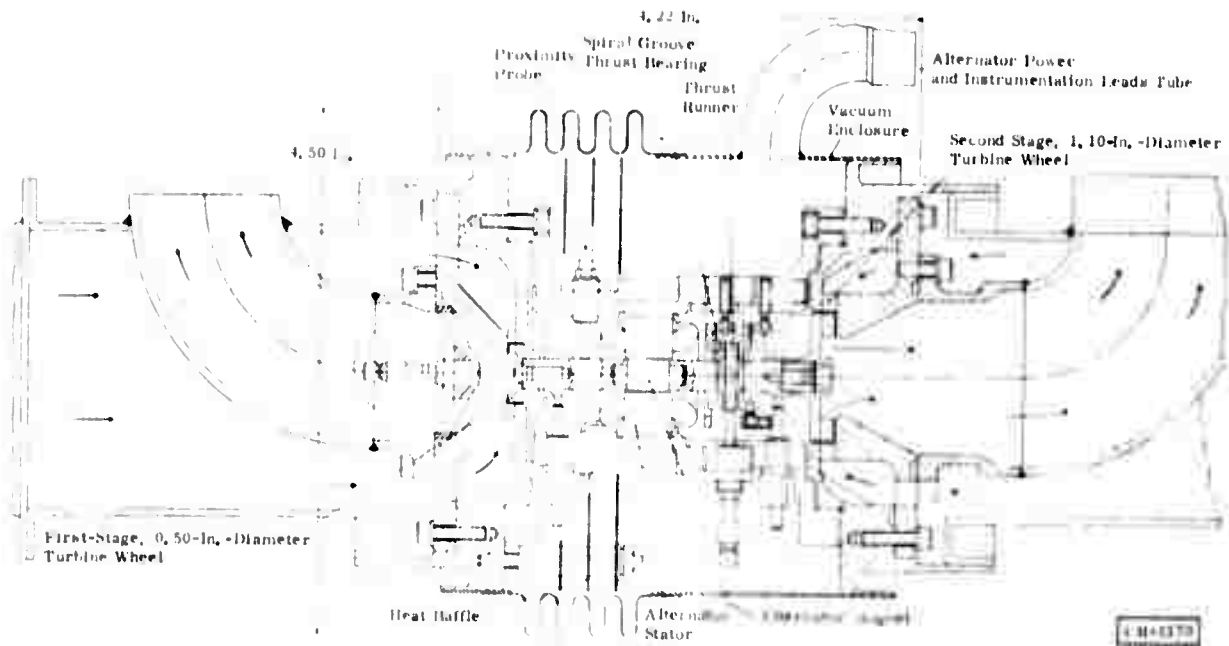


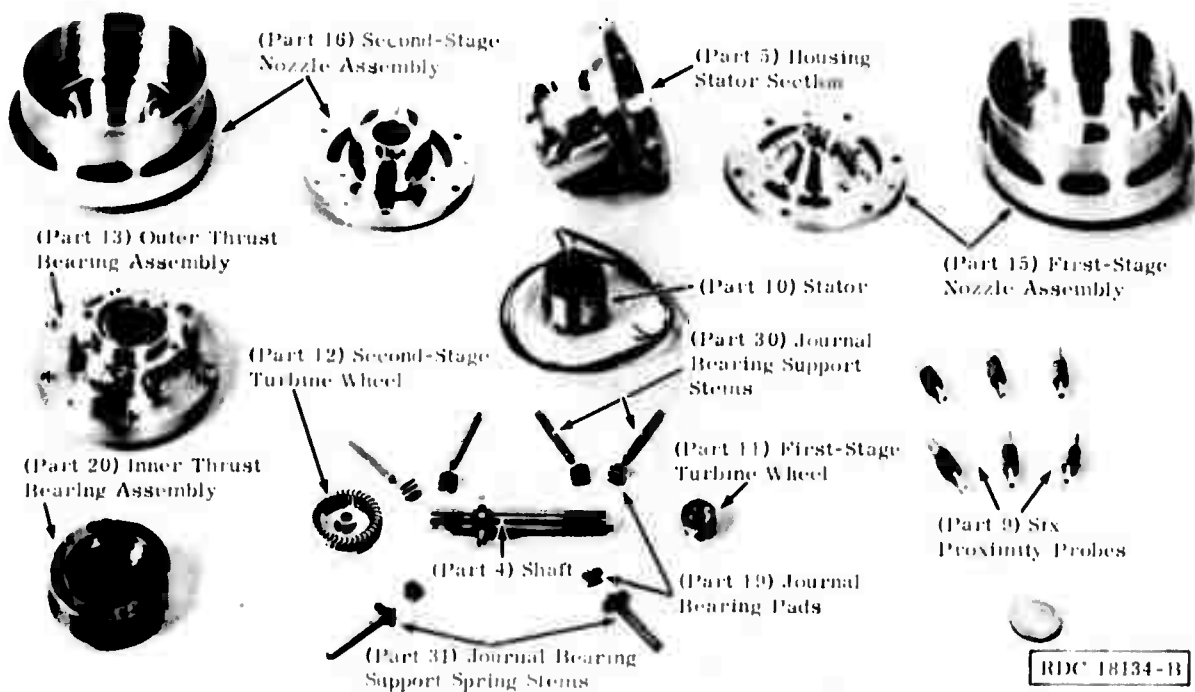
Figure 21. Full-Scale Model of Cryogenic Turboalternator



Figure 22. Turboalternator Test Stand



**Figure 23. Two-Stage Cryogenic Turboalternator**



**Figure 24. Turboalternator Parts for U.S. Air Force Cryogenic Refrigerator**

In addition, a partial-admission, axial inflow, impulse turbine development program has been undertaken, supported by the General Electric Company. This turbine is currently being endurance-tested at 100,000 rpm and at ambient temperature. To date, it has been running for more than 9900 hours without service or maintenance.

The success of miniature turboalternators in cryogenic refrigeration has required the development of self-acting gas bearings and high-efficiency alternators that can operate at low temperature.

The turboalternator arrangement shown in the above figures is a high-speed, radial inflow, impulse turbine mounted on a permanent magnet alternator shaft. The shaft is supported and positioned on self-acting, gas-lubricated bearings. Both the journal and the thrust bearings are free to adjust in the rotating assembly, thereby providing a means for rotating assembly alignment and positioning not available with rigidly fixed bearing surfaces. Tests at speeds up to 400,000 rpm have been conducted. The bearing, windage, and electromagnetic parasitic losses are acceptable.

The high-speed alternator has proven to be of both sound design and efficiency. Tests with electrical loads up to 109 watts have been conducted with electromagnetic efficiencies above 98 percent. This U.S. Army test alternator stator was wound with 265 percent more copper than previous versions, after which it was instrumented with eight thermocouples for test and evaluation.

The bearing system allows operation in any orientation, free from gas bearing and rotor instabilities sometimes found in other bearing systems. This bearing system has also proved capable of many start/stop cycles. At room temperature, a single turboalternator was subjected to start/stop cycles by repeatedly accelerating the rotor to 90,000 rpm and then allowing it to coast to a stop. Both horizontal and vertical positions of the turboalternator were tested. A total of 10,028 start/stop cycles was made, after which the bearing elements and the shaft surfaces were examined. Some wear was evident, but the bearing system was still completely serviceable. Various manufacturing techniques have been developed to produce these turboalternator gas bearing elements. It is significant that the start/stop cycle tests were conducted with elements manufactured by the lowest cost methods.

The turboalternators have been subjected to operation at cryogenic temperatures as low as 58°K in a closed-cycle turborefrigerator for the U.S. Army Mobility Equipment Research and Development Center.

For the present contract, a Big Bertha frame-size turboalternator, with a 0.5-inch-diameter shaft, is to be designed, built, and subjected to extreme environmental tests at 80°K. For this unit, a mechanical arrangement layout has been made, based on the design approach used in the second-generation Tiny Tim turboalternator frame size, which uses a 0.26-inch-diameter shaft.

The single-stage turboalternator is being designed to incorporate elements that could readily be developed to provide suitable performance and that could be adaptable to quantity production. The initial design layout of this turboalternator has been prepared and is shown in Figure 25.

The turboalternator is mounted on gas-lubricated journal bearings. Three hardened pads at each journal bearing support the 0.50-inch-diameter shaft with an operating gas film thickness on the order of 400 microinches. These journal bearings are of the self-acting tilting-pad type and are capable of stable operation throughout the operating range and at any attitude.

Two inward-pumping, self-acting, spiral-grooved, thrust bearings position the shaft axially. Like the journal bearings, the thrust bearings are gas-lubricated and typically operate with a 500-microinch gas film thickness. The entire bearing system is self-aligning, because the thrust bearings are gimbal-mounted and the journal tilting pads are individually self-aligning. Satisfactory operation of the complete bearing system can therefore be somewhat independent of the accuracy with which adjacent parts are manufactured. A radial inflow impulse turbine wheel is shown in Figure 25. The radial inflow wheel is convenient for close blade-tip axial clearances to minimize leakage. Neither the turbine wheel nor the nozzle has been final-designed.

The turbine energy is absorbed by a two-pole permanent magnet alternator. This compact alternator is a very practical device for extracting energy at cryogenic temperatures when that energy will be dissipated at a remote location. The two-pole magnet operates within the stator, which is wound three-phase in a core of low-loss iron laminations.

The vacuum-tight enclosure shown will be welded for the final assembly, but the design allows the use of replaceable static seals for initial tests. Proximity probes are installed to monitor the position of the rotor and gas bearing elements. An axial probe on the outer thrust bearing is shown to monitor thrust bearing motion.

High-speed gas bearing turboalternators require very close tolerances to operate properly. Also, the aerodynamic components require close clearances to achieve maximum performance potentials. Therefore, it is most desirable to establish the assembly procedures of a candidate design at the inception of the design. The results can lead to minimizing the number of critical tolerances on manufactured parts and also can lead to a design that will provide the least development effort. Hence a first draft for the assembly procedure will soon be initiated for this turboalternator, in conjunction with the layout drawing.

A preliminary design drawing of a turboalternator arrangement was made for the full-admission reaction radial inflow turboalternator design (Figure 26). It has a 1.0-inch-diameter shaft and the frame size is called the Grizzly Giant.

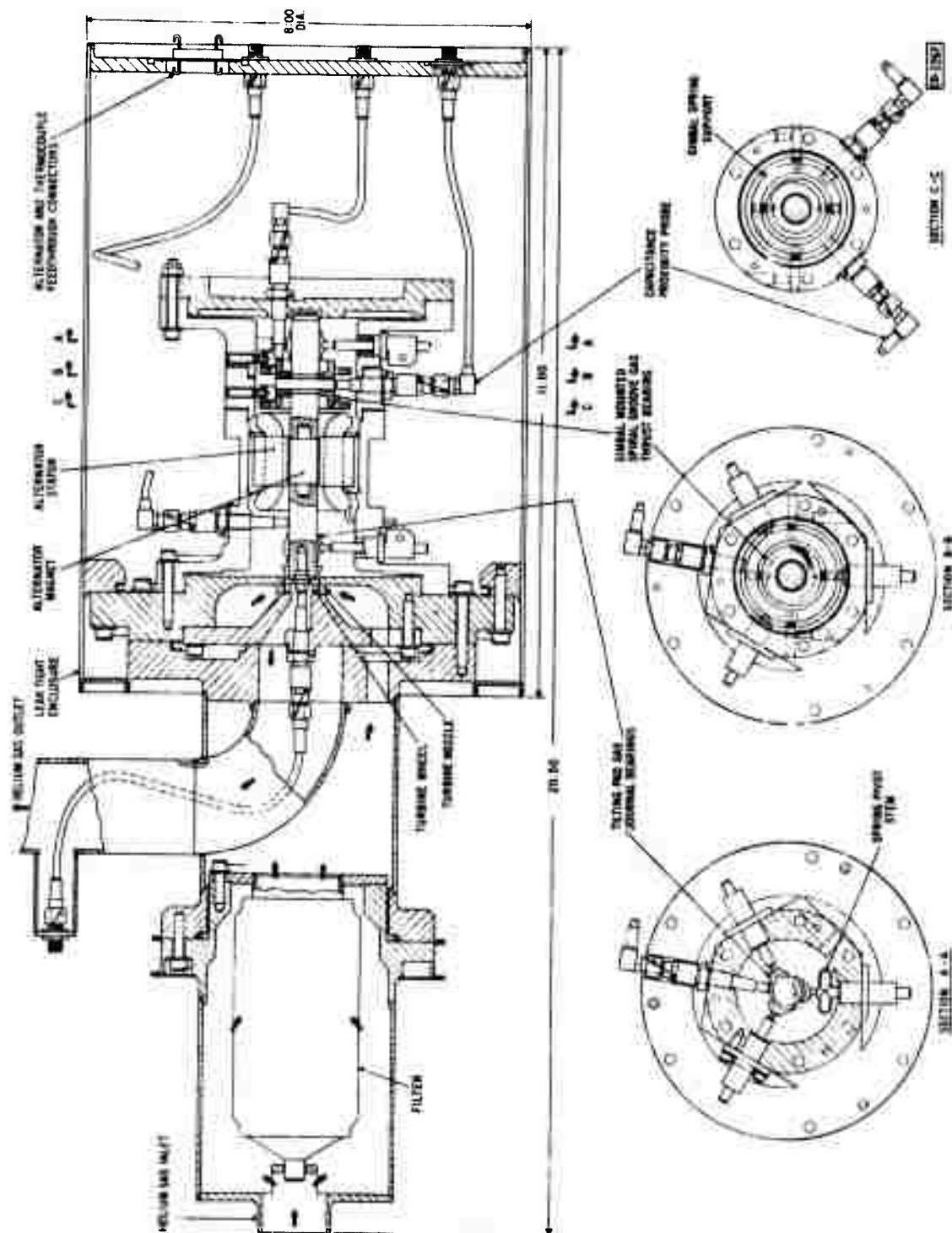


Figure 25. Single-Stage Big Bertha Cryogenic Turboalternator  
(0.50-Inch-Diameter Shaft)

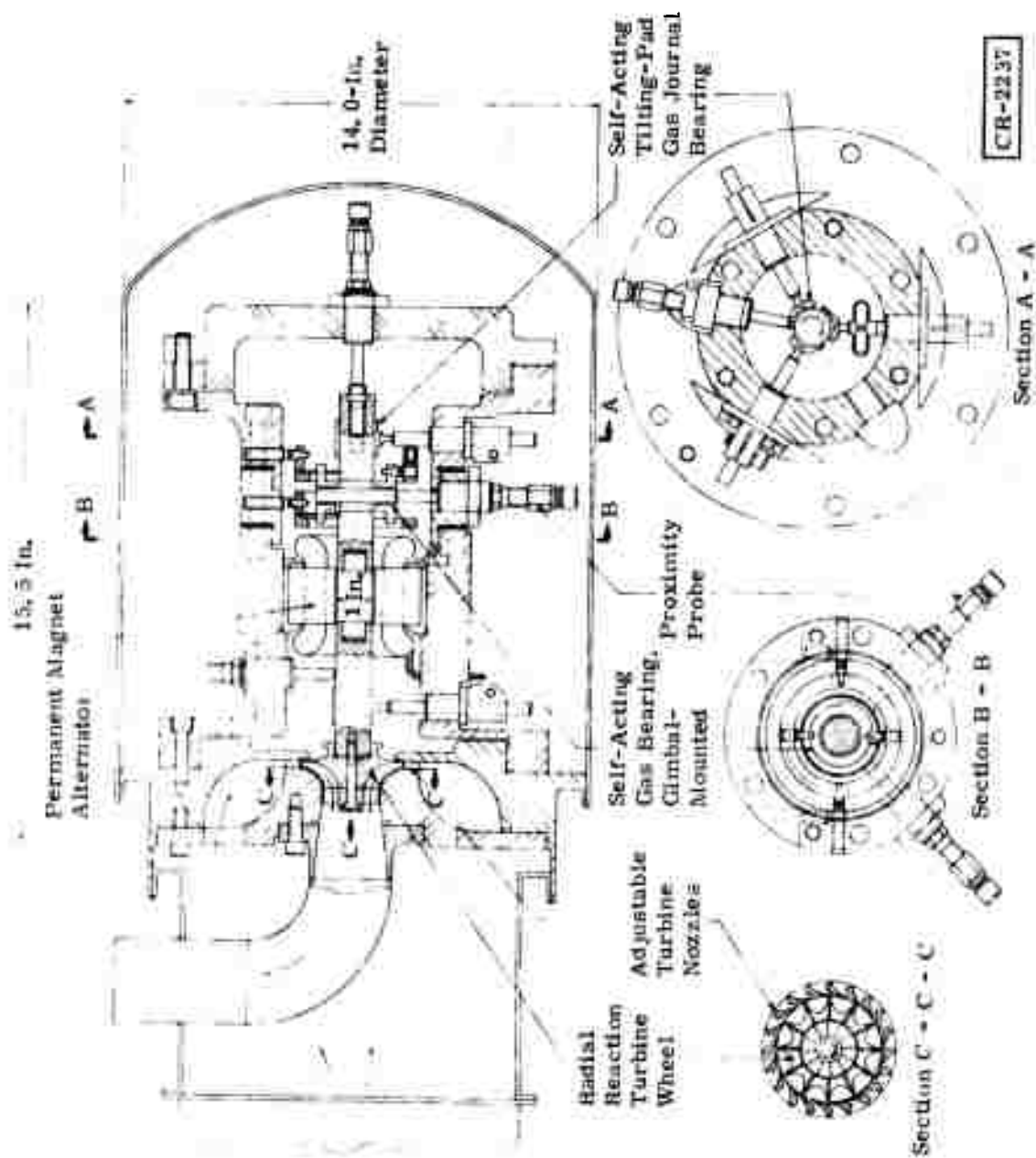


Figure 26. Single-Stage Grizzly Giant Cryogenic Turboalternator  
(1.0-Inch-Diameter Shaft)

This drawing is essentially a scaled-up version of the Tiny Tim and Big Bertha frame sizes, with just the wheel and nozzle geometry changed for the full-admission reaction turbine wheel.

The apparent temperature short circuit from the exit duct to the inlet duct is of no consequence; this problem was resolved with a heat transfer analysis.

The rotating assembly may possibly be shortened by using smaller proximity probes. There is also a possibility that the critical speed on this type of rotating assembly is lower than that desired for the eventual design speed and the initial higher cooldown speed of interest.

A savings in the platinum cobalt magnet volume in the shaft can possibly be achieved by using a hollow cylinder, but with as little change in the design as is practical.

This design is adaptable to provide a turbine wheel on both ends of the rotating assembly but, with most of the applications envisioned at this time, it is not anticipated that this frame size would use two turbine wheels on one shaft.

The radial reaction turbine wheel has been scalloped to reduce the thrust, and it is anticipated that no performance penalties will be incurred. The net turbine thrust can be reduced to almost nothing, with the proper rotor back face scalloping. The thrust generally goes to about zero as the scalloping is at a radius of 0.6 of the tip radius. Because the turbine flow is expanding and a favorable pressure gradient exists, the influence of rotor cutback on efficiency is negligible. Another advantage of rotor cutback on the turbine is that the stress levels will be lower, and the possibility of using aluminum turbine wheels for long-life operation is increased.

The possibility of making a separate exducer and impeller must be examined. Further design attention and stress analysis considerations would be included before these items are finalized. The strength of the nozzle backing plate, which is part of the housing, must be investigated from the diaphragm bending standpoint.

None of the feedthroughs for alternator power, thermocouples, and proximity probe instrumentation are shown on the drawing, but would be incorporated in a final design.

The possibilities of variable area nozzle vanes in this design would be investigated, since a substantial improvement in refrigerator cooldown performance could be obtained.

Only self-acting gas bearings were considered for this design. Externally pressurized bearings were not seriously considered for the following reasons:

- Refrigerator cycle efficiency requires a low ambient pressure, near atmospheric pressure, in the rotor housings.
- Refrigerator cycle efficiency would be lowered because a portion of the cycle gas would have to be diverted through the bearings.
- Ducting the bearing exhaust gas would involve a mechanical and thermal heat leak complication that is considered impractical.
- The bearings must be isolated from the rotor cavity by noncontacting seals. The design of the seals could be equally as complicated as the design of the bearing itself.

Surface features of many self-acting gas bearing types are shown in Figure 27. Tilting-pad journal bearings were selected for the journals because of:

- Confidence in ultimate success.
- Prior manufacturing and cryogenic test experience.
- Broad stability range.
- Inherent self-alignment.
- Reasonable tolerance to dirt ingestion and thermal distortion.

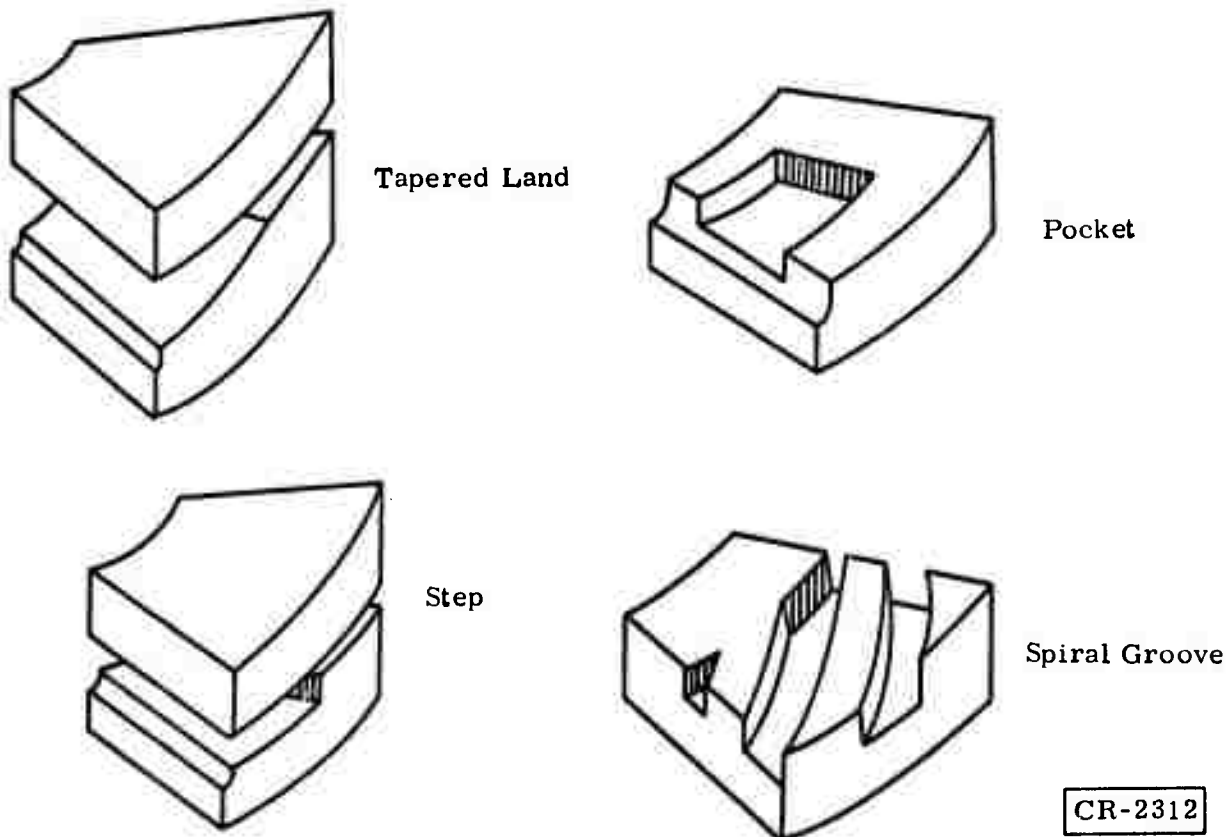


Figure 27. Surface Features of Self-Acting Bearings

Figure 28 shows a scale drawing of the journal bearing for the Big Bertha turboalternator. A double-acting hydrodynamic thrust bearing with a gimbal system mount was selected because of:

- Confidence in ultimate success.
- Prior manufacturing and cryogenic test experience.
- Suitability for any attitude, plus g loading.
- Suitability for complete self-alignment.
- Adequate load capacity.
- Low friction power loss.

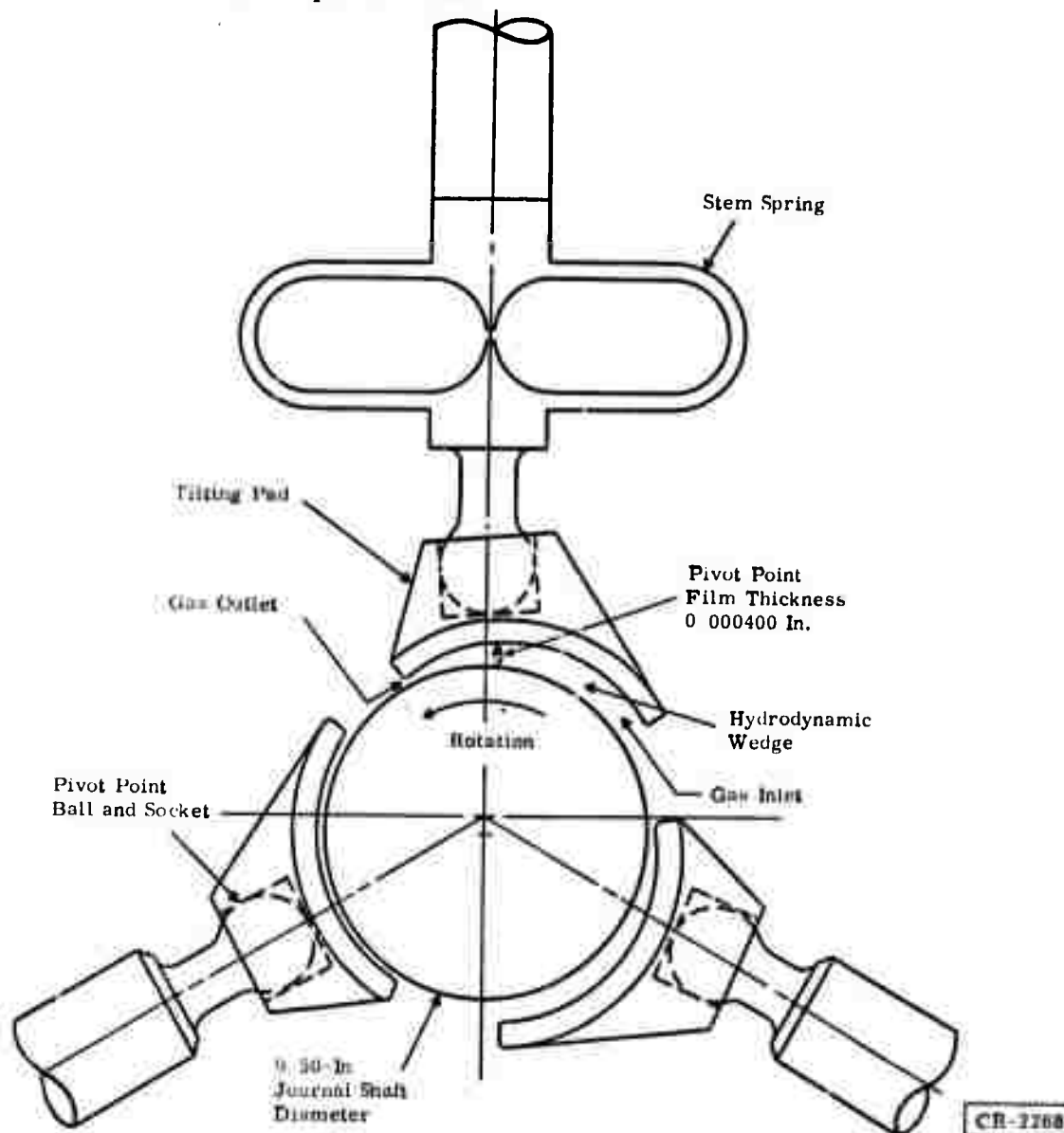


Figure 28. Tilting-Pad Journal Bearing for Big Bertha Turboalternator

Figure 29 shows a gimbal-mounted spiral-groove thrust bearing for the Big Bertha unit.

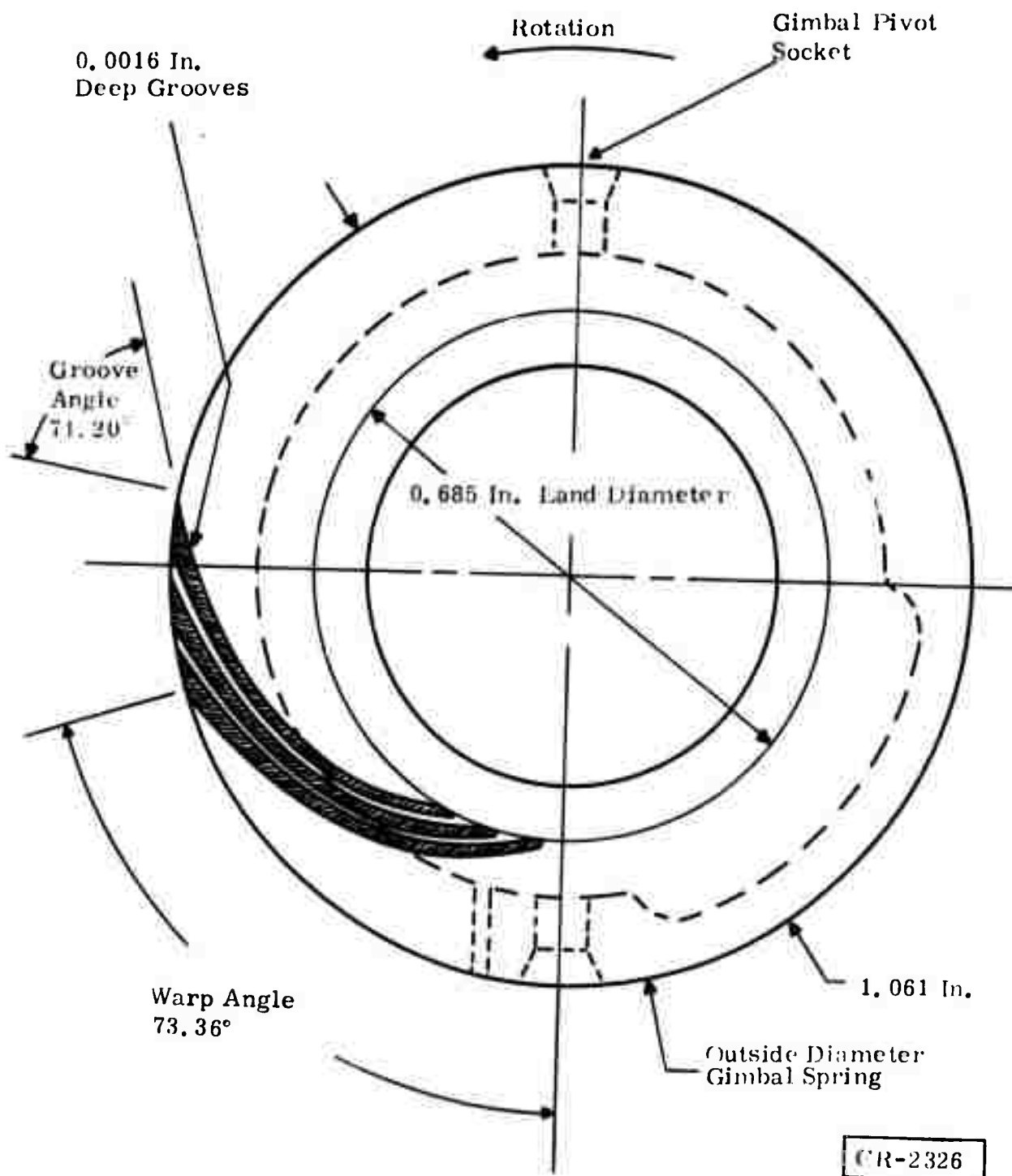


Figure 29. Inward-Pumping Spiral-Groove Thrust Bearing for Big Bertha

## Turboalternator Design Basis

The overall design basis and approach to satisfy the cryogenic refrigerator requirements will be directed toward:

- Reliable continuous operation.
- Long life between service and maintenance intervals.
- Minimum design and development.
- Low cost, size, and weight.
- Compatibility with environment.
- Material selections compatible with refrigerator low contamination requirements.
- Gas bearings capable of operating within complete ranges of speeds, pressures, and temperatures.
- Low-loss gas bearings especially for low-mass-flow designs.
- Alternator load characteristics compatible with control needs.
- Low stress levels for long creep-limited life.
- Short rotating assembly for high critical speed.
- High overall efficiency:
  - High aerodynamic efficiency.
  - High alternator electromagnetic efficiency.
  - Low bearing friction and windage parasitic losses.

Salient features of the gas bearing cryogenic turboalternator design basis include:

- Very long life potential.
- Proven design features.
- Direct turbine-driven alternator.
- Rotor supported on self-acting gas bearings.
- No high-pressure gas to bearings.
- Developed technology that can be applied to large units.
- Minimum system heat leak with alternator.
- Convenient load control with alternator.
- Minimum contamination problems.
- Rational development for extended-life operation.

All of the turboalternator design features of the gas bearing and electromagnetic design of the alternator are essentially the same, irrespective of size, with the only exception being the type of turbine wheel and nozzle used. The partial-admission impulse turbine is used for the low flow regimes and the full-admission reaction turbine is used for the higher flow regimes. The approximate efficiencies and the ranges of specific speeds used for each category of turbine are shown in Figure 30. It can be seen that in the vicinity of a specific speed of 20.0 that it is possible to have either type of turbine providing the best efficiency.

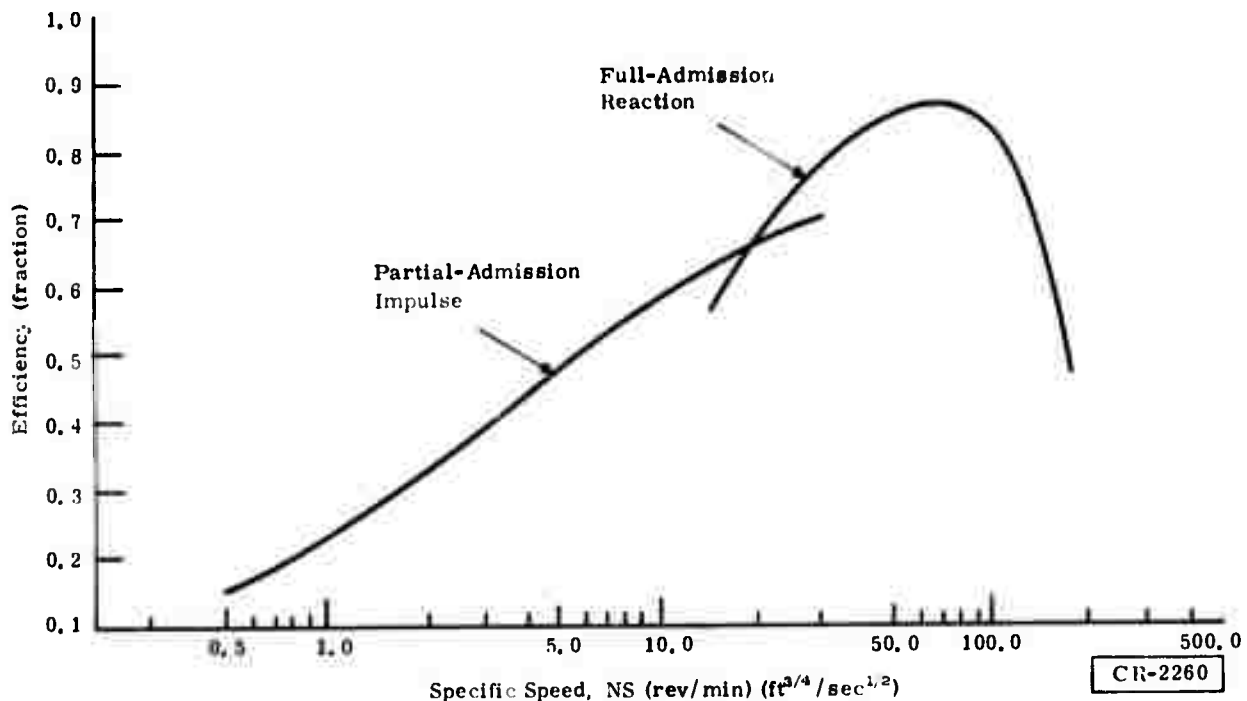


Figure 30. Turbine Aerodynamic Performance

**Alternator Design.** The electromagnetic design of the cryogenic alternator is based on an analysis similar to that for previous designs and substantiated by test results of similar alternators, using a solid platinum cobalt magnet material.

The design is based on a minimum stator overhang from the magnet, in addition to a specified gap between the magnet and the stator. Also, a non-magnetic gap between the magnet and any adjacent element is required. Peak alternator flux density is based on the power and the copper and core loss coefficients, which are both functions of the operating temperature. For a specified operating temperature and speed, along with the desired power output and desired electromagnetic efficiency, the size of the magnet is determined as a function of the core and copper loss coefficients.

Designs using this approach have resulted in electromagnetic efficiencies above 99 percent, operating at cryogenic temperatures. Of course at the higher

temperatures, the copper losses are greater; hence the operating efficiencies are lower.

The alternator load requirements essentially determine the size of the turboalternator frame used. For the two frame sizes described above, all of the turboalternators for the subject study require either a 0.5-inch-diameter Big Bertha frame size or a 1.0-inch diameter with the Grizzly Giant frame-size turboalternator. The approximate alternator power range and speeds are shown in Figure 31.

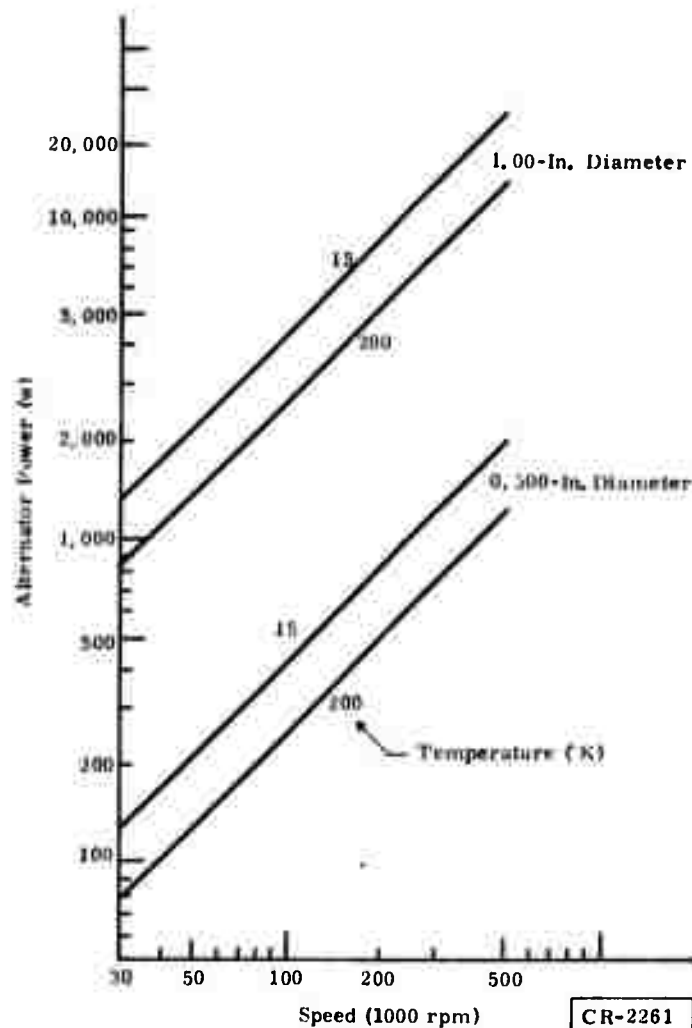


Figure 31. Approximate Cryogenic Alternator Power Characteristics

Partial-Admission Turbine Design. Considerable analysis has been performed on high-energy, low-flow turbines for a variety of applications. Characteristic of these turbine types are small nozzle and blade passages, impulse turbine blades, and high gas velocities. Criteria for analyzing these turbines may be reduced to overall performance similarity parameters of specific speed and diameter and local performance loss-producing parameters of relative blade Mach number and blade Reynolds number. The maximum performance

for design conditions is determined principally on the basis of the specific speed and specific diameter.

The turbine aerodynamic design point is initially established with the overall cycle input conditions to the turbines: turbine inlet total temperature, turbine inlet total pressure, mass flow, and turbine outlet static pressure.

The overall isentropic head is determined from nonideal gas charts or with the perfect gas relationship. Next an initial estimate of the overall turbine efficiency is made to establish the turbine exit conditions. The exit conditions may be determined from the nonideal gas tables or from the perfect gas relationship. Then the specific speed and specific diameter are determined. From these two parameters, with the diameter or the speed fixed, the initial aerodynamic efficiency is determined.

The above approach is used to establish a preliminary design of the turbine wheel and nozzle aerodynamic design. A complete analysis is then conducted for an evaluation of all losses. The various loss categories are:

- Parasitic
  - Journal bearing friction
  - Thrust bearing friction
  - Disk windage
  - Shaft windage
  - Core loss
- Alternator electrical
  - Copper loss
  - Can loss
  - Pole face loss
  - Stray load loss
  - Leakage flux loss
- Aerodynamic
  - Reynolds number
  - Partial admission
  - Housing leakage
  - Axial tip clearance leakage
  - Radial tip clearance effects
  - Blade loading loss
  - Trailing edge thickness loss
  - Blade roughness loss
  - Reaction effect
  - Mach number effect

All of the above design elements of the turboalternator are incorporated into a comprehensive digital computer design program. The design program

accepts refrigeration input cycle conditions and geometry choices. It then provides output of efficiency, individual losses, and a variety of performance information. A simplified version of the partial admission turboalternator design point computer program structure is:

- Input

- Cycle conditions

- Inlet temperature
    - Inlet pressure
    - Outlet pressure
    - Flow

- Geometry

- Wheel diameter
    - Nozzle angle
    - Blade angle
    - Blade trailing edge thickness
    - Number of blades
    - Axial blade clearance
    - Exposed shaft diameter and length
    - Alternator gap, diameter, and length

- Performance

- Alternator core loss coefficient
    - Alternator copper loss coefficient
    - Nozzle velocity coefficient
    - Specific diameter

- Output

- Reynolds numbers

- Disk
    - Shaft
    - Blade
    - Alternator gap

- Efficiencies

- Overall
    - Hydraulic
    - Wheel aerodynamic

- Parasitic Losses

- Electrical (core and copper)
    - Bearing friction
    - Gap windage
    - Shaft windage
    - Disk windage

## Performance

Net power output  
Wheel power  
Shaft power  
Specific speed  
Speed  
Blade inlet relative mach number  
Partial admission arc

## CRYOGENIC HEAT EXCHANGER

Reversed Brayton-cycle and Claude-cycle refrigerators require cryogenic heat exchangers having very high levels of thermal effectiveness (Ref. 1). This requirement is a consequence of the relatively low pressure ratios available with dynamic compressors and the relatively small temperature drops produced by the expanders. These temperature drops must be utilized largely to produce useful refrigeration, leaving only a small available temperature difference to drive heat between the gas streams in the cryogenic heat exchangers. This small temperature difference between streams implies a high thermal effectiveness.

As a consequence of this requirement for high thermal effectiveness, the cryogenic heat exchanger is generally the largest and heaviest component in the cryogenic part of the refrigeration system.

To attain the very high levels of thermal effectiveness required in this cycle, and at the same time to achieve a reasonably small volume, heat exchangers must possess the following characteristics:

- Large heat transfer surface area per unit volume.
- High heat transfer surface coefficients. (These can be realized by designing flow passages with very small equivalent (hydraulic) diameters, which also usually serve to increase the surface area per unit volume.)
- Very small longitudinal heat conduction through the walls and gas in the exchanger.
- Very uniform distribution of flow for each stream throughout any cross section of the exchanger (but high lateral thermal conduction tends to reduce the penalty of flow nonuniformity).

Several types of cryogenic heat exchangers might be considered to satisfy these requirements; however, two general types appear most favorably suited for the particular application under consideration. The first type is the plate-fin heat exchanger, and the second is the metal-plastic-laminate type.

The plate-fin exchanger is frequently used in industrial applications and is extensively described in the literature (Ref. 1). The metal-plastic laminate

exchanger is a newer development that will be briefly described below. Designs for both types of exchanger are carried out by the cycle design computer program. In all designs described in this report, the metal-plastic laminate heat exchanger was found to be considerably lighter and smaller than the corresponding plate-fin exchanger. As a consequence, all cryogenic heat exchanger weights and volumes given in this report are for the metal-plastic laminate type, unless otherwise noted.

### Metal-Plastic Laminate Heat Exchanger

The metal-plastic laminate heat exchanger is a generic type that can utilize several different heat transfer surfaces. Two surfaces will be discussed here: the "perforated plate" and the "wire mesh". The laminate exchanger will be described first utilizing the perforated-plate surface, which has been developed by the General Electric Company and other organizations.

The principle of the perforated-plate heat exchanger is illustrated in Figure 32. The exchanger consists of a large number of parallel perforated plates, with gaps between the plates. The gas streams flow longitudinally in counter-flow, and heat transfers laterally from one stream to the other through the plates, which are constructed of metal of high thermal conductivity.

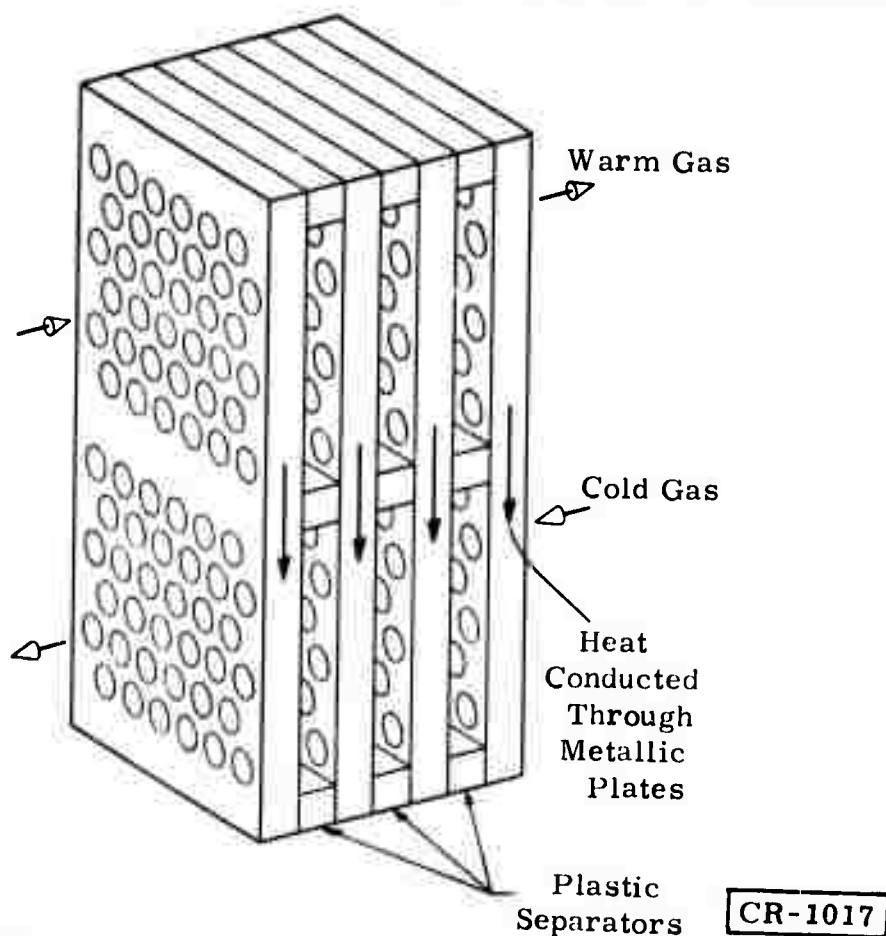


Figure 32. Principle of Perforated-Plate Heat Exchanger

The gaps between plates serve to improve thermal performance by reducing longitudinal heat conduction; for this reason, the separator must be of a low-thermal-conductivity material such as plastic. The separators, when firmly bonded to the plates, not only form a barrier to longitudinal conduction of heat but also serve as gastight seals, from stream to stream and from both streams to the outside. Because very small holes can be produced, the heat-transfer surface area per unit volume can be very large -- a favorable factor in miniaturization. As an example, areas per unit volume of 60 square centimeters per cubic centimeter can be easily attained. This is about five to ten times the surface area density of conventional compact heat exchangers.

The reheadering effect that occurs between each pair of plates tends to produce a highly uniform flow distribution at any cross section. Also, the fact that each hole in a plate is thermally connected to the other holes in the same plate provides additional protection against performance degradation due to flow nonuniformities. Design of headers to eliminate an entrance jet is therefore not as critical as in most types of exchangers.

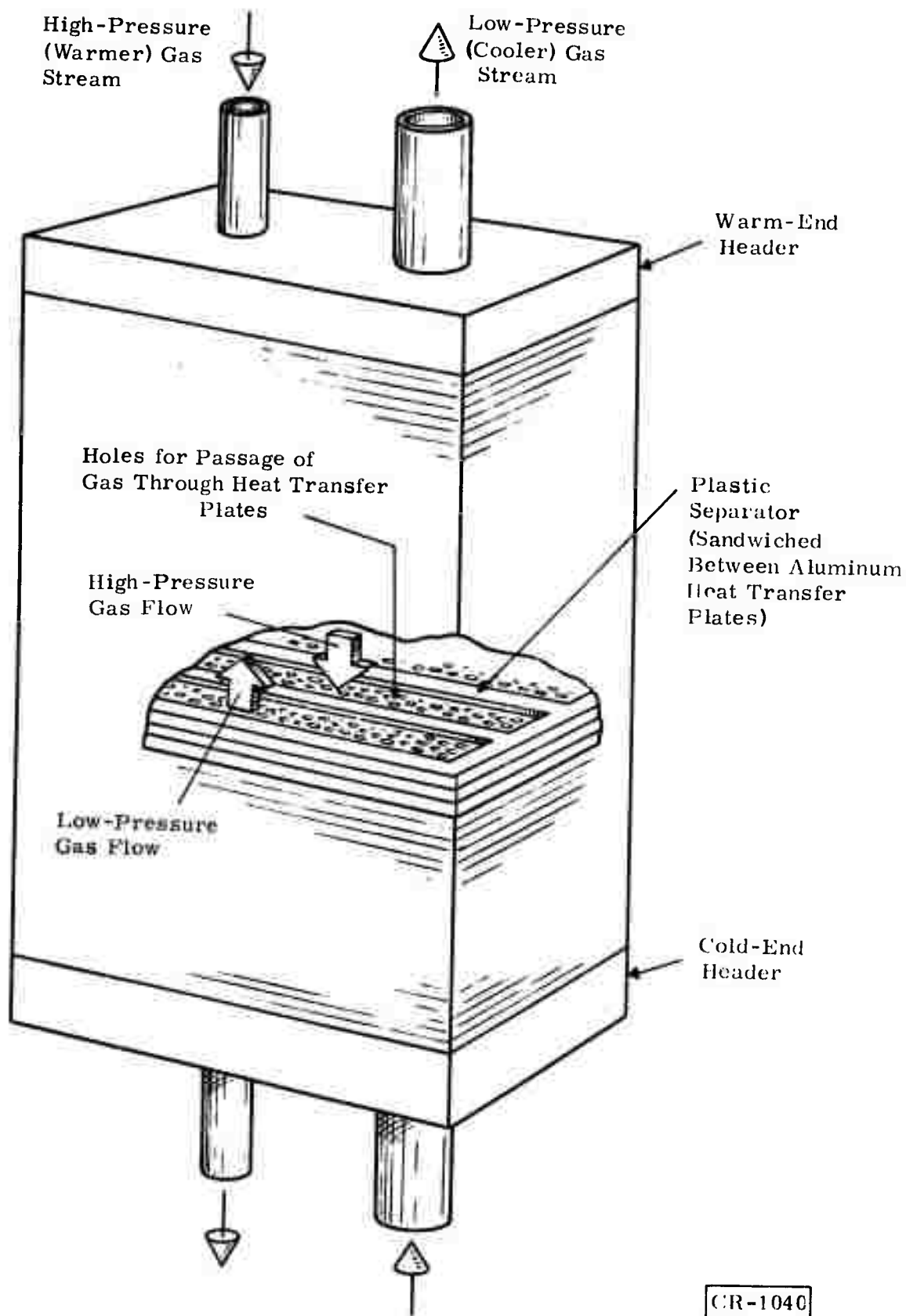
Because each hole in a plate may have a length-to-diameter ratio in the 0.5-to-1.0 range, thermal and hydrodynamic boundary layers are broken up before they have a chance to become fully developed. This results in high heat transfer surface coefficients and, consequently, high friction factors. This effect is enhanced if the holes are misaligned from plate to plate.

A cutaway view of an entire heat exchanger with headers is shown in Figure 33. This figure illustrates the method used to split the hot and cold streams into adjacent channels and shows how the streams flow lengthwise through the exchanger. A photograph of a perforated-plate heat exchanger in a cryogenic test apparatus is shown as Figure 34.

A more detailed description of the perforated-plate heat exchanger can be found in References 2 and 3.

Wire mesh is another type of heat transfer surface that has been used in metal-plastic laminate heat exchangers. Figure 35 shows the heat transfer surface developed by Kinergetics, Inc. With respect to exchanger construction, the wire mesh exchanger is similar to the perforated-plate exchanger described above.

An advantage of the wire mesh design is that larger fractions of open face area can be attained than with the perforated-plate surface, producing a smaller exchanger size and weight in many cases. The cycle design computer program actually calculates the perforated-plate design for the metal-plastic laminate case, but it has been found that if the fraction open face areas corresponding to wire mesh are used as inputs, the resulting heat exchanger weights and sizes are close to those that would be calculated for wire mesh exchangers. All laminate heat exchanger weights and sizes given in this report correspond



CR-1040

Figure 33. Cutaway View of Perforated-Plate Heat Exchanger

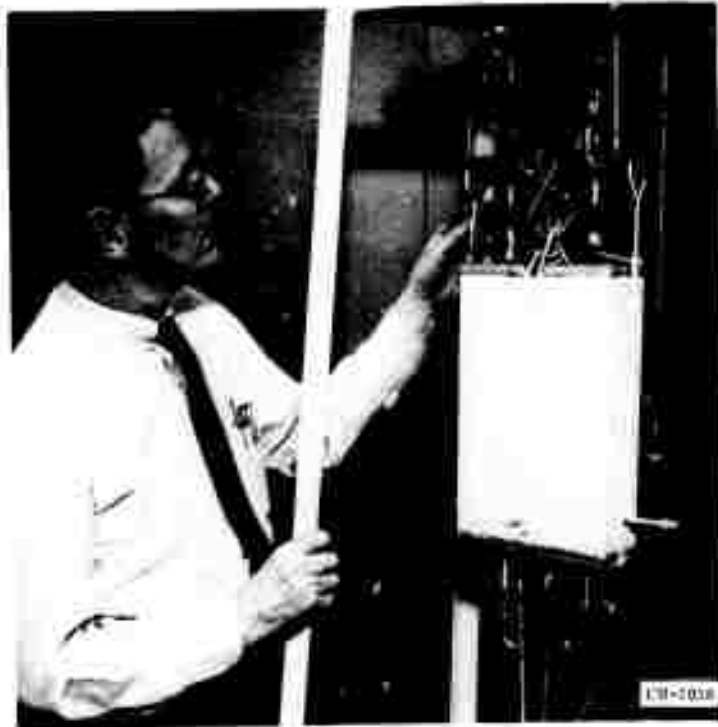


Figure 34. Perforated-Plate Heat Exchanger in Cryogenic Test Apparatus

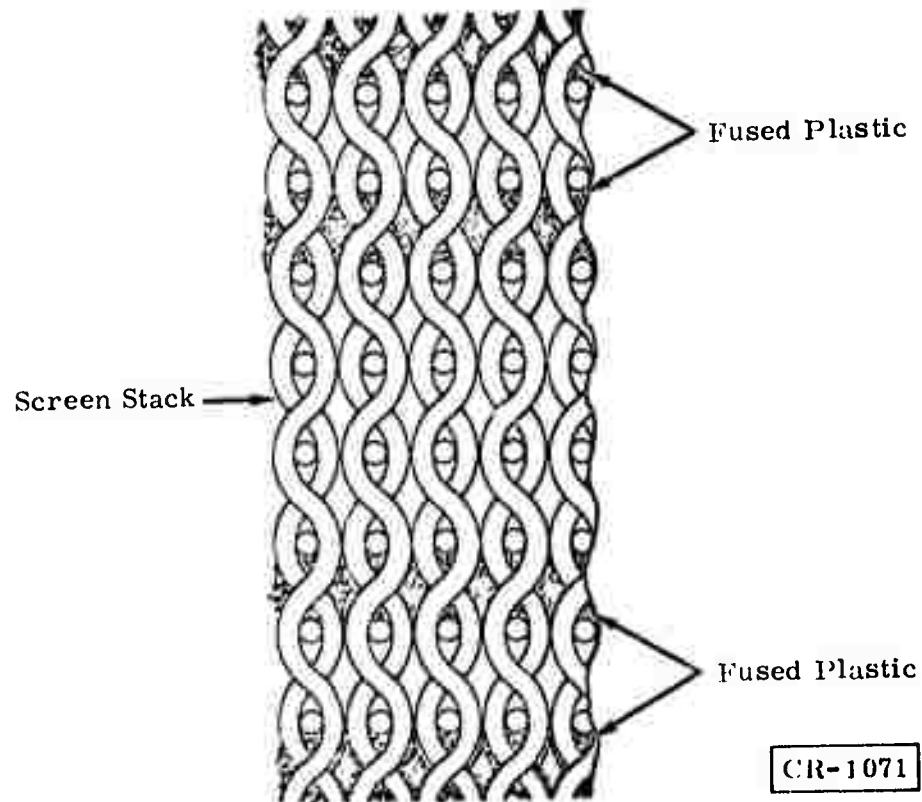


Figure 35. Cross Section of Wire Mesh Heat Exchanger

to the wire mesh exchanger. In the computer output, the word composite is used to designate the metal-plastic laminate (or wire mesh) exchanger.

### **COMPUTER PROGRAM**

In the selection of a cycle design for a cryogenic refrigerator, it is necessary to compare different cycle types, as well as different cycle designs, within one cycle type. The calculations that must be performed for the evaluation of these cycles are long and involved. This is particularly so in a miniature cryogenic refrigerator because:

- The refrigeration cycle itself is a highly coupled system in which the thermal performances of the different components are intimately related.
- Mechanical and thermal losses are a very significant fraction of the gross refrigerative capacity and are thus coupled to the cycle design.
- Some of the refrigeration cycles depend on real gas properties, so it is impossible to use ideal gas properties.

Computer programs have been written that perform calculations for particular cycles and that utilize realistic characterizations for some of the hardware involved (Ref. 4). These programs have been tailored to particular cycle types and are fairly difficult to apply to variations of the cycle.

The approach of having a computer program that itself may select and optimize components has also been taken. This type of computer program considers a decoupled system, so the assembly of a number of optimum components may yield a total system that is not desirable from an overall system point of view. The purpose of the optimization is also not usually well defined.

It is desirable to have available a computer program that can be used simply to try out different designs in a realistic fashion and that will have a short turn-around time so the designer may utilize it efficiently.

Cycle-design programs that will respond in a few seconds have been written for the General Electric time-sharing system. These programs are based upon earlier work funded by the General Electric Company, as well as additions and improvements carried out under U.S. Air Force Contract F33615-71-C-1003. The programs are designed to accommodate reversed Brayton and Claude cycles with up to five turboexpanders, and with liquid withdrawal for electrical lead cooling.

A typical cycle is shown in Figure 36. This figure illustrates a reversed Brayton cycle with a capability of four refrigeration loads at different temperatures. It should be noted that the secondary refrigeration loads have been placed at the turboexpander inlets rather than in the low-pressure stream. This

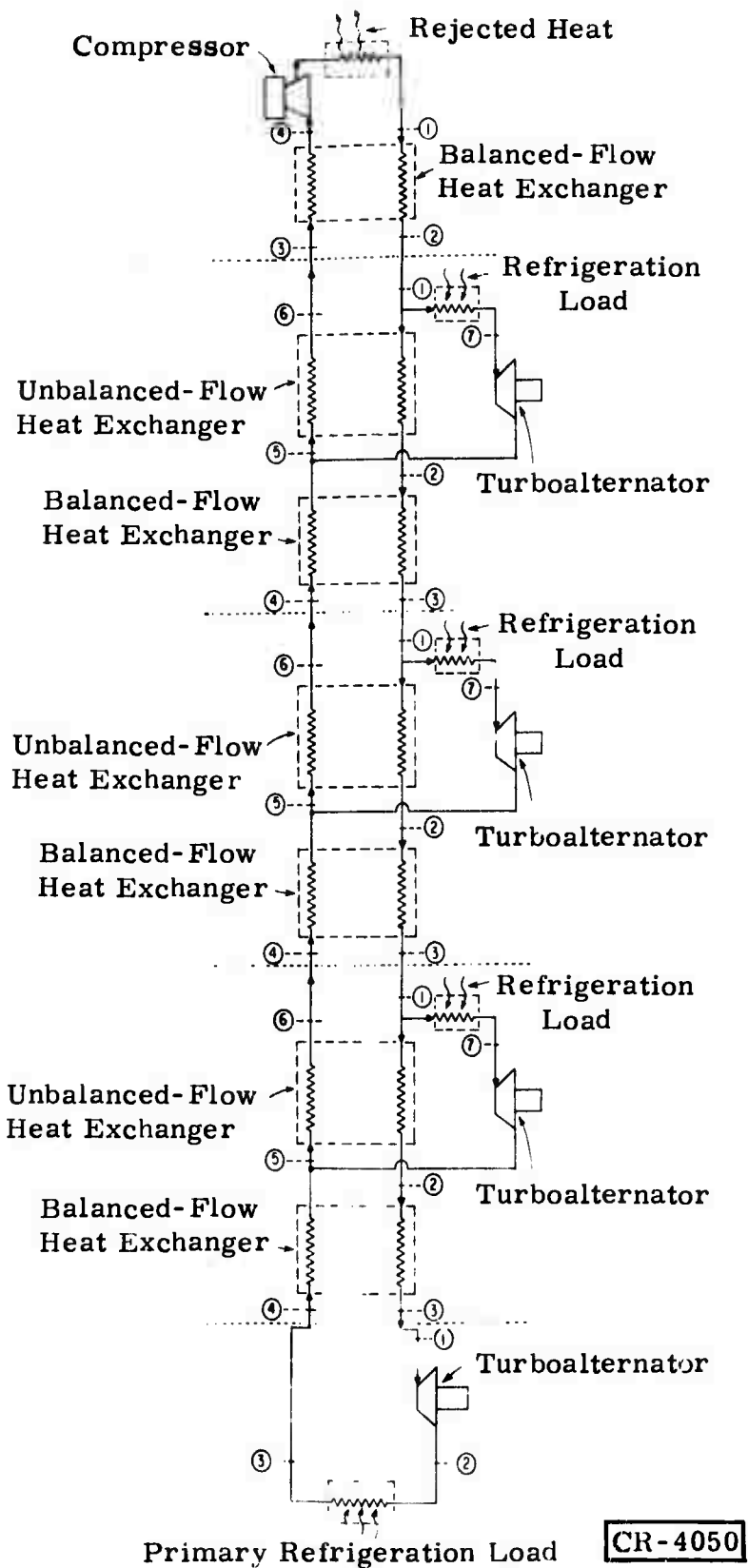


Figure 36. Four-Load Reversed Brayton Cycle

will allow construction of more compact heat exchangers at these loads, because only part of the cycle flow is taken through the refrigeration load, and this flow is at high pressure.

The cycle design computer program will provide designs for perforated-plate heat exchangers in the cryosection; partial-admission, radial-impulse turboexpanders with their corresponding alternators; and centrifugal or regenerative compressors with motors. It will not design such subsystems as the heat rejection system on the structural supports for the cryosection, or calculate the heat leak due to supports and radiation.

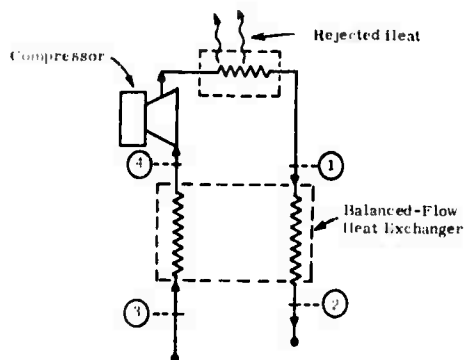
### ELEMENTS AND COMPONENTS

The most important hardware components of a refrigerator are:

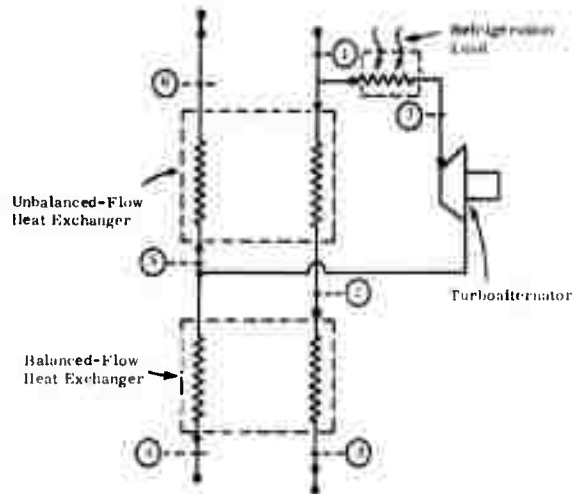
- Compressor system, with its associated hardware (motor, bearings, and aftercoolers).
- Process cryogenic heat exchangers.
- Work-producing expanders.
- Expansion valves.

These components may be arranged into different cycle types, but the different cycle types repeat the arrangement of some of the components. A refrigeration cycle may therefore be characterized by several elements, each of which is composed of more than one component. These elements may then be used as building blocks to construct a complete cycle. The elements that have been used to characterize the cryogenic refrigeration cycles that are desirable for a miniature cryogenic refrigerator are numbered and are shown in Figure 37; the corresponding temperature entropy diagrams are shown in Figure 38. The numbered element types are:

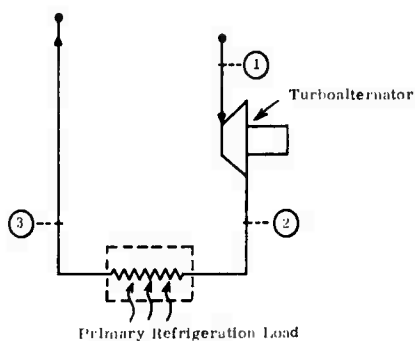
1. Warm-end element, which contains the compressor, its associated coolers, and the warm-end regenerative counterflow heat exchanger.
2. Intermediate section, which includes a balanced-flow and an unbalanced-flow heat exchanger and turboexpander. A secondary refrigeration load has been placed upstream of the turboexpander. (When liquid is withdrawn from the coldest element (Element 6), then all cryogenic heat exchangers are unbalanced-flow exchangers.)
3. Cold end for a reversed Brayton cycle, containing a turboexpander and the primary refrigeration load.
4. Cold end for a Claude cycle, including a Joule-Thomson valve and the primary refrigeration load. Element 4 is used when the refrigerant enters the two-phase region. Element 5 represents the case where a phase change does not take place. These two elements have been considered as different, for convenience in the computer program computation.
- 5.



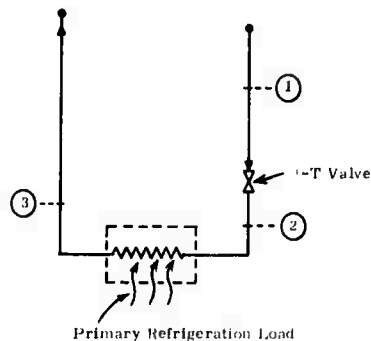
Warm End, Element 1



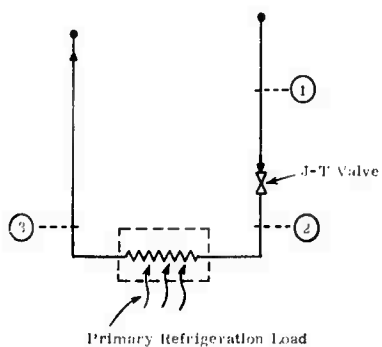
Intermediate-Temperature Cooling Station, Element 2



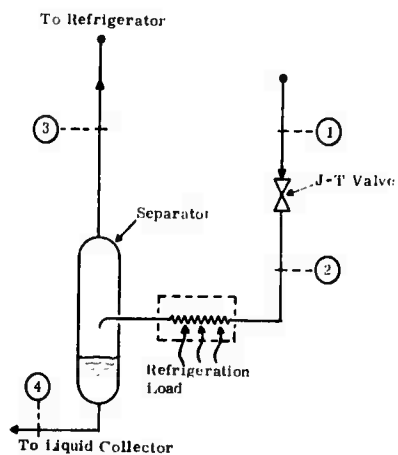
Reversed-Brayton-Cycle Cold End, Element 3



Claude-Cycle Cold End (Liquid), Element 4



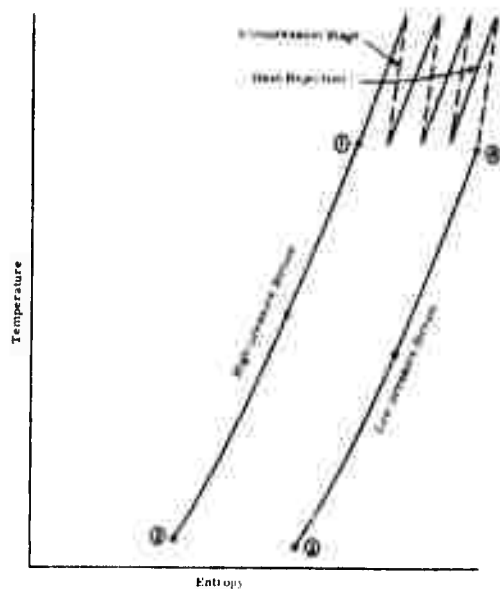
Claude-Cycle Cold End (Gas), Element 5



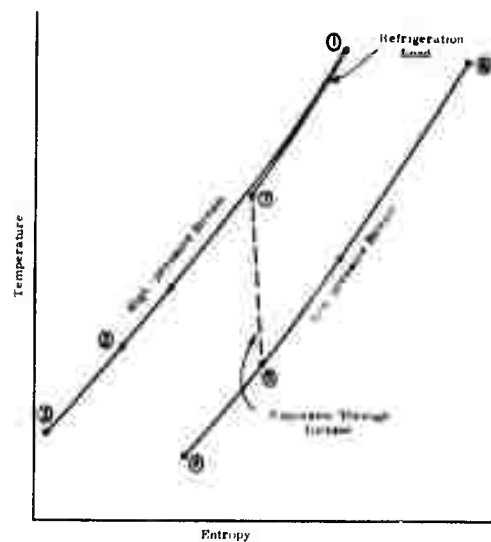
Liquefier Cold End, Element 6

CR-4045

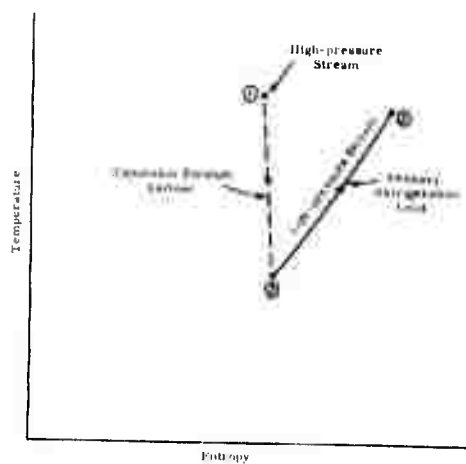
Figure 37. Cryogenic Refrigeration-Cycle Elements



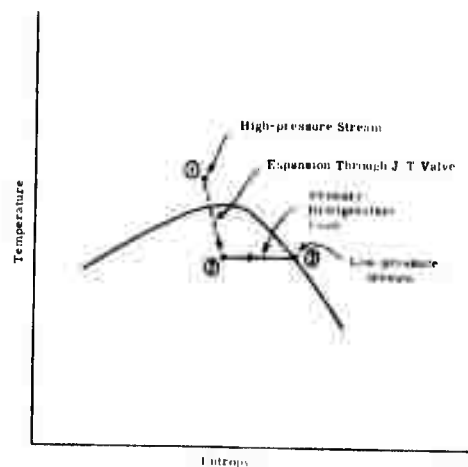
Temperature-Entropy Diagram, Element 1



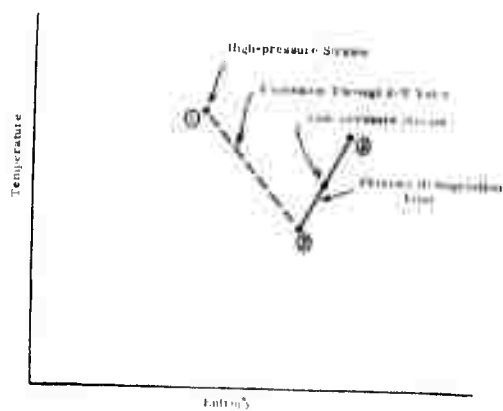
Temperature-Entropy Diagram, Element 2



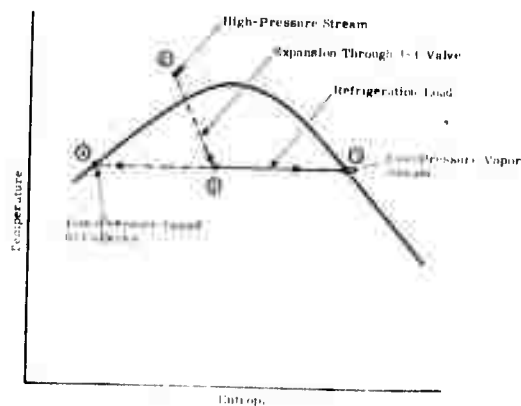
Temperature-Entropy Diagram, Element 3



Temperature-Entropy Diagram, Element 4



Temperature-Entropy Diagram, Element 5



Temperature-Entropy Diagram, Element 6

[6.10.10]

Figure 38. Temperature Entropy Diagrams for Cryogenic Refrigeration-Cycle Elements

6. Cold-end element from which liquid is withdrawn to be used for cooling electrical leads or supports. The resulting vapor is returned to the system at the compressor suction, at the temperature existing at that point.

A cycle type may be constructed from these elements by specifying an element sequence (from the cold end to the warm end). For example, Figure 39 shows the simplest possible reversed Brayton cycle that can be constructed. This cycle is constructed by element sequence 3-1 and has the capability of one refrigeration load that will be at a relatively high temperature.

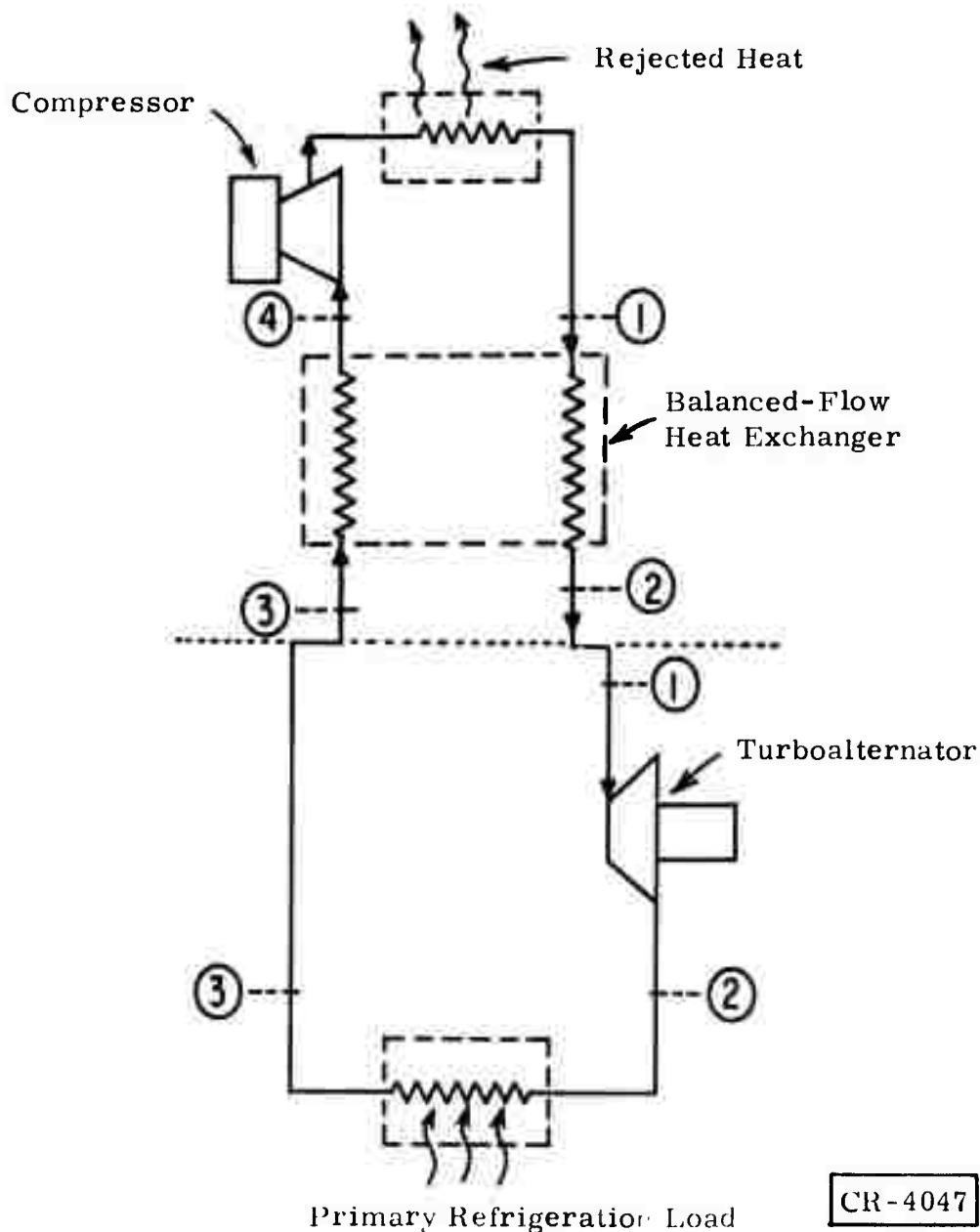


Figure 39. One-Load Reversed Brayton Cycle

This cycle would be suitable for a single  $80^{\circ}\text{K}$  load. For refrigeration at a lower temperature, it is desirable to add one or more turbines. Element sequence 3-2-1 identifies the reversed Brayton cycle in Figure 40. This cycle has the capability of providing refrigeration at two temperature levels.

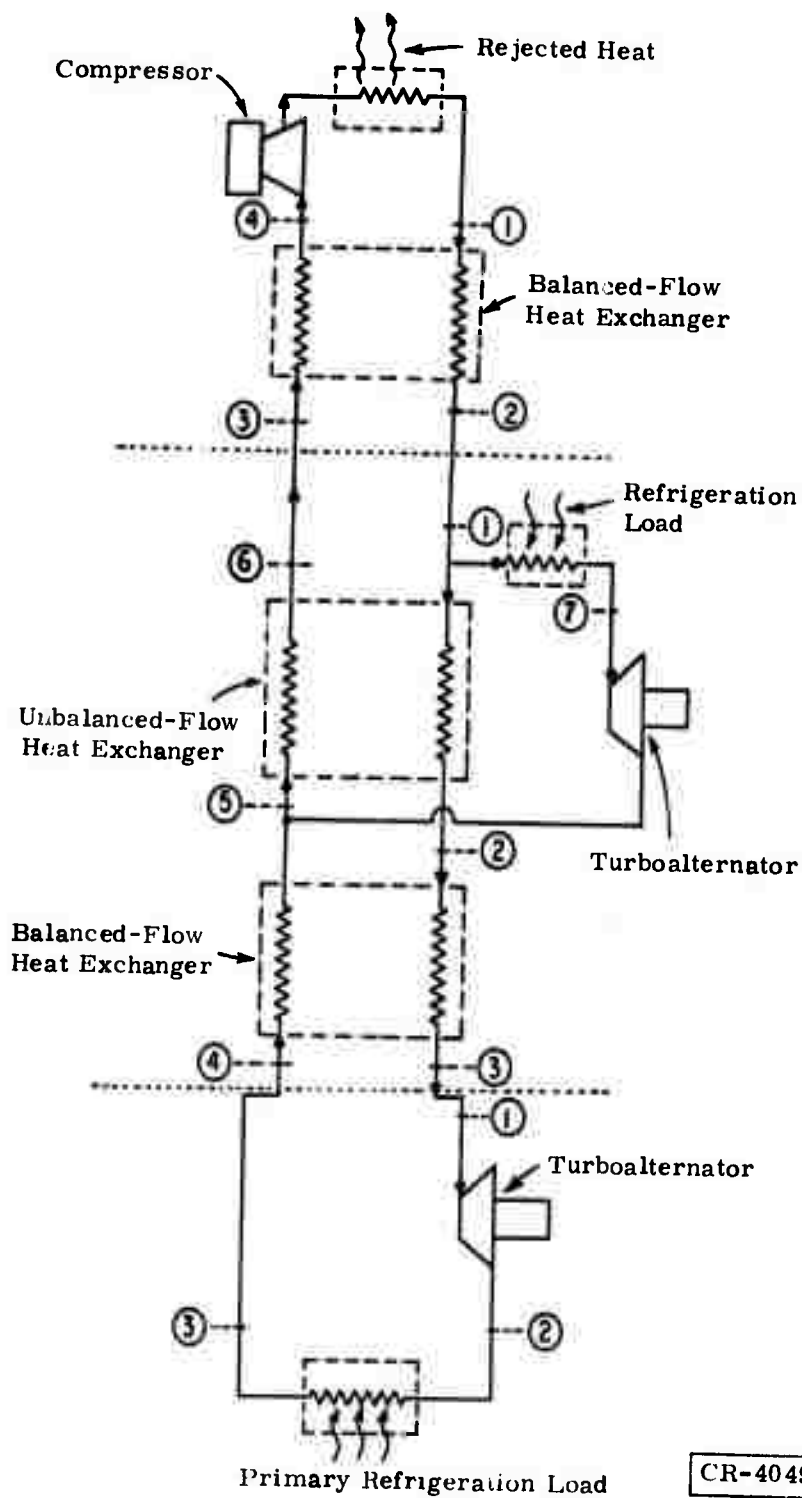


Figure 40. Two-load Reversed Brayton Cycle

A Claude cycle may be constructed in a similar way. Figure 41 represents the cycles with element sequences 4-2-2-1 or 5-2-2-1, depending on whether the primary refrigeration load is in the two-phase region or in the vapor region. Figure 36 represents four-load reversed Brayton cycle 3-2-2-1.

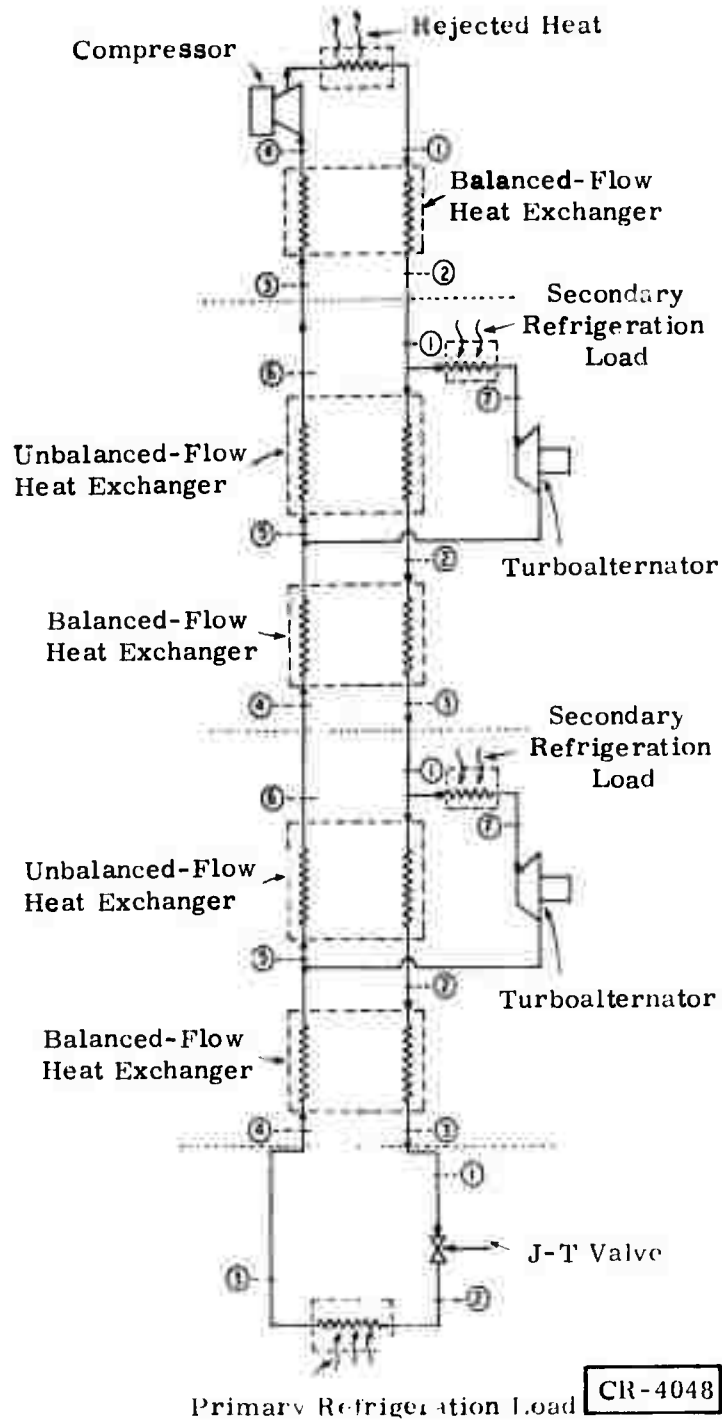


Figure 41. Three-Load Claude Cycle

## CYCLE PROGRAM ORGANIZATION

A short computer program has been written for each of the characteristic elements, so the performance of each element can be calculated when a set of independent operating variables is selected. This set is selected so the elements can be interconnected without a great deal of additional calculations. This is simply done by utilizing the thermodynamic states and mass flows at the coupling points as independent variables. In this way, the program can calculate the cycle performance starting from the coldest element. The input for these programs is entered in a set of files from which the computer will read. The organization of the various programs and input files is shown in Figure 42.

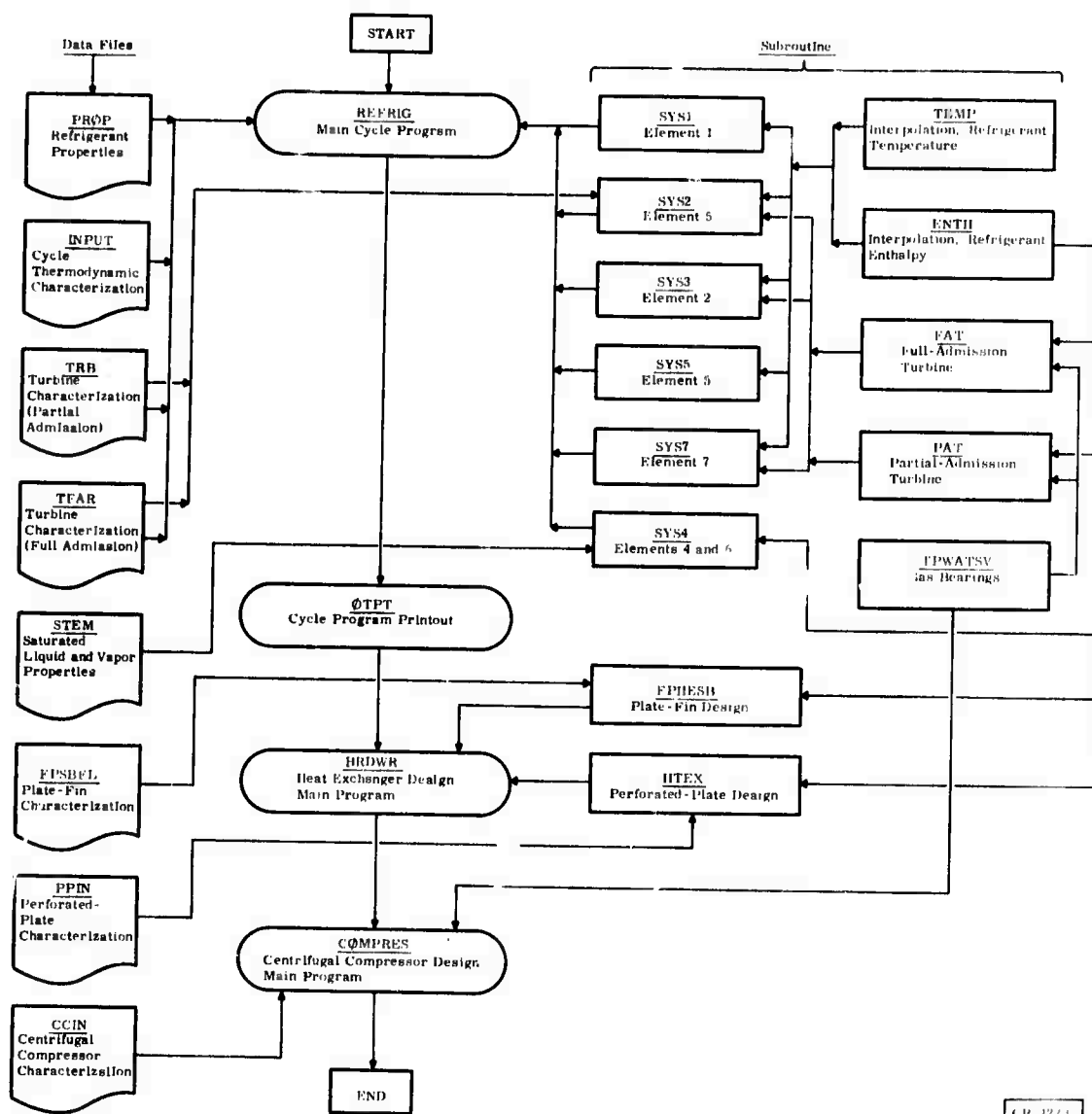


Figure 42. Cycle Design Program Organization

## REFRIGERATOR SYSTEM DESIGN

### DESIGN REQUIREMENTS AND TRADE-OFFS

Design requirements are discussed in detail in Section 3, under "Ship Propulsion System Requirements and Criteria." In general, the refrigeration system must also meet these requirements and at the same time provide refrigeration capacities outlined in Section 3 under "Refrigeration Requirements."

In the design of a cryogenic refrigerator, a number of trade-offs may be considered. As an example, total system weight can be traded off against total refrigerator power input. This trade-off can be accomplished by consideration of heat exchanger effectiveness; as heat exchanger effectiveness increases, the total system weight generally increases, but with the benefit of lower input power. As another example, the distribution of weight between the compressor subsystem and the cryosection can be traded off. As the number of compressor stages is increased, increasing the pressure ratio and the compressor subsystem weight, the cryogenic heat exchanger weight drops, thereby reducing cryosection weight, as a consequence of a lower refrigerant flow rate.

To design toward an optimum system, a set of weighting parameters could be established. However, it is usually very difficult to put numerical values on such parameters; in the absence of quantitative weighting parameters, at least some ordering of importance of the parameters can be established to provide some design guidance.

In the design of the refrigeration system, the following general design guidance was used. It was considered that reliability and refrigerator input power were generally the most important optimization parameters. It was, of course, not possible to calculate a quantitative value for reliability, but generally when there was a choice between a simple system and a more complex system, the simpler system was chosen. For example, a two-turbine system would be chosen over a three-turbine system unless a sizable reduction in input power could be realized. Input refrigerator power is directly calculated by the cycle design computer program and is therefore easily optimized.

Refrigerator weight and size were considered to be next in importance. The cryogenic heat exchanger is the largest and heaviest component in the cryogenic subsystem, and this weight is directly calculated in the cycle design computation. A hand calculation is needed to calculate compressor subsystem weight, but for a given number of compressor stages, the compressor subsystem weight varies by only a small amount, as other system parameters change.

Cost was not considered in the refrigerator optimization because it is difficult to assess without knowing the system quantities and because, for a given system, the cost is relatively insensitive to variations in size, weight, and input power.

For the d-c motor, the size of the cryosection was considered a more important design criterion than for the generators. The reason for this is that the motor is more likely to be cramped for space than are the generators. As a consequence of this criterion, the cryogenic heat exchanger size for the d-c motor refrigerator was greatly reduced by the addition of two more compressor stages, with only a nominal penalty in refrigerator input power. It was assumed that the compressor subsystem for the d-c motor would be remotely located from the motor and thus would not be as limited in space as the cryosection.

The refrigerator loads outlined in Section 3 under "Refrigeration Requirements" are given in Table 3. In the table, temperatures fixed by the design of the generators or motors are noted as "fixed." The remaining temperatures are established by consideration only of the refrigeration system. These temperatures are considered "floating," and while there is no actual useful refrigeration load at these points, the refrigerator itself needs expansion and cooling stations at these points to establish temperature differences between streams in the cryogenic heat exchangers.

Table 3  
REFRIGERATION LOADS USED FOR REFRIGERATOR DESIGNS

Temperature	Basic Heat Load (w)	Heat Load for Transient (w)	Parasitic Heat Load (w)	Total Heat Load (w)	Liquid Helium Withdrawal (g/sec)
<u>A-C Generator</u>					
4.4°K (fixed)	--	--	0.50	0.50	0.245 plus
12°K (floating)	--	--	2.50	2.50	10% for transient
35°K (floating)	--	--	2.50	2.50	= 0.270
120°K (floating)	--	--	10.0	10.0	
<u>D-C Generator</u>					
4.4°K (fixed)	2.5	0.50	--	3.0	0.11
14°K (floating)	--	--	5.0	5.0	
80°K (fixed)	32.0	--	--	32.0	
<u>D-C Motor</u>					
4.4°K (fixed)	4.21	0.84	--	5.05	0.11
14°K (floating)	--	--	5.0	5.0	
80°K (fixed)	106.2	--	--	106.2	

Note: Heat loads and liquid withdrawal rates are for a single, 18-Mw generator or a single, 40,000-hp motor.

The refrigerator "fixed" load temperatures were determined entirely from considerations of electrical equipment design. There was no attempt to iterate the electrical design to select temperatures that were optimum from the refrigerator standpoint. Fortunately, however, the weight and power of the refrigerator is reasonably insensitive to refrigeration temperatures (especially at the higher load temperatures), so this lack of iteration between refrigerator

and electrical equipment design has relatively little effect on refrigerator weight, size, and efficiency.

In Table 3, the floating temperatures given are those temperatures finally optimized for minimum input power. The refrigeration loads shown for the floating temperatures are estimated to be imposed from the refrigerator itself and are therefore considered to be parasitic loads. These parasitic loads include heat from radiation shields and supports that are associated with the refrigerator itself. Generally no parasitic loads were added at the fixed temperature load points. All heat leaks longitudinally within the cryogenic heat exchangers are included in the calculations for heat exchanger thermal effectiveness and therefore are not reflected in the parasitic loads.

Table 3 also includes heat loads calculated to maintain a capacity sufficient to provide for transients within the electrical equipment. Total heat loads shown are those used as inputs to the cycle design computer program.

## A-C GENERATOR

### Refrigeration System for A-C Generator

As was shown in Table 3, the only refrigeration load imposed by the a-c generator is the 0.270-gram-per-second liquid helium withdrawn from the refrigerator. After cooling the superconducting winding, the structural members, and the electrical leads, this helium is returned to the suction of the refrigerator compressor, at near room temperature.

Table 4 is a summary of the significant computer results for the a-c generator, showing the range of parameters studied and giving the effect of variations in some of these parameters. Note that these results are for a single refrigerator cooling a single 18-megawatt generator. Two such generators, each with its own refrigerator, will be required for the application being considered.

Several conclusions can be drawn from the results of Table 4. First, the total compressor input power is relatively insensitive to the temperatures chosen for the refrigeration stations. This can be seen by comparing the first three runs, in which only the Station 2 temperature was varied. The minimum power input was calculated for a station temperature of 13°K, but over the 3°K station temperature range, the variation in input power was only 1.5 percent.

The effect of changes in the warmer station temperature is even less pronounced. Comparing runs 6201, 6204, and 6205, in which only the temperature of the warmer station was changed through a range of 10°K, the input power varied by only 0.4 percent.

Another observation is that the addition of a third turboalternator with its associated cooling station produces a sizable reduction in input power.

Table 4  
COMPUTER RESULTS -- REFRIGERATOR FOR A-C GENERATOR\*

Run	Compressor Stages	Pressure Ratio	Turbines	Liquid-Helium Withdrawal Rate (g/sec)	Refrigeration Capacity (w) / Temperature (°K)				Cryogenic Heat Exchanger Effectiveness	Cryogenic Heat Exchanger Core Weight (lb)	Total Compressor Input Shaft Power (kw)
					Station 1	Station 2	Station 3	Station 4			
6201	6	2.58	2	0.270	0.50/4.4	4.0/13	10/70	--	0.99	618	47.4
6202	6	2.58	2	0.270	0.50/4.4	4.0/12	10/70	--	0.99	632	48.1
6203	6	2.56	2	0.270	0.50/4.4	4.0/14	10/70	--	0.99	--	47.9
6204	6	2.58	2	0.270	0.50/4.4	4.0/13	10/65	--	0.99	600	47.4
6205	6	2.58	2	0.270	0.50/4.4	4.0/13	10/75	--	0.99	--	47.6
6301	6	2.65	3	0.270	0.50/4.4	2.5/12	2.5/50	10/120	0.99	605	36.1
6302	6	2.65	3	0.270	0.50/4.4	2.5/11	2.5/50	10/120	0.99	--	35.4
6303	8	2.85	3	0.270	0.50/4.4	2.5/13	2.5/50	10/120	0.99	--	38.5
6304	6	2.65	3	0.270	0.50/4.4	2.5/12	2.5/45	10/120	0.99	--	35.4
6305	6	2.65	3	0.270	0.50/4.4	2.5/12	2.5/40	10/120	0.99	--	35.0
6306	6	2.65	3	0.270	0.50/4.4	2.5/12	2.5/35	10/120	0.99	541	35.0
6307	6	2.65	3	0.270	0.50/4.4	2.5/12	2.5/30	10/120	0.99	--	35.3
6308	8	2.65	3	0.270	0.50/4.4	2.5/12	2.5/35	10/110	0.99	--	35.0
6309	8	2.85	3	0.270	0.50/4.4	2.5/12	2.5/35	10/130	0.99	--	35.0
6310**	8	2.65	3	0.270	0.50/4.4	2.5/12	2.5/35	10/120	0.99	502	33.7
7301	8	3.80	3	0.270	0.5/4.4	2.5/12	2.5/35	10/120	0.99	352	38.3

\*Results are for a single refrigerator cooling a single 18-Mw generator.  
\*\*Design point.

CR-4231

In all the runs shown, a heat exchanger thermal effectiveness of 99 per cent was used for the major cryogenic heat exchangers. This very high value of effectiveness is extremely difficult to achieve in heat exchangers with balanced flow (that is, with the product of mass flow rate and specific heat the same on both sides of the heat exchanger). However, inasmuch as a sizable amount of liquid helium is withdrawn from the refrigerator and bypasses the cryogenic heat exchangers, there is a significant unbalance in flow between the two helium streams within the heat exchanger system. Because unbalanced-flow exchangers can more easily attain high levels of effectiveness, the 99-per cent design is considered reasonable in this case.

In all cases presented in Table 4, the metal-plastic laminate heat exchanger was considerably lighter and smaller than the plate-fin heat exchanger. For example, for run 6310, the two heat exchanger weights were 502 pounds and 1356 pounds, respectively. All heat exchanger weights shown are for the smaller exchangers.

Run 7301 shows what can be accomplished by the addition of two additional compressor stages and an increased pressure ratio. At the expense of a 14-percent increase in input power, the cryogenic heat exchanger weight is reduced by 30 percent. For the a-c generator, it is believed that the increase in compressor weight, complexity, power, and cost is not justified by the reduction in heat exchanger weight and size.

Run 6310 represents the most favorable overall design. A printout of that computer run is given in Figure 43. This printout is given for record only. The location referred to in the printout progresses from the cold end to the warm end of the cryosection. Under "Turboalternators," the turbine wheel di-

RUN NUMBER 6310

ITERATIONS \* \* \* \* \* 18

ELEMENT SEQUENCE = 6 2 2 2 1

LIQUID FLOW OUT OF REFRIGERATOR= 0.2695E+00 G/SEC

LOCATION	LOAD(W)	TEMP(K)	FLOW(G/SEC)
1	0.5000	4.400	6.257
2	2.500	12.00	7.861
3	2.500	35.00	6.425
4	10.00	120.0	6.294

CYCLE DESIGN POINTS ?YES

L0C.	P(ATM)	TEMP(K)	L0C.	P(ATM)	TEMP(K)
1 1	2.800	5.776	1 2	1.180	4.406
1 3	1.174	4.400			
2 1	2.828	11.95	2 2	2.814	10.37
2 3	2.800	5.776	2 4	1.174	4.400
2 5	1.162	10.31	2 6	1.157	11.07
2 7	2.814	12.00			
3 1	2.856	34.93	3 2	2.842	29.77
3 3	2.828	11.95	3 4	1.157	11.07
3 5	1.145	29.58	3 6	1.139	33.19
3 7	2.842	35.00			
4 1	2.885	119.7	4 2	2.871	103.2
4 3	2.856	34.93	4 4	1.139	33.19
4 5	1.128	102.5	4 6	1.122	115.3
4 7	2.871	120.0			
5 1	2.914	335.0	5 2	2.885	119.7
5 3	1.122	115.3	5 4	1.100	332.8

TURBOALTERNATORS ?YES

-----TURBOALTERNATORS-----				
L0C.	DIA(IN)	PWR(W)	EFFIC.	RPM
2	0.7500	69.00	0.4725	72724.
3	1.250	181.2	0.5086	72615.
4	2.500	572.1	0.4674	63721.

L0C.	ADM.FRACT.	PARA.L0SS(W)	SPEC.SP.D.	SPEC.DIAM.
2	0.3048	4.376	22.66	2.485
3	0.2163	6.324	15.54	3.524
4	0.1453	67.48	9.894	5.237

CR-4234-1

Figure 43. Computer Results for A-C Generator (Run 6310) (Sheet 1 of 3)

LØC.	T.BRG.NØ.	T.LD CØ.	T.MIN F.(IN)	BRG.PWR.(W)
2	0.1279	0.6327E-01	0.5880E-03	0.9320
3	0.2564	0.6587E-01	0.5880E-03	1.777
4	0.6863	0.1261	0.1008E-02	23.85

LØC.	J.BRG.NØ.	J.LD CØ.	J.MIN F.(IN)	BL.HT./CUT.DIA.
2	0.4557	0.8012E-01	0.3006E-03	3.242
3	0.9014	0.8342E-01	0.3006E-03	3.623
4	1.419	0.1596	0.7540E-03	3.123

SKIP HEAT EXCHANGER DESIGN ?NØ

COMPØSITE HEAT EXCHANGERS ?YES

-----HEAT EXCHANGER DESIGN-----				
LØC.	WT(LBS)	LENGTH(CM)	VØL(CU.FT.)	EFFECT
2 B	5.131	17.46	0.7829E-01	0.9901
2 U	1.330	3.929	0.2086E-01	0.9637
3 B	34.98	48.34	0.6442	0.9900
3 U	6.124	8.856	0.1116	0.9649
4 B	133.6	86.35	2.905	0.9900
4 U	15.16	11.55	0.3181	0.9590
5 B	305.7	121.6	7.322	0.9899
TØTALS	502.0		11.40	

FINNED-PLATE HEAT EXCHANGERS ?YES

-----HEAT EXCHANGER DESIGN-----				
LØC.	WT(LBS)	LENGTH(CM)	VØL(CU.FT.)	EFFECT
2 B	FINNED PLATE HYDRAULIC DIA. TØØ BIG			
2 U	FINNED PLATE HYDRAULIC DIA. TØØ BIG			
3 B	95.00	572.2	1.827	0.9900
3 U	14.04	92.03	0.2430	0.9768
4 B	297.0	738.6	7.975	0.9900
4 U	39.56	200.8	1.162	0.9594
5 B	910.7	2494.	43.50	0.9899
TØTALS	1356.		52.70	

CENTRIFUGAL COMPRESSØR?YES

FOR ØUTPUT FOR ALL MØDULES, TYPE ALL  
 FOR ØUTPUT FOR FIRST AND LAST MØDULE ØNLY, TYPE F&L  
 ALL ØR F&L ?ALL

CR-4234-2

Figure 43. Computer Results for A-C Generator (Run 6310) (Sheet 2 of 3)

-----CENTRIFUGAL COMPRESSOR-----

ISENTROPIC COMPR. POWER (KW)	22.09
TOTAL MOTOR SHAFT POWER (KW)	33.74
AMBIENT TEMPERATURE (K)	322.0
PRESSURE RATIO	2.649
MASS FLOW (G/SEC)	26.84
SUPPLY LINE DEL P/P	0.
RETURN LINE DEL P/P	0.

MODULE	SHAFT PWR (KW)	RPM	MOT. SPD. (FPS)
1	11.22	0.5000E+05	667.6
2	11.25	0.5000E+05	667.6
3	11.27	0.5000E+05	667.6

AERODYNAMICS

STAGE	SP. SPEED	AERO. EFF.	TIP SPD (FPS)	DIA. (IN)
1	0.4797E-01	0.6658	1583.	7.255
2	0.4493E-01	0.6473	1583.	7.255
3	0.4223E-01	0.6282	1583.	7.255
4	0.3982E-01	0.6088	1583.	7.255
5	0.3769E-01	0.5895	1583.	7.255
6	0.3573E-01	0.5699	1583.	7.255

STAGE	PRESS. RATIO	COOL. EFFCTV.
1	1.192	0.7405
2	1.185	0.7515
3	1.179	0.7515
4	1.172	0.7515
5	1.166	0.7515
6	1.160	0.7515

BEARINGS

MODULE	T.BRG.NØ.	T.LD.CØ.	T.MIN F.(IN)	BRG. PWR.(W)
1	3.508	0.6089E-01	0.1764E-02	193.2
2	2.522	0.4234E-01	0.1764E-02	209.7
3	1.845	0.3017E-01	0.1764E-02	227.3

MODULE	J.BRG.NØ.	J.LD.CØ.	J.MIN F.(IN)
1	1.644	0.2232	0.1223E-02
2	1.644	0.1552	0.1223E-02
3	1.644	0.1106	0.1223E-02

CR-4234-3

Figure 43. Computer Results for A-C Generator (Run 6310) (Sheet 3 of 3)

ameters can be seen to range from 0.75 inch for the coldest turbine (12°K inlet temperature) to 2.5 inch for the warmest turbine (120°K inlet temperature). Turbine speeds range from 73,000 rpm to 64,000 rpm, and turboalternator efficiencies are in the range of 47 to 51 percent.

The composite heat exchanger is the metal-plastic laminate heat exchanger.

The centrifugal compressor consists of three modules, each with a motor and two centrifugal impellers. Each of the six compression stages is followed by a cooler. Impeller diameters are 7.3 inches, and shaft speeds are 50,000 rpm.

#### Turboalternators for A-C Generators

All three of the turboalternator designs for the a-c generator refrigerator were examined to find satisfactory operating speeds and geometries to satisfy cycle requirements. Cycle Study Computer Run 6310 established the turboalternator requirements listed in Table 5. Also shown are principal turboalternator design results from the cycle run. The three power outputs and overall efficiencies must be achieved for the conditions of the cycle. These turboalternators, of course, were not optimized in the cycle study; hence the wheel tip diameter, admission, and speed are shown only for reference purposes.

Table 5  
TURBOALTERNATOR REQUIREMENTS

Inputs and Results	Inlet Temperature		
	12.0°K	35.0°K	120.0°K
<u>Inputs</u>			
Inlet pressure (atm)	2.814	2.842	2.871
Outlet pressure (atm)	1.162	1.145	1.128
Mass flow (g/sec)	7.861	6.425	6.294
<u>Results</u>			
Refrigerator power output (w)	69.0	181.2	572.1
Overall refrigerator efficiency (fraction)	0.4725	0.5086	0.4674
Wheel tip diameter (in.)	0.75	1.25	2.50
Admission arc (fraction)	0.3048	0.2163	0.1453
Speed (rpm)	72,724	72,615	63,721

Complete partial admission impulse turboalternator preliminary design studies were conducted for all three of the stages for the required cycle conditions. The best operating geometries were established.

Results are shown in Table 6, where the pertinent input, output, performance, and geometry features are listed. It can be seen that the overall efficiencies achieved in the detailed designs all exceed the overall efficiencies required in the cycle. This situation is the result of detailed design improvements made with the turboalternator design program.

Table 6

**TURBOALTERNATOR DESIGN SUMMARY**  
**FOR A-C GENERATOR REFRIGERATOR**  
 Turbine type: partial admission, radial impulse  
 Load alternator type: permanent magnet  
 Journal-bearing type: self-acting tilting pads  
 Thrust-bearing type: inward pumping, spiral groove

Design Parameters	Model and Inlet Temperature		
	Big Bertha (12°K)	Big Bertha (35°K)	Grizzly Giant (120°K)
Total refrigeration power outputs (w)	75.57	191.4	681.5
Design speed (rpm)	72,960	72,820	64,640
Maximum speed (rpm)	200,000	200,000	200,000
<u>Principal Dimensions</u>			
Journal bearing span (in.)	3.82	3.82	7.64
Journal and magnet diameter (in.)	0.50	0.50	1.00
Thrust bearing outside diameter (in.)	0.84	0.84	1.68
Magnet length (in.)	0.705	0.705	1.410
<u>Performance Factors</u>			
Inlet temperature (°R)	21.6	63.0	216.0
Inlet temperature (°K)	12.0	35.0	120.0
Inlet pressure (psia)	41.35	41.77	42.19
Outlet pressure (psia)	17.08	16.83	16.58
Pressure ratio	2.422	2.482	2.545
Mass flow (lb/hr)	67.14	53.44	57.92
Turbine run number	830801006	630602001	630603005
Wheel diameter (in.)	0.750	1.250	2.500
Electromagnetic efficiency (fraction)	0.998	0.985	0.952
Number of blades	37	59	77
Cycle required overall efficiency (fraction)	0.4725	0.5086	0.4674
Overall efficiency (fraction)	0.4809	0.5127	0.4804
Specific Speed	23.57	15.95	10.79
Total friction losses (w)	4.89	9.03	93.66
<u>Design Geometry</u>			
Admission (fraction)	0.3165	0.2216	0.1567
Cutter diameter (in.)	0.0278	0.0243	0.0470
Blade height (in.)	0.0935	0.1085	0.1534
Blade-height-to-diameter ratio	.36	.4707	.3261
Blade angle (deg)	60.0	60.0	60.0
Nozzle angle (deg)	80.0	80.0	80.0

CR-2314

The complete computer design results are shown in Figures 44 through 46. The following paragraphs explain the computer output and define the terms used in these figures.

Below the title, the design case number is used to key the run to the cycle program and to identify the particular turbine design run with a code system. Then the gas selected in the turbine design run is printed.

- Overall Performance. The refrigeration power output for a single-stage turbine is equal to the electrical power output. Electrical power output is the net total refrigeration power output after all the losses have been absorbed, but losses through the three-phase alternator load lines to ambient are not included. The shaft speed is as shown, but the optimum speed is probably about 10 percent lower than shown, because the speed selected was based on the hydraulic efficiency. Then the parasitic losses are added. Hence the net result is that the optimum turboalternator speed should be slightly lower than the design speed shown. The overall efficiency shown is based on the net electrical power or refrigeration power output; hence all turboalternator losses are included.

- Temperatures, Pressures, and Flow. The inlet overall and outlet temperatures are exactly what the refrigeration cycle experiences.

Inlet, nozzle, and outlet pressures are shown next. The inlet pressure is the total pressure into the nozzle. The outlet pressure is the static pressure at the exducer discharge. The pressure ratio is the ratio of the inlet total pressure to the nozzle to the outlet static pressure at the exducer.

Next the mass flow rate in three sets of units is shown.

- Primary Dimensions. The principal aerodynamic derived dimensions around the turbine are shown. The wheel tip diameter is shown, and the blade axial length at the impeller tip diameter is shown. The number of blades listed is an input and is limited for manufacturing considerations.
- Thrust Bearing. The load on the thrust bearing is based on vertical operation and the number of g's of acceleration to be experienced. The thrust bearing outside diameter is next shown as the diameter ratio of the thrust bearing inside diameter to the outside diameter of the thrust runner. The clearance-to-diameter ratio is the actual clearance on the loaded side of the thrust bearing to the thrust runner tip diameter and is an input value. The load coefficient is a dimensionless parameter. The clearance on the loaded side of the thrust bearing is listed, which is a consequence of the thrust bearing diameter and clearance-to-diameter ratio specified. The friction power shown is the friction power for only the loaded side of the thrust bearing.

TURBOALTERNATOR PARTIAL ADMISSION RADIAL IMPULSE  
DESIGN POINT COMPUTER OUTPUT

DESIGN CASE	630601006	
GAS IS HELIUM		
REFRIGERATION PWR OUT (WATTS)	0.7557E+02	PTHL
ELECTRICAL POWER OUTPUT (WATTS)	0.7557E+02	PTA
SPEED (RPM)	0.7296E+05	N
OVERALL EFFICIENCY (FRACTION)	0.4809E+00	ETATA
TEMPERATURES, PRESSURES, FLOW		
INLET TEMPERATURE (R)	0.2160E+02	TO
INLET TEMPERATURE (K)	0.1200E+02	TA
OVERALL TEMPERATURE DROP (R)	0.3089E+01	TEDR
OVERALL TEMPERATURE DROP (K)	0.1716E+01	TEDK
OUTLET TEMPERATURE EXIT (R)	0.1851E+02	T4R
OUTLET TEMPERATURE EXIT (K)	0.1023E+02	T4K
INLET PRESSURE (PSIA)	0.4135E+02	PO
INLET PRESSURE (ATM)	0.2814E+01	PA
OUTLET PRESSURE (PSIA)	0.1708E+02	P3
OUTLET PRESSURE (ATM)	0.1162E+01	PR
PRESSURE RATIO	0.2422E+01	PR
FLOW (LB/SEC)	0.1865E-01	W
FLOW (LB/HR)	0.6714E+02	WR
FLOW (G/SEC)	0.8467E+01	WA
PRIMARY DIMENSIONS		
WHEEL TIP DIAMETER (IN)	0.7500E+00	D
NUMBER OF BLADES	0.3700E+02	Z
BLADE HEIGHT (IN)	0.9353E-01	BH
BLADE HT. CUT. DIA. RATIO	0.3360E+01	BHCD
THRUST BEARING		
LOAD(LBS.),	0.3449E+00	RTL
OUTSIDE DIAMETER(IN),	0.8400E+00	DT
DIAMETER RATIO	0.6548E+00	DR
CLEAR. TO DIA. RATIO	0.7000E-03	RDCR
LOAD COEFFICIENT	0.6380E-01	RTC
BEARING NUMBER	0.1284E+00	RTN
CLEARANCE, LOADSIDE(IN)	0.5880E-03	RLC
FRICTION POWER(WATTS)	0.1089E+00	BTPL
JOURNAL BEARING		
LOAD(LBS.)	0.1725E+00	RJL
LOAD COEFFICIENT	0.8080E-01	RJC
BEARING NUMBER	0.4577E+00	RCN
CLEAR. TO DIA. RATIO	0.7316E-03	RDCR
MACHINED CLEARANCE (IN)	0.3653E-03	RMC
PIV. FILM THICK(IN)	0.3006E-03	RJMF
FRICTION POWER(WATTS)	0.2201E+00	RJPL

CR-2315-1

Figure 44. Turboalternator Partial-Admission Radial Impulse Design Point Computer Output (Design Case 630601006) (Sheet 1 of 3)

DESIGN CASE		630601006
TWO STAGE PERFORMANCE		
OTHER STAGE IN TEMP (K)	0.	TOA
TOTAL HEAT LEAK (WATTS)	0.	PHL
EXIT TEMPERATURE (K)	0.1028E+02	T4KH
SHAFT HEAT LEAK (WATTS)	0.	PHLS
HOUSG HEAT LEAK (WATTS)	0.	PHLH
GAS BEARINGS		
ROTATING ASSEMBLY WEIGHT (LBS)	0.3449E+00	RAW
ACCELERATION OF GRAVITY ("G")	0.1000E+01	ACG
TOT. BEARING FRICTION (WATTS)	0.9394E+00	PLB
PERFORMANCE TERMS		
ISENTROPIC HEAD (FT)	0.6210E+04	HS
HYDRAULIC EFF., FIRST TERM	0.6893E+00	ETAH1
HYDRAULIC EFF., SECOND TERM	0.1246E+00	ETAH2
HYDRAULIC EFF., THIRD TERM	0.5416E-04	ETAH3
TIP CLEARANCE EFF. CORRECTION	0.9769E+00	LC
TRAIL EDGE EFF. CORRECTION	0.9223E+00	LE
BLADE RE. NO. EFF. CORR.	0.1006E+01	LR
ALTERNATOR GAP FLUX (KGAUSS)	0.6158E+01	AR
ALTERNATOR CORE LOSS COEFF.	0.2659E+01	KA
ALTERNATOR COPPER LOSS COEFF.	0.8805E+02	KB
TEMPERATURE WHEEL EXIT GAS (R)	0.1831E+02	T3
TURBINE BLADE DISC VOL. FLOW (CFS)	0.5354E-01	Q3
PERFORMANCE FACTORS		
TIP SPEED TO SPOUTING VEL. RATIO	0.3779E+00	SVR
NOZZLE COEFFICIENT	0.9000E+00	PSIN
SPECIFIC SPEED	0.2357E+02	NS
SPECIFIC DIAMETER	0.2398E+01	DS
FLOW FACTOR	0.3705E+01	ASTP
WHEEL EFFICIENCY (FRACTION)	0.5119E+00	ETAW
HYDRAULIC EFFICIENCY (FRACTION)	0.5846E+00	ETAH
ELECTROMAGNET EFF. (FRACTION)	0.9985E+00	ETEM
ISENTROPIC POWER (WATTS)	0.1572E+03	PTAS
WHEEL POWER OUTPUT (WATTS)	0.8045E+02	PTBW
SHAFT POWER OUTPUT (WATTS)	0.7568E+02	PTR
PARASITIC LOSSES (WATTS)		
ALTERNATOR TOTAL FM	0.1137E+00	PLEL
TURBINE DISC FRICTION	0.4920E+00	PLDF
JOURNAL DIA SHAFT FRICTION	0.3154E+01	PLSF
ALTERNATOR GAP FRICTION	0.1870E+00	PLGF
BEARING FRICTION	0.9394E+00	PLB
SUM ALL PARASITIC LOSSES	0.4886E+01	PLTP



CR-2315-2

Figure 44. Turboalternator Partial-Admission Radial Impulse Design Point  
Computer Output (Design Case 630601006) (Sheet 2 of 3)

## GEOMETRY

WHEEL TIP CLEARANCE (IN)	0.2000E-02	S
BLADE PASSAGE CUTTER DIAMETER (IN)	0.2784E-01	R
BLADE TRAILING EDGE THICKNESS (IN)	0.4000E-02	E
ADMISSION ARC (FRACTION)	0.3165E+00	ARC
ADMISSION ARC (DEGREES)	0.1140E+03	ARCD
NOZZLE ANGLE (DEGREES)	0.8000E+02	ALP2
BLADE ANGLE (DEGREES)	0.6000E+02	BP2
BLADE INCIDENCE ANGLE (DEG)	0.1291E+02	I
BLADE CHORD (IN)	0.9616E-01	C
WHEEL INSIDE DIAMETER (IN)	0.5577E+00	D3
BLADE PRESSURE SURFACE RADIUS (IN)	0.5552E-01	Y
BLADE SUCTION SURFACE RADIUS (IN)	0.2768E-01	X

TOTAL MACHINE SHAFT LENGTH (IN)	0.5050E+01	SL
JOURNAL SHAFT DIAMETER (IN)	0.5000E+00	DJ
JOURNAL FREE SHAFT LENGTH (IN)	0.3249E+01	DSH
ALTERNATOR DIAMETER (IN)	0.5000E+00	DG
ALTERNATOR MAGNET LENGTH (IN)	0.6286E+00	DM
ALTERNATOR PERIF. SPEED(F.P.S.)	0.1593E+03	APS
ALTERNATOR RADIAL GAP (IN)	0.2875E-01	G
STATOR OVERHANG (IN)	0.8625E-01	DA
STATOR LAMINATION DIA. (IN)	0.1845E+01	DL
EMPIR. ALTERNATOR DIA.(IN)	0.3364E+00	DGE
WHEEL BACK SIDE OPTIMUM GAP (IN)	0.1469E-01	GD

## VELOCITIES

SPOUTING VELOCITY (FPS)	0.6324E+03	CO
WHEEL TIP SPEED(FPS)	0.2390E+03	U
NOZZLE DISCHARGE VELOCITY (FPS)	0.5691E+03	C2
BLADE INLET RELATIVE VELOCITY(FPS)	0.1034E+03	W2
BLADE INLET RADIAL VELOCITY (FPS)	0.9883E+02	V2
BLADE INLET RELATIVE MACH NUMBER	0.1776E+00	MW2

## REYNOLDS NUMBERS

BLADE PASSAGE REYNOLDS NO.	0.8474E+05	NREP
TURBINE DISC REYNOLDS NO.	0.1674E+07	NRED
JOURNAL DIAMETER REYNOLDS NO.	0.7441E+06	NREJ
ALTERNATOR GAP REYNOLDS NO.	0.3501E+06	NREG

## DRAG COEFFICIENTS

TURBINE DISC DRAG COEFF.	0.5040E-02	CMD
JOURNAL DIAMETER DRAG COEFF.	0.3027E-02	CDS
ALTERNATOR GAP MOMENT COEFF.	0.9219E-03	CDG

CR-2315-3

Figure 44. Turboalternator Partial-Admission Radial Impulse Design Point  
Computer Output (Design Case 630601006) (Sheet 3 of 3)

Reproduced from  
best available copy.



TURBOALTERNATOR PARTIAL ADMISSION RADIAL IMPULSE  
DESIGN POINT COMPUTER OUTPUT

DESIGN CASE	630602001	
GAS IS HELIUM		
REFRIGERATION PWR OUT (WATTS)	0.1914E+03	PTHL
ELECTRICAL POWER OUTPUT (WATTS)	0.1914E+03	PTA
SPEED (RPM)	0.7282E+05	N
OVERALL EFFICIENCY (FRACTION)	0.5127E+00	ETATA
TEMPERATURES, PRESSURES, FLOW		
INLET TEMPERATURE (R)	0.6300E+02	TO
INLET TEMPERATURE (K)	0.3500E+02	TA
OVERALL TEMPERATURE DROP (R)	0.9827E+01	TEDR
OVERALL TEMPERATURE DROP (K)	0.5459E+01	TEDK
OUTLET TEMPERATURE EXIT (R)	0.5317E+02	T4R
OUTLET TEMPERATURE EXIT (K)	0.2954E+02	T4K
INLET PRESSURE (PSIA)	0.4177E+02	PO
INLET PRESSURE (ATM)	0.2842E+01	PA
OUTLET PRESSURE (PSIA)	0.1683E+02	P3
OUTLET PRESSURE (ATM)	0.1145E+01	PR
PRESSURE RATIO	0.2482E+01	PR
FLOW (LB/SEC)	0.1484E-01	W
FLOW (LB/HR)	0.5344E+02	WR
FLOW (G/SEC)	0.6739E+01	WA
PRIMARY DIMENSIONS		
WHEEL TIP DIAMETER (IN)	0.1250E+01	D
NUMBER OF BLADES	0.5900E+02	Z
BLADE HEIGHT (IN)	0.1085E+00	BH
BLADE HT. CUT. DIA. RATIO	0.3707E+01	BHCD
THRUST BEARING		
LOAD(LBS.),	0.3528E+00	RTL
OUTSIDE DIAMETER(IN),	0.3400E+00	DT
DIAMETER RATIO	0.6548E+00	DR
CLEAR. TO DIA. RATIO	0.7000E-03	BDGR
LOAD COEFFICIENT	0.6622E-01	BTC
BEARING NUMBER	0.2574E+00	RTN
CLEARANCE, LOADSIDE(IN)	0.5880E-03	BLC
FRICTION POWER(WATTS)	0.2147E+00	RTPL
JOURNAL BEARING		
LOAD(LBS.)	0.1764E+00	RJL
LOAD COEFFICIENT	0.8386E-01	RJC
BEARING NUMBER	0.9041E+00	RCN
CLEAR. TO DIA. RATIO	0.7402E-03	RCGR
MACHINED CLEARANCE (IN)	0.3701E-03	BMC
PIV. FILM THICK(IN)	0.3006E-03	RJMF
FRICTION POWER(WATTS)	0.7180E+00	RJPL

CR-2316-1

**Figure 45. Turboalternator Partial-Admission Radial Impulse Design Point Computer Output (Design Case 630602001) (Sheet 1 of 3)**

DESIGN CASE		630602001
TWO STAGE PERFORMANCE		
OTHER STAGE IN TEMP (K)	0.	TOA
TOTAL HEAT LEAK (WATTS)	0.	PHL
EXIT TEMPERATURE (K)	0.2954E+02	T4KH
SHAFT HEAT LEAK (WATTS)	0.	PHLS
HOUSG HEAT LEAK (WATTS)	0.	PHLH
GAS BEARINGS		
ROTATING ASSEMBLY WEIGHT (LBS)	0.3528E+00	RAW
ACCELERATION OF GRAVITY ("G")	0.1000E+01	ACG
TOT. BEARING FRICTION (WATTS)	0.1789E+01	PLB
PERFORMANCE TERMS		
ISENTROPIC HEAD (FT)	0.1853E+05	HS
HYDRAULIC EFF., FIRST TERM	0.6846E+00	ETAH1
HYDRAULIC EFF., SECOND TERM	0.1047E+00	ETAH2
HYDRAULIC EFF., THIRD TERM	0.6602E-04	ETAH3
TIP CLEARANCE EFF. CORRECTION	0.9854E+00	LC
TRAIL EDGE EFF. CORRECTION	0.9408E+00	LE
BLADE RE. NO. EFF. CORR.	0.9987E+00	LR
ALTERNATOR GAP FLUX (KGAUSS)	0.1541E+02	AG
ALTERNATOR CORE LOSS COEFF.	0.1945E+01	KA
ALTERNATOR COPPER LOSS COEFF.	0.2040E+02	KB
TEMPERATURE WHEEL EXIT GAS (R)	0.5272E+02	T3
TURBINE BLADE DISC VOL. FLOW (CFS)	0.1245E+00	Q3
PERFORMANCE FACTORS		
TIP SPEED TO SPOUTING VEL. RATIO	0.3639E+00	SVR
NOZZLE COEFFICIENT	0.9000E+00	PSIN
SPECIFIC SPEED	0.1595E+02	NS
SPECIFIC DIAMETER	0.3444E+01	DS
FLOW FACTOR	0.4986E+01	WSTP
WHEEL EFFICIENCY (FRACTION)	0.5369E+00	ETAH
HYDRAULIC EFFICIENCY (FRACTION)	0.5798E+00	ETAH
ELECTROMAGNET EFF. (FRACTION)	0.9850E+00	ETEM
ISENTROPIC POWER (WATTS)	0.3732E+03	PTAS
WHEEL POWER OUTPUT (WATTS)	0.2004E+03	PTRM
SHAFT POWER OUTPUT (WATTS)	0.1943E+03	PTP
PARASITIC LOSSES (WATTS)		
ALTERNATOR TOTAL EM	0.2959E+01	PLEL
TURBINE DISC FRICTION	0.2532E+01	PLDF
JOURNAL DIAM SHAFT FRICTION	0.1629E+01	PLSF
ALTERNATOR GAP FRICTION	0.1199E+00	PLGF
BEARING FRICTION	0.1789E+01	PLB
SUM ALL PARASITIC LOSSES	0.9029E+01	PLTP

CR-2316-2

Figure 45. Turboalternator Partial-Admission Radial Impulse Design Point  
Computer Output (Design Case 630602001) (Sheet 2 of 3)

## DESIGN CASE

630602001

## GEOMETRY

WHEEL TIP CLEARANCE (IN)	0.2000E-02	S
BLADE PASSAGE CUTTER DIAMETER (IN)	0.2928E-01	B
BLADE TRAILING EDGE THICKNESS (IN)	0.4000E-02	E
ADMISSION ARC (FRACTION)	0.2216E+00	ARC
ADMISSION ARC (DEGREES)	0.7978E+02	ARCD
NOZZLE ANGLE (DEGREES)	0.8000E+02	ALP2
BLADE ANGLE (DEGREES)	0.6000E+02	BP2
BLADE INCIDENCE ANGLE (DEG)	0.1335E+02	I
BLADE CHORD (IN)	0.1055E+00	C
WHEEL INSIDE DIAMETER (IN)	0.1039E+01	D3
BLADE PRESSURE SURFACE RADIUS (IN)	0.6094E-01	Y
BLADE SUCTION SURFACE RADIUS (IN)	0.3166E-01	X

TOTAL MACHINE SHAFT LENGTH (IN)	0.5050E+01	SL
JOURNAL SHAFT DIAMETER (IN)	0.5000E+00	DJ
JOURNAL FREE SHAFT LENGTH (IN)	0.3178E+01	DSH
ALTERNATOR DIAMETER (IN)	0.5000E+00	DG
ALTERNATOR MAGNET LENGTH (IN)	0.6992E+00	DM
ALTERNATOR PERIF. SPEED(F.P.S.)	0.1590E+03	APS
ALTERNATOR RADIAL GAP (IN)	0.2875E-01	G
STATOR OVERHANG (IN)	0.8625E-01	DA
STATOR LAMINATION DIA. (IN)	0.1845E+01	DL
EMPIR. ALTERNATOR DIA. (IN)	0.4286E+00	DGE
WHEEL BACK SIDE OPTIMUM GAP (IN)	0.2215E-01	GD

## VELOCITIES

SPOUTING VELOCITY (FPS)	0.1092E+04	CO
WHEEL TIP SPEED(FPS)	0.3975E+03	U
NOZZLE DISCHARGE VELOCITY (FPS)	0.9832E+03	C2
BLADE INLET RELATIVE VELOCITY(FPS)	0.1782E+03	V2
BLADE INLET RADIAL VELOCITY (FPS)	0.1707E+03	V2
BLADE INLET RELATIVE MACH NUMBER	0.1799E+00	MW2

## REYNOLDS NUMBERS

BLADE PASSAGE REYNOLDS NO.	0.2714E+05	NREP
TURBINE DISC REYNOLDS NO.	0.8026E+06	NRED
JOURNAL DIAMETER REYNOLDS NO.	0.1284E+06	NREJ
ALTERNATOR GAP REYNOLDS NO.	0.6042E+05	NREG

## DRAG COEFFICIENTS

TURBINE DISC DRAG COEFF.	0.5927E-02	CMD
JOURNAL DIAMETER DRAG COEFF.	0.4696E-02	CDS
ALTERNATOR GAP MOMENT COEFF.	0.1562E-02	CDG

CR-2316-3

Figure 45. Turboalternator Partial-Admission Radial Impulse Design Point  
Computer Output (Design Case 630602001) (Sheet 3 of 3)

Reproduced from  
best available copy.



TURBOALTERNATOR PARTIAL ADMISSION RADIAL IMPULSE  
DESIGN POINT COMPUTER OUTPUT

DESIGN CASE		630603005
GAS IS HELIUM		
REFRIGERATION PWR OUT (WATTS)	0.6815E+03	PTHL
ELECTRICAL POWER OUTPUT (WATTS)	0.6815E+03	PTA
SPEED (RPM)	0.6464E+05	N
OVERALL EFFICIENCY (FRACTION)	0.4804E+00	ETATA
 TEMPERATURES, PRESSURES, FLOW		
INLET TEMPERATURE (R)	0.2160E+03	TO
INLET TEMPERATURE (K)	0.1200E+03	TA
OVERALL TEMPERATURE DROP (R)	0.3229E+02	TEDR
OVERALL TEMPERATURE DROP (K)	0.1794E+02	TEDK
OUTLET TEMPERATURE EXIT (R)	0.1837E+03	T4R
OUTLET TEMPERATURE EXIT (K)	0.1021E+03	T4K
 INLET PRESSURE (PSIA)		
INLET PRESSURE (ATM)	0.4219E+02	PO
OUTLET PRESSURE (PSIA)	0.2871E+01	PA
OUTLET PRESSURE (ATM)	0.1658E+02	P3
PRESSURE RATIO	0.1128E+01	PB
FLOW (LR/SEC)	0.2545E+01	PR
FLOW (LR/HR)	0.1609E-01	W
FLOW (G/SEC)	0.5792E+02	WR
	0.7304E+01	WA
 PRIMARY DIMENSIONS		
WHEEL TIP DIAMETER (IN)	0.2500E+01	D
NUMBER OF BLADES	0.7700E+02	Z
BLADE HEIGHT (IN)	0.1534E+00	RH
BLADE HT. CUT. DIA. RATIO	0.3264E+01	RHCD
 THRUST BEARING		
LOAD(LBS.),	0.2687E+01	RTL
OUTSIDE DIAMETER(IN),	0.1680E+01	DT
DIAMETER RATIO	0.6548E+00	DR
CLEAR. TO DIA. RATIO	0.6000E-03	ROCK
LOAD COEFFICIENT	0.1280E+00	RTC
BEARING NUMBER	0.6958E+00	RTN
CLEARANCE, LOADSIDE(IN)	0.1008E-02	RLC
FRICTION POWER(WATTS)	0.3480E+01	RTPL
 JOURNAL BEARING		
LOAD(LBS.)	0.1343E+01	RJL
LOAD COEFFICIENT	0.1621E+00	RJC
BEARING NUMBER	0.1429E+01	RCN
CLEAR. TO DIA. RATIO	0.8318E-03	RCDH
MACHINED CLEARANCE (IN)	0.8318E-03	RVC
PIV. FILM THICK(IN)	0.7540E-03	RJMF
FRICTION POWER(WATTS)	0.8737E+01	RJPL

CR-2317-1

Figure 46. Turboalternator Partial-Admission Radial Impulse Design Point Computer Output (Design Case 630603005) (Sheet 1 of 3)

DESIGN CASE		630603005
TWO STAGE PERFORMANCE		
OTHER STAGE IN TEMP (K)	0.	TOA
TOTAL HEAT LEAK (WATTS)	0.	PHL
EXIT TEMPERATURE (K)	0.1021E+03	T4KH
SHAFT HEAT LEAK (WATTS)	0.	PHLS
HOUSG HEAT LEAK (WATTS)	0.	PHLH
GAS BEARINGS		
ROTATING ASSEMBLY WEIGHT (LBS)	0.2687E+01	RAW
ACCELERATION OF GRAVITY ("G")	0.1000E+01	ACG
TOT. BEARING FRICTION (WATTS)	0.2449E+02	PLR
PERFORMANCE TERMS		
ISENTROPIC HEAD (FT)	0.6498E+05	HS
HYDRAULIC EFF., FIRST TERM	0.6696E+00	ETAH1
HYDRAULIC EFF., SECOND TERM	0.9860E-01	ETAH2
HYDRAULIC EFF., THIRD TERM	0.7247E-04	ETAH3
TIP CLEARANCE EFF. CORRECTION	0.1001E+01	LC
TRAIL EDGE EFF. CORRECTION	0.9745E+00	LE
BLADE RE. NO. EFF. CORR.	0.9809E+00	LR
ALTERNATOR GAP FLUX (KGAUSS)	0.5559E+02	AB
ALTERNATOR CORE LOSS COEFF.	0.1357E+01	KA
ALTERNATOR COPPER LOSS COEFF.	0.3791E+01	KR
TEMPERATURE WHEEL EXIT GAS (R)	0.1793E+03	T3
TURBINE BLADE DISC VOL. FLOW (CFS)	0.4660E+00	Q3
PERFORMANCE FACTORS		
TIP SPEED TO SPOUTING VEL. RATIO	0.3449E+00	SVR
NOZZLE COEFFICIENT	0.9000E+00	PSIN
SPECIFIC SPEED	0.1079E+02	NS
SPECIFIC DIAMETER	0.4873E+01	DS
FLOW FACTOR	0.9906E+01	WSTP
WHEEL EFFICIENCY (FRACTION)	0.5464E+00	ETAW
HYDRAULIC EFFICIENCY (FRACTION)	0.5709E+00	ETAH
ELECTROMAGNET EFF. (FRACTION)	0.9520E+00	ETEM
ISENTROPIC POWER (WATTS)	0.1419E+04	PTAS
WHEEL POWER OUTPUT (WATTS)	0.7751E+03	PTRW
SHAFT POWER OUTPUT (WATTS)	0.7176E+03	PTR
PARASITIC LOSSES (WATTS)		
ALTERNATOR TOTAL EM	0.3618E+02	PLEL
TURBINE DISC FRICTION	0.1941E+02	PLDF
JOURNAL DIAM SHAFT FRICTION	0.1261E+02	PLSF
ALTERNATOR GAP FRICTION	0.9626E+00	PLGF
BEARING FRICTION	0.2449E+02	PLR
SUM ALL PARASITIC LOSSES	0.9366E+02	PLTP

CR-2317-2

Figure 46. Turboalternator Partial-Admission Radial Impulse Design Point Computer Output (Design Case 630603005) (Sheet 2 of 3)

## DESIGN CASE

630603005

## GEOMETRY

WHEEL TIP CLEARANCE (IN)	0.2000E-02	S
BLADE PASSAGE CUTTER DIAMETER (IN)	0.4700E-01	R
BLADE TRAILING EDGE THICKNESS (IN)	0.4000E-02	E
ADMISSION ARC (FRACTION)	0.1567E+00	ARC
ADMISSION ARC (DEGREES)	0.5641E+02	ARCD
NOZZLE ANGLE (DEGREES)	0.8000E+02	ALP2
BLADE ANGLE (DEGREES)	0.6000E+02	BP2
BLADE INCIDENCE ANGLE (DEG)	0.1390E+02	I
BLADE CHORD (IN)	0.1650E+00	C
WHEEL INSIDE DIAMETER (IN)	0.2170E+01	D3
BLADE PRESSURE SURFACE RADIUS (IN)	0.9527E-01	Y
BLADE SUCTION SURFACE RADIUS (IN)	0.4827E-01	X

TOTAL MACHINE SHAFT LENGTH (IN)	0.1000E+02	SL
JOURNAL SHAFT DIAMETER (IN)	0.1000E+01	DJ
JOURNAL FREE SHAFT LENGTH (IN)	0.6277E+01	DSH
ALTERNATOR DIAMETER (IN)	0.1000E+01	DG
ALTERNATOR MAGNET LENGTH (IN)	0.1378E+01	DM
ALTERNATOR PERIF. SPEED(F.P.S.)	0.2823E+03	APS
ALTERNATOR RADIAL GAP (IN)	0.5750E-01	G
STATOR OVERHANG (IN)	0.1725E+00	DA
STATOR LAMINATION DIA. (IN)	0.3690E+01	DL
EMPIR. ALTERNATOR DIA.(IN)	0.6924E+00	DGE
WHEEL BACK SIDE OPTIMUM GAP (IN)	0.3992E-01	GD

## VELOCITIES

SPOUTING VELOCITY (FPS)	0.2046E+04	CO
WHEEL TIP SPEED(FPS)	0.7056E+03	U
NOZZLE DISCHARGE VELOCITY (FPS)	0.1841E+04	C2
BLADE INLET RELATIVE VELOCITY(FPS)	0.3328E+03	W2
BLADE INLET RADIAL VELOCITY (FPS)	0.3197E+03	V2
BLADE INLET RELATIVE MACH NUMBER	0.1821E+00	MW2

## REYNOLDS NUMBERS

BLADE PASSAGE REYNOLDS NO.	0.1039E+05	NPER
TURBINE DISC REYNOLDS NO.	0.3744E+06	NRED
JOURNAL DIAMETER REYNOLDS NO.	0.5990E+05	NREJ
ALTERNATOR GAP REYNOLDS NO.	0.2818E+05	NREG

## DRAG COEFFICIENTS

TURBINE DISC DRAG COEFF.	0.7013E-02	CMD
JOURNAL DIAMETER DRAG COEFF.	0.5683E-02	CDS
ALTERNATOR GAP MOMENT COEFF.	0.1963E-02	CDG

CR-2317-3

Figure 46. Turboalternator Partial-Admission Radial Impulse Design Point  
Computer Output (Design Case 630603005) (Sheet 3 of 3)

- Journal Bearing. The load is based on the load to a single journal bearing with the number of g accelerations included. The load coefficient is a dimensionless parameter. The bearing number is the journal bearing compressibility number, and the clearance-to-diameter ratio is a calculation of the bearing subroutine and is the ratio of the machined pivot film clearance to the journal bearing diameter. The machined clearance is also selected from the bearing subroutine, as is the pivot film thickness. The minimum film thickness not shown is about 0.8 of the pivot film thickness and is at the trailing edge of the pad. The friction power shown is the total friction power for one of the two identical journal bearings.
- Gas Bearings. Rotating assembly weight is the entire rotating assembly weight including the alternator magnet and turbine wheel. Acceleration of gravity is the input g value desired. The total bearing friction loss is the total of both journal bearings and the total of both sides of the thrust bearing.
- Performance Terms. The isentropic head is the available ideal expansion head across the entire turbine from the inlet total pressure to the exit static pressure, based on the inlet total temperature. The first hydraulic efficiency term is the basic impulse turbine efficiency, with a partial-admission correction that allows the leaving velocity to be lower than the full-admission counterpart, because of the filling and emptying process at each end of the active arc. The second term accounts for momentum and mixing losses at each end of the active arc, where the high-velocity gas enters the blade passage and mixes with the latent stagnant gas. The third term accounts for the pumping losses in unshrouded blades, with the residual gas pumping and churning in the blade passage.

The alternator gap flux is the next item listed above with the alternator core loss coefficient and the copper loss coefficient. The wheel exit gas temperature is a static temperature. Next shown is the wheel discharge volume flow rate.

- Performance Factors. The tip-speed-to-spouting-velocity ratio is the classical performance term and is ideally 0.707 for a radial reaction turbine and 0.5 for impulse turbines. For partial-admission turbines, the ratio is characteristically around 0.30. The nozzle coefficient is a semiempirical input value characteristically 0.90. The specific speed is a parameter used extensively that includes the operating variables of rotating speed, volume flow, and isentropic head. The value of specific speed provides a general index of flow capability relative to work; low values are associated with relatively small passages and high values are associated with relatively large passages. The specific diameter is another overall performance parameter that includes the volume flow, isentropic head, and turbine diameter. Both specific speed and specific diameter are widely used

as an indication of achievable efficiency, as shown by pertinent performance curves for turbine design.

The flow factor, a turbine characteristic, is a function of mass flow, inlet temperature and pressure, and pressure ratio. The wheel efficiency is the actual efficiency across the wheel, including the Reynolds number penalty, if any. The hydraulic efficiency is the wheel efficiency before the Reynolds number correction has been made. The electromagnetic efficiency is the overall electromagnetic performance of the permanent magnet alternator. The isentropic power is the ideal power available with the isentropic head and mass flow to the turbine nozzle. The wheel power output is the actual power from the wheel to the shaft. The shaft output is the wheel power output less the windage and bearing losses.

- Parasitic Losses. The sum of the alternator electromagnetic losses is shown. The journal diameter shaft friction loss is the net friction loss of the journal diameter that does not include the bearing losses or alternator windage friction loss. The alternator gap friction loss is the windage loss between the stator and the magnet. The bearing friction loss shown is the total of all the gas bearing friction losses. The sum of all parasitic losses is the sum of all preceding losses listed.
- Geometry. The wheel tip clearance is the axial tip clearance of the blades at the wheel tip outside diameter. The blade passage cutter diameter is the selected input value based on the diameter and desired ratio of the blade height to the cutter diameter. The blade trailing edge thickness is an input value that critically affects the efficiency. The partial-admission arc is shown as a fraction and in degrees.

The nozzle angle is the nozzle input angle. The blade angle is the entrance angle of the blade and is typically around 60 degrees. The blade incidence angle is the angle required for zero flow separation for this particular design. The blade chord is the radial distance across the blade. The blade inside diameter is at the blade trailing edges. The approximate blade pressure and suction surface radii are listed for a constant gas passage-width design.

The total machine shaft length is from one end of the shaft to the other and is an input specification. The journal shaft diameter is an input value. The journal shaft length is the length required for the journal bearings and the alternator stator. The alternator diameter is an input value and is usually set equal to the journal diameter. The magnet has no hole in the center.

The alternator magnet length is a value calculated by the computer program. It is based on the electromagnetic efficiency and the power output requirements. The alternator peripheral speed is an index

for the strength of the platinum cobalt magnet. The alternator radial gap is between the shaft and stator. The stator overhang is the amount of stator overhanging each end of the magnet. The stator lamination diameter is outside the diameter of the lamination.

- Velocities. Spouting velocity is the ideal isentropic velocity based on the isentropic head. The wheel tip speed is shown for stress considerations. The nozzle discharge velocity is based on the flow geometry and number of blades. The blade inlet relative velocity, radial velocity, and relative Mach number are based on the geometry and nozzle discharge velocity.

The empirical alternator diameter is an alternate relationship for sizing the alternator magnet. The wheel backside optimum gap is the best operating clearance to minimize friction and pumping losses.

- Reynolds Numbers. The blade passage Reynolds number shown is a performance correction factor. The turbine disk Reynolds number is needed to determine the turbine disk losses. The journal diameter Reynolds number is used for the free shaft length windage losses. The alternator gap Reynolds number, based on the alternator stator-rotor gap, is for the windage loss determination.
- Drag Coefficients. The turbine disk drag coefficient is used to obtain the friction drag. Then the journal diameter drag coefficient and alternator gap drag coefficient are determined from their respective Reynolds numbers.

Because the lowest temperature turbine for this refrigerator resulted in a design specific speed of 23.57, it appeared worthwhile to evaluate the full-admission reaction turboalternator counterpart. Hence a design study was conducted to determine the best efficiency and operating conditions for the full-admission turbine. A comparison of results is shown in Table 7.

The overall efficiency shows an improvement from 0.481 for the partial-admission turbine to 0.704 for the full-admission turbine. The partial-admission turbine design shown is certainly within the realm of producibility and is practical, based on past experience. Some of the design entries for the full-admission turbine may be considered uncertain until further detailed engineering evaluations have been conducted.

The most outstanding point of conjecture can be within the design of the turbine wheel itself, where a 0.80-inch-diameter turbine wheel will require 44 blades to achieve the relatively high efficiency shown. The manufacture of such a turbine wheel is expected to be possible, but at the same time no turbine wheel this exotic has been built, because a three-dimensional milling approach will be necessary with very small cutters and sophisticated tooling. On the other hand, it is very possible that the 44 blades can be reduced in number, with some loss in efficiency, and yet be able to achieve a greater ef-

Table 7

**COMPARISON OF PARTIAL- AND FULL-ADMISSION  
TURBOALTERNATORS**

Model: Big Bertha

Load alternator type: permanent magnet

Journal-bearing type: self-acting tilting pads

Thrust-bearing type: inward pumping, spiral groove

Design Parameters	Turbine Type	
	Partial-Admission Radial Impulse	Full-Admission Radial Reaction
Total refrigeration power outputs (w)	75.59	110.6
Design speed (rpm)	72,960	96,900
Maximum speed (rpm)	200,000	200,000
<u>Principal Dimensions</u>		
Journal-bearing span (in.)	3.82	3.82
Journal and magnet diameter (in.)	0.50	0.50
Thrust-bearing outside diameter (in.)	0.84	0.84
Magnet length (in.)	0.705	0.705
<u>Performance Factors</u>		
Inlet temperature ( $^{\circ}$ R)	21.6	21.6
Inlet temperature ( $^{\circ}$ K)	12.0	12.0
Inlet pressure (psia)	41.35	41.35
Outlet pressure (psia)	17.08	17.08
Pressure ratio	2.422	2.422
Mass flow (lb/hr)	67.14	67.14
Turbine run number	630601006	630601007
Wheel diameter (in.)	0.750	0.800
Electromagnetic efficiency (fraction)	0.998	0.998
Number of blades	37	44
Overall efficiency (fraction)	0.481	0.704
Specific speed	23.57	30.50
Total friction losses (w)	4.89	9.90
<u>Design Geometry</u>		
Admission (fraction)	0.3165	1.00
Cutter diameter (in.)	0.0278	--
Blade height (in.)	0.0935	0.0222
Blade-height-to-diameter ratio	3.36	--
Blade angle (deg)	60.0	0.0
Nozzle angle (deg)	80.0	81.9

CR-2313

efficiency than that shown for the partial-admission turbine. All of these factors should be investigated further in Phase II of this program.

The complete full-admission radial turbine design is shown on Figure 47. The computer printout has many elements the same as the partial-admission turbine design program; a detailed description of the radial reaction turboalternator design point program output follows.

Below the title, the design case number (up to 13 digits) is used to key the run to the cycle program and to identify the particular turbine design run with any convenient code system. Then the gas selected in the turbine design run is printed.

- Overall Performance. Electrical power output is the net total refrigeration power output after all the losses have been absorbed, but losses through the three-phase alternator load lines to ambient are not included. The speed is as shown, but the optimum speed is probably 5 to 10 percent lower than that shown, because the speed selected was based on the hydraulic efficiency. Then the parasitic losses were added. Hence the net result is that the optimum turboalternator speed should be slightly lower than the design speed shown. The overall efficiency is shown based on the net electrical power or refrigeration power output; hence all turboalternator losses are included.
- Temperatures, Pressures, and Flow. The inlet, overall, and outlet temperature drop and outlet temperatures are exactly the temperatures the refrigeration cycle experiences.

Inlet, nozzle, and outlet pressures are shown next. The inlet pressure is the total pressure into the nozzle. The nozzle exit pressure is the local static pressure out of the nozzle and into the radial reaction wheel. The outlet pressure is the static pressure at the exducer discharge. The pressure ratio is the ratio of the inlet total pressure to the nozzle to the outlet static pressure at the exducer. Next the mass flow in three sets of units is shown.

- Primary Dimensions. The principal aerodynamic-derived dimensions around the turbine are shown. The wheel tip diameter is also shown.

The blade axial length at the impeller tip diameter is shown, and the exducer tip diameter and hub diameter are listed. The number of blades listed is a function of the optimum aerodynamic performance based on a negative incidence angle, which results in no flow separation at the entrance into the wheel. The apparent resulting large number of blades shown will have to be considered in conjunction with practical manufacturing considerations. Then the performance will have to be decreased from that shown.

- Thrust Bearing. The load on the thrust bearing is based on vertical operation and the number of g's of acceleration to be experienced.

TURBOALTERNATOR FULL ADMISSION RADIAL REACTION  
DESIGN POINT COMPUTER OUTPUT

DESIGN CASE  
GAS IS HELIUM

630601007

OVERALL PERFORMANCE

ELECTRICAL POWER OUTPUT (WATTS)	0.1106E+03	PIA
SPEED (RPM)	0.9690E+05	N
OVERALL EFFICIENCY (FRACTION)	0.7039E+00	ETA

TEMPERATURES, PRESSURES, FLOW

INLET TEMPERATURE (K)	0.2160E+02	T0
INLET TEMPERATURE (K)	0.1200E+02	T1
OVERALL TEMPERATURE DROP (K)	0.4521E+01	TEMP
OVERALL TEMPERATURE DROP (K)	0.2512E+01	TEMP
OUTLET TEMPERATURE EXIT (K)	0.1708E+02	T4K
OUTLET TEMPERATURE EXIT (K)	0.9488E+01	T4K

INLET PRESSURE (PSIA)	0.4135E+02	P0
INLET PRESSURE (ATM)	0.2814E+01	PA
NOZZLE EXIT PRESSURE (PSIA)	0.3251E+02	P2
OUTLET PRESSURE (PSIA)	0.1708E+02	P3
OUTLET PRESSURE (ATM)	0.1162E+01	PP
PRESSURE RATIO	0.2422E+01	PR

FLOW (LB/SEC)	0.1865E-01	W
FLOW (LB/HR)	0.6714E+02	WR
FLOW (G/SEC)	0.8467E+01	WA



PRIMARY DIMENSIONS

WHEEL TIP DIAMETER (IN)	0.8000E+00	D
TIP BLADE HEIGHT (IN)	0.2224E-01	PH
EXDUCER TIP DIA. (IN)	0.2630E+00	ED
EXDUCER HUB DIA. (IN)	0.1052E+00	END
NUMBER OF BLADES	0.4404E+02	Z

THRUST BEARING

LOAD(LBS.),	0.3324E+00	RTL
OUTSIDE DIAMETER(IN),	0.8400E+00	DT
DIAMETER RATIO	0.6548E+00	DR
CLEAR. TO DIA. RATIO	0.7000E-03	RDCK
LOAD COEFFICIENT	0.6148E-01	RLC
BEARING NUMBER	0.1605E+00	RLN
CLEARANCE, LOADSIDE(IN)	0.5880E-03	RLC
FRICITION POWER(WATTS)	0.1808E+00	PIFL

CR-2318-1

Figure 47. Turboalternator Full-Admission Radial Reaction Design Point Computer Output (Design Case 630601007) (Sheet 1 of 3)

DESIGN CASE		630601007
JOURNAL BEARING		
LOAD(LBS.)	0.1662E+00	RJL
LOAD COEFFICIENT	0.7785E-01	RJC
BEARING NUMBER	0.6160E+00	RCN
CLEAR. TO DIA. RATIO	0.7268E-03	RCDR
MACHINED CLEARANCE (IN)	0.3634E-03	RMC
PIVOT FILM THICK(IN)	0.3006E-03	RJMF
FRICTION POWER(WATTS)	0.6621E+00	RJPL
GAS BEARINGS		
ROTATING ASSEMBLY WEIGHT (LBS)	0.3324E+00	RAV
ACCELERATION OF GRAVITY ("G")	0.1000E+01	ACG
TOT. BEARING FRICTION (WATTS)	0.1622E+01	PLP
PERFORMANCE TERMS		
ISENTROPIC HEAD (FT)	0.6210E+04	HS
EXDUCER LEAVING LOSS (FT)	0.3682E+03	HE
LEAVING LOSS FRACTION, ISEN. HEAD	0.5929E-01	HLF
ALTERNATOR GAP FLUX (KGAUSS)	0.5611E+01	AP
ALTERNATOR CORE LOSS COEFF.	0.2659E+01	KA
ALTERNATOR COPPER LOSS COEFF.	0.8805E+02	KP
NOZZLE EXIT GAS TEMP.(R)	0.1989E+02	12
EXDUCER EXIT GAS TEMP.(R)	0.1668E+02	13
EXDUCER DISC VOL. FLOW (CPS)	0.4879E-01	Q3
PERFORMANCE FACTORS		
TIP SPEED TO SPOUTING VEL. RATIO	0.5349E+00	SVR
TURB. PRESSURE REACT. RATIO	0.6357E+00	PRR
SPECIFIC SPEED	0.3050E+02	VS
SPECIFIC DIAMETER	0.2688E+01	DS
FLOW FACTOR	0.3705E+01	WSIF
WHEEL EFFICIENCY (FRACTION)	0.7669E+00	FIAB
HYDRAULIC EFFICIENCY (FRACTION)	0.7840E+00	FIA
ELECTROMAGNET EFF. (FRACTION)	0.9980E+00	FIFM
ISENTROPIC POWER (WATTS)	0.1572E+03	FIAS
WHEEL POWER OUTPUT (WATTS)	0.1205E+03	PIRW
SHAFT POWER OUTPUT (WATTS)	0.1108E+03	PIR

CR-2318-2

Figure 47. Turboalternator Full-Admission Radial Reaction Design Point  
Computer Output (Design Case 630601007) (Sheet 2 of 3)

DESIGN CASE		630601007
PARASITIC LOSSES (WATTS)		
ALTERNATOR TOTAL E-M	0.2221E+00	PLEI
JOURNAL DIAM SHAFT FRICTION	0.7801E+01	PLSF
ALTERNATOR GAP FRICTION	0.2626E+00	PLGF
BEARING FRICTION	0.1622E+01	PLR
SUM ALL PARASITIC LOSSES	0.9907E+01	PLTP
GEOMETRY		
WHEEL TIP CLEARANCE (IN)	0.1600E-02	S
EXDUCER TIP CLEARANCE (IN)	0.6574E-03	SE
NØZZLE ANGLE (DEGREES)	0.8188E+02	ALP2
BLADE ANGLE (DEGREES)	0.	BP2
BLADE INCIDENCE ANGLE (DEG.)	-0.1844E+02	I
EXDUCER TIP BLADE ANGLE (DEG)	0.3583E+02	R3
TOTAL MACHINE SHAFT LENGTH (IN)	0.5050E+01	SL
JOURNAL SHAFT DIAMETER (IN)	0.5000E+00	DJ
JOURNAL FREE SHAFT LENGTH (IN)	0.3486E+01	DSH
ALTERNATOR DIAMETER (IN)	0.5000E+00	DG
ALTERNATOR MAGNET LENGTH (IN)	0.3915E+00	DM
ALTERNATOR PERIF. SPEED(F.P.S.)	0.2114E+03	APS
ALTERNATOR RADIAL GAP (IN)	0.2875E-01	G
STATOR OVERHANG (IN)	0.8625E-01	DA
STATOR LAMINATION DIA. (IN)	0.1845E+01	DL
EMPIR. ALTERNATOR DIA.(IN)	0.3462E+00	DGE
VELOCITIES		
SPOUTING VELOCITY (FPS)	0.6324E+03	CO
WHEEL TIP SPEED(FPS)	0.3383E+03	U
NØZZLE DISCHARGE VELOCITY (FPS)	0.3262E+03	C2
BLADE INLET RELATIVE VELOCITY(FPS)	0.4856E+02	W2
BLADE INLET RADIAL VELOCITY (FPS)	0.4607E+02	V2
BLADE INLET RELATIVE MACH NUMBER	0.7576E-01	MW2
SLIP FACTOR	0.1362E+00	SLIP
EXDUCER AXIAL VELOCITY (FPS)	0.1540E+03	V3
EXDUCER TIP REL. VELOCITY (FPS)	0.1899E+03	W3
EXDUCER TIP REL. MACH NUMBER	0.3236E+00	MW3
REYNOLDS NUMBERS		
TURBINE DISC REYNOLDS NØ.	0.3042E+07	NRED
JOURNAL DIAMETER REYNOLDS NØ.	0.1152E+07	NREJ
ALTERNATOR GAP REYNOLDS NØ.	0.5420E+06	NREG
DRAG COEFFICIENTS		
WHEEL REYNOLDS NUMBER CORRECTION	0.9782E+00	RNC
JOURNAL DIAMETER DRAG COEFF.	0.2714E-02	CDS
ALTERNATOR GAP MOMENT COEFF.	0.8086E-03	CDG

CR-2318-3

Figure 47. Turboalternator Full-Admission Radial Reaction Design Point  
Computer Output (Design Case 630601007) (Sheet 3 of 3)

The thrust bearing outside diameter is next shown. The diameter ratio is the ratio of the thrust bearing inside diameter to the outside diameter of the runner. The clearance-to-diameter ratio is the actual clearance on the loaded side of the thrust bearing to the thrust runner tip diameter and is an input value.

The load coefficient is a dimensionless parameter. The clearance on the loaded side of the thrust bearing is listed, which is a consequence of the thrust bearing diameter and clearance-to-diameter ratio specified. The friction power shown is the friction power for only the loaded side of the thrust bearing.

- Journal Bearing. The load is based on the load to a single journal bearing with the number of g accelerations included. The load coefficient is a dimensionless load parameter. The bearing number is the journal bearing compressibility number, and the clearance-to-diameter ratio is a result of the bearing subroutine program and is the machined pivot-film-clearance-to-journal-bearing-diameter ratio. The machined clearance is the clearance selected from the bearing subroutine program. The pivot film thickness is taken from the bearing subroutine program. The minimum film thickness not shown is about 0.8 of the pivot film thickness and is at the trailing edge of the pad. The friction power shown is the total friction power for one of the two identical journal bearings.
- Gas Bearings. Rotating assembly weight is the entire rotating assembly weight including the alternator magnet and turbine wheel. Acceleration of gravity is the input g value desired. The total bearing friction loss is the total of both journal bearings and the total of both sides of the thrust bearing.
- Performance Terms. Isentropic head is the available ideal expansion head across the entire turbine from the inlet total pressure to the exit static pressure, based on the inlet total temperature. The exducer leaving loss is the axial velocity head loss leaving the exducer. The leaving loss is expressed as a fraction of the total isentropic head.

The alternator gap flux is next listed, along with the alternator core loss coefficient and the copper loss coefficient. The nozzle exit gas static temperature is the static temperature. The exducer gas temperature is the static temperature. Next shown is the exducer discharge flow.

- Performance Factors. The tip-speed-to-spouting-velocity ratio is the classical performance term and is ideally 0.707 for a radial reaction turbine and 0.5 for classical impulse turbines. The turbine pressure reaction ratio is the reaction ratio based on the pressure at the inlet to the nozzle, at the exit of the nozzle, and at the exit of the turbine wheel exducer. The pressure reaction ratio is the frac-

tion of the pressure drop across the turbine wheel, as compared with the overall pressure drop across the stage. This pressure reaction ratio is slightly different from the classical enthalpy reaction ratio expression.

The specific speed is a parameter used extensively that includes the operating variables of rotating speed, volume flow, and isentropic head. The value of specific speed provides a general index of flow capability relative to work with low values associated with relatively small passages and high value associated with relatively large flow passages.

The specific diameter is another overall performance parameter that includes the volume flow, ideal specific work, and diameter of the turbine. Both specific speed and specific diameter are widely used as an indication of achievable efficiency, as shown by pertinent performance curves for turbine design.

The flow factor is a characteristic of the turbine as a function of mass flow, inlet temperature, and pressure and is a function of pressure ratio. The wheel efficiency is the actual efficiency across the wheel, with the Reynolds number penalty, if any, included. The hydraulic efficiency is the wheel efficiency before the Reynolds number correction has been made, and the electromagnetic efficiency is the overall electromagnetic performance of the permanent magnet alternator. The isentropic power is the ideal power available with the isentropic head and mass flow to turbine nozzle. The wheel power output is the actual power from the wheel to the shaft, and the shaft output is the wheel power output less the windage and bearing losses.

- Parasitic Losses. The total alternator electromagnetic losses are shown. The journal diameter shaft friction loss is the net friction loss of the journal diameter that does include the bearing losses or alternator windage friction loss. The alternator gap friction loss is the windage loss between the stator and the magnet. The bearing friction loss shown is the total of all the gas bearing friction losses. The sum of all parasitic losses is the sum of all the preceding losses.
- Geometry. The wheel tip clearance is the axial tip clearance of the blades at the wheel tip outside diameter. The exducer tip clearance is the radial tip clearance at the tip of the exducer. The nozzle angle is the nozzle angle based on the best aerodynamic conditions. The blade angle is the entrance of the blade and is zero for all radial reaction turbine wheels. Any other blade angle is not consistent with the rest of this design computer program.

The blade incidence angle is the angle required for zero flow separation for this particular design. It is the same angle as the relative velocity from the radial velocity component. The exducer tip blade angle is the resultant angle at the exducer tip, based on no swirl in the exit velocity.

The total machine shaft length is from one end of the shaft to the other and is input variable. The journal shaft diameter is an input value, and the journal free shaft length is the length of the shaft less the journal bearings and the alternator stator. The alternator diameter is an input value and is usually set equal to the journal diameter. The magnet has no hole in the center, to save weight and cost.

The alternator magnet length is a value derived from the computer program. It is based on the electromagnetic efficiency and the power output requirements. The alternator peripheral speed is an index for the strength of the platinum cobalt magnet. The alternator radial gap is between the shaft and the stator.

The stator overhang is the amount of stator overhanging each end of the magnet. The stator lamination diameter is the outside diameter of the lamination. The empirical alternator diameter is an alternate relationship for sizing the alternator magnet.

- Velocities. Spouting velocity is the ideal isentropic velocity based on the isentropic head. The wheel tip speed is shown for stress considerations. The nozzle discharge velocity is based on the flow geometry and number of blades. The blade inlet relative velocity, radial velocity, and relative Mach number are based on the geometry and nozzle discharge velocity.

The exducer axial velocity is based on the exit volume flow area with the assumption that no swirl remains. From this, the exducer tip relative velocity is obtained and the local relative Mach number is determined.

- Reynolds Numbers. The turbine Reynolds number is used to obtain the turbine wheel Reynolds number correction. The journal diameter Reynolds number is used for the free shaft length windage losses. The alternator gap Reynolds number is based on the alternator stator-to-rotor gap for the windage loss determination.
- Drag Coefficients. The wheel Reynolds correction shown is based on the turbine wheel. Then the journal diameter drag coefficient and alternator gap drag coefficient are determined from their respective Reynolds numbers.

### Compressors for A-C Generator

For this refrigerator, the cycle study resulted in the requirement for three compressor modules with two centrifugal compressor stages on each end of the rotor.

A detailed compressor design study was conducted, using the compressor design computer program. The resulting overall performance and features are shown in Table 8. Also shown are the features of the first and last modules.

Table 8

# A-C GENERATOR REFRIGERATOR TURBOCOMPRESSOR DESIGN SUMMARY

Design Case 6310001

Impeller type: centrifugal

Motor type: induction

Journal-bearing type: self-acting tilting pads

Thrust-bearing type: inward-pumping, spiral groove

Feature	Performance			
Inlet temperature	322.8°K			
Inlet pressure	1.10 atm			
Pressure ratio	2.649			
Flow	26.84 g/sec			
Speed	50,000 rpm			
Input power	43.34 kw			
Number of modules	3			
Number of stages	6			
<u>First and Last Module Features</u>	<u>First</u>		<u>Last</u>	
Motor diameter (in.)	3.041		3.041	
Motor lamination outside diameter (in.)	6.993		6.993	
Motor power output (hp)	16.46		16.66	
Total windage loss (w)	181.2		283.2	
Total bearing friction loss (w)	1219.0		1275.0	
<u>First- and Last-Stage Features</u>	<u>First</u>	<u>Last</u>	<u>First</u>	<u>Last</u>
Pressure ratio	1.196	1.183	1.165	1.159
Volume flow (cfm)	341.9	296.6	181.9	156.1
Aerodynamic efficiency (fraction)	0.6641	0.6486	0.5913	0.5719
Specific speed (nondimensional)	0.04768	0.04513	0.03788	0.0359
Tip speed (fps)	1575	1575	1575	1575
Tip diameter (in.)	7.217	7.217	7.217	7.217
Tip width (in.)	0.1847	0.1734	0.1402	0.1320

CR-3331

Because the detailed compressor design uses somewhat different inputs and calculation procedures from those used in the system calculation (Figure 43), the answers are slightly different. A conception of an arrangement for this compressor system is shown in Figure 48. Included are the individual plate-fin aftercoolers for each stage and the interconnecting piping.

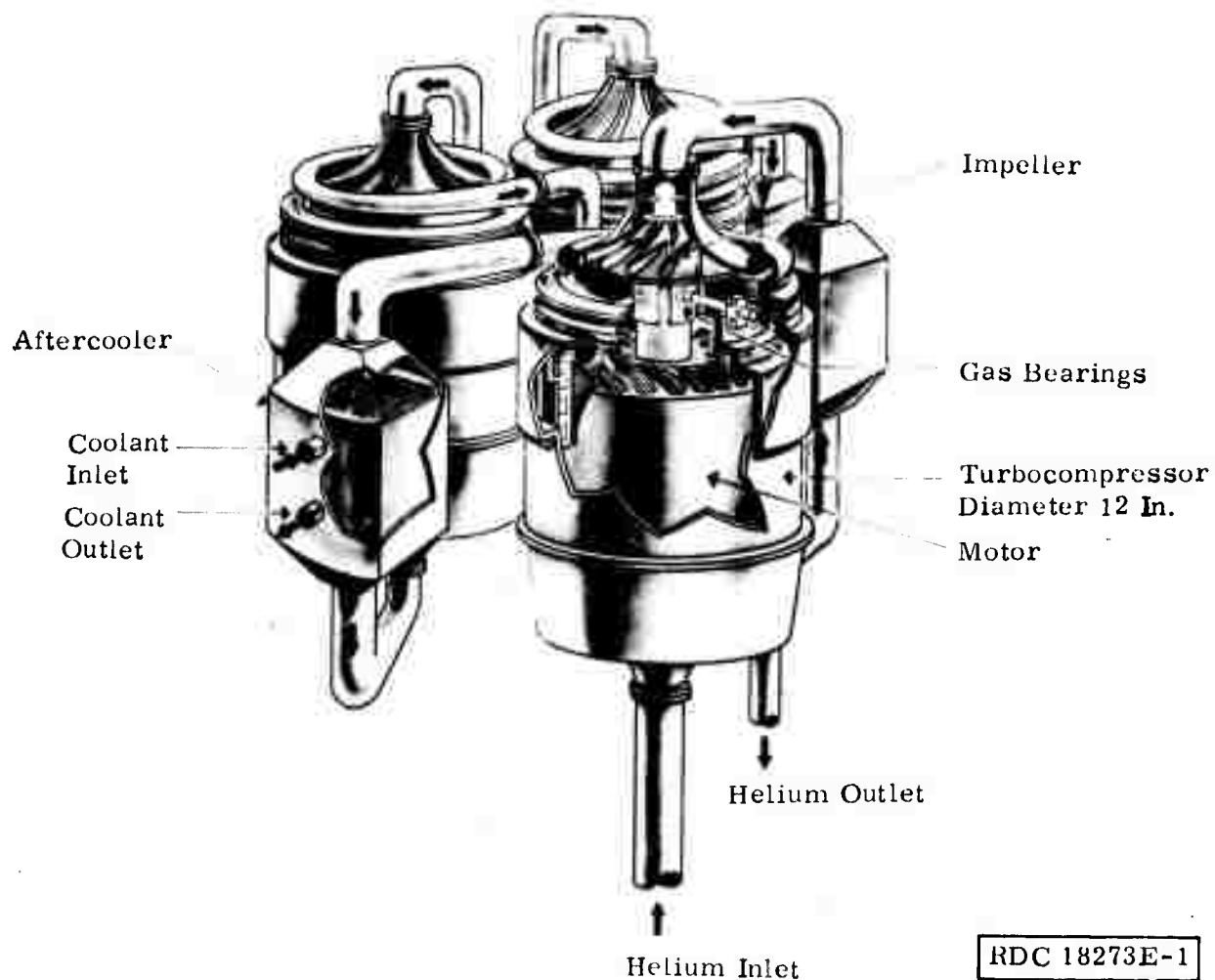


Figure 48. Compressor System Arrangement

A complete computer design point printout for the compressor system is shown in Figure 49. Only the first and last modules are shown to provide a basis for evaluating the extremes of performance factors.

For this centrifugal compressor design point computer program, qualifications are listed to explain every entry on the output sheets.

Below the title, the design case number is shown to key the run to the cycle program and to identify the particular compressor system design run with a selected code system. Then the gas selected for the compressor design run is printed.

**Overall Performance.** The overall compressor system performance is shown with the inlet temperature and pressure and the outlet temperature. The overall

# GAS IS HELIUM

## OVERALL COMPRESSOR PERFORMANCE

INLET TEMPERATURE (K)	322.8	T4
INLET PRESSURE (ATM)	1.100	P4
OUTLET TEMPERATURE (K)	335.0	T1
OUTLET PRESSURE (ATM)	2.914	P1
PRESSURE RATIO	2.649	PR1
FLOW (G/SEC)	26.84	FL0
SPEED (RPM)	0.5000E+05	N
AMBIENT TEMPERATURE (K)	322.0	TAMK
INPUT POWER (KW)	43.34	POWER
NUMBER OF MODULES	3.000	AMDN
CONDIT-CONTROL EFFICIENCY	0.9200	FICC
NUMBER OF STAGES	6	M
OVERALL EFFICIENCY	0.4939	EQCS
NUMBER OF MOD. WITH SAME TIP SPEED	3.000	VIDM
TIP SPEED MULTIPLIER	1.000	AKU

## MODULE NO. 1

### PERFORMANCE

STAGE NO.	1	2	
INLET TEMPERATURE (K)	581.0	603.0	TEMI
INLET PRESSURE (PSIA)	16.16	19.33	PREI
OUTLET TEMPERATURE (K)	651.1	673.1	TEMD
PRESSURE RATIO	1.196	1.183	PR
ACCUM. PRESS. RATIO	1.196	1.415	PRSU
VOLUME FLOW (CFM)	341.9	296.6	Q
AERO EFFICIENCY	0.6641	0.6486	EE
SPECIFIC SPEED	0.4768E-01	0.4513E-01	ANS
AERO POWER (HP)	7.295	7.295	HP
ISENTROPIC HEAD (FT)	0.4498E+05	0.4403E+05	HAD
TEMPERATURE RISE (K)	70.09	70.09	DT
TIP SPEED (FPS)	1575.	1575.	UT
TIP DIAMETER (IN)	7.217	7.217	DTI
EYE DIAMETER (IN)	2.464	2.391	DE
HUB DIAMETER (IN)	0.5096	0.5298	DHL
TIP WIDTH (IN)	0.1847	0.1734	HZIT
COOLER EFFECTIVENESS	0.6729	0.7497	ECI
COOLER PRESS. DROP. RATIO	0.1400E-01	0.1400E-01	DPCOP
AFTERCoolER WEIGHT (LBS)	7.795	10.000	WIC

CR-3332-1

Figure 49. Centrifugal Compressor Design Point Computer Output  
(Case No. 631C001) (Sheet 1 of 4)

# MOTOR DESIGN

ELECTROMAG. EFF. (FR)	0.9300	EIM
DIAMETER (IN)	3.041	DE
LENGTH (IN)	3.662	DM
LAMINATION Ø.DIA.(IN)	6.993	DL
RADIAL GAP (IN)	0.4409E-01	G
PERIF. SPEED (FPS)	663.3	APS
MOTOR POWER OUTPUT (HP)	16.46	PMO
MOTOR POWER LOSS (WATTS)	924.5	PHLM
CONDIT-CONTRÖLLER LOSS (W)	1148.	PHLC
CONDIT-CONTR. IN. POWER(KW)	14.36	PCC

# WINDAGE POWER LOSSES (WATTS)

JOURNAL FREE SHAFT LENGTH	70.20	PLSF
MOTOR END RINGS	73.76	PLEF
MOTOR ROTOR GAP	37.22	PLGF
TOTAL WINDAGE LOSS	181.2	PLWS

# GAS BEARINGS DESIGN

## THRUST BEARING

LOAD(LBS.)	32.95	RIL
OUTSIDE DIAMETER(IN)	4.500	PTH
DIAMETER RATIO	0.7333	DR
CLEAR. TO DIA. RATIO	0.3300E-03	RDCR
LOAD COEFFICIENT	0.2319	BTC
BEARING NUMBER	2.839	RTN
CLEARANCE, LOADSIDE(IN)	0.1485E-02	PLC
FRICTION POWER(WATTS)	145.7	RIFL

## JOURNAL BEARING

LOAD(LBS.)	16.48	RJL
LOAD COEFFICIENT	0.1894	RJC
BEARING NUMBER	2.000	RCN
CLEAR. TO DIA. RATIO	0.9887E-03	RCDR
MACHINED CLEARANCE	0.2966E-02	RMC
PIV. FILM THICK.(IN)	0.1582E-02	RJMF
FRICTION POWER(WATTS)	465.3	RJPL

CR-3332-2

Figure 49. Centrifugal Compressor Design Point Computer Output  
(Case No. 6310001) (Sheet 2 of 4)

Reproduced from  
best available copy.



## GAS BEARINGS

ROTATING ASSY. WEIGHT(LBS)	32.95	RAW
ACCELERATION OF GRAVITY("G")	1.000	ACG
131. BEARING FRICTION(WATTS)	1219.	PLR
SHAFT LENGTH (IN)	14.41	SL
JOURNAL DIA.(IN)	3.000	DJ
VISCOSITY (LB-SEC/SQ-IN)	0.3363E-08	MU

## MODULE NO. 3

## PERFORMANCE

STAGE NO.	1	2	
INLET TEMPERATURE (R)	603.0	603.0	TEMI
INLET PRESSURE (PSIA)	31.53	36.72	PREI
OUTLET TEMPERATURE (R)	673.1	673.1	TEMD
PRESSURE RATIO	1.165	1.159	PR
ACCUM. PRESS. RATIO	2.273	2.633	PRSU
VOLUME FLOW (CFM)	181.9	156.1	Q
AERO EFFICIENCY	0.5913	0.5719	EF
SPECIFIC SPEED	0.3788E-01	0.3592E-01	ANS
AERO POWER (HP)	7.295	7.295	PP
ISENTHROPIC HEAD (FT)	0.4013E+05	0.3891E+05	HAD
TEMPERATURE RISE (R)	70.09	70.09	DT
TIP SPEED (FPS)	1575.	1575.	UT
TIP DIAMETER (IN)	7.217	7.217	DTI
EYE DIAMETER (IN)	2.162	2.098	DE
HUB DIAMETER (IN)	0.5554	0.5447	DHL
TIP WIDTH (IN)	0.1402	0.1320	H/TI
COOLER EFFECTIVENESS	0.7497	0.7497	ECI
COOLER PRESS. DROP. RATIO	0.1400E-01	0.1400E-01	OPC3P
AFTERCooler WEIGHT (LBS)	10.000	10.000	WIC

## MOTOR DESIGN

ELECTROMAG. EFF. (FR)	0.9300	EIM
DIAMETER (IN)	3.041	DC
LENGTH (IN)	3.708	DM
LAMINATION Ø.DIA.(IN)	6.993	DL
RADIAL GAP (IN)	0.4409E-01	G
PERIF. SPEED (FPS)	663.3	APS
MOTOR POWER OUTPUT (HP)	16.68	PMO
MOTOR POWER LOSS (WATTS)	936.4	PHLM
CONDIT-CONTROLLER LOSS (W)	1163.	PHLC
CONDIT-CONTR. IN. POWER(KW)	14.54	PCC

CR-3332-3

Figure 49. Centrifugal Compressor Design Point Computer Output  
(Case No. 6310001) (Sheet 3 of 4)

# WINDAGE POWER LOSSES (WATTS)

JOURNAL FREE SHAFT LENGTH	111.8	PLSF
MOTOR END RINGS	117.0	PLEF
MOTOR MOTOR GAP	54.33	PLGF
TOTAL WINDAGE LOSS	283.2	PLWS

# GAS BEARINGS DESIGN

## THRUST BEARING

LOAD(LBS.)	32.45	PTL
OUTSIDE DIAMETER(IN)	4.500	DTM
DIAMETER RATIO	0.7333	DR
CLEAR. TO DIA. RATIO	0.3300E-03	RDCR
LOAD COEFFICIENT	0.1202	RTC
BEARING NUMBER	1.527	RTN
CLEARANCE, LOADSIDE(IN)	0.1485E-02	RLC
FRICITION POWER(WATTS)	148.9	PTPL

## JOURNAL BEARING

LOAD(LBS.)	16.22	RJL
LOAD COEFFICIENT	0.9817E-01	RJC
BEARING NUMBER	2.000	RCN
CLEAR. TO DIA. RATIO	0.7173E-03	RCLR
MACHINED CLEARANCE	0.2152E-02	RMC
PIV. FILM THICK.(IN)	0.1582E-02	RJMF
FRICITION POWER(WATTS)	490.3	RJPL

## GAS BEARINGS

ROTATING ASSY. WEIGHT(LBS)	32.45	RAW
ACCELERATION OF GRAVITY("G")	1.000	ACG
TOT. BEARING FRICITION(WATTS)	1275.	PLP
SHAFT LENGTH (IN)	14.46	SL
JOURNAL DIA.(IN)	3.000	DJ
VISCOSITY (LB-SEC/SQ-IN)	0.3363E-08	MU

CR-3332-4

Figure 49. Centrifugal Compressor Design Point Computer Output  
(Case No. 6310001) (Sheet 4 of 4)

pressure ratio for the entire compressor system shown includes all pressure drop losses. The flow rate to the compressor is shown, followed by the design speed of all modules. The ambient temperature is shown next. The total electrical input power to the compressor system shown accounts for all losses.

Next the number of modules is shown, followed by the conditioner-controller efficiency. Then the number of stages making up the complete compressor system is shown. The overall efficiency is the power input to the conditioner-controller, as compared with the entire isentropic power output of the compressor. Hence all windage, bearing, motor electromagnetic, conditioner-controller, and cooler pressure drop losses are included in this value. The number of modules with the same tip speed is then listed followed by the tip speed multiplier, which is different from 1.0 if not all modules have the same tip speed.

Stage Performance. The stage number of each of the stages within the module is shown, followed by the local inlet temperature, the inlet pressure, and the outlet temperature before the cooler. Then the pressure ratio of the individual stage is followed by the accumulated pressure ratio across all stages, up through the particular stage listed. Next the inlet volume flow and wheel aerodynamic efficiency are shown. The specific speed and aerodynamic power are then listed.

The isentropic head across each stage is next shown along with the actual stage temperature rise. Then the impeller peripheral speed is shown, followed by the tip diameter, eye diameter, and hub diameter. The impeller inlet tip width is shown next, followed by the effectiveness of the cooler following the stage, the cooler pressure drop ratio, and an estimated cooler weight.

Motor Design. Electromagnetic efficiency of only the motor itself is first listed, and the motor diameter and the length of the motor without the end rings is shown. The radial gap between the motor and stator is next listed. The motor peripheral speed is shown (it is a criterion for stress considerations) and then the motor power output is shown in units of horsepower. The motor power loss is the amount of electromagnetic losses to be removed from the stator. Then the conditioner-controller input power requirement is listed.

Windage Power Losses. The individual windage power losses are shown, first with the journal shaft free area loss. Then the friction from the motor end rings is listed, followed by the motor rotor gap windage loss. Then the total windage loss is shown. The disk friction loss for the impeller was included within the overall impeller aerodynamic efficiency.

Gas Bearing Design. The thrust bearing design is shown first with the load given in pounds, which is the entire rotating assembly weight for vertical operation and includes any additional load for acceleration. Next the outside diameter of the thrust bearing is shown, along with the diameter ratio of the

thrust-bearing-to-journal-bearing diameter. Next the thrust bearing clearance-to-diameter ratio, which is for the most highly loaded thrust bearing surface, is listed. The load coefficient is the load over the projected area and the ambient pressure. The bearing number is the gas bearing compressibility number, which is a significant design parameter. Clearance on the most heavily loaded side is next listed. This is the direct result of the clearance-to-diameter ratio established. The friction power loss shown is the friction for only the most heavily loaded thrust surface.

Next the journal bearing design parameters are shown, with the journal bearing load being half of the rotating assembly weight, plus any acceleration load imposed. The load coefficient listed is the unit load over the journal projected area times ambient pressure. This is a first-order selection criterion number. The bearing number is the bearing compressibility number, which is a significant design parameter.

The efficiency of the gas bearing decreases as the bearing number increases. The clearance-to-diameter ratio listed is the ratio of the pivot film clearance to the journal shaft. The machined clearance is the clearance machined in the tilting-pad bearing. It is the difference between the actual journal radius and the actual pad radius. The pivot film thickness listed is the design operating film thickness at the pivot point. The total friction power loss for only one journal bearing is next listed.

The combined gas bearing performance is shown next with the calculated rotating assembly weight shown first, followed by the imposed acceleration of gravity. The total bearing friction loss consists of the friction loss of both journal bearings plus the friction loss of both the loaded and unloaded sides of the thrust bearing.

The final entry is the total shaft length. This length is determined by stacking all of the bearing and motor elements plus allowing for gaps between the various elements along the shaft.

## D-C GENERATOR

### Refrigeration System for D-C Generator

As was shown in Table 3, the d-c generator imposes refrigeration loads at 4.4°K and 80°K, in addition to requiring a withdrawal of liquid helium from the refrigerator. Table 9 is a summary of the significant computer output for the d-c generator. As in the case of the a-c generator, these results are for a single refrigerator cooling a single, 18-megawatt generator.

Some of the same general conclusions as were drawn earlier for the a-c generator can be drawn from this table. The effect of varying only the Station 2 temperature can be seen by comparing the compressor input shaft power for the first three runs in Table 3. The Station 2 temperature giving

Table 9  
COMPUTER RESULTS -- REFRIGERATOR FOR D-C GENERATOR\*

Run	Compressor Stages	Pressure Ratio	Turbines	Liquid Helium Withdrawal Rate (g/sec)	Refrigeration Capacity (w/ Temperature (°K))			Cryogenic Heat Exchanger Effectiveness	Cryogenic Heat Exchanger Core Weight (lb)	Total Compressor Input Shaft Power (kw)
					Station 1	Station 2	Station 3			
10202	6	2.58	2	0.11	3.0/4.4	5.13	86.80	0.985	405	37.8
10201	6	2.88	2	0.11	3.0/4.4	5.14	64.80	0.985	401	37.3
10203	6	2.58	2	0.11	3.0/4.4	5.15	64.80	0.985	420	38.2
10204	8	2.58	2	0.11	2.0/4.4	5.14	64.80	0.985	387	36.5
20205*	8	2.58	2	0.11	3.0/4.4	5/14	32.80	0.985	161	38.0
11201	8	3.51	2	0.11	3.0/4.4	5.14	64.80	0.985	200	38.0

\*Results are for a single refrigerator cooling a single 18-Mw generator.  
\*Design point.

CH-4232

the minimum input power, is about 14°K, but the change in power is not very sensitive to the station temperature.

The difference between Runs 10201 and 10204 is that for the latter run, turbine wheel diameters and other turbine geometry were chosen closer to optimum values, thereby increasing turbine efficiencies. These changes in turbine geometry were worked out using a turbine design computer program that is separate from the cycle design program.

Run 11201 illustrates the effect of increasing the pressure ratio by the addition of two compressor stages. The input power increases 4 percent (compared to Run 10204), but the cryogenic heat exchanger weight drops by 48 percent. Because this effect is accomplished at the expense of increased weight, complexity, and cost of the compressor subsystem, and because there is no strong inducement to decrease the weight and size of the cryosection, it was felt that the lower compressor ratio would be more suitable for the d-c generator.

In all the runs shown in Table 9, a heat exchanger effectiveness of 98.5 percent was used for the major cryogenic heat exchangers. The reason for this is that the amount of liquid helium withdrawn is small relative to the total flow (in contrast with the a-c generator system). The degree of unbalanced flow between helium streams within the refrigerator is therefore small, and the difficulty of achieving 99-percent effectiveness is increased. The effectiveness of 98.5 percent is considered a safe upper limit under these circumstances.

In all cases the metal-plastic laminate heat exchanger was lighter and smaller than the plate-fin exchanger. For example, for Run 20205, the heat exchanger weights were 381 pounds and 606 pounds, respectively. All weights given in the table are for the lighter exchangers.

It is interesting to compare Runs 10204 and 20205. Every run in the table, except for Run 20205, used an incorrect value of 64 watts for the Station 3 heat load. When the correct value of 32 watts was used (Run 20205), the he-

helium flow rates changed only slightly, as reflected in only small changes in heat exchanger weight and compressor input power. The reason for this small change is that the principal heat load at the warmest turbine station is internal to the refrigerator; that is, the principal requirement of the warmest expansion turbine is to provide the cooling necessary to maintain the temperature difference between helium streams within the cryogenic heat exchangers, thus compensating for the inefficiencies of the heat exchangers.

The relative importance of the internal heat load and the external heat load is illustrated by the fact that the warmer turbine extracts about 730 watts of power from the system, while the external heat load at that point is only 32 watts. It is therefore apparent that a major change in external heat load will have only a small effect on the refrigerator design.

Run 20205 is chosen to represent the most favorable design. A printout of that run is shown in Figure 50. The cold and warm turbine diameters are 1.3 and 2.0 inches, and the shaft speeds are 44,200 and 68,800 rpm, respectively. Turboalternator efficiencies are in the 51- to 53-percent range.

RUN NUMBER 20205

ITERATIONS \* \* \* \* \* 9

ELEMENT SEQUENCE = 6 2 2 1

LIQUID FLOW OUT OF REFRIGERATOR= 0.1100E+00 G/SEC

LOCATION	LOAD(W)	TEMP(K)	FLOW(G/SEC)
1	3.000	4.400	6.028
2	5.000	14.00	13.43
3	32.00	80.00	11.26

CYCLE DESIGN POINTS ?YES

LOC.	P(ATM)	TEMP(K)	LOC.	P(ATM)	TEMP(K)
1 1	2.800	5.780	1 2	1.180	4.406
1 3	1.174	4.400			
2 1	2.828	13.94	2 2	2.814	11.89
2 3	2.800	5.780	2 4	1.174	4.400
2 5	1.162	11.78	2 6	1.157	12.44
2 7	2.814	14.00			
3 1	2.856	79.45	3 2	2.842	68.39
3 3	2.828	13.94	3 4	1.157	12.44
3 5	1.145	67.55	3 6	1.139	74.60
3 7	2.842	80.00			
4 1	2.885	335.0	4 2	2.856	79.45
4 3	1.139	74.60	4 4	1.117	331.1

TURBOALTERNATORS ?YES

CR-4235-1

Figure 50. Computer Results for D-C Generator (Run 20205) (Sheet 1 of 3)

-----TURBOALTERNATORS-----

LØC.	DIA(IN)	PWR(W)	EFFIC.	RPM
2	1.300	155.3	0.5336	44198.
3	2.000	729.9	0.5113	68769.

LØC.	ADM.FRACT.	PARA.LØSS(W)	SPEC.SPD.	SPEC.DIAM.
2	0.2406	2.744	17.38	3.193
3	0.2213	63.81	15.85	3.482

LØC.	T.BRG.NØ.	T.LD CØ.	T.MIN F.(IN)	BRG.PWR.(W)
2	0.8506E-01	0.6490E-01	0.5880E-03	0.3874
3	0.5597	0.1249	0.1008E-02	22.20

LØC.	J.BRG.NØ.	J.LD CØ.	J.MIN F.(IN)	BL.HT./CUT.DIA.
2	0.2999	0.8219E-01	0.3006E-03	3.526
3	1.280	0.1581	0.7540E-03	3.488

SKIP HEAT EXCHANGER DESIGN ?NØ

COMPOSITE HEAT EXCHANGERS ?YES

-----HEAT EXCHANGER DESIGN-----

LØC.	WT(LBS)	LENGTH(CM)	VØL(CU.FT.)	EFFECT
2 B	4.741	16.13	0.7233E-01	0.9850
2 U	0.8553	2.387	0.1356E-01	0.9478
3 B	75.71	67.80	1.535	0.9851
3 U	6.661	6.451	0.1327	0.9299
4 B	293.2	119.5	6.992	0.9851
TØTALS	381.2		8.745	

FINNED-PLATE HEAT EXCHANGERS ?YES

-----HEAT EXCHANGER DESIGN-----

LØC.	WT(LBS)	LENGTH(CM)	VØL(CU.FT.)	EFFECT
2 B	FINNED PLATE HYDRAULIC DIA. TØØ BIG			
2 U	FINNED PLATE HYDRAULIC DIA. TØØ BIG			
3 B	122.9	436.1	2.687	0.9850
3 U	12.25	58.12	0.2484	0.9305
4 B	471.2	1234.	19.49	0.9850
TØTALS	606.4		20.43	

CENTRIFUGAL COMPRESSØR?YES

FOR OUTPUT FOR ALL MØDULES, TYPE ALL  
 FOR OUTPUT FOR FIRST AND LAST MØDULE ØNLY, TYPE F&L  
 ALL ØR F&L ?ALL

CR-4235-2

Figure 50. Computer Results for D-C Generator (Run 20205) (Sheet 2 of 3)

-----CENTRIFUGAL COMPRESSOR-----

ISENTHROPIC COMP. POWER (KW)	24.38
TOTAL MOTOR SHAFT POWER (KW)	36.02
AMBIENT TEMPERATURE (K)	322.0
PRESSURE RATIO	2.584
MASS FLOW (G/SEC)	30.72
SUPPLY LINE DEL P/P	0.
RETURN LINE DEL P/P	0.

MODULE	SHAFT PWR (KW)	RPM	MOT. SPD. (FPS)
1	11.98	0.5000E+05	667.6
2	12.00	0.5000E+05	667.6
3	12.03	0.5000E+05	667.6

AERODYNAMICS

STAGE	SP. SPEED	AERO. EFF.	TIP SPD (FPS)	DIA. (IN)
1	0.5224E-01	0.6872	1529.	7.010
2	0.4901E-01	0.6715	1529.	7.010
3	0.4604E-01	0.6544	1529.	7.010
4	0.4339E-01	0.6367	1529.	7.010
5	0.4102E-01	0.6188	1529.	7.010
6	0.3891E-01	0.6008	1529.	7.010

STAGE	PRESS. RATIO	COOL. EFFCTV.
1	1.185	0.7163
2	1.178	0.7385
3	1.173	0.7385
4	1.168	0.7385
5	1.162	0.7385
6	1.157	0.7385

BEARINGS

MODULE	T.BRG.NØ.	T.LD.CØ.	T.MIN F.(IN)	BRG.PWR.(W)
1	3.450	0.5761E-01	0.1764E-02	192.4
2	2.513	0.4049E-01	0.1764E-02	208.6
3	1.852	0.2908E-01	0.1764E-02	225.7

MODULE	J.BRG.NØ.	J.LD.CØ.	J.MIN F.(IN)
1	1.639	0.2111	0.1223E-02
2	1.639	0.1484	0.1223E-02
3	1.639	0.1066	0.1223E-02

CR-4235-3

Figure 50. Computer Results for D-C Generator (Run 20205) (Sheet 3 of 3)

The centrifugal compressor consists of three modules, each with two centrifugal impellers. Impeller diameters are about 7.0 inches and shaft speeds are 50,000 rpm.

### Turboalternators for D-C Generator

Both of the turboalternator designs for the d-c generator refrigerator were examined to find satisfactory operating speeds and geometries to satisfy cycle requirements. Cycle Study Computer Run 10204 established the turboalternator requirements listed in Table 10.

Table 10  
TURBOALTERNATOR REQUIREMENTS (RUN 10204)

Inputs and Results	Inlet Temperature	
	14.0°K	80.0°K
<u>Inputs</u>		
Inlet pressure (atm)	2.814	2.842
Outlet pressure (atm)	1.162	1.145
Mass flow (g/sec)	13.40	11.84
<u>Results</u>		
Refrigerator power output (w)	154.9	775.3
Overall refrigerator efficiency (fraction)	0.5334	0.5165
Wheel tip diameter (in.)	1.30	2.00
Admission arc (fraction)	0.2404	0.2271
Speed (rpm)	44,193	68,987

Also shown in Table 10 are principal turboalternator design results from the cycle run. The two power outputs and overall efficiencies must be achieved for the conditions of the cycle points. These turboalternators, of course, were not optimized in the cycle study; hence the wheel tip diameter, admission, and speed are shown only for reference purposes.

Complete partial-admission turboalternator preliminary design studies were conducted for both of the stages for the required cycle conditions. The best operating geometries were established.

Design summary results are shown in Table 11. Complete design computer result listings are shown in Figures 51 and 52.

### Compressors for D-C Generator

For this refrigerator, the cycle study resulted in the requirement for three compressor modules with two centrifugal compressor stages on each end of the rotor.

Table 11

**TURBOALTERNATOR DESIGN SUMMARY  
FOR D-C GENERATOR REFRIGERATOR**

( Turbine type: partial admission, radial impulse  
Load alternator type: permanent magnet  
Journal-bearing type: self-acting tilting pads  
Thrust-bearing type: inward-pumping, spiral groove )

Design Parameters	Model and Inlet Temperature	
	Big Bertha (14°K)	Grizzly Giant (80°K)
Total refrigeration power outputs (w)	161.7	804.4
Design speed (rpm)	44,290	69,110
Maximum speed (rpm)	200,000	200,000
<u>Principal Dimensions</u>		
Journal bearing span (in. )	3.82	7.64
Journal and magnet diameter (in. )	0.50	1.0
Thrust bearing outside diameter (in. )	0.84	1.68
Magnet length (in. )	0.705	1.410
<u>Performance Factors</u>		
Inlet temperature (°R)	25.2	144.0
Inlet temperature (°K)	14.0	80.0
Inlet pressure (psia)	41.35	41.77
Outlet pressure (psia)	17.08	16.83
Pressure ratio	2.422	2.482
Mass flow (lb/hr)	110.4	96.98
Turbine run number	102010103	102010202
Wheel diameter (in. )	1.30	2.00
Electromagnetic efficiency (fraction)	0.990	0.973
Number of blades	53	59
Cycle required overall efficiency (fraction)	0.5334	0.5165
Overall efficiency (fraction)	0.5364	0.5195
Specific Speed	17.72	16.58
Total friction losses (w)	4.19	77.34
<u>Design Geometry</u>		
Admission (fraction)	0.2450	0.2308
Cutter diameter (in. )	0.0345	0.04925
Blade height (in. )	0.1238	0.1787
Blade-height-to-diameter ratio	3.586	3.629
Blade angle (deg)	60.0	60.0
Nozzle angle (deg)	80.0	80.0

CR-2319

TURBOALTERNATOR PARTIAL ADMISSION RADIAL IMPULSE  
DESIGN POINT COMPUTER OUTPUT

DESIGN CASE	102010103	
GAS IS HELIUM		
REFRIGERATION PWR OUT (WATTS)	0.1617E+03	PTHL
ELECTRICAL POWER OUTPUT (WATTS)	0.1617E+03	PTA
SPEED (RPM)	0.4429E+05	N
OVERALL EFFICIENCY (FRACTION)	0.5364E+00	ETATA
TEMPERATURES, PRESSURES, FLOW		
INLET TEMPERATURE (R)	0.2520E+02	TO
INLET TEMPERATURE (K)	0.1400E+02	TA
OVERALL TEMPERATURE DROP (R)	0.4020E+01	TEDR
OVERALL TEMPERATURE DROP (K)	0.2233E+01	TEDK
OUTLET TEMPERATURE EXIT (R)	0.2113E+02	T4R
OUTLET TEMPERATURE EXIT (K)	0.1177E+02	T4K
INLET PRESSURE (PSIA)	0.4135E+02	PO
INLET PRESSURE (ATM)	0.2814E+01	PA
OUTLET PRESSURE (PSIA)	0.1706E+02	P3
OUTLET PRESSURE (ATM)	0.1162E+01	PB
PRESSURE RATIO	0.2422E+01	PR
FLOW (LB/SEC)	0.3066E-01	W
FLOW (LB/HR)	0.1104E+03	WB
FLOW (G/SEC)	0.1392E+02	WA
PRIMARY DIMENSIONS		
WHEEL TIP DIAMETER (IN)	0.1300E+01	D
NUMBER OF BLADES	0.5300E+02	Z
BLADE HEIGHT (IN)	0.1238E+00	BH
BLADE HT. CUT. DIA. RATIO	0.3586E+01	BHCD
THRUST BEARING		
LOAD(LBS.),	0.3523E+00	RTL
OUTSIDE DIAMETER(IN),	0.3400E+00	DT
DIAMETER RATIO	0.6548E+00	DR
CLEAR. TO DIA. RATIO	0.7000E-03	RDGR
LOAD COEFFICIENT	0.6517E-01	RTC
BEARING NUMBER	0.8534E-01	RTN
CLEARANCE, LOADSIDE(IN)	0.5880E-03	RLC
FRICTION POWER(WATTS)	0.4394E-01	RTPL
JOURNAL BEARING		
LOAD(LBS.)	0.1762E+00	RJL
LOAD COEFFICIENT	0.8253E-01	RJC
BEARING NUMBER	0.3008E+00	RCN
CLEAR. TO DIA. RATIO	0.7391E-03	RCDR
MACHINED CLEARANCE (IN)	0.3695E-03	RMC
PIV. FILM THICK(IN)	0.3006E-03	RJMF
FRICTION POWER(WATTS)	0.1586E+00	RJPL

CR-2320-1

Figure 51. Turboalternator Partial-Admission Radial Impulse Design Point Computer Output (Design Case 102010103) (Sheet 1 of 3)

DESIGN CASE		102010103
TWO STAGE PERFORMANCE		
OTHER STAGE IN TEMP (K)	0.	TOA
TOTAL HEAT LEAK (WATTS)	0.	PHL
EXIT TEMPERATURE (K)	0.1177E+02	T4KH
SHAFT HEAT LEAK (WATTS)	0.	PHLS
HOUSE HEAT LEAK (WATTS)	0.	PHLH
GAS BEARINGS		
ROTATING ASSEMBLY WEIGHT (LBS)	0.3523E+00	RAW
ACCELERATION OF GRAVITY ("G")	0.1000E+01	ACG
TOT. BEARING FRICTION (WATTS)	0.3896E+00	PLR
PERFORMANCE TERMS		
ISENTROPIC HEAD (FT)	0.7245E+04	HS
HYDRAULIC EFF., FIRST TERM	0.6867E+00	ETAH1
HYDRAULIC EFF., SECOND TERM	0.1081E+00	ETAH2
HYDRAULIC EFF., THIRD TERM	0.6323E-04	ETAH3
TIP CLEARANCE EFF. CORRECTION	0.9921E+00	LC
TRAIL EDGE EFF. CORRECTION	0.9525E+00	LE
BLADE RE. NO. EFF. CORR.	0.1007E+01	LR
ALTERNATOR GAP FLUX (KGAUSS)	0.1589E+02	AB
ALTERNATOR CORE LOSS COEFF.	0.2542E+01	KA
ALTERNATOR COPPER LOSS COEFF.	0.7133E+02	KB
TEMPERATURE WHEEL EXIT GAS (R)	0.2108E+02	T3
TURBINE BLADE DISC VOL. FLOW (CFS)	0.1013E+00	Q3
PERFORMANCE FACTORS		
TIP SPEED TO SPOUTING VEL. RATIO	0.3681E+00	SVR
NOZZLE COEFFICIENT	0.9000E+00	PSIN
SPECIFIC SPEED	0.1772E+02	NS
SPECIFIC DIAMETER	0.3140E+01	DS
FLOW FACTOR	0.6579E+01	WSTP
WHEEL EFFICIENCY (FRACTION)	0.5503E+00	ETAW
HYDRAULIC EFFICIENCY (FRACTION)	0.5785E+00	ETAH
ELECTROMAGNET EFF. (FRACTION)	0.9900E+00	ETEM
ISENTROPIC POWER (WATTS)	0.3014E+03	PTAS
WHEEL POWER OUTPUT (WATTS)	0.1659E+03	PTRW
SHAFT POWER OUTPUT (WATTS)	0.1633E+03	PT3
PARASITIC LOSSES (WATTS)		
ALTERNATOR TOTAL EM	0.1650E+01	PLFL
TURBINE DISC FRICTION	0.1379E+01	PLDF
JOURNAL DIAM SHAFT FRICTION	0.7236E+00	PLSF
ALTERNATOR GAP FRICTION	0.4906E-01	PLGF
BEARING FRICTION	0.3896E+00	PLR
SUM ALL PARASITIC LOSSES	0.4191E+01	PLTP

CR-2320-2

Figure 51. Turboalternator Partial-Admission Radial Impulse Design Point  
Computer Output (Design Case 102010103) (Sheet 2 of 3)

## DESIGN CASE

102010103

## GEOMETRY

WHEEL TIP CLEARANCE (IN)	0.2000E-02	S
BLADE PASSAGE CUTTER DIAMETER (IN)	0.3453E-01	R
BLADE TRAILING EDGE THICKNESS (IN)	0.4000E-02	E
ADMISSION ARC (FRACTION)	0.2450E+00	ARC
ADMISSION ARC (DEGREES)	0.8819E+02	ARCD
NOZZLE ANGLE (DEGREES)	0.8000E+02	ALP2
BLADE ANGLE (DEGREES)	0.6000E+02	BP2
BLADE INCIDENCE ANGLE (DEG)	0.1322E+02	I
BLADE CHORD (IN)	0.1210E+00	C
WHEEL INSIDE DIAMETER (IN)	0.1058E+01	D3
BLADE PRESSURE SURFACE RADIUS (IN)	0.6988E-01	Y
BLADE SUCTION SURFACE RADIUS (IN)	0.3535E-01	X

TOTAL MACHINE SHAFT LENGTH (IN)	0.5050E+01	SL
JOURNAL SHAFT DIAMETER (IN)	0.5000E+00	DJ
JOURNAL FREE SHAFT LENGTH (IN)	0.3196E+01	DSL
ALTERNATOR DIAMETER (IN)	0.5000E+00	DG
ALTERNATOR MAGNET LENGTH (IN)	0.6817E+00	DM
ALTERNATOR PERIF. SPEED(F.P.S.)	0.9670E+02	APS
ALTERNATOR RADIAL GAP (IN)	0.2875E-01	G
STATOR OVERHANG (IN)	0.8625E-01	DA
STATOR LAMINATION DIA. (IN)	0.1845E+01	DL
EMPIR. ALTERNATOR DIA.(IN)	0.4856E+00	DGE
WHEEL BACK SIDE OPTIMUM GAP (IN)	0.2679E-01	GD

## VELOCITIES

SPOUING VELOCITY (FPS)	0.6830E+03	CO
WHEEL TIP SPEED(FPS)	0.2514E+03	U
NOZZLE DISCHARGE VELOCITY (FPS)	0.6147E+03	C2
BLADE INLET RELATIVE VELOCITY(FPS)	0.1115E+03	W2
BLADE INLET RADIAL VELOCITY (FPS)	0.1067E+03	V2
BLADE INLET RELATIVE MACH NUMBER	0.1774E+00	MW2

## REYNOLDS NUMBERS

BLADE PASSAGE REYNOLDS NO.	0.9120E+05	NREF
TURBINE DISC REYNOLDS NO.	0.2422E+07	NRED
JOURNAL DIAMETER REYNOLDS NO.	0.3583E+06	NREJ
ALTERNATOR GAP REYNOLDS NO.	0.1666E+06	NREG

## DRAG COEFFICIENTS

TURBINE DISC DRAG COEFF.	0.4646E-02	CMD
JOURNAL DIAMETER DRAG COEFF.	0.3634E-02	CDS
ALTERNATOR GAP MOMENT COEFF.	0.1148E-02	CDG

CR-2320-3

Figure 51. Turboalternator Partial-Admission Radial Impulse Design Point Computer Output (Design Case 102010103) (Sheet 3 of 3)

**TURBOALTERNATOR PARTIAL ADMISSION RADIAL IMPULSE  
DESIGN POINT COMPUTER OUTPUT**

DESIGN CASE		102010202
GAS IS HELIUM		
REFRIGERATION PWR OUT (WATTS)	0.8044E+03	PTHL
ELECTRICAL POWER OUTPUT (WATTS)	0.8044E+03	PTA
SPEED (RPM)	0.6911E+05	N
OVERALL EFFICIENCY (FRACTION)	0.5195E+00	ETATA
 TEMPERATURES, PRESSURES, FLOW		
INLET TEMPERATURE (R)	0.1440E+03	TO
INLET TEMPERATURE (K)	0.8000E+02	TA
OVERALL TEMPERATURE DROP (R)	0.2276E+02	TEDP
OVERALL TEMPERATURE DROP (K)	0.1264E+02	TEDK
OUTLET TEMPERATURE EXIT (R)	0.1212E+03	T4R
OUTLET TEMPERATURE EXIT (K)	0.6736E+02	T4K
 INLET PRESSURE (PSIA)		
INLET PRESSURE (ATM)	0.4177E+02	PO
OUTLET PRESSURE (PSIA)	0.2842E+01	PA
OUTLET PRESSURE (ATM)	0.1683E+02	P3
PRESSURE RATIO	0.1145E+01	PR
FLOW (LB/SEC)	0.2482E+01	PR
FLOW (LB/HR)	0.2694E-01	W
FLOW (G/SEC)	0.9698E+02	WR
	0.1223E+02	WA
 PRIMARY DIMENSIONS		
WHEEL TIP DIAMETER (IN)	0.2000E+01	D
NUMBER OF BLADES	0.5900E+02	Z
BLADE HEIGHT (IN)	0.1787E+00	BH
BLADE HT. CUT. DIA. RATIO	0.3629E+01	BHCD
 THRUST BEARING		
LOAD(LBS.),	0.2687E+01	BTL
OUTSIDE DIAMETER(IN),	0.1600E+01	DT
DIAMETER RATIO	0.6548E+00	DR
CLEAR. TO DIA. RATIO	0.6000E-03	BDCH
LOAD COEFFICIENT	0.1261E+00	RTC
BEARING NUMBER	0.5626E+00	BTN
CLEARANCE, LOADSIDE(IN)	0.1003E-02	RLC
FRICTION POWER(WATTS)	0.3054E+01	BTPL
 JOURNAL BEARING		
LOAD(LBS.)	0.1344E+01	RJL
LOAD COEFFICIENT	0.1597E+00	RJC
BEARING NUMBER	0.1284E+01	RCN
CLEAR. TO DIA. RATIO	0.7900E-03	BCDH
MACHINED CLEARANCE (IN)	0.7900E-03	PMC
PIV. FILM THICK(IN)	0.7540E-03	RJMF
FRICTION POWER(WATTS)	0.8132E+01	RJPL

CR-2321-1

**Figure 52. Turboalternator Partial-Admission Radial Impulse Design Point Computer Output (Design Case 102010202) (Sheet 1 of 3)**

DESIGN CASE	102010202	
TWO STAGE PERFORMANCE		
OTHER STAGE IN TEMP (K)	0.	TOA
TOTAL HEAT LEAK (WATTS)	0.	PHL
EXIT TEMPERATURE (K)	0.6736E+02	T4K1
SHAFT HEAT LEAK (WATTS)	0.	PHLS
HOUSG HEAT LEAK (WATTS)	0.	PHLH
GAS BEARINGS		
ROTATING ASSEMBLY WEIGHT (LBS)	0.2687E+01	RAW
ACCELERATION OF GRAVITY ("G")	0.1000E+01	ACG
TOT. BEARING FRICTION (WATTS)	0.2242E+02	PLR
PERFORMANCE TERMS		
ISENTROPIC HEAD (FT)	0.4235E+05	HS
HYDRAULIC EFF., FIRST TERM	0.6865E+00	ETAH1
HYDRAULIC EFF., SECOND TERM	0.1019E+00	ETAH2
HYDRAULIC EFF., THIRD TERM	0.6515E-04	ETAH3
TIP CLEARANCE EFF. CORRECTION	0.1007E+01	LC
TRAIL EDGE EFF. CORRECTION	0.9745E+00	LE
BLADE RE. NO. EFF. CORR.	0.9930E+00	LR
ALTERNATOR GAP FLUX (KGAUSS)	0.4719E+02	AR
ALTERNATOR CORE LOSS COEFF.	0.1528E+01	KA
ALTERNATOR COPPER LOSS COEFF.	0.6596E+01	KR
TEMPERATURE WHEEL EXIT GAS (R)	0.1191E+03	T3
TURBINE BLADE DISC VOL. FLOW (CFS)	0.5104E+00	Q3
PERFORMANCE FACTORS		
TIP SPEED TO SPOUTING VEL. RATIO	0.3655E+00	SVR
NOZZLE COEFFICIENT	0.9000E+00	PSIN
SPECIFIC SPEED	0.1658E+02	NS
SPECIFIC DIAMETER	0.3347E+01	DS
FLOW FACTOR	0.1368E+02	WSTP
WHEEL EFFICIENCY (FRACTION)	0.5695E+00	ETAH
HYDRAULIC EFFICIENCY (FRACTION)	0.5846E+00	ETAH
ELECTROMAGNET EFF. (FRACTION)	0.9730E+00	ETEM
ISENTROPIC POWER (WATTS)	0.1548E+04	PTAS
WHEEL POWER OUTPUT (WATTS)	0.8817E+03	PTRW
SHAFT POWER OUTPUT (WATTS)	0.8273E+03	PTB
PARASITIC LOSSES (WATTS)		
ALTERNATOR TOTAL F <sup>2</sup>	0.2296E+02	PLEL
TURBINE DISC FRICTION	0.1110E+02	PLDF
JOURNAL DIAM SHAFT FRICTION	0.1938E+02	PLSF
ALTERNATOR GAP FRICTION	0.1477E+01	PLGF
BEARING FRICTION	0.2242E+02	PLR
SUM ALL PARASITIC LOSSES	0.7734E+02	PLTP

CR-2321-2

Figure 52. Turboalternator Partial-Admission Radial Impulse Design Point  
Computer Output (Design Case 102010202) (Sheet 2 of 3)

## DESIGN CASE

102010202

## GEOMETRY

WHEEL TIP CLEARANCE (IN)	0.2000E-02	S
BLADE PASSAGE CUTTER DIAMETER (IN)	0.4925E-01	R
BLADE TRAILING EDGE THICKNESS (IN)	0.4000E-02	F
ADMISSION ARC (FRACTION)	0.2308E+00	ARC
ADMISSION ARC (DEGREES)	0.8308E+02	ARCD
NOZZLE ANGLE (DEGREES)	0.8000E+02	ALP2
BLADE ANGLE (DEGREES)	0.6000E+02	BP2
BLADE INCIDENCE ANGLE (DEG)	0.1330E+02	I
BLADE CHORD (IN)	0.1689E+00	C
WHEEL INSIDE DIAMETER (IN)	0.1662E+01	D3
BLADE PRESSURE SURFACE RADIUS (IN)	0.9750E-01	Y
BLADE SUCTION SURFACE RADIUS (IN)	0.4826E-01	X

TOTAL MACHINE SHAFT LENGTH (IN)	0.1000E+02	SL
JOURNAL SHAFT DIAMETER (IN)	0.1000E+01	DJ
JOURNAL FREE SHAFT LENGTH (IN)	0.6235E+01	DSH
ALTERNATOR DIAMETER (IN)	0.1000E+01	DG
ALTERNATOR MAGNET LENGTH (IN)	0.1420E+01	DM
ALTERNATOR PERIF. SPEED(F.P.S.)	0.3018E+03	APS
ALTERNATOR RADIAL GAP (IN)	0.5750E-01	G
STATOR OVERHANG (IN)	0.1725E+00	DA
STATOR LAMINATION DIA. (IN)	0.3690E+01	DL
EMPIR. ALTERNATOR DIA.(IN)	0.6657E+00	DGF
WHEEL BACK SIDE OPTIMUM GAP (IN)	0.3331E-01	GD

## VELOCITIES

SPOUTING VELOCITY (FPS)	0.1652E+04	CU
WHEEL TIP SPEED(FPS)	0.6076E+03	U
NOZZLE DISCHARGE VELOCITY (FPS)	0.1486E+04	C2
BLADE INLET RELATIVE VELOCITY(FPS)	0.2695E+03	U2
BLADE INLET RADIAL VELOCITY (FPS)	0.2581E+03	V2
BLADE INLET RELATIVE MACH NUMBER	0.1800E+00	M2

## REYNOLDS NUMBERS

BLADE PASSAGE REYNOLDS NO.	0.1797E+05	NRPF
TURBINE DISC REYNOLDS NO.	0.5101E+06	NRED
JOURNAL DIAMETER REYNOLDS NO.	0.1275E+06	NRFD
ALTERNATOR GAP REYNOLDS NO.	0.6000E+05	NREG

## DRAG COEFFICIENTS

TURBINE DISC DRAG COEFF.	0.6550E-02	CMD
JOURNAL DIAMETER DRAG COEFF.	0.4704E-02	CDS
ALTERNATOR GAP MOMENT COEFF.	0.1565E-02	CDG

CR-2321-3

Figure 52. Turboalternator Partial-Admission Radial Impulse Design Point Computer Output (Design Case 102010202) (Sheet 3 of 3)

Reproduced from  
best available copy.

The overall performance and features are shown in Table 12. Also shown are the first and last module features. A conception of an arrangement for this compressor system would be very similar to that shown in Figure 48.

The complete computer program printout of the design is shown in Figure 53 for the first and last of the three modules.

Table 12

**D-C GENERATOR REFRIGERATOR TURBOCOMPRESSOR  
DESIGN SUMMARY**

Design Case 10204001

Impeller type: centrifugal

Motor type: induction

Journal bearing type: self-acting tilting pads

Thrust bearing type: inward-pumping spiral groove

Feature	Performance			
Inlet temperature	331.4°K			
Inlet pressure	1.117 atm			
Pressure ratio	2.584			
Flow	31.27 g/sec			
Speed	48,000 rpm			
Input power	44.48 kw			
Number of modules	3			
Number of stages	6			
<u>First and Last Module Features</u>	First	Last		
Motor diameter (in.)	3.152	3.152		
Motor lamination outside diameter (in.)	7.249	7.249		
Motor power output (hp)	16.92	17.10		
Total windage loss (w)	124.8	194.1		
Total bearing friction loss (w)	367.6	430.8		
<u>First- and Last-Stage Features</u>	First	Last	First	Last
Pressure ratio	1.186	1.178	1.162	1.156
Volume flow (cfm)	402.4	343.3	212.7	183.0
Aerodynamic efficiency (fraction)	0.6792	0.6626	0.6085	0.5898
Specific speed (nondimensional)	0.05053	0.04741	0.03979	0.03772
Tip speed (fps)	1540	1540	1540	1540
Tip diameter (in.)	7.353	7.353	7.353	7.353
Tip width (in.)	0.2012	0.1880	0.1517	0.1426

CR-3333

GAS IS HELIUM

# OVERALL COMPRESSOR PERFORMANCE

INLET TEMPERATURE (K)	331.1	T4
INLET PRESSURE (ATM)	1.117	P4
OUTLET TEMPERATURE (K)	335.0	T1
OUTLET PRESSURE (ATM)	2.386	P1
PRESSURE RATIO	2.134	PRT
FLOW (G/SEC)	31.27	FLD
SPEED (RPM)	0.4300E+05	N
AIR FLOW TEMPERATURE (K)	222.0	TAMK
INPUT POWER (KW)	44.42	POWER
NUMBER OF MODULES	3.000	AMDN
CONTROL-CONTROL EFFICIENCY	0.1200	ETCC
NUMBER OF STAGES	3	M
OVERALL EFFICIENCY	0.5575	EOCS
NUMBER OF STD. WITH SAME TIP SPEED	3.000	NIDM
TIP SPEED MULTIPLIER	1.000	AKU

MODULE NO. 1

## PERFORMANCE

Reproduced from  
best available copy.

STAGE NO.	1	2	
INLET TEMPERATURE (K)	556.0	603.0	TEMP1
INLET PRESSURE (PSIA)	15.41	19.46	PRE1
OUTLET TEMPERATURE (K)	653.0	670.0	TEMP2
PRESSURE RATIO	1.176	1.178	PR
ACCU. PRESS. RATIO	1.176	1.393	PRSU
VOLUME FLOW (CFM)	402.4	343.3	Q
AERO EFFICIENCY	0.5792	0.6626	EE
SPECIFIC SPEED	0.5063E-01	0.4741E-01	ANS
AERO POWER (HP)	8.130	8.130	HP
ISOTHERMAL HEAD (FT)	0.4224E+05	0.4304E+05	HAD
TEMPERATURE RISE (K)	67.05	67.05	DT
TIP SPEED (FPS)	1540.	1540.	UT
TIP DIAMETER (IN)	7.353	7.353	DIT
RY DIAMETER (IN)	2.612	2.610	DE
HP DIAMETER (IN)	0.5330	0.5564	DHL
TIP WIDTH (IN)	0.2012	0.1880	BZIF
COOLER EFFICIENCY	0.7195	0.7413	ECF
COOLER PRESS. DROP. RATIO	0.1400E-01	0.1400E-01	OPGDP
HEAT EXCHANGER HEAT (BTU)	10.55	11.33	ATC

CR-3334-1

Figure 53. Centrifugal Compressor Design Point Computer Output  
(Case No. 10204001) (Sheet 1 of 4)

# MOTOR DESIGN

ELECTRODIA. EFF. (FR)	0.9300	EFF
DIAMETER (IN)	2.122	DC
LENGTH (IN)	3.427	DC
LAMINATIONS DIA. (IN)	7.249	DL
RADIAL GAP (IN)	0.1570E-01	DC
PERIF. SPEED (FPS)	650.1	SPS
MOTOR POWER OUTPUT (HP)	15.62	PH
MOTOR POWER LOSS (WATTS)	250.0	PHL
CONDIT-CONTROLLER LOSS (W)	11.00	PHL
CONDIT-CONT. LL. POWER (KW)	14.75	PHL

## WINDAGE LOSS LOCATES (WATTS)

JOURNAL SHAFT LENGTH	12.00	PL
MOTOR SHAFT LOSS	77.06	PL
MOTOR SHAFT GAP	35.00	PL
TOTAL WINDAGE LOSS	124.4	PL

# GAS BEARINGS DESIGN

Reproduced from  
best available copy.

## INDUST BEARING

LOAD (LBS.)	17.23	FL
OUTSIDE DIAMETER (IN)	4.000	FL
DIAMETER RATIO	0.5500	FL
CLEAR. TO DIA. RATIO	0.0007E-03	FL
LOAD COEFFICIENT	0.1010	FL
BEARING NUMBER	1.800	FL
CLEARANCE LOADS (IN)	0.2000E-02	FL
FRICTION POWER (WATTS)	20.50	FL

## JOURNAL BEARING

LOAD (LBS.)	4.517	FL
LOAD COEFFICIENT	0.2214	FL
BEARING NUMBER	2.000	FL
CLEAR. TO DIA. RATIO	0.2711E-03	FL
MACHINE CLEARANCE	0.1042E-02	FL
PIV. FIL THICK. (IN)	0.1375E-02	FL
FRICTION POWER (WATTS)	103.3	FL

CR-3334-2

Figure 53. Centrifugal Compressor Design Point Computer Output  
(Case No. 10204001) (Sheet 2 of 4)

# GAS BEARINGS

ROTATING ASSY. WEIGHT(LBS)	17.23	RAA
ACCELERATION OF GRAVITY("G")	1.000	ACG
TOT. BEARING FRICTION(WATTS)	367.6	PLF
SHAFT LENGTH (IN)	11.50	SL
JOURNAL DIA.(IN)	2.000	BJ
VISCOSITY (LB-SEC/SQ-IN)	0.3354E-02	AV

MODULE NO. 3

Reproduced from  
best available copy.

## PERFORMANCE

STAGE NO.	1	2	
INLET TEMPERATURE (R)	603.0	603.0	TEMP
INLET PRESSURE (PSIA)	31.41	36.50	PRFI
OUTLET TEMPERATURE (R)	670.0	670.0	TEMP
PRESSURE RATIO	1.162	1.156	PR
ACCEL. PRESS. RATIO	2.224	2.572	PRSU
VOLUME FLOW (CFM)	212.7	113.0	Q
AIR EFFICIENCY	0.6085	0.5203	EF
SPECIFIC SPEED	0.3779E-01	0.3772E-01	SPS
AIR POWER (HP)	8.130	8.130	P
ISOTHERMIC HEAD (FT)	0.3951E+05	0.3638E+05	HAD
TEMPERATURE RISE (R)	67.05	67.05	DT
TIP SPEED (RPS)	1540.	1540.	UT
TIP DIA. (IN)	7.353	7.353	DIT
KEY DIA. (IN)	2.270	2.270	DK
HUB DIA. (IN)	0.5280	0.5110	DHL
TIP HUB (IN)	0.1517	0.1517	DZIT
COOLER EFFECTIVENESS	0.7413	0.7413	ECF
COOLER PRESS. DROP. RATIO	0.1400E-01	0.1100E-01	PPCDP
AFTERCOLER WEIGHT (LBS)	11.33	11.33	WC

## MODULE DESIGN

ELECTRO. A. EFF. (FR)	0.9300	ETM
SHAFT (IN)	3.152	SG
CO. DIA. (IN)	3.524	SC
LA. DIA. (IN)	7.242	DL
RADIAL GAP (IN)	0.4570E-01	G
ACCEL. SP. (RPS)	660.1	APS
TOT. POWER OUTPUT (HP)	17.10	PPO
TOT. POWER LOSS (WATTS)	960.0	PLP
COOLIT-CONTROLLED LOSS (W)	1107.	CLC
COOLIT-CONTROL. IT. POWER (W)	14.91	PCP

CR-3334-3

Figure 53. Centrifugal Compressor Design Point Computer Output  
(Case No. 10204001) (Sheet 3 of 4)

# WINDAGE POWER LOSSES (WATTS)

JOURNAL FREE SHAFT LENGTH	19.26	PLSF
MOTOR END RINGS	122.7	PLTF
MOTOR MOTOR CAP	52.14	PLCF
TOTAL WINDAGE LOSS	175.1	PLWS

# GAS BEARINGS DESIGN

## THRUST BEARING

LOAD(LBS.)	16.60	RTL
OUTSIDE DIAMETER(IN)	4.000	OTD
DIAMETER RATIO	0.5500	ODR
CLEAR. TO DIA. RATIO	0.0000E-03	ODCR
LOAD COEFFICIENT	0.5120E-01	RTC
BEARING NUMBER	0.2665	RTM
CLEARANCE, LOAD SIDE(IN)	0.2000E-02	RLC
FRICTION POWER(WATTS)	31.05	RTPL

## JOURNAL BEARINGS

LOAD(LBS.)	8.302	PJL
LOAD COEFFICIENT	0.1137	PJC
BEARING NUMBER	2.000	PJM
CLEAR. TO DIA. RATIO	0.7021E-03	PJCR
WHAISTLE CLEARANCE	0.1413E-02	PJWC
PIV. FILM THICK.(IN)	0.1373E-02	PJTF
FRICTION POWER(WATTS)	134.4	PJPL

## GAS BEARINGS

ROTATING ASSY. WEIGHT(LBS)	16.60	PA
ACCELERATION OF GRAVITY("G")	1.000	AG
TOT. BEARING FRICTION(WATTS)	420.5	PLS
SHAFT LENGTH(IN)	11.55	SL
JOURNAL DIA.(IN)	2.000	DJ
VISCOSITY (LB-SEC/IN <sup>2</sup> -IN)	0.2354E-02	AV

CR-3334-4

Figure 53. Centrifugal Compressor Design Point Computer Output  
(Case No. 10204001) (Sheet 4 of 4)

Reproduced from  
best available copy.

## D-C MOTOR

### Refrigeration System for D-C Motor

Table 3 indicated that the d-c motor requires refrigeration at 4.4°K and 80°K, in addition to the withdrawal of liquid helium from the refrigerator. Table 13 is a summary of the significant computer results for the d-c motor. These results are for a single refrigerator cooling a 40,000-hp motor.

The same general trends can be observed from Table 13 as from Tables 4 and 9. The first five runs in Table 13 showed a Station 2 temperature of 14°K to result in minimum power input.

Runs 8208 and 8306 showed the effect of increasing the thermal effectiveness of the major heat exchangers from 98.5 percent to 99 percent. While the reduction in input power was significant, a 99-percent effectiveness is considered a risky design with nearly balanced-flow heat exchangers. The more conservative choice of 98.5 percent was therefore made for the remainder of the runs, including design point Run 9206.

Runs 9201 through 9206 showed the effect of increasing the pressure ratio by the addition of two more compressor stages. With only a slight penalty in input power, the heat exchanger weight was reduced by roughly a factor of two. One of the reasons for this reduction is that, with higher pressure ratios, the same amount of refrigeration can be accomplished with lower helium flow rates, resulting in smaller exchangers. In addition, smaller high-pressure-side hydraulic diameters can be used for the same pressure drop, further reducing heat exchanger size. It was felt that in the case of the d-c motor, there is good reason to pay the penalty of increased compressor weight, complexity, and cost in order to realize the benefit of greatly reduced cryosection size. Design point Run 9206 was therefore chosen from among the high-pressure ratio runs.

The series of runs beginning with Run 8301 utilizes three turbines. In contrast with the a-c generator, the addition of a third turbine did not significantly reduce either input power or heat exchanger weight because the Station 3 temperature was fixed at 80°K, and the three turbines were forced to operate at temperatures deviating considerably from optimum.

In all cases presented in Table 13, the metal-plastic laminate heat exchanger was considerably lighter and smaller than the plate-fin heat exchanger. For example, in Run 9206 the two heat exchanger weights were 206 and 356 pounds, respectively. All heat exchanger weights shown are for the lighter exchangers.

Run 9206 was chosen to represent the most favorable design. A printout of that run is shown in Figure 54. The warm and cold turbine diameters are

Table 13  
COMPUTER RESULTS -- REFRIGERATOR FOR D-C MOTOR

Run	Compressor Stages	Pressure Ratio	Turbines	Liquid Helium Withdrawal Rate (g/sec)	Refrigeration Capacity (w)				Cryogenic Heat Exchanger Effectiveness	Cryogenic Heat Exchanger Core Weight (lb)	Total Compressor Input Shaft Power (kw)
					Station 1	Station 2	Station 3	Station 4			
8202	6	2.58	2	0.11	4.63/4.4	5.0/11	106.2/80	--	0.985	605	47.9
8201	6	2.58	2	0.11	4.63/4.4	5.0/12	106.2/80	--	0.985	509	43.0
8203	6	2.58	2	0.11	4.63/4.4	5.0/13	106.2/80	--	0.985	465	39.9
8204	6	2.58	2	0.11	4.63/4.4	5.0/14	106.2/80	--	0.985	464	40.8
8205	6	2.58	2	0.11	4.63/4.4	5.0/15	106.2/80	--	0.985	--	41.9
8207(2)	6	2.58	2	0.11	4.63/4.4	5.0/14	106.2/80	--	0.985	445	39.9
8208	6	2.58	2	0.11	4.63/4.4	5.0/14	106.2/80	--	0.99	374	32.7
8210(3)	6	2.58	2	0.11	5.05/4.4	5.0/14	106.2/80	--	0.985	455	40.4
9201	8	3.51	2	0.11	4.63/4.4	5.0/14	106.2/80	--	0.985	240	41.0
9202(4)	8	3.51	2	0.11	4.63/4.4	5.0/14	106.2/80	--	0.985	235	40.7
9203(5)	8	3.51	2	0.11	5.05/4.4	5.0/14	106.2/80	--	0.985	240	41.0
9206(2)(5)	8	3.51	2	0.11	5.05/4.4	5.0/14	106.2/80	--	0.985	206	38.3
9301	6	2.65	3	0.11	4.63/4.4	5.0/14	106.2/80	0.0/120	0.985	675	39.1
8300	6	2.65	3	0.11	4.63/4.4	5.0/14	106.2/80	0.0/150	0.985	673	37.5
8303	6	2.65	3	0.11	4.63/4.4	5.0/14	106.2/80	0.0/180	0.985	--	36.9
8304	6	2.65	3	0.11	4.63/4.4	5.0/14	106.2/80	0.0/200	0.985	--	36.9
8305(2)	6	2.65	3	0.11	4.63/4.4	5.0/14	106.2/80	0.0/200	0.985	657	35.2
8306	6	2.65	3	0.11	4.63/4.4	5.0/14	106.2/80	0.0/200	0.99	626	30.1
9301	8	3.60	3	0.11	4.63/4.4	5.0/14	106.2/80	0.0/200	0.985	337	37.1

1) Results are for single refrigerator cooling a single, 40,000-hp motor.

2) Increased Turbine wheel diameters.

3) Increase Station 1 capacity to account for transients.

4) Reduced turbine wheel diameters.

5) Design point.

CR-4233

RUN NUMBER 9206

ITERATIONS \* \* \* \* \* 12

ELEMENT SEQUENCE = 6 2 2 1

LIQUID FLOW OUT OF REFRIGERATOR= 0.1100E+00 G/SEC

LOCATION	LOAD(W)	TEMP(K)	FLOW(G/SEC)
1	5.052	4.400	3.546
2	5.000	14.00	9.195
3	106.2	80.00	8.304

CYCLE DESIGN POINTS ?YES

L0C.	P(ATM)	TEMP(K)	L0C.	P(ATM)	TEMP(K)
1 1	3.800	6.214	1 2	1.180	4.406
1 3	1.174	4.400			
2 1	3.838	13.91	2 2	3.819	11.44
2 3	3.800	6.214	2 4	1.174	4.400
2 5	1.162	11.33	2 6	1.157	12.07
2 7	3.819	14.00			
3 1	3.877	77.54	3 2	3.857	65.78
3 3	3.838	13.91	3 4	1.157	12.07
3 5	1.145	64.97	3 6	1.139	72.15
3 7	3.857	80.00			
4 1	3.915	335.0	4 2	3.877	77.54
4 3	1.139	72.15	4 4	1.117	331.0

TURBOALTERNATORS ?YES

-----TURBOALTERNATORS-----

L0C.	DIA(IN)	PWR(W)	EFFIC.	RPM
2	1.300	127.7	0.5041	47970.
3	2.600	650.0	0.4892	54555.

L0C.	ADM.FRACT.	PARA.L0SS(W)	SPEC.SPD.	SPEC.DIAM.
2	0.1750	2.496	12.73	4.184
3	0.1291	54.74	8.922	5.719

L0C.	T.BRG.N0.	T.LD C0.	T.MIN F.(IN)	BRG.PWR.(W)
2	0.8987E-01	0.6405E-01	0.5880E-03	0.4515
3	0.4308	0.1247	0.1008E-02	14.33

L0C.	J.BRG.N0.	J.LD C0.	J.MIN F.(IN)	BL.HT./CUT.DIA.
2	0.3261	0.8111E-01	0.3006E-03	3.509
3	1.098	0.1579	0.7540E-03	3.325

CR-4236-1

Figure 54. Computer Results for D-C Motor (Run 9206) (Sheet 1 of 3)

SKIP HEAT EXCHANGER DESIGN ?NO

COMPOSITE HEAT EXCHANGERS ?YES

```

-----HEAT EXCHANGER DESIGN-----
LOC.   WT(LBS)   LENGTH(CM)   VOL(CU.FT.)   EFFECT
2 B      2.433      8.280      0.3712E-01      0.9849
2 U      0.5157     1.755      0.7869E-02      0.9588
3 B      44.90      53.99      0.8527          0.9850
3 U      3.408      4.479      0.6346E-01      0.9358
4 B      154.9      84.41      3.487          0.9849
TOTALS   206.1                4.448

```

FINNED-PLATE HEAT EXCHANGERS ?YES

```

-----HEAT EXCHANGER DESIGN-----
LOC.   WT(LBS)   LENGTH(CM)   VOL(CU.FT.)   EFFECT
2 B      FINNED PLATE HYDRAULIC DIA. T00 BIG
2 U      FINNED PLATE HYDRAULIC DIA. T00 BIG
3 B      79.38      453.9      1.590          0.9851
3 U      8.959      61.77      0.1647         0.9357
4 B      268.1      874.1      8.950          0.9849
TOTALS   356.5                8.705

```

CENTRIFUGAL COMPRESSOR?YES

FOR OUTPUT FOR ALL MODULES, TYPE ALL  
 FOR OUTPUT FOR FIRST AND LAST MODULE ONLY, TYPE F&L  
 ALL OR F&L ?ALL

```

-----CENTRIFUGAL COMPRESSOR-----
ISENTROPIC COMPR. POWER (KW)      23.56
TOTAL MOTOR SHAFT POWER (KW)      38.28
AMBIENT TEMPERATURE (K)           322.0
PRESSURE RATIO                     3.507
MASS FLOW (G/SEC)                  21.05
SUPPLY LINE DEL P/P                0.
RETURN LINE DEL P/P                0.

```

```

MODULE SHAFT PWR (KW)   RPM      MOT.SPD.(FPS)
1      9.531      0.5000E+05      667.6
2      9.555      0.5000E+05      667.6
3      9.583      0.5000E+05      667.6
4      9.613      0.5000E+05      667.6

```

CR-4236-2

Figure 54. Computer Results for D-C Motor (Run 9206) (Sheet 2 of 3)

## AERODYNAMICS

STAGE	SP.SPEED	AERØ.EFF.	TIP SPD(FPS)	DIA. (IN)
1	0.4163E-01	0.6236	1644.	7.536
2	0.3925E-01	0.6038	1644.	7.536
3	0.3701E-01	0.5829	1644.	7.536
4	0.3498E-01	0.5619	1644.	7.536
5	0.3322E-01	0.5418	1644.	7.536
6	0.3164E-01	0.5225	1644.	7.536
7	0.3023E-01	0.5038	1644.	7.536
8	0.2895E-01	0.4858	1644.	7.536

STAGE	PRESS.RATIO	COØL.EFFCTV.
1	1.196	0.7473
2	1.186	0.7654
3	1.179	0.7654
4	1.171	0.7654
5	1.165	0.7654
6	1.158	0.7654
7	1.151	0.7654
8	1.145	0.7654

## BEARINGS

MØDULE	T.BRG.NØ.	T.LD.CØ.	T.MIN F.(IN)	BRG.PWR.(W)
1	3.454	0.6277E-01	0.1764E-02	194.4
2	2.487	0.4365E-01	0.1764E-02	211.4
3	1.823	0.3121E-01	0.1764E-02	229.2
4	1.367	0.2291E-01	0.1764E-02	248.2

MØDULE	J.BRG.NØ.	J.LD.CØ.	J.MIN F.(IN)
1	1.646	0.2301	0.1223E-02
2	1.646	0.1600	0.1223E-02
3	1.646	0.1144	0.1223E-02
4	1.646	0.8399E-01	0.1223E-02

CR-4236-3

Figure 54. Computer Results for D-C Motor (Run 9206) (Sheet 3 of 3)

1.3 and 2.6 inches, and the shaft speeds are 48,000 and 54,600 rpm, respectively. Turboalternator efficiencies are in the 49- to 50-percent range.

The centrifugal compressor consists of four modules, each with a motor and two centrifugal impellers. Impeller diameters are about 7.5 inches, and shaft speeds are 50,000 rpm.

### Turboalternators for D-C Motor

Both of the turboalternator designs for the d-c motor refrigerator were examined to find satisfactory operating speeds and geometries to satisfy

cycle requirements. Cycle Study Computer Run 9206 established the turbo-alternator requirements listed in Table 14.

Table 14  
TURBOALTERNATOR REQUIREMENTS

Inputs and Results	Inlet Temperature	
	14.0°K	80.0°K
<u>Inputs</u>		
Inlet pressure (atm)	3.819	3.857
Outlet pressure (atm)	1.162	1.145
Mass flow (g/sec)	9.195	8.304
<u>Results</u>		
Refrigerator power output (w)	127.7	650.0
Overall refrigerator efficiency (fraction)	0.5041	0.4892
Wheel tip diameter (in.)	1.30	2.60
Admission arc (fraction)	0.1750	0.1291
Speed (rpm)	47,970	54,555

Also shown in Table 14 are principal turboalternator design results from the cycle run. The two power outputs and overall efficiencies must be achieved for the conditions of the cycle points. These turboalternators, of course, were not optimized in the cycle study; hence the wheel tip diameter, admission, and speed are shown only for reference purposes.

Complete partial-admission turboalternator preliminary design studies were conducted for both of the stages for the required cycle conditions. The best operating geometries were established. Design summary results are shown in Table 15. Complete design computer result listings are shown in Figures 55 and 56.

#### Compressors for D-C Motor

For this refrigerator, the cycle study resulted in the requirement for four compressor modules with two centrifugal compressor stages on each end of the rotor.

The overall performance and features are shown in Table 16. Also shown are the first and last module features. A conception of an arrangement for this compressor system would be very similar to that shown for the three module arrangement shown in Figure 48, but with the addition of one more module.

Table 15

**TURBOALTERNATOR DESIGN SUMMARY  
FOR D-C MOTOR REFRIGERATOR**

( Turbine type: partial admission, radial impulse  
Load alternator type: permanent magnet  
Journal-bearing type: self-acting tilting pads  
Thrust-bearing type: inward pumping, spiral groove )

Design Parameters	Model and Inlet Temperature	
	Big Bertha (14°K)	Giant Grizzly (80°K)
Total refrigeration power outputs (w)	143.6	762.3
Design speed (rpm)	48,340	55,340
Maximum speed (rpm)	200,000	200,000
<u>Principal Dimensions</u>		
Journal bearing span (in.)	3.82	7.64
Journal and magnet diameter (in.)	0.50	1.00
Thrust bearing outside diameter (in.)	0.84	1.68
Magnet length (in.)	0.705	1.410
<u>Performance Factors</u>		
Inlet temperature (°R)	25.2	144.0
Inlet temperature (°K)	14.0	80.0
Inlet pressure (psia)	56.12	56.68
Outlet pressure (psia)	17.08	16.83
Pressure ratio	3.287	3.369
Mass flow (lb/hr)	80.72	75.41
Turbine run number	920301006	920302006
Wheel diameter (in.)	1.30	2.60
Electromagnetic efficiency (fraction)	0.992	0.959
Number of blades	67	91
Cycle required overall efficiency (fraction)	0.5041	0.4892
Overall efficiency (fraction)	0.5128	0.5016
Specific speed	13.47	9.66
Total friction losses (w)	4.45	80.88
<u>Design Geometry</u>		
Admission (fraction)	0.1844	0.1384
Cutter diameter (in.)	0.0265	0.0409
Blade height (in.)	0.09754	0.1451
Blade-height-to-diameter ratio	3.684	3.548
Blade angle (deg)	60.0	60.0
Nozzle angle (deg)	80.0	80.0

CR-2322

TURBOALTERNATOR PARTIAL ADMISSION RADIAL IMPULSE  
DESIGN POINT COMPUTER OUTPUT

DESIGN CASE		920301006
GAS IS HELIUM		
REFRIGERATION PWR OUT (WATTS)	0.1436E+03	PTHL
ELECTRICAL POWER OUTPUT (WATTS)	0.1436E+03	PTA
SPEED (RPM)	0.4834E+05	N
OVERALL EFFICIENCY (FRACTION)	0.5127E+00	FIATA
TEMPERATURES, PRESSURES, FLOW		
INLET TEMPERATURE (R)	0.2520E+02	T0
INLET TEMPERATURE (K)	0.1400E+02	TA
OVERALL TEMPERATURE DROP (R)	0.4883E+01	TFDP
OVERALL TEMPERATURE DROP (K)	0.2713E+01	TEOK
OUTLET TEMPERATURE EXIT (R)	0.2032E+02	TDR
OUTLET TEMPERATURE EXIT (K)	0.1120E+02	TK
INLET PRESSURE (PSIA)	0.5612E+02	P0
INLET PRESSURE (ATM)	0.3810E+01	PA
OUTLET PRESSURE (PSIA)	0.1703E+02	P2
OUTLET PRESSURE (ATM)	0.1162E+01	PA
PRESSURE RATIO	0.3267E+01	PR
FLOW (LB/SEC)	0.2242E+01	W
FLOW (LB/HR)	0.2072E+02	W
FLOW (G/SEC)	0.1013E+02	W
PRIMARY DIMENSIONS		
WHEEL TIP DIAMETER (IN)	0.1200E+01	D
NUMBER OF BLADES	0.6700E+02	Z
BLADE HEIGHT (IN)	0.0754E+01	H
BLADE HT. OUT. DIA. RATIO	0.3684E+01	H/D
THRUST BEARING		
LOAD(LBS.),	0.3407E+01	BT
OUTSIDE DIAMETER(IN),	0.3403E+00	BT
DIAMETER RATIO	0.6543E+00	BT
CLEAR. TO DIA. RATIO	0.7000E-02	BT
LOAD COEFFICIENT	0.463E-01	BT
BEARING NUMBER	0.0053E+01	BT
CLEARANCE, LOADSIDE(IN)	0.5390E-03	BT
FRICTION POWER(WATTS)	0.5088E-01	BTPL
JOURNAL BEARING		
LOAD(LBS.)	0.1740E+00	JBL
LOAD COEFFICIENT	0.3192E-01	JBC
BEARING NUMBER	0.3200E+00	JBN
CLEAR. TO DIA. RATIO	0.7382E-02	JBC
MACHINED CLEARANCE (IN)	0.2691E-03	JBC
PIV. FILM THICK(IN)	0.3005E-02	JBC
FRICTION POWER(WATTS)	0.1375E-01	JBPL

Reproduced from  
best available copy.

CR-2323-1

Figure 55. Turboalternator Partial-Admission Radial Impulse Design Point Computer Output (Design Case 920301006) (Sheet 1 of 3)

DESIGN CASE		920301006
TWO STAGE PERFORMANCE		
OTHER STAGE IN TEMP (K)	0.	TOA
TOTAL HEAT LEAK (WATTS)	0.	PHL
EXIT TEMPERATURE (K)	0.1129E+02	T4KH
SHAFT HEAT LEAK (WATTS)	0.	PHLS
HOUSG HEAT LEAK (WATTS)	0.	PHLH
GAS BEARINGS		
ROTATING ASSEMBLY WEIGHT (LBS)	0.3497E+00	RAW
ACCELERATION OF GRAVITY ("G")	0.1000E+01	ACG
TOT. BEARING FRICTION (WATTS)	0.4589E+00	PLP
PERFORMANCE TERMS		
ISENTROPIC HEAD (FT)	0.9209E+04	HS
HYDRAULIC EFF., FIRST TERM	0.6796E+00	ETAH1
HYDRAULIC EFF., SECOND TERM	0.1051E+00	ETAH2
HYDRAULIC EFF., THIRD TERM	0.6989E-04	ETAH3
TIP CLEARANCE EFF. CORRECTION	0.9744E+00	LC
TRAIL EDGE EFF. CORRECTION	0.9336E+00	LE
BLADE RE. NO. EFF. CORR.	0.1006E+01	LR
ALTERNATOR GAP FLUX (KGAUSS)	0.1370E+02	AR
ALTERNATOR CORE LOSS COEFF.	0.2542E+01	KA
ALTERNATOR COPPER LOSS COEFF.	0.7133E+02	KR
TEMPERATURE WHEEL EXIT GAS (R)	0.2017E+02	T3
TURBINE BLADE DISC VOL. FLOW (CFS)	0.7090E-01	Q3
PERFORMANCE FACTORS		
TIP SPEED TO SPOUTING VEL. RATIO	0.3564E+00	SVR
NOZZLE COEFFICIENT	0.9000E+00	PSIN
SPECIFIC SPEED	0.1347E+02	NS
SPECIFIC DIAMETER	0.3986E+01	DS
FLOW FACTOR	0.3545E+01	WSTP
WHEEL EFFICIENCY (FRACTION)	0.5286E+00	ETAW
HYDRAULIC EFFICIENCY (FRACTION)	0.5743E+00	ETAH
ELECTROMAGNET EFF. (FRACTION)	0.9920E+00	ETEM
ISENTROPIC POWER (WATTS)	0.2802E+03	PTAS
WHEEL POWER OUTPUT (WATTS)	0.1481E+03	PTRW
SHAFT POWER OUTPUT (WATTS)	0.1448E+03	PTR
PARASITIC LOSSES (WATTS)		
ALTERNATOR TOTAL FM	0.1168E+01	PLFL
TURBINE DISC FRICTION	0.1809E+01	PLDF
JOURNAL DIAM SHAFT FRICTION	0.9590E+00	PLSF
ALTERNATOR GAP FRICTION	0.5912E-01	PLGF
BEARING FRICTION	0.4589E+00	PLR
SUM ALL PARASITIC LOSSES	0.4454E+01	PLTP

CR-2323-2

Figure 55. Turboalternator Partial-Admission Radial Impulse Design Point  
Computer Output (Design Case 920301006) (Sheet 2 of 3)

## DESIGN CASE

920301006

## GEOMETRY

WHEEL TIP CLEARANCE (IN)	0.2000E-02	S
BLADE PASSAGE CUTTER DIAMETER (IN)	0.2648E-01	R
BLADE TRAILING EDGE THICKNESS (IN)	0.4000E-02	E
ADMISSION ARC (FRACTION)	0.1844E+00	ARC
ADMISSION ARC (DEGREES)	0.6638E+02	ARCD
NOZZLE ANGLE (DEGREES)	0.8000E+02	ALP2
BLADE ANGLE (DEGREES)	0.6000E+02	BP2
BLADE INCIDENCE ANGLE (DEG)	0.1357E+02	I
BLADE CHORD (IN)	0.9765E-01	C
WHEEL INSIDE DIAMETER (IN)	0.1105E+01	D3
BLADE PRESSURE SURFACE RADIUS (IN)	0.5638E-01	Y
BLADE SUCTION SURFACE RADIUS (IN)	0.2990E-01	X

TOTAL MACHINE SHAFT LENGTH (IN)	0.5050E+01	SL
JOURNAL SHAFT DIAMETER (IN)	0.5000E+00	DJ
JOURNAL FREE SHAFT LENGTH (IN)	0.3243E+01	DSH
ALTERNATOR DIAMETER (IN)	0.5000E+00	DG
ALTERNATOR MAGNET LENGTH (IN)	0.6342E+00	DM
ALTERNATOR PERIF. SPEED(F.P.S.)	0.1055E+03	APS
ALTERNATOR RADIAL GAP (IN)	0.2875E-01	G
STATOR OVERHANG (IN)	0.8625E-01	DA
STATOR LAMINATION DIA. (IN)	0.1845E+01	DL
EMPIR. ALTERNATOR DIA.(IN)	0.4571E+00	DGE
WHEEL BACK SIDE OPTIMUM GAP (IN)	0.2738E-01	GD

## VELOCITIES

SPOUTING VELOCITY (FPS)	0.7701E+03	C0
WHEEL TIP SPEED(FPS)	0.2744E+03	U
NOZZLE DISCHARGE VELOCITY (FPS)	0.6931E+03	C2
BLADE INLET RELATIVE VELOCITY(FPS)	0.1255E+03	W2
BLADE INLET RADIAL VELOCITY (FPS)	0.1204E+03	V2
BLADE INLET RELATIVE MACH NUMBER	0.2038E+00	MW2

## REYNOLDS NUMBERS

BLADE PASSAGE REYNOLDS NO.	0.8514E+05	NREP
TURBINE DISC REYNOLDS NO.	0.2843E+07	NRED
JOURNAL DIAMETER REYNOLDS NO.	0.4206E+06	NREJ
ALTERNATOR GAP REYNOLDS NO.	0.1979E+05	NREG

## DRAG COEFFICIENTS

TURBINE DISC DRAG COEFF.	0.4485E-02	CD0
JOURNAL DIAMETER DRAG COEFF.	0.3401E-02	CDJ
ALTERNATOR GAP MOMENT COEFF.	0.1094E-02	CDG

CR-2323-3

Figure 55. Turboalternator Partial-Admission Radial Impulse Design Point  
Computer Output (Design Case 920301006) (Sheet 3 of 3)

Reproduced from  
best available copy.

TURBOALTERNATOR PARTIAL ADMISSION RADIAL IMPULSE  
DESIGN POINT COMPUTER OUTPUT

DESIGN CASE		920302006
GAS IS HELIUM		
REFRIGERATION PWR OUT (WATTS)	0.7623E+03	PTHL
ELECTRICAL POWER OUTPUT (WATTS)	0.7623E+03	PTA
SPEED (RPM)	0.5534E+05	N
OVERALL EFFICIENCY (FRACTION)	0.5016E+00	ETATA
TEMPERATURES, PRESSURES, FLOW		
INLET TEMPERATURE (R)	0.1440E+03	TO
INLET TEMPERATURE (K)	0.8000E+02	TA
OVERALL TEMPERATURE DROP (R)	0.2774E+02	TEDR
OVERALL TEMPERATURE DROP (K)	0.1541E+02	TEDK
OUTLET TEMPERATURE EXIT (R)	0.1163E+03	T4R
OUTLET TEMPERATURE EXIT (K)	0.6459E+02	T4K
INLET PRESSURE (PSIA)	0.5668E+02	PO
INLET PRESSURE (ATM)	0.3857E+01	PA
OUTLET PRESSURE (PSIA)	0.1683E+02	P3
OUTLET PRESSURE (ATM)	0.1145E+01	PB
PRESSURE RATIO	0.3369E+01	PR
FLOW (LB/SEC)	0.2095E+01	W
FLOW (LB/HR)	0.7541E+02	WR
FLOW (G/SEC)	0.9510E+01	WA
PRIMARY DIMENSIONS		
WHEEL TIP DIAMETER (IN)	0.2600E+01	D
NUMBER OF BLADES	0.9100E+02	Z
BLADE HEIGHT (IN)	0.1451E+00	BH
BLADE HT. CUT. DIA. RATIO	0.3548E+01	BHCD
THRUST BEARING		
LOAD(LBS.),	0.2695E+01	RTL
OUTSIDE DIAMETER(IN),	0.1630E+01	DT
DIAMETER RATIO	0.6548E+00	DR
CLEAR. TO DIA. RATIO	0.6000E-03	RDOR
LOAD COEFFICIENT	0.1265E+00	RTC
BEARING NUMBER	0.4364E+00	RTN
CLEARANCE, LOADSIDE(IN)	0.1008E-02	RLC
FRICTION POWER(WATTS)	0.1897E+01	RTPL
JOURNAL BEARING		
LOAD(LBS.)	0.1347E+01	RJL
LOAD COEFFICIENT	0.1601E+00	RJC
BEARING NUMBER	0.1110E+01	RCN
CLEAR. TO DIA. RATIO	0.7606E-03	RCOR
MACHINED CLEARANCE (IN)	0.7606E-03	RJC
PIV. FILM THICK(IN)	0.7540E-03	RJMF
FRICTION POWER(WATTS)	0.5452E+01	RJPL

Reproduced from  
best available copy.

CR-2324-1

Figure 56. Turboalternator Partial-Admission Radial Impulse Design Point Computer Output (Design Case 920302006) (Sheet 1 of 3)

DESIGN CASE	920302006	
TWO STAGE PERFORMANCE		
OTHER STAGE IN TEMP (K)	0.	TOA
TOTAL HEAT LEAK (WATTS)	0.	PHL
EXIT TEMPERATURE (K)	0.6459E+02	T4KH
SHAFT HEAT LEAK (WATTS)	0.	PHLS
HOUSG HEAT LEAK (WATTS)	0.	PHLH
GAS BEARINGS		
ROTATING ASSEMBLY WEIGHT (LBS)	0.2695E+01	RAW
ACCELERATION OF GRAVITY ("G")	0.1000E+01	ACG
TOT. BEARING FRICTION (WATTS)	0.1473E+02	PLR
PERFORMANCE TERMS		
ISENTROPIC HEAD (FT)	0.5347E+05	HS
HYDRAULIC EFF., FIRST TERM	0.6674E+00	ETAH1
HYDRAULIC EFF., SECOND TERM	0.9028E-01	ETAH2
HYDRAULIC EFF., THIRD TERM	0.7345E-04	ETAH3
TIP CLEARANCE EFF. CORRECTION	0.9990E+00	LC
TRAIL EDGE EFF. CORRECTION	0.9691E+00	LE
BLADE RE. NO. EFF. CORR.	0.9931E+00	LR
ALTERNATOR GAP FLUX (KGAUSS)	0.5781E+02	AB
ALTERNATOR CORE LOSS COEFF.	0.1528E+01	KA
ALTERNATOR COPPER LOSS COEFF.	0.6596E+01	KR
TEMPERATURE WHEEL EXIT GAS (R)	0.1133E+03	T3
TURBINE BLADE DISC VOL. FLOW (CFS)	0.3779E+00	Q3
PERFORMANCE FACTORS		
TIP SPEED TO SPOUTING VEL. RATIO	0.3386E+00	SVR
NOZZLE COEFFICIENT	0.9000E+00	PSIN
SPECIFIC SPEED	0.9660E+01	NS
SPECIFIC DIAMETER	0.5360E+01	DS
FLOW FACTOR	0.7839E+01	WSTP
WHEEL EFFICIENCY (FRACTION)	0.5548E+00	ETAW
HYDRAULIC EFFICIENCY (FRACTION)	0.5771E+00	ETAH
ELECTROMAGNET EFF. (FRACTION)	0.9590E+00	ETEM
ISENTROPIC POWER (WATTS)	0.1520E+04	PTAS
WHEEL POWER OUTPUT (WATTS)	0.8432E+03	PTRW
SHAFT POWER OUTPUT (WATTS)	0.7964E+03	PTR
PARASITIC LOSSES (WATTS)		
ALTERNATOR TOTAL EM	0.3405E+02	PLEL
TURBINE DISC FRICTION	0.2043E+02	PLDF
JOURNAL DIAM SHAFT FRICTION	0.1086E+02	PLSF
ALTERNATOR GAP FRICTION	0.8218E+00	PLGF
BEARING FRICTION	0.1473E+02	PLR
SUM ALL PARASITIC LOSSES	0.8088E+02	PLTP

CR-2324-2

Figure 56. Turboalternator Partial-Admission Radial Impulse Design Point  
Computer Output (Design Case 920302006) (Sheet 2 of 3)

## DESIGN CASE

920302006

## GEOMETRY

WHEEL TIP CLEARANCE (IN)	0.2000E-02	S
BLADE PASSAGE CUTTER DIAMETER (IN)	0.4088E-01	R
BLADE TRAILING EDGE THICKNESS (IN)	0.4000E-02	E
ADMISSION ARC (FRACTION)	0.1384E+00	ARC
ADMISSION ARC (DEGREES)	0.4981E+02	ARCD
NOZZLE ANGLE (DEGREES)	0.8000E+02	ALP2
BLADE ANGLE (DEGREES)	0.6000E+02	BP2
BLADE INCIDENCE ANGLE (DEG)	0.1407E+02	I
BLADE CHORD (IN)	0.1467E+00	C
WHEEL INSIDE DIAMETER (IN)	0.2307E+01	D3
BLADE PRESSURE SURFACE RADIUS (IN)	0.8470E-01	Y
BLADE SUCTION SURFACE RADIUS (IN)	0.4382E-01	X

TOTAL MACHINE SHAFT LENGTH (IN)	0.1000E+02	SL
JOURNAL SHAFT DIAMETER (IN)	0.1000E+01	DJ
JOURNAL FREE SHAFT LENGTH (IN)	0.6251E+01	DSH
ALTERNATOR DIAMETER (IN)	0.1000E+01	DG
ALTERNATOR MAGNET LENGTH (IN)	0.1404E+01	DM
ALTERNATOR PERIF. SPEED(F.P.S.)	0.2417E+03	APS
ALTERNATOR RADIAL GAP (IN)	0.5750E-01	G
STATOR OVERHANG (IN)	0.1725E+00	DA
STATOR LAMINATION DIA. (IN)	0.3690E+01	DL
EMPIR. ALTERNATOR DIA.(IN)	0.6995E+00	DGE
WHEEL BACK SIDE OPTIMUM GAP (IN)	0.4564E-01	GD

## VELOCITIES

SPRUITING VELOCITY (FPS)	0.1856E+04	CO
WHEEL TIP SPEED(FPS)	0.6283E+03	U
NOZZLE DISCHARGE VELOCITY (FPS)	0.1670E+04	C2
BLADE INLET RELATIVE VELOCITY(FPS)	0.3016E+03	W2
BLADE INLET RADIAL VELOCITY (FPS)	0.2900E+03	V2
BLADE INLET RELATIVE MACH NUMBER	0.2107E+00	MW2

## REYNOLDS NUMBERS

BLADE PASSAGE REYNOLDS NO.	0.1801E+05	NRER
TURBINE DISC REYNOLDS NO.	0.7485E+06	NRED
JOURNAL DIAMETER REYNOLDS NO.	0.1107E+06	NREJ
ALTERNATOR GAP REYNOLDS NO.	0.5210E+05	NREG

## DRAG COEFFICIENTS

TURBINE DISC DRAG COEFF.	0.6019E-02	CDT
JOURNAL DIAMETER DRAG COEFF.	0.4873E-02	CDS
ALTERNATOR GAP MOMENT COEFF.	0.1633E-02	CDG

CR-2324-3

Figure 56. Turboalternator Partial-Admission Radial Impulse Design Point  
Computer Output (Design Case 920302006) (Sheet 3 of 3)

Table 16

**TURBOCOMPRESSOR DESIGN SUMMARY  
FOR D-C MOTOR REFRIGERATOR**

Design Case 9206001  
Impeller type: centrifugal  
Motor type: induction  
Journal bearing type: self-acting tilting pads  
Thrust bearing type: inward-pumping spiral groove

Feature	Performance			
Inlet temperature	331.0°K			
Inlet pressure	1.117 atm			
Pressure ratio	3.507			
Flow	21.05 g/sec			
Speed	50,000 rpm			
Input power	50.98 kw			
Number of modules	4			
Number of stages	8			
<u>First and Last Module Features</u>	<u>First</u>		<u>Last</u>	
Motor Diameter (in. )	3.041		3.041	
Motor lamination outside diameter (in. )	6.993		6.993	
Motor power output (hp)	14.42		14.90	
Total windage loss (w)	172.9		342.5	
Total bearing friction loss (w)	1244		1431	
<u>First- and Last-Stage Features</u>	<u>First</u>	<u>Last</u>	<u>First</u>	<u>Last</u>
Pressure ratio	1.196	1.187	1.152	1.146
Volume flow (cfm)	270.8	229.1	103.5	89.8
Aerodynamic efficiency (fraction)	0.6227	0.6029	0.5025	0.4845
Specific speed (nondimensional)	0.04152	0.03914	0.03013	0.02886
Tip speed (fps)	1647	1647	1647	1647
Tip diameter (in. )	7.551	7.551	7.551	7.551
Tip width (in. )	0.1633	0.1515	0.1128	0.1074

CR-3335

The complete computer program printout is shown in Figure 57 for the first and last of the four modules.

GAS IS HELIUM  
OVERALL COMPRESSOR PERFORMANCE

INLET TEMPERATURE (K)	331.0	14
INLET PRESSURE (ATM)	1.117	P4
OUTLET TEMPERATURE (K)	335.0	11
OUTLET PRESSURE (ATM)	3.917	P1
PRESSURE RATIO	3.507	PR1
FLW (G/SEC)	21.05	FL0
SPEED (RPM)	0.5000E+05	N
AMBIENT TEMPERATURE (K)	322.0	TAMB
INPUT POWER (KW)	50.98	POWER
NUMBER OF MODULES	4.000	AMDN
CONDIT-CONTROL EFFICIENCY	0.9200	EICC
NUMBER OF STAGES	8	M
OVERALL EFFICIENCY	0.4618	ECCS
NUMBER OF MOD. WITH SAME TIP SPEED	4.000	NIDM
TIP SPEED MULTIPLIER	1.000	AKU

MODULE NO. 1

PERFORMANCE

STAGE NO.	1	2	
INLET TEMPERATURE (K)	595.8	603.0	TFMI
INLET PRESSURE (PSIA)	16.41	19.63	PREI
OUTLET TEMPERATURE (K)	672.5	679.7	TEMD
PRESSURE RATIO	1.196	1.187	PR
ACCUM. PRESS. RATIO	1.196	1.420	PRSU
VOLUME FLOW (CFM)	270.8	229.1	Q
AERO EFFICIENCY	0.6227	0.6029	EF
SPECIFIC SPEED	0.4152E-01	0.3914E-01	ANS
AERO POWER (HP)	6.263	6.263	HP
ISENTHROPIC HEAD (FT)	0.4630E+05	0.4480E+05	HAD
TEMPERATURE RISE (K)	76.72	76.72	DT
TIP SPEED (FPS)	1647.	1647.	U1
TIP DIAMETER (IN)	7.551	7.551	D11
EYE DIAMETER (IN)	2.379	2.308	DE
HUB DIAMETER (IN)	0.5307	0.5954	DHL
TIP WIDTH (IN)	0.1633	0.1515	HZ11
COOLER EFFECTIVENESS	0.7482	0.7663	ECT
COOLER PRESS. DROP. RATIO	0.1400E-01	0.1400E-01	DPCOP
AFTERCoolER WEIGHT (LBS)	7.803	8.293	WTC

CR-3336-1

Figure 57. Centrifugal Compressor Design Point Computer Output  
(Case No. 9206001) (Sheet 1 of 4)

# MOTOR DESIGN

ELECTROMAG. EFF. (FR)	0.9300	EIM
DIAMETER (IN)	3.041	DF
LENGTH (IN)	3.207	DM
LAMINATION Ø.DIA.(IN)	6.993	DL
RADIAL GAP (IN)	0.4409E-01	G
PERIF. SPEED (FPS)	663.3	APS
MOTOR POWER OUTPUT (HP)	14.42	PMO
MOTOR POWER LOSS (WATTS)	809.8	PHLM
CONDIT-CONTROLLER LOSS (W)	1006.	PHLC
CONDIT-CONTR. IN. POWER(KW)	12.58	PCG

# WINDAGE POWER LOSSES (WATTS)

JOURNAL FREE SHAFT LENGTH	67.04	PLSF
MOTOR END RINGS	73.21	PLEF
MOTOR ROTOR GAP	32.66	PLGF
TOTAL WINDAGE LOSS	172.9	PLWS

# GAS BEARINGS DESIGN

Reproduced from  
best available copy.

## THRUST BEARING

LOAD(LBS.)	32.56	PIL
ØUTSIDE DIAMETER(IN)	4.500	DIH
DIAMETER RATIO	0.7333	DR
CLEAR. TO DIA. RATIO	0.3300E-03	PDCK
LOAD COEFFICIENT	0.2256	PLC
BEARING NUMBER	2.854	RIN
CLEARANCE, LOADSIDE(IN)	0.1485E-02	RLC
FRICTION POWER(WATTS)	148.8	RIPL

## JOURNAL BEARING

LOAD(LBS.)	16.28	FJL
LOAD COEFFICIENT	0.1843	FJC
BEARING NUMBER	2.000	FCN
CLEAR. TO DIA. RATIO	0.9913E-03	FCDK
MACHINED CLEARANCE	0.2974E-02	FMC
PIV. FILM THICK.(IN)	0.1582E-02	FIMP
FRICTION POWER(WATTS)	474.9	FJPL

## GAS BEARINGS

ROTATING ASSY. WEIGHT(LBS)	32.56	RAW
ACCELERATION OF GRAVITY("G")	1.000	ACC
TOT. BEARING FRICTION(WATTS)	1244.	PLF
SHAFT LENGTH (IN)	13.86	SL
JOURNAL DIA.(IN)	3.000	DJ
VISCOSITY (LP-SEC/SQ-IN)	0.3385E-08	MJ

CR-3336-2

Figure 57. Centrifugal Compressor Design Point Computer Output  
(Case No. 9206001) (Sheet 2 of 4)

PERFORMANCE

STAGE NO.	1	2	
INLET TEMPERATURE (K)	603.0	603.0	ITEM1
INLET PRESSURE (PSIA)	43.47	50.07	PREI
OUTLET TEMPERATURE (K)	679.7	679.7	ITEMD
PRESSURE RATIO	1.152	1.146	PR
ACCUM. PRESS. RATIO	3.051	3.496	PRSU
VOLUME FLOW (CFM)	103.5	89.82	Q
AERO EFFICIENCY	0.5025	0.4845	FF
SPECIFIC SPEED	0.3013E-01	0.2886E-01	ANS
AERO POWER (HP)	6.263	6.263	HP
ISENTROPIC HEAD (FT)	0.3738E+05	0.3603E+05	HAD
TEMPERATURE RISE (K)	76.72	76.72	DT
TIP SPEED (FPS)	1647.	1647.	UT
TIP DIAMETER (IN)	7.551	7.551	DI1
EYE DIAMETER (IN)	1.985	1.946	DE
HUB DIAMETER (IN)	0.5311	0.5540	DHL
TIP WIDTH (IN)	0.1128	0.1074	HZ11
COOLER EFFECTIVENESS	0.7663	0.7663	EC1
COOLER PRESS. DROP. RATIO	0.1400E-01	0.1400E-01	DPCOP
AFTERCooler WEIGHT (LBS)	8.293	8.293	WTC

MOTOR DESIGN

ELECTROMAG. EFF. (FR)	0.9300	EIM
DIAMETER (IN)	3.041	DC
LENGTH (IN)	3.312	DM
LAMINATION O.DIA.(IN)	6.993	DL
RADIAL GAP (IN)	0.4409E-01	G
PERIF. SPEED (FPS)	663.3	AFS
MOTOR POWER OUTPUT (HP)	14.90	PMO
MOTOR POWER LOSS (WATTS)	836.6	PHLM
CONDIT-CONTROLLER LOSS (W)	1039.	PHLC
CONDIT-CONTR. IN. POWER(KW)	12.99	PCC

WINDAGE POWER LOSSES (WATTS)

JOURNAL FREE SHAFT LENGTH	135.7	PLSF
MOTOR END RINGS	146.8	PLEF
MOTOR ROTOR GAP	59.98	PLGF
TOTAL WINDAGE LOSS	342.5	PLWS

CR-3336-3

Figure 57. Centrifugal Compressor Design Point Computer Output  
(Case No. 9206001) (Sheet 3 of 4)

Reproduced from  
best available copy.

## GAS BEARINGS DESIGN

### THRUST BEARING

LOAD(LBS.)	31.91	RIL
OUTSIDE DIAMETER(IN)	4.500	DIH
DIAMETER RATIO	0.7333	DR
CLEAR. 10 DIA. RATIO	0.3300E-03	PDGR
LOAD COEFFICIENT	0.8669E-01	RIC
BEARING NUMBER	1.127	RIN
CLEARANCE, LOADSIDE(IN)	0.1485E-02	RLC
FRICTION POWER(WATTS)	149.8	RIPL

### JOURNAL BEARING

LOAD(LBS.)	15.95	RJL
LOAD COEFFICIENT	0.7081E-01	RJC
BEARING NUMBER	2.000	PCN
CLEAR. 10 DIA. RATIO	0.6208E-03	PCDR
MACHINED CLEARANCE	0.1862E-02	RMC
PIV. FILM THICK.(IN)	0.1582E-02	PJMF
FRICTION POWER(WATTS)	567.3	RJPL

### GAS BEARINGS

ROTATING ASSY. WEIGHT(LBS)	31.91	RAW
ACCELERATION OF GRAVITY("G")	1.000	ACG
TOT. BEARING FRICTION(WATTS)	1431.	PLR
SHAFT LENGTH (IN)	13.99	SL
JOURNAL DIA.(IN)	3.000	DJ
VISCOSITY (LB-SEC/SQ-IN)	0.3485E-08	MU

CR-3336-4

Figure 57. Centrifugal Compressor Design Point Computer Output  
(Case No. 9206001) (Sheet 4 of 4)

## SUMMARY OF SYSTEM DESIGNS

Table 17 presents a summary of information on the design-point refrigeration systems presented above in Tables 4, 9, and 13. In addition, Table 17 includes weights and sizes of the compressor subsystems.

Table 17 shows that the total power inputs to the three systems do not differ greatly -- the range being from 33.7 to 38.3 kilowatts. It is difficult to make direct comparisons among the three systems, because of the different system arrangements. Each system differs from the other two with respect to the number of turbines, pressure ratio, or heat exchanger effectiveness; all of these parameters have a strong effect on input power, as can be seen from the above tables.

The heat exchanger weights shown in the table are for the heat exchanger cores only. The weights do not include heat exchanger headers, piping, filters, turboalternators, or radiation shields. An estimated 10 to 20 percent can be added to the heat exchanger weight to account for these items. Weights for vacuum jackets surrounding the cryosection are also not included in the table.

Table 17  
SUMMARY OF REFRIGERATION SYSTEMS

Parameter	A-C Generator	D-C Generator	D-C Motor
Design point computer Run No.	6310	20205	9206
Liquid helium withdrawal rate for cooling (g/sec)	0.270	0.11	0.11
Refrigeration capacity (w) temperature (°K)			
Station 1 (coldest)	0.5/4.4*	3.0/4.4	5.05/4.4
Station 2	2.5/12*	5.0/14*	5.0/14*
Station 3	2.5/35*	32/80	106.2/80
Station 4 (warmest)	10/120*	--	--
Turbines	3	2	2
Number of compressor stages/ pressure ratio	6/2.65	6/2.58	8/3.51
Thermal effectiveness of major cryogenic heat exchangers	0.990	0.985	0.985
Total compressor input shaft power (kw)	33.7	36.0	38.3
Cryogenic heat exchanger			
Weight (lb)	502	381	206
Compressor subsystem			
Weight (lb)	600	600	690
Size (in. outside diameter x in. high)	36 x 32	36 x 32	42 x 32

\*Parasitic heat load (internal to refrigerator).

CR-4237

added to the heat exchanger weight to account for these items. Weights for vacuum jackets surrounding the cryosection are also not included in the table.

#### Compressor Subsystem Weight and Size

The last item in Table 17 is an estimate of the compressor subsystem weight and size. The weights were calculated on the basis of equations presented in detail in Reference 5. The weights include:

- Power conditioner-controllers.
- Motors.

- Compressors (frames, impellers, etc. ).
- Heat rejectors (one water-cooled heat exchanger after each compression stage).

The compressor subsystem weight does not include any cover or housing that may be needed to protect the compressor.

### Refrigeration System Arrangements

Various arrangements of the compressor subsystem and the cryosection are possible. Because the only connections between the compressor subsystem and the cryosection are ambient temperature supply and return lines for helium gas, the compressors and the cryosection can conveniently be separated by a considerable distance. This may be an advantage in some layouts. For example, it may be desirable to locate the compressor subsection at some distance from the d-c motor, which may be limited for space. It may also be an advantage to locate the compressors for the motor and both generators in the same vicinity.

Figure 48 is a drawing of a typical three-module (six-stage) compressor subsystem. Each of the three modules contains a motor and two centrifugal compressor impellers. Following each of the six compression stages is a water-cooled heat rejector. The shafts are oriented vertically, and the impellers are mounted at each end of each shaft.

A typical cryosection arrangement is shown in Figure 58. This unit has three single-stage turboalternators and a circular cryogenic heat exchanger

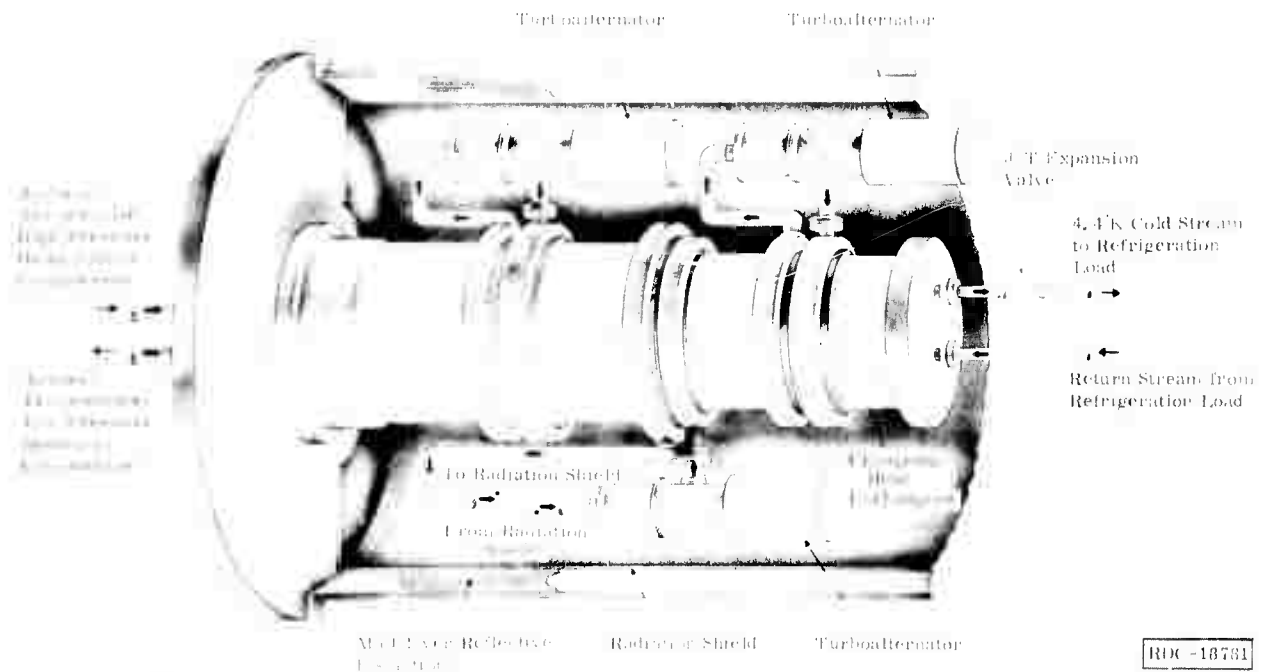


Figure 58. Cryosection with Circular Heat Exchanger

of the metal-plastic laminate type. At the intermediate-temperature turbine, a connection to a radiation shield is shown. Cold helium gas from any of the three turbines could be piped to a cooling station, if needed.

Figure 59 shows a cryosection arrangement especially designed from the standpoints of compactness and structural rigidity to withstand shock and vibration. The heat exchanger is in the shape of a "Y," to give it a large second moment of area and to accommodate the turboalternators with a minimum of wasted space.

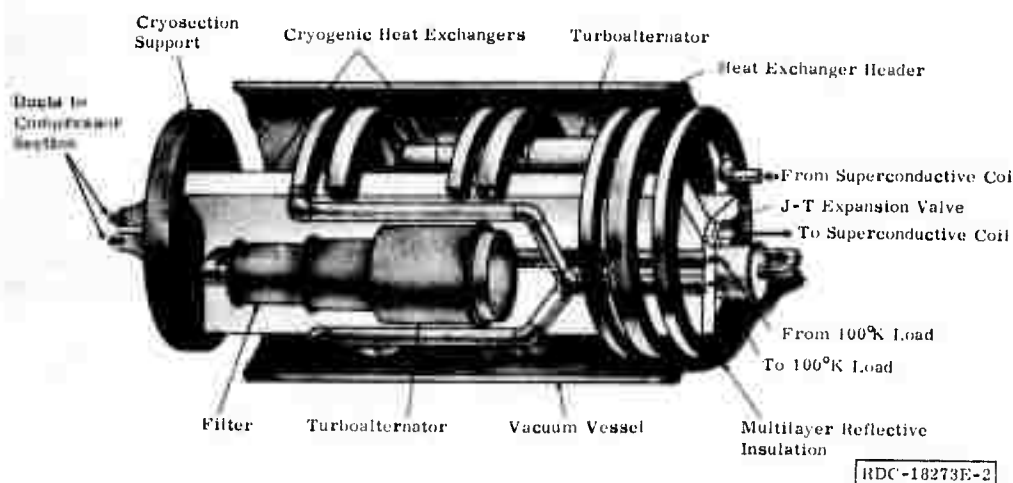


Figure 59. Cryosection with Y-Shaped Heat Exchanger

Comparisons of refrigerator weights, sizes, and power relative to the generators and motors being cooled are given in Section 3 of this report.

### COMPARISON OF REFRIGERATION TURBOMACHINERY

From the review of refrigeration requirements for the Department of Defense, it is apparent that three categories of cryogenic refrigeration are required:

- Special lightweight low-input-power refrigerators used for space applications. These refrigerators can be 1- to 2-watt refrigerators operating as low as 4°K and as high as 100°K. For this type of refrigerator, very special component designs are necessary to meet the generally limited input power capability of the spacecraft.
- Small refrigerators for ground, shipboard, and aircraft applications, where the input power and weight restrictions are not as severe as for the space applications.
- Large refrigerator requirements for ground and ship applications to satisfy Department of Defense requirements. In general, these cryo-

genic refrigeration needs are more similar to commercial requirements.

For these large refrigerators, the key to the success for long life will eventually be the use of advanced turbomachinery components, which can be made to approach a reasonable production cost.

It is anticipated that the adaptability of long-life turborefrigerators can and will be proven in studies that are anticipated for ARPA, the U.S. Army in Huntsville, the U.S. Navy, and the National Bureau of Standards. Turbo-refrigeration systems will be the best selection in most of these studies, from the standpoints of life and maintenance.

The costs of turborefrigeration systems must be considered, and a means of standardizing components needs to be adopted.

The anticipated cost breakdown of typical large turborefrigerators is:

<u>Component</u>	<u>Percent</u>
Compressors	40-60
Turboalternators	25-35
Cryogenic exchangers	5-15
All other costs	5-15

Taking the above list in reverse order, "all other costs" includes filters, plumbing, vacuum equipment, controls, power supply, and any other specialized necessities.

The cryogenic heat exchanger can be either the laminated or the plate-fin type. For small refrigerators, the laminated type will probably be the most compact. As far as cost is concerned, it is anticipated that the two types are reasonably competitive.

The second largest item of cost is the turboalternators. The approach at the General Electric Research and Development Center is believed to be a unique and effective means of providing this refrigerator component. The cost of such devices can be expected to be reduced as development proceeds and manufacturing methods are advanced.

Development and manufacturing tooling costs can be minimized by limiting the number of different frame sizes. The number of different turboalternator designs can be limited to the extent that probably a minimum of four different frame sizes with alternator diameters 0.25 to 2.0 inches will provide loads

for powers from 10 to 10,000 watts. These four frame sizes should be sufficient to satisfy all Department of Defense refrigerator needs. This approach has been applied to the selection of turboalternators in the cycle studies.

A comparison of all turborefrigeration turboalternators for the three refrigerator applications is shown in Table 18. It can be seen that the turboalternator requirements can be conveniently met by the two different frame sizes, the Big Bertha and the Grizzly Giant units. It can also be seen that the design of these turboalternators generally vary along with the design temperatures, and the loads vary with the particular operating conditions. Hence it can be concluded that with the exception of specific turbine wheel and turbine nozzle designs, all parts of all three refrigerator applications can be made identical within the two frame sizes selected.

The most costly components in the refrigeration system are the high-speed turbocompressors. Cost is high because there are so many precision elements within each rotating assembly, and there are many units required. Hence minimizing the number of different rotating assembly designs can result in substantial savings.

A comparison of all the refrigerator turbocompressors is shown in Table 19. It can be seen that there are many similarities in the design results.

The motor dimensions shown are similar in size and rating for all three applications. The motor for the d-c generator application is adequate and it is justified as a design basis for all three applications. Variations in frequency and voltage are easily accommodated by simply changing the number of turns in the stator winding.

Because the rotating speed can be made the same, the first stage of each compressor system could be made identical. Further, for the a-c generator and d-c generator, all three modules should be made with identical components on a stage-by-stage basis. Further, the first three modules of the d-c motor refrigerator would be identical to the first three modules of the a-c and d-c generators. Then, for the fourth module of the d-c motor refrigerator turbocompressor, the entire motor and bearing system would be identical to the other units, except that the seventh- and eighth-stage impellers would be slightly different because of the volume flow conditions. It is also anticipated that all of the aftercoolers for all the refrigeration turbocompressors should be identical.

#### OFF-DESIGN PERFORMANCE STUDY (TASK R-30)

The off-design performance study is primarily a Phase II Task; however, work on this task was started during Phase I. The following discussion describes this preliminary work, which was performed during Phase I.

Table 18

## COMPARISON OF ALL REFRIGERATOR TURBOALTERNATORS

Design Parameters	A-C Generator			D-C Generator			D-C Motor	
	Model and Inlet Temperature	Big Bertha 12° K	Grizzly Giant 120° K	Model and Inlet Temperature	Big Bertha 14° K	Grizzly Giant 80° K	Model and Inlet Temperature	Grizzly Giant 80° K
Total refrigeration power outputs (w)		75.57	681.5		161.7	804.4		762.3
Design speed (rpm)		72,960	64,640		14,290	69,110		55,340
Maximum speed (rpm)		200,000	200,000		200,000	200,000		200,000
<u>Principal Dimensions</u>								
Journal bearing span (in.)		3.82	7.64		3.9/2	7.64		7.64
Journal and magnet diameter (in.)		0.50	1.00		0.50	1.0		1.00
Thrust bearing outside diameter (in.)		0.84	1.68		0.84	1.68		1.68
Magnet length (in.)		0.705	1.410		0.705	1.410		1.410
<u>Performance Factors</u>								
Inlet pressure (psia)		41.35	42.19		41.35	41.77		56.68
Outlet pressure (psia)		17.08	16.58		17.08	16.83		16.83
Pressure ratio		2.422	2.545		2.422	2.482		3.369
Mass flow (lb/hr)		67.14	57.92		110.4	96.98		75.41
Turbine run number		630601006	630603005		102010103	102010202		920302006
Wheel diameter (in.)		0.750	2.500		1.30	2.00		2.60
Electromagnetic efficiency (fraction)		0.998	0.952		0.990	0.973		0.959
Number of blades		37	77		53	59		91
Overall efficiency (fraction)		0.4809	0.4804		0.5364	0.5195		0.5016
Specific speed		23.57	10.79		17.72	16.58		9.66
<u>Design Geometry</u>								
Admission (fraction)		0.3165	0.1567		0.2450	0.2308		0.1384
Cutter diameter (in.)		0.0278	0.0470		0.0345	0.04925		0.0409
Blade height (in.)		0.0935	0.1534		0.1238	0.1787		0.1451
Blade angle (deg)		60.0	60.0		60.0	60.0		60.0
Nozzle angle (deg)		80.0	80.0		80.0	80.0		80.0

CR-2325

Table 19  
COMPARISON OF ALL REFRIGERATOR TURBOCOMPRESSORS

Features	A-C Generator		D-C Generator		D-C Motor	
Inlet temperature (°K)	322.8		331.4		331.0	
Inlet pressure (atm)	1.10		1.117		1.117	
Pressure ratio	2.649		2.584		3.507	
Flow (g/sec)	26.84		31.27		21.05	
Speed (rpm)	50,000		48,000		50,000	
Input power (kw)	43.34		44.48		50.98	
Number of modules	3		3		4	
Number of stages	6		6		8	
<u>First and Last Module Features</u>	First	Last	First	Last	First	Last
Motor diameter (in.)	3.041	3.041	3.152	3.152	3.041	3.041
Motor lamination outside diameter (in.)	6.993	6.993	7.249	7.249	6.993	6.993
Motor power output (hp)	16.46	16.66	16.92	17.10	14.42	14.90
<u>First- and Last-Stage Features</u>	First	Last	First	Last	First	Last
Pressure ratio	1.196	1.183	1.186	1.159	1.196	1.152
Volume flow (cfm)	341.9	296.6	402.4	156.1	270.8	103.5
Aerodynamic efficiency (fraction)	0.6641	0.6486	0.6792	0.5719	0.6227	0.5025
Specific speed (nondimensional)	0.04768	0.04513	0.03788	0.03592	0.04152	0.03013
Tip speed (fps)	1575	1575	1540	1575	1647	1647
Tip diameter (in.)	7.217	7.217	7.353	7.217	7.551	7.551
Tip width (in.)	0.1847	0.1734	0.2012	0.1320	0.1633	0.1074

CR-3337

To predict off-design performance of the system, the behavior of its elements individually and collectively must be expressed in mathematical terms. This can be looked upon as construction of a mathematical model that can be used to simulate various system operating conditions.

It is most useful to assemble such a model in modular form, much as the physical assembly of the system must take place. The complete assembly is therefore visualized as a set of models of the essential system elements plus their interconnections and a computational method for exercising them.

In general, a performance model of the system can be significantly simplified in comparison with a design model because, in most cases, only the external characteristics of a given device are of interest. Where important, the nonideal behavior of an actual device can often be represented by some modifying empirical function added to an ideal model. Under these considerations, and exploiting the advantages of a modular approach, it is most practical to start with the basic first-order functions of the system and add refinements later.

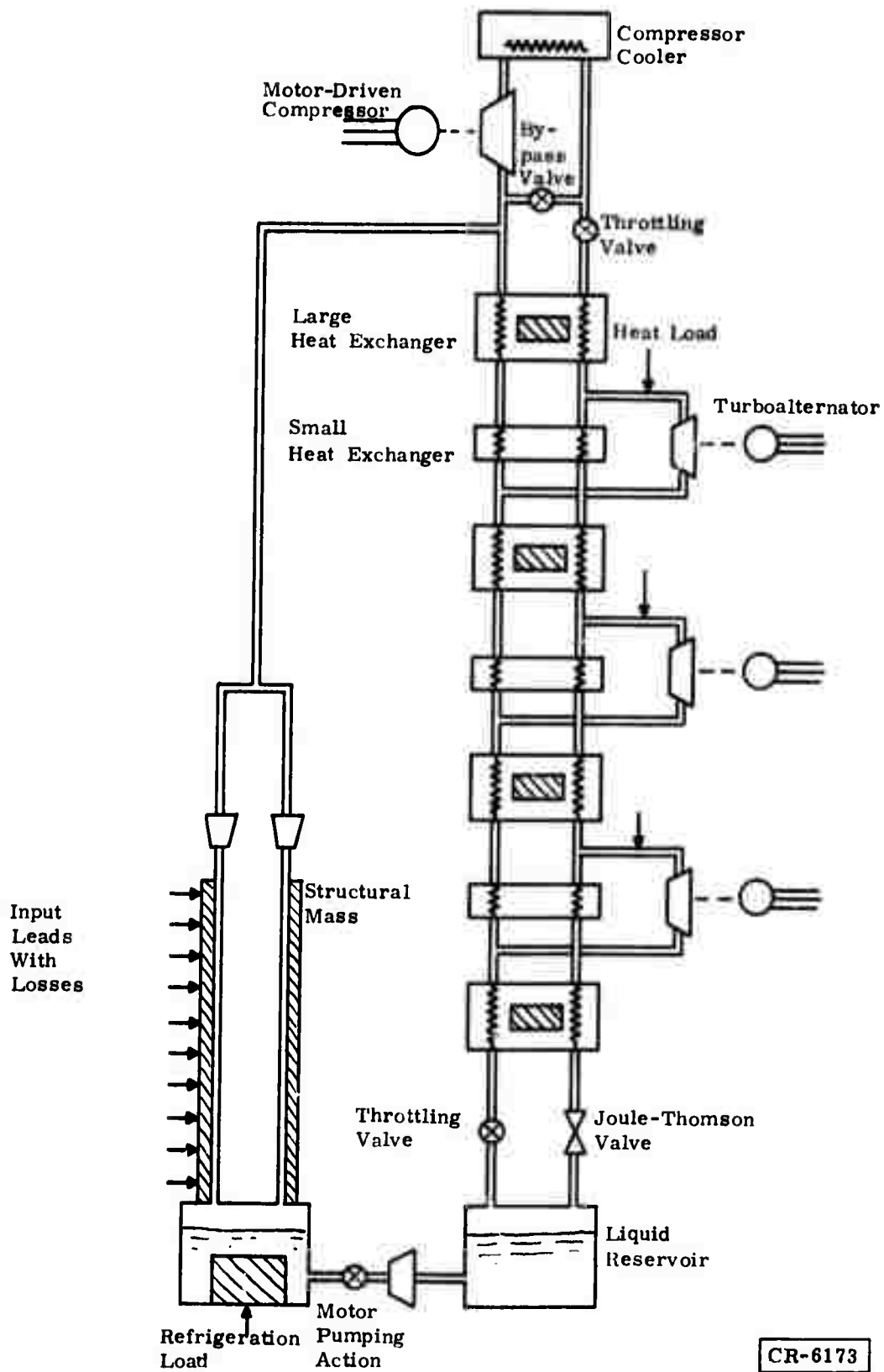
In the present case satisfactory models for compressors and turbo-alternators are available from work on preceding programs, such as U. S. Air Force Contract F33615-71-C-1003, described below. The major element for which a working model was needed was the cryogenic heat exchanger, and that derivation is presented below. The other elements required are the Joule-Thomson valve, the liquid-gas interface, and the refrigeration load. The first two of these elements are seen as quite straightforward relationships; however, a convenient form for representation remains to be chosen. The refrigeration load is, of course, central to the program. However, from the standpoint of the refrigerator, its first-order effect is simply to withdraw a certain fraction of liquid helium from the total mass flow of helium.

For reasons discussed more fully below, it does not appear meaningful to separate off-design and transient models of the system, except perhaps in the level of detail of the refrigeration load effects. The model is therefore visualized as a single entity, which will evolve as more refinements are added but which will simulate transient behavior in moving from one off-design state to another.

Any modeling/computation activity is subject to a variety of modifications and corrections until finally working to complete satisfaction. In that sense, and noting that a number of steps remain to complete the model, the following description must be regarded as preliminary.

#### CONCEPTUAL MODEL SYSTEM

From a performance-modeling standpoint, the system is seen to contain the elements shown in Figure 60.



CR-6173

Figure 60. Conceptual Model System

The motor-driven compressor maintains a driving pressure ratio across the stack of heat exchangers and turboalternators, which extract energy from the fluid, thereby reducing its temperature in a boot-strapping manner until liquefaction finally takes place as a result of expansion through a Joule-Thomson valve. Bypass and throttling valves are provided for control purposes, to keep the compressor operating in a proper thermodynamic state without overpowering the turbomachinery during cooldown and/or other off-design conditions. The several elements present in the refrigeration load are seen to have a resultant effect, on the refrigerator proper, of diverting some fraction of the mass flow from the low-pressure side of the heat exchangers.

### REFERENCE MODEL

A model of a cryogenic turborefrigerator system was developed under Contract F33615-71-C-1003 for the Department of the Air Force. The model is described in detail in Reference 6.

The model contains a basic representation of the compressor and turboalternators and their interrelationships; the model has been successfully operated over a range of synthetic, off-design conditions. Its general form is shown in Figures 61 and 62.

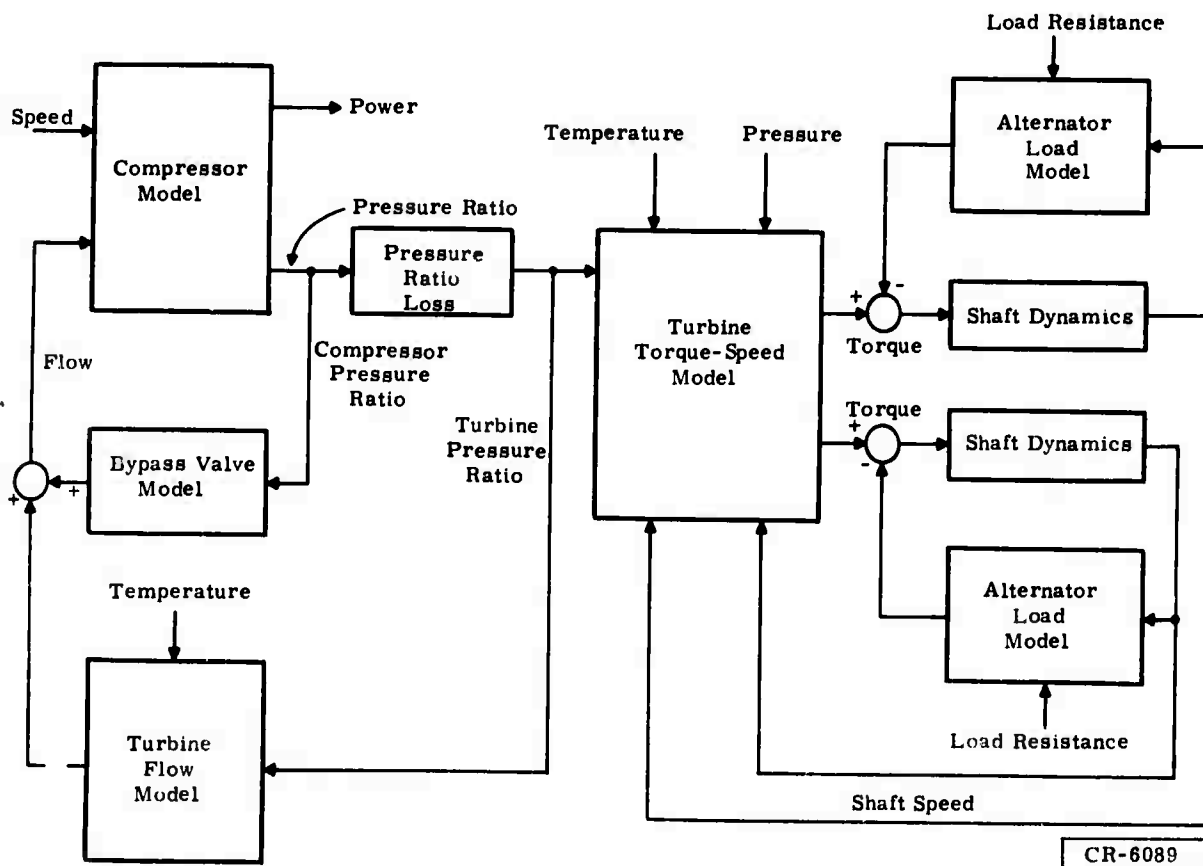


Figure 61. Reference Model Block Diagram



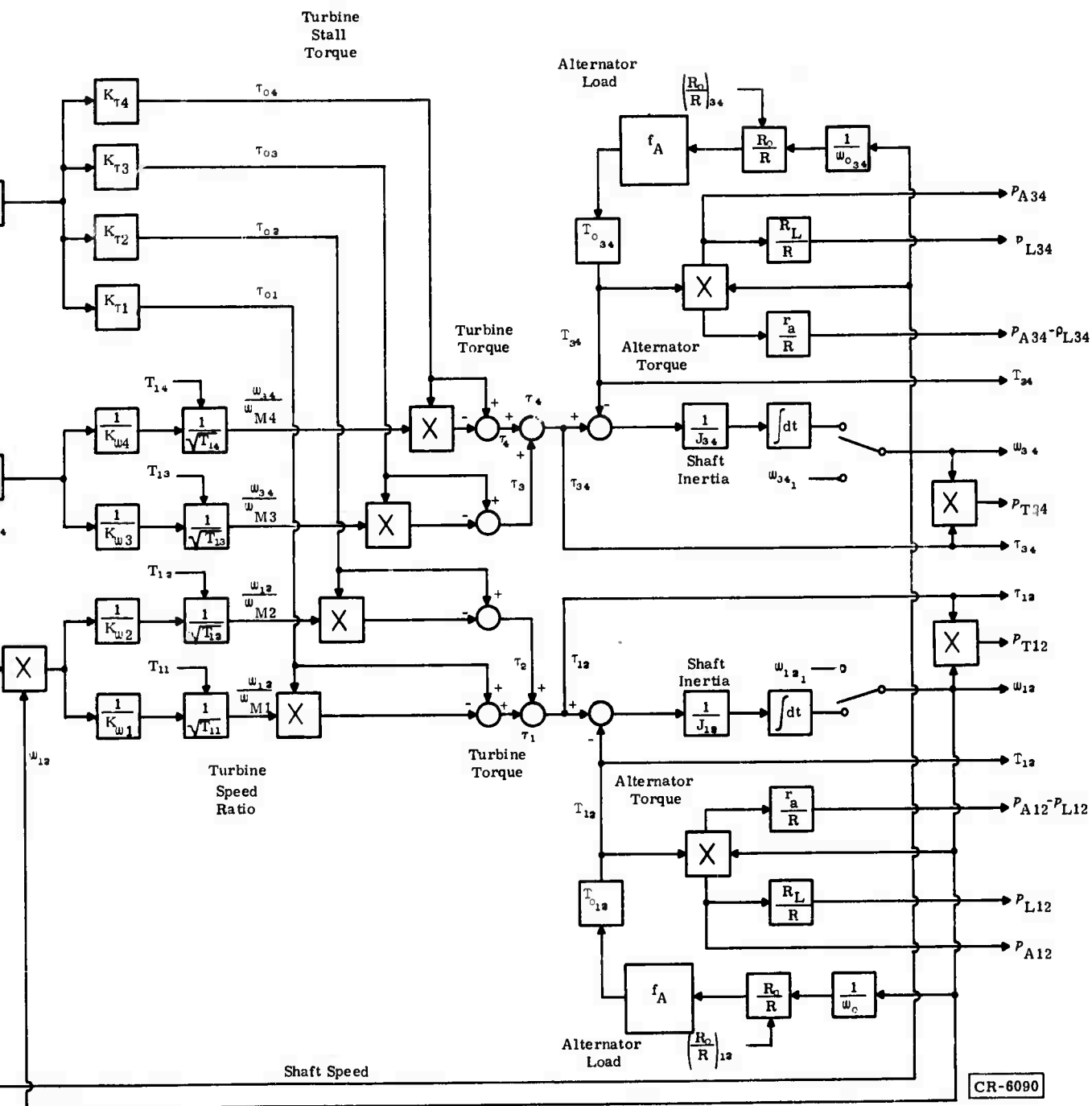


Figure 62. Reference Model

B

It is planned to use all of the elements of that model as a base and to add to it the additional elements and interrelationships required for the present application. The primary deficiency of the reference model is the absence of the heat exchanger elements and the consequent requirement for independently determined temperature inputs. For this purpose, a heat exchanger model has been synthesized and is described below. By properly using this model with the turboalternator energy and mass flow relations in hand from the reference model, it is planned to synthesize a temperature calculation loop about the structure of the reference model. To this the essential characteristics of the Joule-Thomson valve and the flow diversion of the refrigeration load will then be added.

### HEAT EXCHANGER MODEL

Consideration was given to synthesis of a heat exchanger model on the basis of transient heat flow equations for a distributed configuration. It was soon apparent that the solution of the resulting simultaneous partial differential equations would require laborious calculation to solve the implied boundary value problem for each particular configuration and thermal state -- a situation impractical for the type of modeling desired and unjustified for the level of input information anticipated and the accuracy needed.

It was therefore decided to approximate the heat exchanger on the basis of an idealized, distributed, steady-state model and an arbitrarily applied single time constant transient relationship. The derivation of the steady-state model is included in Appendix 1, "Ideal Heat Exchanger Model," and the basic transient concept is below. The results of the steady-state model synthesis are:

It is assumed that in the calculation process, values will be obtained for the input temperature and mass flow at each side of the heat exchanger. The derived relationships will then be used to determine the temperature at the corresponding heat exchanger outputs. (Figure 63).

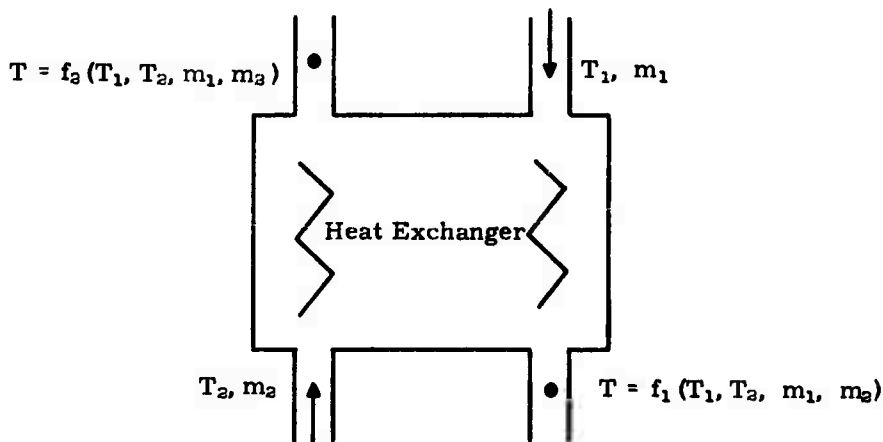


Figure 63. Heat Exchanger Outputs

The results are:

$$f_1 = \frac{\left(\frac{m_1}{m_2} - 1\right) e^{\frac{m_1 - m_2}{m_1 m_2} \frac{hA}{Cp}} T_1 + \left(e^{\frac{m_1 - m_2}{m_1 m_2} \frac{hA}{Cp}} - 1\right) T_2}{\frac{m_1}{m_2} e^{\frac{m_1 - m_2}{m_1 m_2} \frac{hA}{Cp}} - 1} \quad (1)$$

$$f_2 = \frac{\frac{m_1}{m_2} \left(e^{\frac{m_1 - m_2}{m_1 m_2} \frac{hA}{Cp}} - 1\right) T_1 + \left(\frac{m_1}{m_2} - 1\right) T_2}{\frac{m_1}{m_2} e^{\frac{m_1 - m_2}{m_1 m_2} \frac{hA}{Cp}} - 1} \quad (2)$$

Where the constant parameter ( $hA/Cp$ ) will be determined by calibration against data for the physical unit.

### COMPUTATIONAL AND TRANSIENT CONSIDERATIONS

Whether seeking a new off-design balance point or the behavior of the system under transient conditions, it is going to be necessary to slew the model variables from some initial state toward a new stable-balance state.

In very general terms, referring to the conceptual model system of Figure 61, and given an initial state, the energy and mass flow for each turbo-alternator and load can be calculated. In a chain calculation, this information can then be used to establish a new system thermodynamic state and the process can be repeated until a stable solution is reached.

To carry out such iterative processes in an efficient and stable manner, it is usually necessary to introduce algorithms with appropriate convergence factors. Certain forms of these functions can be shown to be equivalent to physical time constants. For this reason, it is anticipated that there will, in this case, be no essential difference in form between an off-design and a transient model. By inserting appropriate time constants for transient purposes, these constants are expected to function as aids in stable convergence to off-design states. The only difference then would likely be in the choice of numerical values for the time constants.

Among the system elements, the time constants for the turboalternators are on the order of seconds, whereas those for the large heat exchangers and probably for the motor load are on the order of minutes to hours and therefore are dominant as far as the system is concerned.

For the heat exchangers, it is planned to establish a single equivalent time constant for each on the basis of extrapolation of test data for represen-

tative types. For each present heat exchanger output temperature,  $T$ , the expressions given on page 144 under "Heat Exchanger Model" will permit calculation of the corresponding final steady-state temperature,  $T'$ . Assuming a single time constant,  $\tau$ , for the device:

$$T = \frac{T'}{1 + \tau s}$$

$$sT = \frac{dT}{dt} = \frac{1}{\tau} (T' - T)$$

$$\Delta T = \frac{1}{\tau} (T' - T) \Delta t \quad (3)$$

or:

$$T_{i+1} = T_i + \frac{1}{\tau} (T' - T)_i \Delta t$$

where  $\Delta t$  is a time step input for the transient problem.

### Section 3

## SUPERCONDUCTIVE POWER SYSTEMS

### SUPERCONDUCTIVE POWER APPLICATIONS STUDY

The purpose of this Task is to survey potential Defense Department applications for superconductivity and cryogenics in the category of electric power and/or propulsion requirements.

The applications, which have been identified, are described below in detail, with an indication of the degree to which each is being pursued by the individual services. A summary of the findings is also presented below:

<u>Application</u>	<u>Description</u>
1. Ship Propulsion	Superconductive generator-motor electric drives connecting gas turbines to ship propellers. Pursued by Navy. Major development request expected.
2. Superconductive Alternators	Superconductive alternators in the 1- to 10-Mw range for base power sources. Potential application in Air Force and Army. Actively pursued in several organizations.
3. MHD Power Generation	Magnetohydrodynamic (MHD) power generators with superconductive field coils. Competing for applications similar to those of Item 2. Pursued by Air Force.
4. Pulse Energy Storage	Use of switched superconductive inductors as pulse energy sources for lasers (replaces capacitors). Air Force pursuing (relatively) low-energy, long-pulse systems for driving flash lamps. Flash lamp lasers are being supplanted by other types for weapons application. Existence of three competing types (one electrical) and the embryonic state of their development makes the requirement for an energy source difficult to quantify. For matching present experimental electric lasers, capacitor sources would be too bulky, and inductor sources cannot be switched in the short time required. Neither source fits the requirement well. A blue sky study of the total system (energy source, pulse condi-

<u>Application</u>	<u>Description</u>
4. Pulse Energy Storage (Cont'd)	tioner, and laser) is indicated, but the laser technology still may be too fluid to make this meaningful.
5. Refrigeration Requirements	The above devices imply a need for compact, reliable refrigerators; however, devices themselves are speculative enough to make firm formulation of the number and timing of refrigerator need difficult. The Air Force leans to batch cooling for short missions, eliminating the need for refrigeration.
6. New Superconductor Stimulation	Niobium titanium is adequate for demonstration models and is not the limiting item in demonstration of useful devices. Conceivable breakthroughs in superconductive materials do not appear to materially ease the development job or make advantages of superconductive devices overwhelming. Continuing development of high-critical-temperature filamentary superconductors is indicated.

The detailed basis for the above conclusions is set forth in the following pages. A list of U.S. Air Force-supported work appears in Table 20.

### SHIP PROPULSION

Superconductive machinery can be applied to ship propulsion with potentially beneficial results. The ship drive system might consist of one or more gas turbines per propeller. The gas turbines directly drive electric generators that, in turn, power electric motors coupled directly to the propeller shaft. The use of electric drives permits the propeller speed to be independent of the gas turbine speed (as opposed to fixed ratio gearing). Because of this independence, the gas turbine can be operated at all times at speeds consistent with minimum fuel consumption. In addition, the number of gas turbines connected to the propellers may be varied to suit operating conditions, and the gas turbines can be cross-connected (one turbine can drive both propellers). All of the above operating modes can be beneficial in achieving minimum fuel consumption for a given operating condition.

The use of superconductive machines is aimed at reduced size and weight for the propulsion system. Two distinct types of machines may be suitable for this application. The first is the acyclic (homopolar) d-c motor and generator, and the second is the synchronous (a-c) motor and generator. A hybrid system, using an a-c generator, rectifiers, and a d-c motor, is also conceivable.

Table 20  
HIGH-POWER PROGRAMS

Program	Contractor	Description
4-Mw APU (Phase I -- complete; Phase II -- AFWL)	Rocketdyne/Westinghouse	Modify the existing turbine to run on $N_2H_4$ , fabricate a gearbox, design an alternator and build a rotor.
Advanced turbine (FY74)	Unassigned -- future	Design the optimum turbine in the 3000- to 10,000 hp range.
Advanced generator (deferred)	Unassigned -- future	Design the optimum, high-speed, high-frequency generator.
Superconducting generator	Westinghouse	Design and fabricate a 1- to 5-Mw superconducting alternator.
High-power fuel cell	Pratt and Whitney	Reduce the specific weight of high-power-density fuel cells to ~0.5 lb/kw.
Multiburst MHD	Avco	Investigate MHD generator operation, repetitive bursts, and rapid starts at 2 to 3 Mw.
Explosive MHD	Avco	Investigate explosive MHD, redirection to design a 10-Mw, prototype, conventional MHD generator.
Explosive MHD	Hercules	Investigate explosive MHD, redirection to explore a solid-fuel MHD.
High-voltage MHD	In-house	Study MHD generator, inverter and load interactions.
Limiting mechanisms in MHD	Stanford University	Investigate MHD phenomena.
Capacitive energy storage	Unassigned -- future	Increase the specific energy density of capacitors to 400 to 500 j/lb.
Inductive energy storage	MCA	Demonstrate inductive energy storage at 100 kilojoules.
High-power switching	Hughes (gas tube) MCA (rotary) Westinghouse (Vacuum interrupter) Purdue University (solid state)	Investigate various means of accomplishing inductive energy storage (opening) switching.
Capacitor switching (FY74)	Unassigned -- future	Build a high-power closing switch.
Transformer	Thermal Technology	Reduce the specific weight of a high-power transformer to < 0.4 lb/kw.
Transient effects in superconductors	National Bureau of Standards	Develop helium pump and conduct transient superconductivity analysis.
Computer-aided design	University of Kentucky	Perform computer modeling of high-power systems.

AFWL = Air Force Weapons Laboratory  
APU = Auxiliary power unit  
MHD = Magnetohydrodynamic

Homopolar machines would use superconductive field windings and normal armature elements. The armature elements can be either disks or drums, series-connected to produce the required output voltage. Because homopolar machines are low-voltage, high-current devices, liquid-metal current collectors are usually assumed. The homopolar, d-c machines have the advantage that the superconductive field coil is stationary, making the cryogenics and coil construction essentially state of the art. In addition, no intermediate power conditioning is required. The disadvantage is the large current required, necessitating the use of heavy bus work and also the use of liquid metal in the current collectors, which, with some metals (e. g., mercury and sodium potassium), may present a potential operating hazard.

A-C synchronous motors and generators would consist of a superconductive field winding on the rotor and a normal-temperature armature winding

on the stator. Typical operating speed ratios are from 3600 rpm at the turbine to 200 rpm at the motor. In conventional electric drives, the speed ratio can be obtained by matching the number of poles on the motor and generator to their respective speeds (e. g., a 3600-rpm, 2-pole generator and a 200-rpm, 36-pole motor). Superconductive machines do not lend themselves to a large number of poles; power density falls off rapidly above 6 to 8 poles. Hence a superconductive motor-generator system will require a frequency changer, such as a cycle converter, in order to meet the basic speed ratio between the turbine and the propeller. The frequency changer will also serve as a speed regulator device for the drive motor.

Advantages of an a-c/a-c system would be higher system voltage, allowing small cables in intercollections, and possibly faster response through the use of the frequency changer as a speed control. Disadvantages might be the size and weight of the frequency changer and increased cryogenic complexity leading to higher refrigeration requirements and increased development time.

The U. S. Navy has been pursuing, at a low level, the application of superconductive ship drives for a number of years. A number of study contracts have been funded, and there is an ongoing development program at the U. S. Naval Ship Research and Development Laboratory in Annapolis, Maryland. Present plans call for the issuance of a request for proposal for a more detailed study and construction of a 3000-hp model system (40,000 hp is typical full-scale power). There appear to be no basic technological barriers to the development of such a system.

### SUPERCONDUCTIVE ALTERNATORS

The use of superconductive field windings in alternators is an application that has the potential advantage of increased power density (decreased size and weight). In principle, a superconductive alternator could be constructed without any magnetic iron; in practice, most conceptual designs have included an iron yoke for the field return circuit, in order to eliminate stray a-c fields, which might be undesirable. All concepts presume that only the field winding (d-c) is superconductive; the armature winding (a-c) is more or less conventional, operating at normal temperatures. (A satisfactory power frequency superconductor has not been developed.)

In most concepts, the superconductive field winding is carried on the rotor (as it is in conventional alternators), which increases the complexity of the cryogenic cooling design. Flux densities in the armature, three to four times those of conventional air gap flux densities, can be achieved. The elimination of the need for iron teeth in the stator also allows more space for conductor and, thus, increased current loading, so the theoretical gain in power density is on the order of six to eight. Practical configurations show gains of about three to four.

The development of successful superconductive alternators appears to be possible using straightforward (although sophisticated) engineering. Cryogenic cooling requirements do not appear excessive, and available superconductor technology appears adequate. It is possible that there may be some surprises in helium flow behavior and/or in superconductor stability in rotating assemblies under high centrifugal loading, although this is not considered likely.

Superconductive alternators are under study in several organizations in the United States. The bulk of this study effort is aimed at evaluation of central-station steam turbine applications (60 hertz). Westinghouse has built an experimental, 5-megavolt-ampere model, which is undergoing testing. The Massachusetts Institute of Technology has a 2-megavolt ampere machine nearly ready for testing (sponsored by the Edison Electric Institute). Within the General Electric Company, activity has been concentrated on design studies of large machines; no working models have been built. In terms of direct military applications, the U. S. Air Force Power and Propulsion Laboratory is funding the construction of a 1- to 5-megawatt, 400-hertz, 12,000-rpm, superconductive alternator. The work on 60-hertz machines can be translated, with a high degree of correlation, to the higher speed, higher frequency, Air Force requirement.

The U. S. Army Mobility Equipment Research and Development Center (MERDC) is interested in smaller, lighter alternators for generation in command post (base load) operations where the generator set is transported primarily by truck. The 1- to 5-megawatt range suits their projected needs for the near term, and further forecasts are not available.

In the case of the U. S. Air Force, the need is not so much for a prime aircraft power supply as it is for powering special purpose loads. In the latter case, the generator would probably be driven by a separate chemical turbine, as opposed to being tied to the turbojet propulsion engines. Although public identification has not been made, it is generally supposed that the load requirement is basically premised on high-energy laser weapons (discussed below), although other high-power load needs may exist or arise.

Laser weapon development is not concentrated in the Air Force. All three Department of Defense services, as well as ARPA, have an interest in laser deployment, but so far there has been no differentiation in type; that is, the present assumption is that the Air Force development will be commonly applicable to all three services. To this extent, the power source requirement is common, although it is obvious that size and weight are not so critical in a landbased or ship-based system.

In summary, a need is foreseen for lightweight electrical power sources in the 1- to 10-megawatt decade by at least two of the three services. It is possible that superconductive alternators may help meet this need.

The development is being actively pursued at the present, and no areas where a technical breakthrough is needed to implement the application have been identified.

### MHD POWER GENERATION

Special purpose, magnetohydrodynamic (MHD) generators are being considered by the Air Force as an alternate power source to the turbine-alternator for laser weapons power. The MHD device would use stored fuel and oxidizer (liquid or high-pressure gas), discharging the combustion products overboard. Fuels considered have been mundane, such as JP-4, or exotic, such as toluene, benzene, cyanogen, and so forth. The use of solid rocket propellants is still under consideration.

Selection of fuel will depend on mission duration, specific fuel consumption, and so forth. Few MHD machines have been built, and those have been laboratory devices. The Avco Everett Research Laboratory has operated a 2-megawatt machine and also a 30-megawatt industrial prototype. A 200-kilowatt machine has been operated at Wright-Patterson Air Force Base.

MHD generators need superconductive field coils. Here again the coil is stationary, rather than rotating, as in the alternator application. The Air Force has contracted for a few prototype coils, with reasonable success. It appears that satisfactory coils can be made, applying current technology (1 to 2m long with an 8- to 12-inch active bore for 5 to 10 Mw). When optimized for total weight, MHD generators are optimum at a working flux density of about 50 kilogauss.

Technical factors other than coil technology and cryogenics will be limiting in the development of MHD generators. MHD generators may have a size and weight advantage over rotating generators. A further advantage may be fast startup; that is, a rotating machine must spin at idle for the duration of the mission period to be ready for fast loading at arbitrary command, when the weapon is actually being used in fast, short bursts. The MHD generator may have the capability of starting from shutdown in fractions of seconds, through the use of fast valving on the fuel and oxidizer. However, the MHD field coil would have to remain charged. A subsidiary advantage may be the lack of interaction between the field and the fluid (drawing power suddenly does not load the field or require sudden changes in field current). There is no analog of the reactance of a synchronous generator.

### PULSE ENERGY STORAGE

A need exists for short, high-energy, electrical pulses for Department of Defense laser applications. Conventional capacitors prove to be too bulky for airborne missions. The theoretical energy density available in a magnetic field created by a superconductive inductor is attractive; however, pulse length

requirements are short, and switching emerges as a major technical problem. Because the discussion illustrating the above thesis and leading to conclusions has turned out to be extensive, the conclusions appear first:

- Application of superconductive inductors to pulse energy duty requires development, mostly in switching, for relatively modest power levels.
- Any applications compatible with today's technology in inductive storage are probably being supplanted by other forms of high-energy lasers.
- In the high-energy laser technology, there are three competing systems, only one of which is electric. The state of development is not far enough to pick a winner.
- The trend in high-energy electric lasers (electric discharge lasers) is toward shorter and more frequent pulses. Based on today's knowledge, upgrading capacitors may be more fruitful than developing inductive systems. Switching techniques may require new inventions for inductive systems.
- Probably neither inductors nor capacitors are fully satisfactory approaches. A fruitful activity would be a fresh look at the total system integration, including modifying the laser itself to arrive at the optimum direction of development. The present state of laser technology is not stable enough to allow firm conclusions from such a study.

In addition to requirements for large blocks of basic electric power generation, laser weapons systems may create requirements for power conditioning, the principal one being the delivery of electric power in short pulses of high energy. The classic example of this requirement is the glass laser, which is pumped by pulses of light delivered by a bank of flash lamps.

The traditional source of pulsed power is the capacitor bank; however, capacitors are low-energy-density devices and unsuited to mobile or airborne applications. In terms of fundamental energy density, inductors (and particularly superconductive coils) are much more compact. This can be seen by looking at the basic equations for the volume density of stored energy in the electrostatic and electromagnetic field:

$$W = \frac{\epsilon\epsilon_0 E^2}{2} \quad \text{and} \quad W = \frac{B^2}{2\mu\mu_0} \quad (4)$$

Where  $E$  is the electric field intensity,  $B$  is the magnetic flux density,  $\epsilon_0$  is the permittivity of free space, and  $\mu_0$  is the permeability of free space.

Typical orders of magnitude for working electric field strengths in the best commercial capacitors is about 2.5 megavolts per inch and the dielectric (e. g., castor oil and paper) may have a dielectric constant of about five.

This figure yields a theoretical energy density of about 3.5 joules per cubic inch. Commercial energy storage capacitors have an overall energy density of about 2.5 joules per cubic inch (based on the volume of the can only) and a specific density of about 40 joules per pound. In contrast, a magnetic field (created by a superconductive coil) of 5.0 webers per square meter has a theoretical energy density of 164.5 joules per cubic inch. This comparison reveals the incentive for investigating superconductive, inductive energy storage.

Two factors have inhibited the use of inductors as substitutes for capacitors in energy storage applications. The first factor is the inherent resistive loss during charging and during charged, waiting intervals (hopefully this loss is eliminated by superconductivity). The second factor is that the transfer of energy to the load must be accomplished by interrupting the coil current. For short pulses of high energy, this factor imposes severe duty on the interrupting element (switch). Capacitors have little inherent loss and the energy transfer is accomplished by closing a switch, a relatively simple operation.

Although superconductors are lossless in the presence of steady currents and fields, a time-varying field produces losses. These losses are delivered directly to liquid helium. An appreciation of the sensitivity may be gained by observing that mechanical refrigeration at helium temperatures requires 1000 watts input per watt extracted; thus, the inductor losses must be kept on the order of 0.1 percent or less to avoid a refrigeration requirement equal to the energy stored.

Mechanisms for superconductor loss are understood, and partially adequate technology exists for coping with them. Losses are hysteretic (rate-independent) in the superconductor. Minimization of losses is presently accomplished by codrawing the superconductor in fine filaments in a metal matrix. The presence of a metal matrix introduces eddy current losses, which are rate-dependent. For pulses in the microsecond range, the eddy currents dominate for present designs. The remedy for losses is finely stranded conductors, fully transposed, and can be handled for reasonable cases with today's technology. The switch problems are less well defined, because less study for cases of practical interest has been undertaken to date.

The results of a specific case can be briefly cited for purposes of example. A U.S. Air Force-funded program studied the production of pulses of 50 to 100,000 joules, rise time of about 100 microseconds, pulse duration of 250 microseconds, and a pulse repetition frequency of five per second. At 50,000 joules, the load (bank of flash lamps) requirement was on the order of peak currents of 20,000 amperes at 15 kilovolts, (250- $\mu$ s pulse), or some other combination of current and voltage yielding 300-megawatt peak power. These values (along with the rise time) serve to define the switch requirement.

The results of preliminary evaluation of these requirements have been published (Refs. 7 and 8). The requirement for a superconductor is a composite strand of a few (one to three) thousandths of an inch in diameter. The superconductor can be a single or multifilament diameter of one thousandth of an inch or less. These dimensions, though not common, are within today's state of the art.

All investigators have rejected, as switching elements, silicon-controlled rectifiers, ignitrons, and triggered vacuum gaps (ignitrons are the most common capacitor switch, but the clearing times are too long for inductive applications) in favor of vacuum breakers with movable contacts. One contractor estimated that a series-parallel combination of 17 of the best commercial switches would be required. All circuit breakers require a current-zero to extinguish the arc; commercial a-c breakers rely on the natural 60-hertz current zero.

In the present application, the switch would be commutated by discharging a capacitor through the contacts in the reverse direction. After the current zero, the switch has a characteristic recovery time during which the metal ions and electrons created by the arc must condense or be otherwise removed to prevent a restrike when voltage is reapplied. Recovery times of commercial vacuum breakers appear adequate, if marginal, for the 100-microsecond voltage rise time considered here. Mechanical limitations and reliability at a pulse repetition frequency of five per second have yet to be evaluated.

In terms of laser weapons, the above example represents a relatively low-level requirement. Flashlamp lasers for high-energy pulses are being deemphasized, and it is likely that flashlamp systems of the above characteristics will never be deployed.

Laser weapons research has evolved to the point where it is now estimated that light power levels higher than those obtainable with flashlamps will be required. Three types of systems are being investigated for this purpose:

- Gas Dynamic Lasers. The pumping mechanism is primarily thermal excitation by combustion, followed by expansion of the working gas into the optical cavity.
- Chemical Lasers. A chemical reaction at temperatures and pressures less than those required for thermal excitation produces the excited species.
- Electric Discharge Lasers. Electron bombardment produces the pumping excitation.

In order of the state of development, the ranking is:

1. Gas dynamic lasers
2. Electric discharge lasers
3. Chemical lasers

It is not appropriate, in this document, to delve into the technical details of each method. The subject is presented only to cast some light on the probability of a need for pulse energy systems. Possible requirements can be discussed briefly; for the present, it is sufficient to note that there are two nonelectric competitors for the laser weapons mission.

Electric discharge lasers, as applied to the weapons field, are adaptations of the gas discharge carbon dioxide laser. The latter, in its present embodiment, is pumped by a continuous glow discharge in a tube, the optic axis being parallel to the electric discharge. These lasers operate at reduced pressure and are capable of producing a few kilowatts of output, but cannot be reasonably scaled up in power.

To upgrade the energy density as well as total power for the weapons application, it is desirable to operate near atmospheric pressure. To accomplish this, the electric discharge laser has the electric discharge perpendicular to the optic axis and is of considerably shorter length (for reasonable voltages). To remove waste heat, the gas is circulated, the flow generally being in the third dimension.

The emitted light is at 10.6 microns in both cases, characteristic of a transition between carbon dioxide vibrational states. One recent version of the electric discharge laser is called the pulser sustainer electric discharge laser. Ionization is created by an electron beam injected into the gas from an external electron source. The primary energy comes from so-called sustainer electrodes, which bound the active volume. In this way, the sustainer voltage is too low to sustain continuous ionization (and degeneration into an arc) but is of just the right magnitude to produce a maximum concentration of excited molecules. The free electrons are produced by the injected beam. The plasma electron temperature is thus controlled by the sustainer voltage, and the density or current is controlled by the injection source.

Electric discharge lasers can operate in a continuous-wave mode; however, this mode is not presently favored, because the gas density must be reduced to 1/3 atmosphere or less and the light output is less than the average power produced by a pulse mode electric discharge laser.

In the pulse mode, limitations are placed on pulse length by the fact that a sudden release of energy in the gas creates a pressure wave that propagates with the speed of sound. Once the wave is reflected at the walls of the cavity, the optical quality of the cavity is spoiled. (These sound waves create severe structural and vibrational problems for the electric discharge laser as well.) Present pulse length is approximately 20 microseconds.

The above sonic limitation on pulse length implies that a maximum of 100 microseconds may be tolerable, even for high-power systems. As now visualized, a trapezoidal pulse of 20 to 100 microseconds will be required with a

rise time on the order of 3 microseconds. Such pulses are within the capabilities of capacitor banks; however, a 3-microsecond rise time would appear to be so short that it is beyond presently reasonable capability of switches that could be used to interrupt an inductor current.

Finally, it should be mentioned that in addition to the short pulse duration required, the electric discharge laser requires a pulse whose voltage is flat to within about 10 percent, because the pulse voltage determines the electron energy, which must be kept within close limits for maximum efficiency.

Capacitor banks are amenable to pulse shaping by arranging the capacitors along with small inductors in the form of a transmission line. The mechanism (with associated additional hardware) for precise pulse shaping with an inductive store have not been fully investigated.

The short pulse requirement cited above for electric discharge lasers complicates the inductive storage picture further, as illustrated by the earlier discussion.

Designing the inductor for low loss is accentuated by short pulses, although this design is probably not prohibitive. However, the production of high-energy pulses with rise times on the order of a few microseconds, would appear to be well beyond the state of the art for switching, and new inventions may be required.

## REFRIGERATION REQUIREMENTS

Implementation of any of the above power generation machinery concepts will create a need for compact, reliable refrigeration machinery. It does not appear possible to arrive at a numerical measure of this requirement in units per year or watt load per year, because a requirement for deployment of the machinery itself cannot be arrived at in any firm way. Firm data on which to base the refrigeration load of any individual machine are also not really available; however, most studies have shown that machines of this general size will have refrigeration loads in the range 5 to 20 watts. Hence, refrigerator development for machines in this capacity range seems indicated.

In addition, the more sophisticated cooling studies show that the most effective cooling is obtained by systems that remove heat at the highest possible temperature level, either by absorption of the heat in the exhaust helium gas, returning it to the refrigerator at a temperature near room temperature, or by using a combined-cycle refrigerator with one or more elevated temperature stages. The 5- to 20-watt range quoted above presupposes such a cooling cycle. Hence, any refrigerator development program should address itself to cooling requirements of this general nature.

A further complication in evaluating refrigeration needs is introduced in consideration of airborne applications. Generally speaking, contacts with the

U.S. Air Force indicate that studies performed to date have resulted in the general conclusion that the mission duration for the superconductive equipment in question is usually taken as about two hours (total airborne time may be more than this; reference is to the time of active use). In these cases, weight trade-offs usually result in the conclusion that for short mission duration, it is preferable to provide cooling with batch liquid helium, venting the exhaust gas overboard. Hence a requirement for refrigeration machines is not forthcoming. In the case of equipment that must be continuously kept cold (cooldown time is usually visualized on the order of large fractions of days) for combat readiness, the usual assumption is that a more conventional (commercial perhaps) refrigerator in the form of ground support equipment will be used.

Navy, Army, and space applications, however, all require compact, reliable, continuous refrigeration systems.

### POTENTIAL FOR ADVANCED SUPERCONDUCTORS

Niobium titanium remains the material on which most superconductor applications are based. In recent years, significant advances have been made in producing niobium titanium in twisted filament form. This configuration makes possible the control of losses in pulse applications (e. g., synchrotrons) at low frequencies (one per second), for which it was first conceived. However, more important, the mechanism that contributes to low loss also contributes to stability against flux jumps in steady-field applications, and coils are now constructed in which practically all electromagnetic instabilities have been eliminated.

The suppression of magnetic instabilities has allowed another form to surface: mechanical instabilities due to wire and/or coil motion. These instabilities operate in a similar way; superconductor deformation or frictional motion creates enough energy to raise the superconductor above its critical temperature, defined by the extant condition of current density and magnetic field strength. This instability is remedied by firm restraint of the superconductor -- mostly the use of coil potting.

Although niobium-titanium properties are no longer the limiting item in the exploitation of superconductive devices, it is pertinent to raise the question as to what improved superconductor properties would enhance the scope of application. The critical field is an obvious possibility; however, increases in critical field, per se, may not be of primary significance at the moment. Rotating machinery concepts generally retain iron shielding and increasing the operating flux density serves mainly to increase the required shielding without a substantial gain in overall power density. In the case of magneto-hydrodynamic generators, it is found that a generator weight optimum usually comes out at about 40 kilogauss because increased fields require increasing amounts of superconductor and, if high enough, the addition of structural material to contain magnetic forces. Similar factors exist in the design of energy storage coils.

Niobium tin ( $\text{Nb}_3\text{Sn}$ ) is the second most developed superconductor. Although it has better properties than niobium titanium, it is intrinsically brittle and harder to fabricate into useful shapes; this latter property has retarded its use, except where high field strength is indispensable. In view of the remarks about high fields in the above paragraph, it appears that this property may not be sufficient to displace niobium titanium. However, niobium tin has a critical temperature of  $18^\circ\text{K}$ , compared to  $10^\circ\text{K}$  for niobium titanium. This property may prove advantageous in allowing the superconductor to operate near  $10^\circ\text{K}$ , as opposed to  $4.2^\circ\text{K}$ , as is customary for niobium titanium. (Niobium tin has properties at  $10^\circ\text{K}$  almost as good as those of niobium titanium at  $4.2^\circ\text{K}$ .)

Higher temperature operation allows an improvement in the cycle efficiency of cryogenic cooling. For higher temperature operation, the effectiveness of liquid cooling, with its attendant high nucleate boiling coefficient is sacrificed (the critical temperature of helium is  $5.2^\circ\text{K}$ ). To realize the cycle efficiency, cooling would be produced by gas entering at approximately  $8^\circ\text{K}$  and exiting at  $10^\circ\text{K}$ . In such a system, the refrigerator input might be halved for a given load. It should be noted that freely boiling liquid automatically provides a fixed temperature point, while in gas cooling, the flow rate must be controlled to maintain the temperature. In the case of batch cooling, the helium must be carried as the liquid, in any event; however, the amount required would be about half if the total enthalpy of the gas between  $4.2^\circ\text{K}$  and  $10^\circ\text{K}$  could be utilized.

It seems safe to predict that the filamentary form of superconductor is firmly enough entrenched so that a filamentary, flexible form of niobium tin would be required before it would be used extensively, even with the above refrigeration requirement. However, the increased critical temperature might have a second (and more important) benefit in this case. Instability (either magnetic or mechanical) depends on a balance between the potential for energy release (mechanical or magnetic) and the specific heat required to raise the superconductor above the critical temperature. Because the specific heat of metals (niobium) increases from  $3 \times 10^{-4}$  at  $4.2^\circ\text{K}$  to  $25 \times 10^{-4}$  joules per gram at about  $8^\circ\text{K}$ , this available energy absorption may prove to be a powerful influence on stability. Experimental work is required to verify this supposition.

Another superconductor that has properties similar to those of niobium tin is  $\text{V}_3\text{Ga}$  gallium. Its critical temperature is somewhat lower ( $14^\circ\text{K}$ ); however, at low temperatures its critical field and critical current density (at high fields) appear to be somewhat better. The Japanese are actively pursuing its development as a commercial product; indications are that it may be somewhat simpler to produce in filamentary form than niobium tin.

Other processes that have been considered for producing fine-filament superconductors include the impregnation of vicor glass with lead or lead-bismuth alloys. This process produces very fine filaments (which have en-

hanced the critical field), but the resulting composite is limited in critical temperature. Niobium carbonitride has been produced in reactions starting with synthetic fibers. Its critical temperature can range from 9°K to 18°K, depending on structure, and its critical field is comparable to that of niobium tin. Critical current densities have not been accurately measured. The above processes have the advantage that the filament production is not associated with the presence of a metal matrix; therefore, these may have the potential for the creation of a true a-c superconductor.

In conclusion, it appears that the direction of research will be most profitably aimed at producing twisted filament superconductors with higher critical temperature from the standpoints of stability, operating margin, and cooling efficiency. Success in this regard could conceivably lead to superconductors whose a-c losses would be acceptable at power frequencies; these superconductors might lead to more effective electrical apparatus concepts.

## SHIP PROPULSION SYSTEM REQUIREMENTS AND CRITERIA (TASK S-10)

### SYSTEM REQUIREMENTS

System requirements for this study have been established by considering various types of naval ships to which superconductive propulsion machinery might be applied, reviewing the specific requirements of each of these ships, and considering requirements generally applicable to Navy ships. From this information, a set of system requirements has been prepared that is considered to be typical of those that a superconductive propulsion system should be able to meet in one or more promising naval applications.

### System Description and Potential Advantages

The basic system (Figure 64) consists of a generator driven from the prime mover, suitable power conditioning equipment, an adjustable-speed

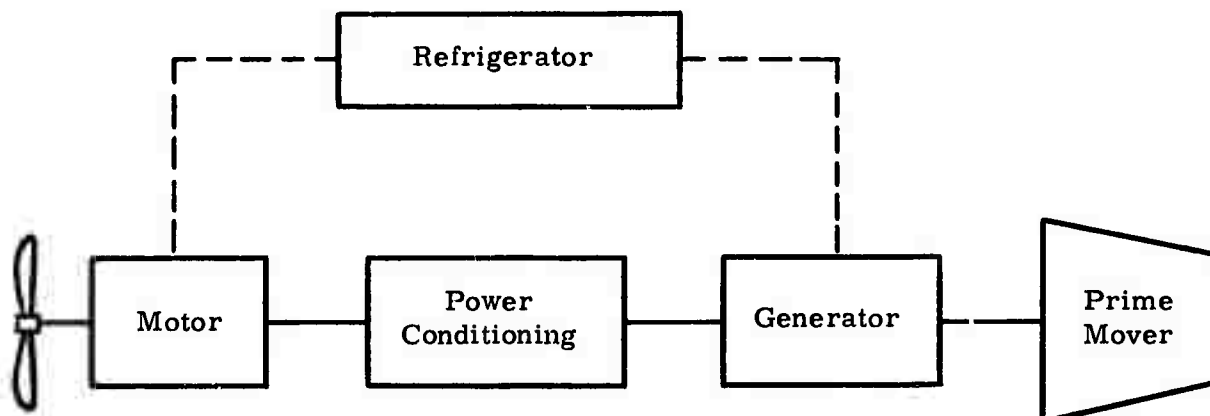


Figure 64. Schematic Diagram of Basic System

motor driving the propeller, and cryogenic refrigeration equipment for maintaining the field windings of the motor and generator at superconducting temperatures. Suitable control equipment (not shown) is, of course, required for the complete system.

In cases where more than one prime mover and generator is involved, the system lends itself well to having capability for cross connection, where motors and generators can be electrically connected in any combination. Figure 65 illustrates such a system. In accordance with the proposal and program plan for this study, attention has been directed toward two basic systems:

- D-c generator/d-c motor
- A-c generator/d-c motor

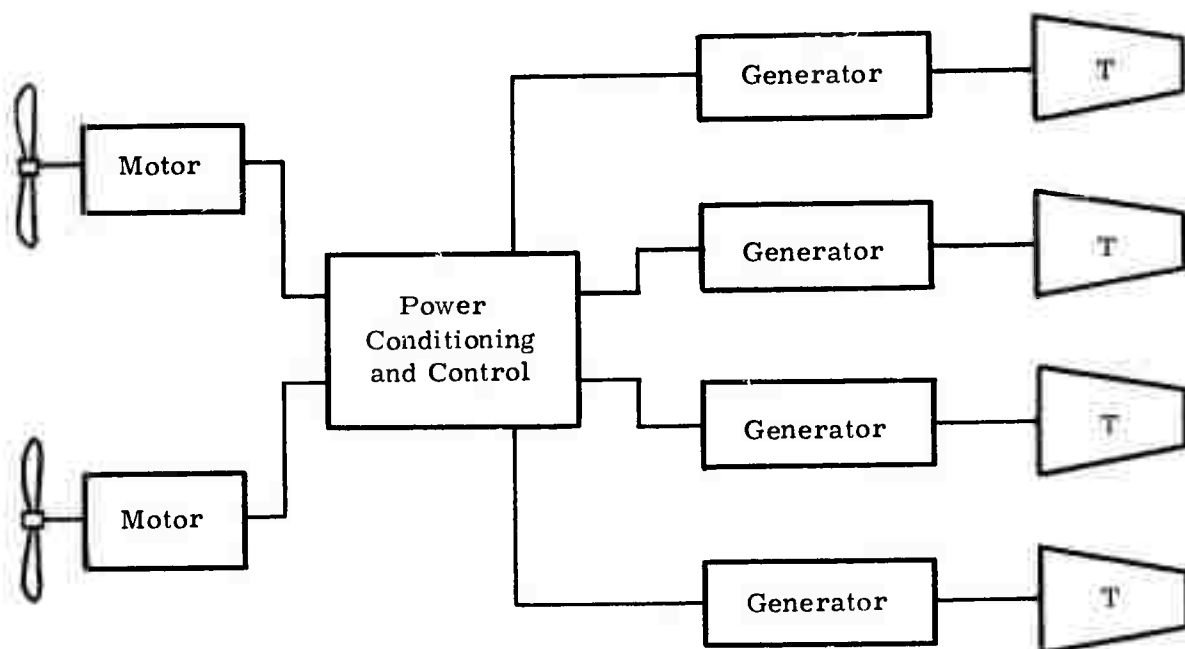


Figure 65. Cross-Connection Capability

Potential advantages of the superconductive system can be categorized into three main areas:

- Flexibility of Mechanical Arrangement. Because the prime mover and propeller are no longer connected through gearing, there is a great deal of freedom available for choosing the location of the prime mover. For example, in a destroyer application using a gas turbine, the turbine could be located at or near deck level, eliminating the very bulky and heavy inlet air and exhaust ducting required for a turbine located deep in the hull. Or, in the case of a hydrofoil or surface ship, generally simpler electrical leads could replace complex gear trains.

- Cross-Connection Capability. The capability for cross connection (Figure 65) provides the potential for improved specific fuel consumption by making it possible to shut down one or more prime movers under a partial load, enabling the remaining units to operate nearer the point of best fuel consumption. A possibility that can also be considered in this connection is use of one or more relatively small prime mover/generator units at cruise speed, achieving better fuel consumption than would be possible using the larger units.

In addition to improving specific fuel consumption, this cross-connection capability can significantly reduce the operating time for the main prime movers on any given mission, resulting in longer effective life and reductions in cost.

- Reduced Size and Weight. The preceding two advantages are basic to electric drives in general and do not require use of superconductive machinery. The major incentive for the superconductive machinery, on the other hand, is its potential for reducing size and weight. This potential could lead to increased payload or improved ship performance. Possibly more important, it might also make an approach practicable that otherwise might not be. Direct drive of hydrofoil propellers by use of motors in the pods might be such a case, where low frontal area is vital.

### Potential Naval Applications

Five types of naval ships have been considered:

- Conventional surface
- Swath
- Hydrofoil
- Surface effects
- Submarine

The first four of these types are shown in Figure 66.

Conventional Surface. Major advantages are believed to be the possibilities of relocating the prime mover near deck level and of improved specific fuel consumption due to the cross-connection capability. These advantages appear to be greater if the prime mover is a gas turbine than if it is a steam turbine, because of the ducting required for the gas turbine and because its fuel consumption is more load-sensitive. In this connection, because of the trend toward use of gas turbines in destroyer-size ships, attention in this study has concentrated on destroyer-type conventional surface ships.

Swath. Potential advantages for this advanced-type ship are the same as those for the conventional surface ship, with the additional desirability of low

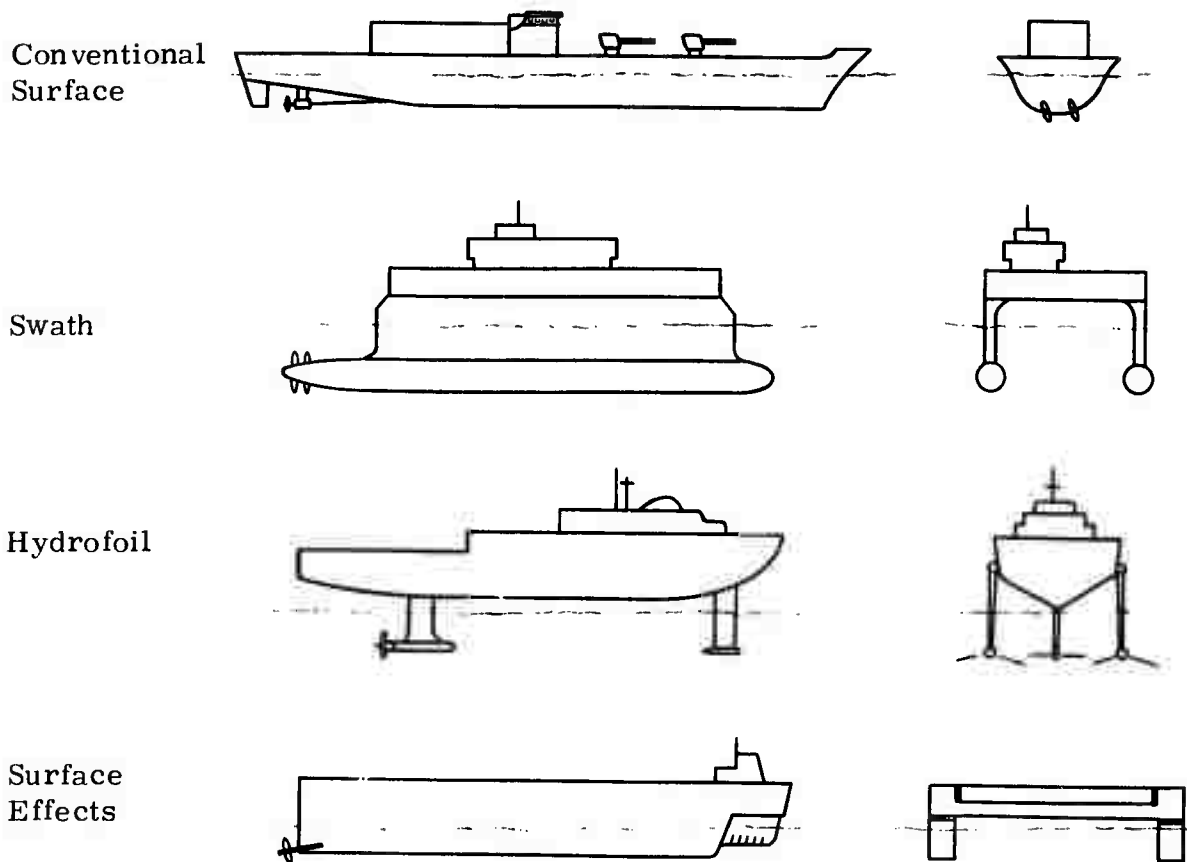


Figure 66. Potential Naval Applications

weight. Reduced size, to a lesser extent, is also of interest, because it provides increased accessibility and a reduction in propeller shaft lengths.

Hydrofoil. The major advantage in this case appears to be elimination of complex gear trains. Motor size, especially frontal area, is of prime importance, in order to locate the motors in the pods.

Surface Effects Ship. These ships are characterized by the need for power, in many different parts of the ship, for propulsion and lift. Consequently, the major advantages appear to be elimination of complex gear trains and possible consolidation of a number of prime movers into fewer, more efficient, centrally located units.

Submarine. The major potential advantage in this case appears to be the possibility of locating the motor outside the pressure hull, eliminating penetration of that hull by a rotating shaft and the consequent problems of providing an adequate seal around this shaft for deep submergence depths. Because of the more sensitive nature of submarine requirements, no further consideration has been given in this study to submarine application, but the possibility is noted for future reference.

## Investigation of Specific Ships

From the above ship types, six specific ships have been investigated in more detail, and Table 21 compares their power requirements. The DD963,

Table 21  
COMPARISON OF POWER REQUIREMENTS

Characteristic	DD963	Patrol Frigate	Twin-Screw Destroyer	Swath	Hydrofoil	SES <sup>a</sup>
Displacement (tons)	7000	~4000	4000	2800	750	300
Total power (hp)	80,000	40,000	80,000	40,000	40,000	100,000
Number of shafts	2	1	2	2	2	2 + 4
Prime mover						
Type	Gas turbine	Gas turbine	Gas turbine	Gas turbine	Gas turbine	Gas turbine
Rating (hp)	20,000	20,000	20,000	20,000	20,000	20,000
Speed (rpm)	3600	3600	3600	3600	3600	3600
Propeller speed (rpm)	168	180	180	200	800	800
Motor rating (hp)	Gear	40,000	40,000	20,000	20,000	30,000 (2) 10,000 (4)

\* Two propellers of 30,000 hp each and four lift fans of 10,000 hp each

the patrol frigate, and the twin-screw destroyer are all conventional surface ships of destroyer size. The DD963 is currently being constructed by Litton Industries, Inc. The patrol frigate is under active study by the Bath Iron-works Corporation and Gibbs and Cox. The twin-screw destroyer is a hypothetical, but typical, advanced ship called out in the initial version of Reference 9, which provides preproposal information for a forthcoming Navy request for quotation for a study of superconductive ship propulsion.

The swath ship described in Table 21 is somewhat smaller and is of the double-submerged-hull construction indicated in Figure 66. It has been studied extensively by the Navy and is expected to replace the twin-screw destroyer in the forthcoming Navy request for quotation. The hydrofoil and surface effects ship are typical advanced ships also called out in the initial version of Reference 9; they are expected to remain in the final version.

### Selection of System Rating and Type of Ship

Selection of prime mover and generator ratings and of the speed to be used in this study was relatively straightforward. The commonality indicated in Table 21 makes it quite apparent that very typical conditions are represented by use of a gas turbine prime mover of about 20,000 hp at 3600 rpm, with the generator having the same rating and speed.

Selection of a typical motor rating and speed was not so straightforward. Table 21 indicates that the differences in ship motor requirements mean that a basic decision must be made as to which ship type should be studied (conven-

tional destroyer, swath, hydrofoil, or surface effects ship). The decision was to use the conventional destroyer, because:

- Comparative information for conventional propulsion for this ship type is more readily available, and such comparison is considered an important part of this study.
- One can concentrate more on the superconductive aspects for this type of ship than with the hydrofoil or surface effects ship, because the latter would necessarily get involved with various types of gear trains and a multiplicity of sizes of motors. At this stage of study, and for the scope of this program, such concentration is considered appropriate.

With the decision to base studies on a conventional destroyer-type ship, a motor rating of 40,000 hp and 200 rpm was also selected. The rating of 40,000 hp is apparent from Table 21. The 200 rpm is somewhat higher than the 180 rpm indicated in the table, but is used because a preliminary selection of that rating and speed had been made early in the program, based upon data from the patrol frigate, which at that time had a propeller speed of 200 rpm.

#### System Requirements

System requirements are given in Appendix II, "System Requirements for Superconducting Naval Ship Propulsion System." Explanation of this appendix, where appropriate, is provided below.

Performance Requirements. The system performance requirements are:

- Ratings. Because of inefficiencies, motor, generator, and prime mover ratings are not equal. Of the two basic choices available (fix the prime mover rating or fix the motor rating), the motor rating was chosen to be fixed. This is because it eliminated perturbing motor size and makes ship performance constant. Also, it can be argued that the gas turbine output, because of the wide variety and growth capabilities of these units, can be allowed to fluctuate insofar as it is required in this study. A fixed generator rating was selected for sizing and layout studies, in order to avoid unnecessary perturbations in these areas. The size (18,000 kw) is somewhat larger than actually needed, even with inefficiencies, but is convenient and sufficiently close for size studies.
- Size. The required generator envelope dimensions were selected to assure that the generator is no wider or higher than the LM2500 gas turbine prime mover and thus does not determine mounting spacing. Motor-required envelope dimensions were selected so the motor would fit within the machinery space noted for the twin-screw destroyer described in Reference 9 (height of 14 ft). Required refrigeration equipment envelope dimensions were arbitrarily selected so they

are no larger than the equipment being serviced (motor and generator), a requirement that should be very conservative.

The goal dimensions for the generator and motor are approximately equal to machinery sizes obtained in early studies and are used herein with the rationale that it should be possible to better these numbers. Again, refrigeration equipment size is arbitrarily made no larger than the machines serviced.

- Cross-Connect Switching Time. The goal of 1 minute is based upon information indicating that the time required to do this for a conventional gas turbine/gear drive is 1 to 2 minutes.
- Cooldown and Warmup. Cooldown time is taken from Reference 9. Warmup time is somewhat arbitrary, being selected on the grounds that it is not critical if it is but a small portion of the cooldown time and that it should be possible to warm up considerably faster than it is possible to cool down.
- Generator and Motor Starting Times. These are typical times for the gas turbine and are selected so the generator and motor will be no more restrictive than the turbine.
- Crash Reversal. This requirement is taken from Reference 9.
- Overspeed. The motor value of 25 percent is standard practice for Navy electrical equipment (MILG 18473). The generator value of 10 percent is the same as that of the gas turbine to which it is coupled, the standard 25 percent for electrical equipment being unneeded in this case.
- Short Circuit and Loss of Superconductivity. These are very real possibilities, in spite of care taken to prevent them; therefore the requirements are considered prudent.
- Resonant Frequencies. Speed is adjustable and the possibility exists of running for some time at any speed within the operating range.

Operational Requirements and Goals. Operational requirements and goals include:

- Duty Cycle. These data are taken from Reference 9.
- Life. This requirement is comparable to that for conventional steam turbine gear drive systems, and it is argued that this equipment should be able to do as well.
- Reliability. The mean time between failure of 140,000 hours is comparable to that of marine steam turbines, and it is argued that the goal of this equipment should be to do as well.

- Maintainability. Time between major inspections or overhaul of 45,000 hours is consistent with current Navy practice for d-c motors and generators.

Environmental Requirements. Environmental requirements include:

- Shock and Vibration. The comments in general are based on perusal of applicable specifications. The steady-state acceleration design guidelines for shock are based on experience with marine gear design.
- Magnetic Field Strength. This requirement is taken from Reference 9.
- Inclination. This requirement is the same as that called out in the LM2500 gas turbine specification as well as in MIL-E-17341C, the specification covering gas turbine engines for naval shipboard use. Because a gas turbine is the prime mover in this study, inclination requirements for the electrical and refrigeration equipment should equal, but need not exceed those of the gas turbine.
- Other. All other environmental requirements are taken from Reference 9.

Refrigeration Requirements

Refrigeration requirements of a general nature are contained in Appendix II, "System Requirements for Superconducting Naval Ship Propulsion Systems." The following paragraphs provide requirements that are unique to the refrigeration equipment needed for the specific preliminary designs, which have been prepared in this study, of an a-c generator, a d-c generator, and a d-c motor. These latter designs are consistent with the system requirements listed in Appendix II.

Following is a summary of the refrigeration requirements:

- Refrigeration Approach. The a-c generator utilizes an all-liquefier refrigeration system, wherein saturated liquid helium at about 4.4°K and 1-atmosphere pressure is supplied to the rotor. This helium cools the winding and the current leads, takes care of all heat leakage into the cryogenic portion of the rotor, and exits as a gas at room temperature. Losses in the room temperature outer portion of the rotor are expected to be absorbed by air circulating in the rotor/stator gap.

The d-c generator and d-c motor have a more complex set of temperature stations. Some saturated liquid helium at about 4.4°K and 1-atmosphere pressure is used to cool the electrical leads, exiting from the machine as a gas at room temperature. The winding is cooled by a refrigerator loop, wherein saturated liquid helium at about 4.4°K, and 1-atmosphere pressure is supplied to the winding, cools it, and exits as gas at a maximum allowable temperature of

5.5°K. An intermediate temperature radiation shield at 80°K is also cooled by a refrigeration loop operating at that temperature, using helium gas.

- Steady-State Requirements. Table 22 summarizes the steady-state helium flow and refrigerator loop requirements, as determined in this study, for the a-c generator, d-c generator, and the d-c motor. A word of caution is in order regarding these results, to the extent that they represent reasonable, but not fully optimized, results. This caution should be kept in mind when making comparisons from machine to machine.
- Transient Requirements. Under transient conditions, the heat load increases considerably above the steady-state value. For the a-c generator, it is believed that the most severe of such conditions would occur during a three-phase armature short circuit, wherein additional heat is generated in and around the winding. For the d-c generator, it is believed that the most severe of such conditions would occur during a crash-back maneuver when the field might have to be reversed in 15 seconds or less. Again, this condition produces heat loads in and around the winding. For the d-c motor, the transient analysis indicates that no field ramping will be required during this maneuver.

For the generators, it has been determined that the best way to handle these transient loads is to evaporate a portion of the liquid helium contained in the winding during steady-state operation. This helium is then replaced over a period of time by providing refrigeration system capacity somewhat in excess of the steady-state requirement. The same approach is used for the d-c motor.

Table 23 summarizes results of the transient loads, the suggested increase in refrigeration system capacity over the steady-state value, and the corresponding recovery time from the transients.

Table 22  
SUMMARY OF STEADY-STATE REFRIGERATION REQUIREMENTS

Machine Type	A-C Generator	D-C Generator	D-C Motor
Rating (hp)	24, 000	24, 000	40, 000
Liquefier requirement (g/sec) (at 4.4°K inlet)	0.25	0.11	0.11
Refrigerator requirement (w)			
At 4.4°K - 5.5°K	--	2.5	4.2
At 80°K	--	32	106

Table 23  
TRANSIENT REFRIGERATION LOADS

Machine Type	A-C Generator	D-C Generator	D-C Motor
Rating (hp)	24, 000	24, 000	40, 000
Transient heat load at winding			
Watt-sec	89	510	--
Duration (sec)	0.3	15	--
Average (w)	295	34	--
Helium evaporated during transient			
Gram	4.6	27	--
Liter	0.037	0.22	--
Average rate (g/sec)	15	1.8	--
Steady-state winding requirements			
Helium flow (g/sec)	0.22	--	--
Watts	--	2.5	--
Ratio of transient rate/steady rate	68	14	--
Suggested excess refrigeration			
Capacity at winding (%)*	10	20	20
Recharge time after transient (min)*	~3	~9	--

\*Including latent heat at 4.4°K of helium used to cool conductor leads.

Table 23 shows that an excess refrigeration capacity of 10 percent for the a-c generator will allow recharging the helium evaporated during the transient in about 3 minutes, while 20-percent excess capacity for the d-c generator will allow a recharge in about 9 minutes. These times appear to offer reasonable operation flexibility. It is therefore suggested that refrigeration capacities at 4.4°K of the a-c and d-c generators be 10 and 20 percent, respectively, in excess of steady-state requirements, in order to handle transients. For the purpose of refrigeration system design, a 20-percent extra capacity for the motor has also been specified.

Operational procedures and resultant effects on refrigeration size, to meet the 72-hour cooldown requirements of Appendix III, have not yet been determined.

A-C Generator Steady-State Refrigeration Requirements. A schematic diagram of the generator rotor, to emphasize sources of heating that must be removed by refrigeration, is given in Figure 67. The generator rotor consists of an annular field winding, enclosed within a cylindrical steel shell called a torque ring. This ring supports the winding centrifugal load and also transmits torque to the shaft through what is termed the torque ring extension, but which is an integral part of the torque ring.

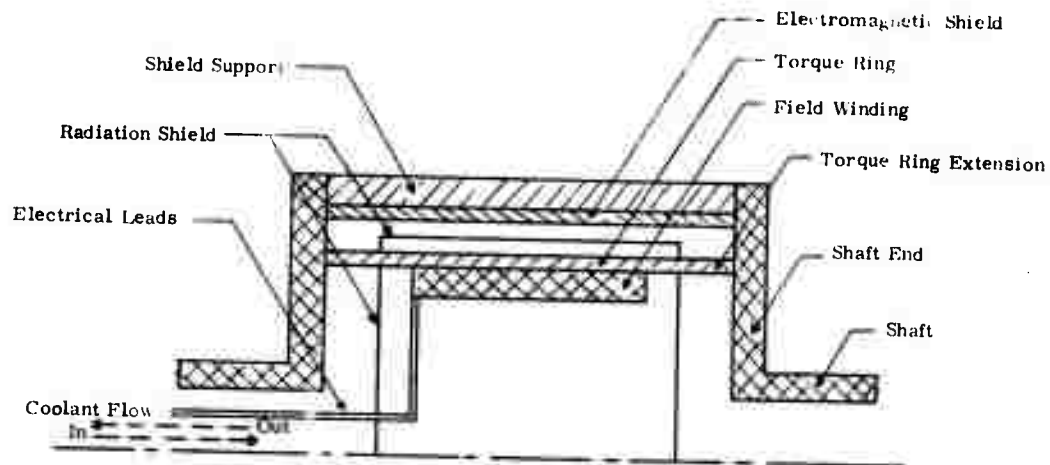


Figure 67. Schematic of A-C Generator Rotor

Another annular cylinder encloses the torque ring and is separated from it by a vacuum gap. This cylinder is a thermal radiation shield, and end bells are also supplied for the same purpose. The radiation shield is maintained at about  $80^{\circ}\text{K}$  by fastening it to an appropriate location of the torque ring extension.

Outside this radiation shield is another cylinder, the electromagnetic shield. The function of this shield is to protect the field winding from non-synchronous fields produced by the armature. It, together with the shaft ends, also maintains the entire rotor interior at a high vacuum. The electromagnetic shield operates at room temperature, and the ends of the torque ring extensions, where they fasten to the shaft ends, are also at room temperature. The winding and the torque ring immediately adjacent to it are maintained at superconducting temperatures.

The design requirement in this case is that the temperature in this region shall not exceed  $5.5^{\circ}\text{K}$  at any time, in order to provide an adequate margin of assurance that the field winding will not go normal. Electrical leads, as indicated in the figure, connect the winding to room temperature conductors.

For this configuration, the sources of heat leak to the winding are:

- Thermal radiation from the electromagnetic shield and shaft ends, partially intercepted by the thermal radiation shield.

- Thermal conduction from the shaft ends, in along the torque ring extensions, with some additional conduction in along the torque ring extensions from the thermal radiation shields, from their points of attachment.
- Conduction in along the current leads.
- Heat generated in and near the field winding, due to time-varying flux such as might be produced by negative sequence currents in the armature, arising from unbalanced loads in the armature circuit.

The steady-state value of this latter heating, in the present analysis, has been assumed to be negligible. This should be a rather reasonable assumption, based on the ability to provide well-balanced armature loads as well as effective attenuation by the electromagnetic shield.

The cooling approach that has been selected is an all-liquefier refrigeration system. Liquid helium at about 4.2 to 4.4°K and approximately 1-atmosphere pressure is supplied to the rotor through a rotating joint along the rotor centerline. This helium is used to absorb the previously mentioned heat leakages and exits from the machine at room temperature. This particular approach has been selected based upon General Electric Company-funded studies of a number of different approaches for larger machines. In all cases, the all-liquefier approach was either better or essentially as good as the other approaches in terms of estimated power input requirements. Because it is a simpler system, and judged to be of comparable or smaller size, it was therefore also selected for the a-c generator to be applied to this study.

In this connection, detailed design layouts and analyses of this a-c generator were separately and previously prepared using General Electric Company funds, as part of a study covering a range of sizes and ratings. Application of the all-liquefier cooling approach to this size and quantitative determination of the refrigeration requirements were also done under the Company-funded study. Details are contained in a General Electric internal report that is available to appropriate persons.

A-C Generator Transient Refrigeration Requirements. A-C generator transient refrigeration requirements include:

- Transient Heating. Transient heating of the field winding and nearby structure will occur whenever the magnetic field seen by the rotor changes magnitude with time. In considering the various possibilities, it is believed that the worst case will be that for a three-phase terminal short circuit of the armature, and the transient heating has been estimated for this condition using the following major assumptions: (1) the losses in the torque ring are predominant, compared with the losses in the superconductor and its copper matrix, (2) the total losses in the

support structure, including end effects, are twice the losses calculated for the active length of the structure, and (3) power dissipation caused by a-c components of armature current is negligible compared to that caused by d-c components, due to the rapid decay time of the former.

Results indicate a transient heating of about 89 watt-seconds over a 0.3-second period, for an average rate of 295 watts in this time.

- Effect on Refrigeration Requirements. For a useful helium cooling capability of about 28 watt-seconds/gram, between the rotor center-line and winding exit temperature of 5.5°K, the transient heating just noted would result in a flow requirement of about 11 grams per second, some 45 times the steady-state helium usage rate. Obviously some means of using thermal capacity to average this out over a longer period is preferred to increasing the capacity of the refrigeration system by such a drastic amount.

A review of this possibility indicates that it should be quite feasible to accommodate the increased transient heat load simply by letting it evaporate some of the liquid helium already present in the winding. A longer time period can then be used to restore conditions in the winding to those prevailing just before the transient.

Calculations indicate that evaporation of a little more than 4 grams of helium will absorb this transient load and that it should be possible to provide adequate volume for helium storage within the winding in such a way that this evaporation will result in a negligible pressure and temperature rise within the winding. With this situation, a refrigeration system having a capacity 10 percent in excess of the steady-state value is capable of restoring the helium stored in the winding to its original condition in about 6 minutes, even if two shorts occur in rapid succession. This situation is considered quite adequate; it has therefore been concluded that transient heating will be accommodated by boiling off liquid helium already stored in the winding region and sizing the refrigeration system for about 10-percent greater capacity than required for steady-state operation.

In connection with this problem, it is noted that the liquid helium in the winding, because of the centrifugal field present, will be immediately adjacent to the torque ring, where the major transient heat is generated, and thus should effectively insulate the winding from this heat.

D-C Generator. To withstand the shock requirements of a marine drive application, the support structure of the superconducting field coil must be designed for high strength and rigidity while minimizing the heat leaks. The design approach used in the present study can be seen in Figure 68.

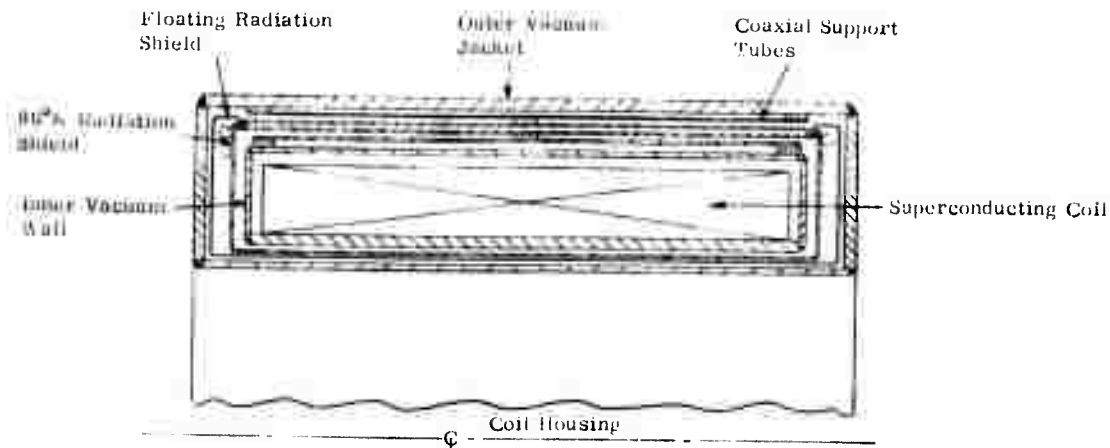


Figure 68. Acyclic Generator -- Dewar Construction

The coil is contained in a vacuum-tight annular can suspended within an enclosing vacuum jacket, the whole of which can be called the dewar. The inner cold chamber, containing the coil, is at nominally atmospheric pressure and is supported through the vacuum region by four coaxial, thin-walled tubes. These support tubes are very rigid, yet present a path of high thermal resistance between the outer walls and the inner cold chamber.

The surfaces of the support tubes are coated with a highly reflective layer to minimize radiation. An enclosing radiation shield, and the intermediate joint of the support tube assembly, are heat-sunk at 80°K.

D-C generator steady-state and transient refrigeration requirements are discussed below:

- Steady-State Refrigeration Requirements. Steady-state thermal loads on the superconducting coil are of three types: current lead conduction, support conduction, and radiation. The current leads can be treated in three different ways: (1) the leads can be uncooled, (2) the leads can be uncooled but have intermediate temperature sinking, and (3) the leads can be vapor-cooled by liquid helium boiloff. Reference 13 shows the superiority of the last method, which takes a portion of the helium boiloff gas as a counterflow coolant up the length of the leads and returns the gas to the refrigeration cycle at ambient temperature. In the present study, vapor cooling was chosen to handle the current lead heat conduction, and a consumption of 4.5 liquid liters of helium per 1000 amperes for a pair of leads was assumed. This value is conservative and could probably be reduced by a third, with careful design.

The degree of conduction heat leak through the support structure is a function of the type of support, the construction material, and the strength level at which it was designed. In the present study the coil support was designed to withstand an acceleration loading of 60g, as a first approximation to meeting the shock requirements of Appendix II,

"System Requirements for Superconducting Naval Ship Propulsion System." The calculation of conduction and radiation heat leaks appears in Appendix III, "Calculation of D-C Generator and Conduction and Radiation Heat Leaks to Superconducting Field Coil."

For the configuration in Figure 68, with all radiation surfaces having an emissivity of 0.03, the following heat leaks result:

<u>Leak</u>	<u>Rate</u>
Heat to 80°K shield	
Conduction	22.8w
Radiation	$\frac{8.9w}{31.7w}$
Heat to coil enclosure	
Conduction	2.4w
Radiation	$\frac{0.1w}{2.5w}$
LHe consumption of leads	0.11 g/sec

A support structure of the same general design, but using glass-filament-reinforced epoxy composite, was also investigated. The additional thickness of the support shells was compensated for by the lower thermal conductivity of the composite, so that within the known accuracy of the parameters, the above results were substantially unchanged.

- D-C Transient Refrigeration Requirements. During a change of magnetic field strength, as when imposed by control requirements, there is a partial conversion of the stored energy of the magnetic field into heat in the refrigerated region. These conversions are the so-called ramping losses, and they are of two types: ohmic losses associated with circulating currents induced in the structure and hysteretic losses within the superconductor itself.

Ramping losses due to induced currents can be controlled by interrupting the circumferential current paths with nonconductors inserted in closed metallic current paths and by using nonconductors, such as glass-epoxy composites, where possible. By careful design, all of the possible current paths in the cold region can be interrupted, except for a thin-walled container, in the coil enclosure, which serves as a hermetic seal to prevent helium diffusion into the vacuum region. In

the present study, it has been assumed that a stainless steel container having 0.010-inch walls will be used as a helium barrier.

Hysteretic losses in the superconductor are a function of the physical properties and geometric construction of the superconducting composite. The calculation of these losses and the above losses is presented in Appendix IV, "Transient Refrigeration Loads Due to Ramping."

Taking a representative extreme maneuver in a marine propulsion system as being a propeller reversal from full ahead to full astern in 15 seconds, the resulting refrigeration load due to the generator field reversal is calculated to be 520 joules (see Appendix IV).

This transient refrigeration load can be adequately handled by the evaporation of a quantity of the liquid helium in which the coil is submerged. Because the quantity of liquid helium needed to furnish 520 joules of refrigeration effect at 4.4°K is only 220 milliliters, it is no problem to provide enough excess liquid storage in the coil dewar to furnish several such reversals in quick succession. The amount of liquid helium consumed during these transients can be made up by excess refrigeration capacity.

A 20-percent refrigeration capacity excess over steady state will restore the liquid helium used during a reversal in less than 9 minutes. This recovery rate, coupled with a few liters of excess storage capacity in the coil dewar, is considered quite adequate. It has therefore been concluded that transient refrigeration demand will be met by providing excess liquid capacity in the coil dewar and a 20-percent capacity increase of the refrigerator over steady-state requirements.

D-C Motor. The construction of the dewar containing the superconducting field coil of the motor is essentially the same as that described above for the d-c generator. As in the generator, the inner cold chamber is supported by concentric thin-walled tubes, heat-sunk at 80°K midway between ambient and coil temperatures. The main difference between motor and generator coil supports is that the former uses two concentric support tubes rather than four. Fewer tubes are needed because the much greater length of the motor coil provides room for a larger conduction path with fewer tubes in series.

Only steady-state conditions were investigated for the d-c motor, because the system analysis indicated that rapid transients of field strength, as required for control purposes, would be required only in the generator. The steady-state refrigeration requirements for the motor were calculated on the same basis as those of the d-c generator, as described above and in Appendix III.

To support the motor coil at an acceleration loading of 60g, the required thickness of A-286 support tubes was found to be 0.078 inch. The following heat leaks result:

<u>Leak</u>	<u>Rate</u>
Heat to 80°K shield	
Conduction	31.8w
Radiation	74.4w
	<u>106.2w</u>
Heat to coil enclosure	
Conduction	3.45w
Radiation	0.76w
	<u>4.21w</u>
LHe consumption of leads	0.11 g/sec at 700 amperes

### COMPARISON CRITERIA

Following are comparison criteria suitable for comparing superconductive ship propulsion systems with each other and with conventional gear drive:

- Performance
  - Efficiency
  - Size and shape
  - Weight
  - Response to speed commands
  - Startup time
  - Field strength external to the machine
- Operation
  - Reliability
  - Life
  - Maintenance requirements
  - Vulnerability to accident or enemy action
  - Noise
  - Safety
  - Detection
  - Cost effectiveness
- Adaptability to Various Ships and Missions
  - Power level (any limitations)
  - Compatibility with prime movers
  - Compatibility with propellers
  - Flexibility of component arrangement

- Development Risk

- Technical barriers
  - Unknowns
  - Probability of success
  - Cost
  - Time

These criteria have been used to the extent practicable in this study, in order to make the comparisons that are described in more detail below.

## COMPARATIVE PERFORMANCE AND RECOMMENDED APPROACH

### Scope

As part of this study, data have been generated to provide a preliminary comparison of the following ship propulsion systems:

- Conventional gear drive
- D-C generator and d-c motor
- A-C generator and a-c motor

These data also make it possible to make a preliminary comparison of various items of individual equipment within these systems. System rating is that called out on pages 164 and 165 under "Selection of System Rating and Type of Ship," namely two 20,000-hp gas turbine-generators driving a single 40,000-hp motor. The type of ship, where study requires this information, is a conventional destroyer.

The following information has been prepared:

- Comparison of fuel consumption for conventional gear drive and superconductive ship propulsion using mission profile information from Reference 9 and for both a single-screw and twin-screw ship. Details of this study are contained on pages 191 through 204.
- Preliminary designs of an a-c generator, a d-c generator, and a d-c motor, as described in detail beginning on pages 204, 207, and 211, respectively.
- Refrigeration requirements for the generator and motor preliminary designs, as already described on page 168 under "Refrigeration Requirements."
- Preliminary design and estimates of size, weight, and performance of the refrigeration equipment required for the generator and motor preliminary designs. Details are contained on pages 60 through 135.

- Preliminary size and weight estimates of transformer/rectifier equipment required for the a-c/d-c system. Details are contained on pages 217 and 218.
- Preliminary study of circuitry and switching for the d-c/d-c system. Details appear on pages 218 through 224.
- Study of optimum bus size and losses for the d-c/d-c system, with details also contained on pages 224 through 228.
- Compilation and extension of the foregoing information into a tabulation of size and weight of the conventional gear drive, d-c/d-c, and a-c/d-c systems for a twin-screw destroyer using the mission profile for that ship (Ref. 9).

The objective of the following paragraphs in this section is to take the pertinent information generated in the foregoing studies and to summarize and compare it.

### Summary and Conclusions

Summary Comparisons. The cross-connection capability of superconductive propulsion results in significant reduction in fuel requirements for the typical destroyer mission described in Reference 9. For a twin-screw ship, this reduction is on the order of 17 percent, without use of small cruise turbine-generator sets and on the order of 22 percent, using small cruise turbine-generator sets (see page 162). For a single-screw ship, no advantage results unless a small cruise turbine-generator set is used, in which case the reduction is on the order of 17 percent.

The cross-connection capability also results in a significant reduction in operating time of the 20,000-hp prime movers for the typical destroyer mission described in Reference 9. The average operating time of these units is 51 percent for both twin-screw and single-screw ships using conventional gear drive.

For the twin-screw ship using superconductive drive, it is reduced to about 27 percent if no cruise unit is used and to about 5 percent if a cruise unit is used. For the single-screw ship with superconducting drive, no reduction is achieved unless the cruise unit is used, in which case the average operating time of the large units is about 9 percent. This reduction in operating time should be significant in increasing overall mission life for the large units and in reducing costs.

Size and weight of the a-c generator and of the d-c generator are very nearly the same and should not be a significant factor in making a system selection.

Size, weight, and power requirements of the refrigeration equipment for the a-c and d-c generators are very similar and should not be significant in making a system selection; indeed, it appears that the refrigeration system, in itself, will have very little impact in choosing between a d-c/d-c and an a-c/d-c system. (Refrigeration system weight for the generators is about 5% of the generator weight while volumes are about 75% of the generator volume.)

The size and weight of the refrigeration system for the d-c motor are small relative to the motor (total volume is < 10% of motor volume, cryosection volume is < 1% and weight is < 1/2%).

The weight, volume, and area of d-c buswork, though large compared to conventional higher voltage buses, are quite reasonable in relation to the rest of the equipment for the twin-screw destroyer mission profile of Reference 9. For example, the bus weight using copper buses at minimum system weight is about half the total generator weight, about 12% of the total motor weight, about 1/3 of the weight of gas turbine inlet and exit exhaust ducts in a conventional gear drive, and about 1/4 the weight of reduction gearing for a conventional gear drive. This weight includes allowance for cooling but does not include the support structure. Use of aluminum buses would reduce this weight by about 25 percent at minimum system weight.

Correspondingly, the bus volume using copper buswork at minimum system weight is about 60% of the total generator volume, about 11% of the total motor volume, about 1% of the volume of gas turbine inlet and exit exhaust ducts in a conventional gear drive, and about 4 percent of the volume of reduction gearing for a conventional gear drive. This volume includes allowance for cooling. Use of aluminum buswork would increase the volume by about 140% at minimum system weight.

The area of each copper bus (two required per generator) at minimum system weight is about 61 square inches, including a 35-percent area allowance for cooling. Minimum system weight for copper buses occurs for a bus loss of about 3 percent, while for aluminum bus work it is at a loss of about 2 percent for the twin-screw mission profile of Reference 9.

Preliminary indications are that transformer/rectifier sizes are significantly larger than the d-c motor and, of course, much larger than the d-c bus volume (perhaps 15 or more times as large as copper buswork). Weight of these items also appears to be very large compared to d-c/bus weight (perhaps twice as heavy as copper buses), while losses are expected to be about the same as the d-c/d-c buswork. However, some caution should be exercised here, in that transformer/rectifier sizing studies were quite limited. More work should be done before drawing definite conclusions.

For the twin-screw destroyer mission profile of Reference 9, the weights of all three systems (conventional gear, d-c/d-c without cruise units, and a-c/d-c without cruise units) are equal to one another within the accuracy of the study, differing by less than 1.5 percent. In this connection, the reduced weight of fuel and gas turbine inlet and exhaust ducting attributable to the superconducting systems is essentially offset by the greater weight of their electrical equipment compared to reduction gearing.

For the same mission profile, both superconducting systems, however, have a total volume about 30 percent less than that of the conventional gear drive.

The requirement for shielding the d-c motor results in a significant weight and volume penalty. The weight increment for the twin-screw ship is about 370,000 pounds for two motors. This increment is about 14 percent of the total system weight for the mission profile of Reference 9. The motor diameter and length could be reduced about 40 percent and 20 percent, respectively, if the shielding requirement did not exist.

Major Conclusions. For conventional destroyer application, the following appear to be the prime advantages of the superconducting system relative to a gear drive:

- Capability for locating the prime movers at or near deck level, with consequent implications on accessibility in maintenance, overhaul, replacement of units, and manning requirements.
- Significant reductions in average operating time of the prime movers, with consequent implications on overall mission life and cost.

Concurrently, there appears to be no significant weight saving for a fully shielded superconductive system compared to gear drive. Although there is a volume saving of about 30 percent, the value of this saving may be somewhat limited, because the need for tight volume restrictions for this type of ship is not too evident, as far as the destroyer-type ship used in this study is concerned.

A true evaluation of the real merit of the advantages cited above (because it is closely associated with the intended use and ship type considered) is beyond the scope of this study, so no firm conclusion has been drawn. However, as an opinion, it would seem that there is not a great deal of incentive for applying superconducting propulsion to conventional destroyer-type ships unless something additional is done, such as using contrarotating propellers. In this connection, a d-c superconducting motor is considered to be highly

suited to driving contrarotating propellers, offering, in effect, the possibility of doubling motor power output in the same frame size. When this possibility is coupled with the increased efficiency obtainable by the application of such propellers, a significant improvement in performance for conventional destroyer-type ships might result. This potential improvement has not been studied in this contract.

The foregoing conclusion would also be expected to apply to the swath-type ship, assuming a similar mission profile and based on current information on volume availability for such a ship.

Hydrofoil and surface effects ship applications may be much more promising for superconductive propulsion because of the additional possibility of eliminating complex gear trains.

From results of this study, concern over large d-c buswork that has been evidenced from time to time appears to be overdrawn. Viewed in its proper perspective as another item of equipment in the system, d-c bus size, volume, cost, and losses are very reasonable. In this connection, better perspective might be gained by comparing d-c buswork to the gas turbine inlet and exhaust ducting, a highly fair comparison.

The major trade-offs between a-c/d-c and d-c/d-c systems appear to be:

- Relative development and operational risk of the a-c generator versus the d-c generator.
- Size, weight, and efficiency of transformer/rectifier equipment versus d-c buswork.

In the first category, the d-c system clearly has the advantage due to its stationary superconductive coil. Results of the present study indicate it also has an advantage in the second category, but more transformer/rectifier studies are required before a definite conclusion can be drawn.

While no firm conclusion can yet be drawn, due to uncertainties in transformer/rectifier sizes and weights, the weight of evidence to date indicates that the d-c/d-c system is preferable to the a-c/d-c system. Such a conclusion would receive added support, it is believed, in hydrofoil applications where the transformer/rectifier equipment must also be placed in the pod with the motor, in order to avoid buswork and bus losses comparable to those of the d-c system.

### Performance Comparisons

Weight and Volume. Table 24 is a summary of the weight and volume estimates for major system elements as determined during this study. One of

Table 24  
WEIGHT AND VOLUME OF MAJOR COMPONENTS

Component	Weight (lb)		Volume (ft <sup>3</sup> )	
Gas turbine*	--	44,500	--	600
Turbine	10,300	--	--	--
Enclosure/base/accessories	34,200	--	--	--
Reduction gear**	--	116,000	--	1,950
A-c generator*	--	20,000	--	55
D-c generator*	--	26,000	--	58
D-c motor**	--	244,000	--	590
Transformers/rectifiers**	--	70,000	--	1,170
Refrigeration				
A-c generator	--	1,132	--	43
Cryosection	532	--	11	--
Compressor subsystem	600	--	32	--
D-c generator	--	1,007	--	41
Cryosection	407	--	9	--
Compressor subsystem	600	--	32	--
D-c motor	--	916	--	47
Cryosection	226	--	5	--
Compressor subsystem	690	--	42	--

\*20,000-hp nominal

\*\*40,000-hp nominal

the more interesting aspects of this table is the small weight of the refrigeration equipment, relative to the equipment it is cooling, and the small volume of the refrigeration equipment for the motor, relative to the motor size. Volume of refrigeration equipment for each generator is roughly comparable to the corresponding generator volume. Motor volume is seen to be about one third that of the reduction gear for a conventional drive. Transformer/rectifier volume is relatively large.

Using the basic building blocks from Table 24, plus results of studies on fuel consumption and d-c bus weight and volume from pages 201, 226, and 227, a

compilation of weights and volumes has been prepared for the twin-screw destroyer-type ship of Reference 9, using four 20,000-hp gas turbines driving four 20,000-hp generators, with two 40,000-hp motors per shaft. The two 5000-hp turbine-generator sets suggested in Reference 9 for this ship have been omitted in this compilation.

Three systems, as previously mentioned, have been considered:

- Conventional gear drive
- D-C/D-C
- A-C/D-C

Weight and volume summaries are provided in Tables 25 and 26, respectively. More detailed breakdown of these weights and volumes is contained in Tables 27 and 28, respectively. Figures 69 through 71 provide a graphic picture of each system, showing the arrangement and relative volumes of equipment. For convenience, only half of the system is shown in each figure; that is, the equipment associated with one of the two shafts. Volumes, where appropriate, are prorated accordingly. For example, the fuel volume shown is half the volume required for the complete, two-shaft system. In these figures, the equipment size is drawn to scale. Some averaging of height and depth dimensions has been made, where needed, so each figure can be viewed, on a volume basis, as having a depth equal to the height shown in the figures.

Table 25  
SUMMARY OF WEIGHT FOR TWIN-SCREW SHIP

System Type	Conventional Gear (lb)	D-C Generator D-C Motor (lb)	A-C Generator D-C Motor (lb)
Gas turbines	358,000	237,000	237,000
Gear	232,000	--	--
Electrical system	--	680,000*	708,000*
Refrigeration system	--	5,900	6,400
Fuel	2,093,000	1,723,000	1,715,000
Total	2,683,000	2,645,900**	2,666,400
Increment	0	-37,100	-16,600
Percent increment	0	-1.4	-0.6

\*Motor shielding weight = 370,000 lb

\*\*Use of aluminum buswork could decrease total weight by ~33,000 lb

Table 26  
SUMMARY OF VOLUME FOR TWIN-SCREW SHIP

System Type	Conventional Gear (ft <sup>3</sup> )	D-C Generator D-C Motor (ft <sup>3</sup> )	A-C Generator D-C Motor (ft <sup>3</sup> )
Gas turbines	15,400	4,400	4,400
Gear	3,900	--	--
Electrical system	--	1,660	3,740
Refrigeration system	--	257	265
Fuel	37,250	30,700	30,550
Total	56,550	37,017	38,955
Increment	0	-19,533	-17,595
Percent increment	0	-35	-32

Table 27  
SUMMARY OF SYSTEM WEIGHT FOR TWIN-SCREW SHIP<sup>(1)</sup>

System Type	Conventional Gear (lb)		D-C Generator D-C Motor (lb)		A-C Generator A-C Motor (lb)	
Gas turbine	--	358,000	--	237,000	--	237,000
Turbines	41,000	--	41,000	--	41,000	--
Enclosures/base/accessories	137,000	--	137,000	--	137,000	--
Ductwork <sup>(5)</sup>	180,000	--	59,000	--	59,000	--
Gear	--	232,000	--	--	--	--
Generator	--	--	--	105,000	--	80,000
Motor	--	--	--	488,000	--	488,000
Switches	--	--	--	28,000	--	Assumed
Buswork	--	--	--	59,000 <sup>(2)</sup>	--	Negligible
Transformers/rectifiers	--	--	--	--	--	Assumed
Controls	Not estimated		Not estimated		Not estimated	
Refrigeration						
Generator	--	--	--	5900	--	6400
Cryosection	--	--	1600	--	2100	--
Compressor subsystem	--	--	2400	--	2400	--
Subtotal	--	--	4000	--	4500	--
Motor						
Cryosection	--	--	500	--	500	--
Compressor subsystem	--	--	1400	--	1400	--
Subtotal	--	--	1900	--	1900	--
Fuel	2,093,000		1,723,000 <sup>(4)</sup>		1,715,000	
Total	2,683,000		2,645,900		2,666,400	

1) Two motors--nominal rating = 40,000 hp each.

Four generators and four turbines - nominal rating - 20,000 hp each.

2) Use of aluminum bases could reduce this by ~17,000 lb. Includes ~4% allowance for weight of coolant, consistent with coolant area allowance.

3) Assumes weight of transformer = 50% of commercial practice.

4) Use of aluminum buses could reduce this by ~16,000 lb.

5) Not including inlet and exit silencers, which could add ~79,000 pounds.

Table 28

## SUMMARY OF SYSTEM VOLUME FOR TWIN-SCREW SHIP\*

System Type	Conventional Gear (ft <sup>3</sup> )		D-C Generator/D-C Motor (ft <sup>3</sup> )		A-C Generator/D-C Motor (ft <sup>3</sup> )	
Gas turbine						
Turbines	2400	15,400	2400	4400	2400	4400
Enclosures/base/accessories**	--	--	--	--	--	--
Ductwork	13,000	--	2000	--	2000	--
Gear	--	3900	--	--	--	--
Generator	--	--	--	230	--	220
Motor	--	--	--	1180	--	1180
Switches	--	--	--	115	--	Assumed negligible
Buswork	--	--	--	135†	--	Assumed negligible
Transformers/rectifiers	--	--	--	--	--	2340††
Controls	Not estimated		Not estimated		Not estimated	
Refrigeration	--	--	--	257	--	265
Generator	--	--	--	--	--	--
Cryosection	--	--	36	--	44	--
Compressor subsystem	--	--	<u>128</u>	--	<u>128</u>	--
Subtotal	--	--	164	--	172	--
Motor	--	--	--	--	--	--
Cryosection	--	--	9	--	9	--
Compressor subsystem	--	--	<u>84</u>	--	<u>84</u>	--
Subtotal	--	--	93	--	93	--
Fuel		37,250		30,700		30,550
Total		56,550		37,017		38,955

\*Two motors-nominal rating = 40,000 hp each.

Four generators and four turbines-nominal rating = 20,000 hp each.

\*\*Added volume of enclosure and base not included.

†Use of aluminum could increase this by ~190ft<sup>3</sup> for operation at minimum weight of fuel and bus.

Includes 35% allowance for coolant volume.

†† Rectifier volume not included. Assumes volume  $\pm$  50% of commercial practice.

A few background comments concerning these tables and figures are in order before discussing them in more detail:

- Fuel weights and volumes are based on the mission profile for this ship, as given in Reference 9, and include realistic gas turbine specific fuel consumption characteristics and system component efficiencies. These calculations are described in detail beginning on page 191.
- D-C bus size and losses have been optimized to result in minimum weight of buswork plus fuel (which will very nearly minimize the total system weight). D-C bus volume and weight also include an allowance for cooling. These calculations are described in more detail beginning on page 224.

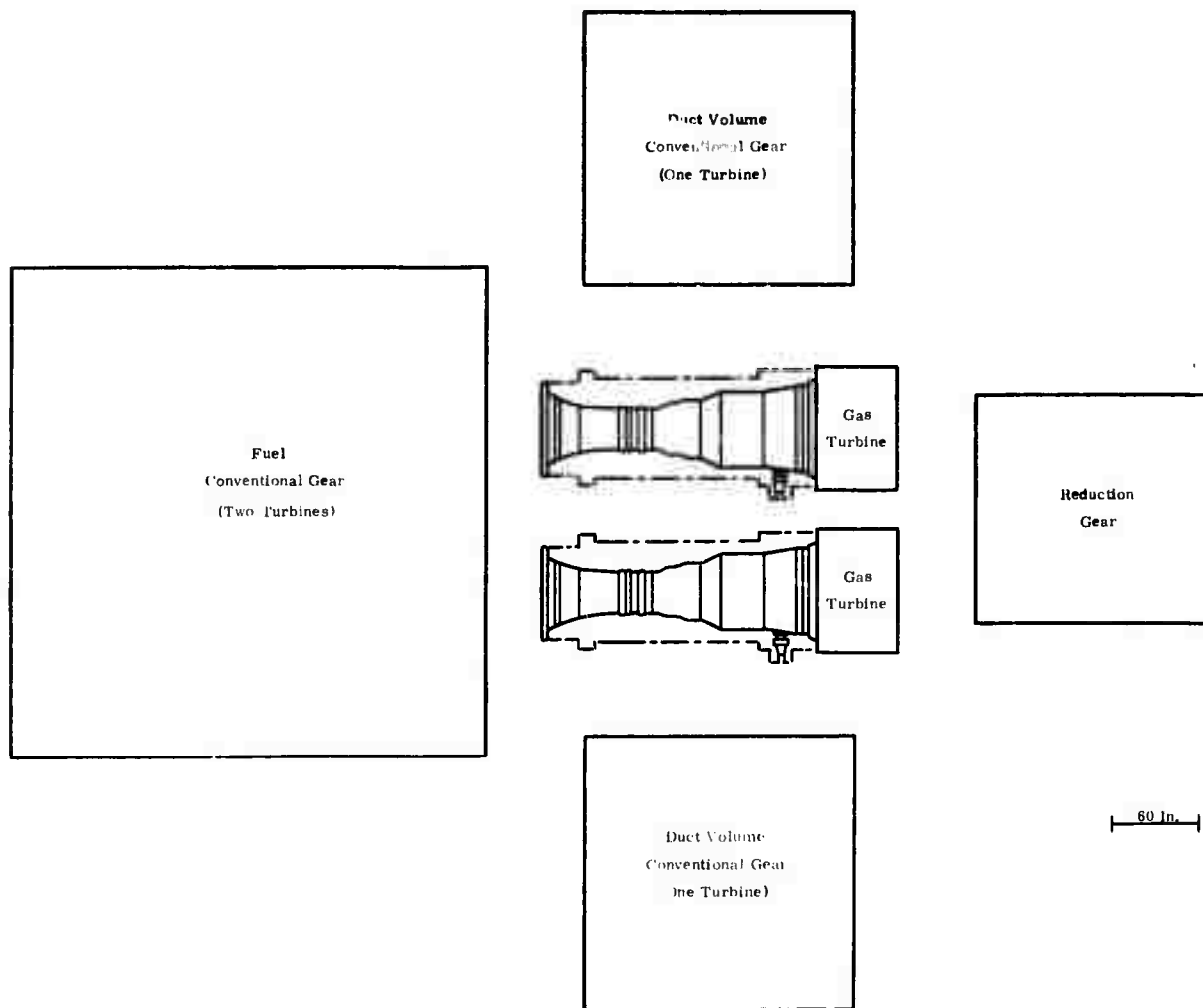


Figure 69. Conventional Gear Propulsion System

- Reduction gear weight and volume estimates are based on General Electric Company studies of similar ships, but are not otherwise detailed here.
- Transformer-rectifier weights are based on rather limited studies, as described in more detail on pages 217 and 218.
- The analysis resulting in refrigeration equipment sizes and weights is discussed in detail on pages 60 through 135.

The most striking feature of Table 25 is that the weight of all three systems is equal within the accuracy of this study. The superconductive systems result in a significant fuel weight saving, compared to the gear drive, due to their cross-connect capability. They also result in a saving in gas turbine weight due to reduction of inlet and exhaust ducting weights occasioned by placing the turbines at or nearer the deck level (see Table 27 for a breakdown). However, these are essentially offset by the greater weight of electrical equipment relative to the reduction gear.

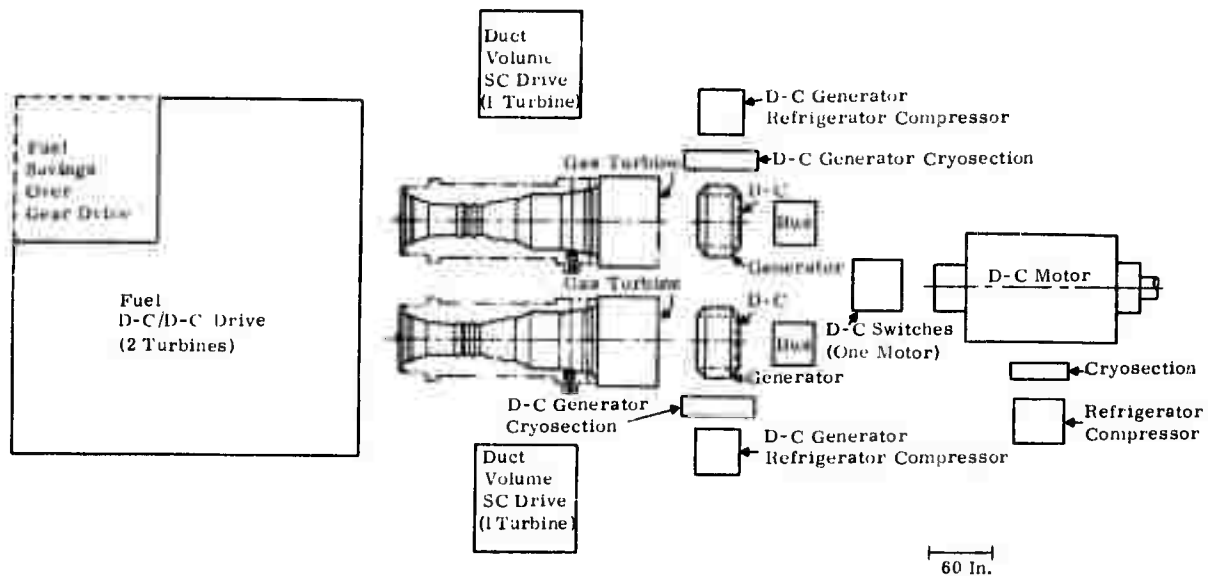


Figure 70. D-C/D-C Propulsion System

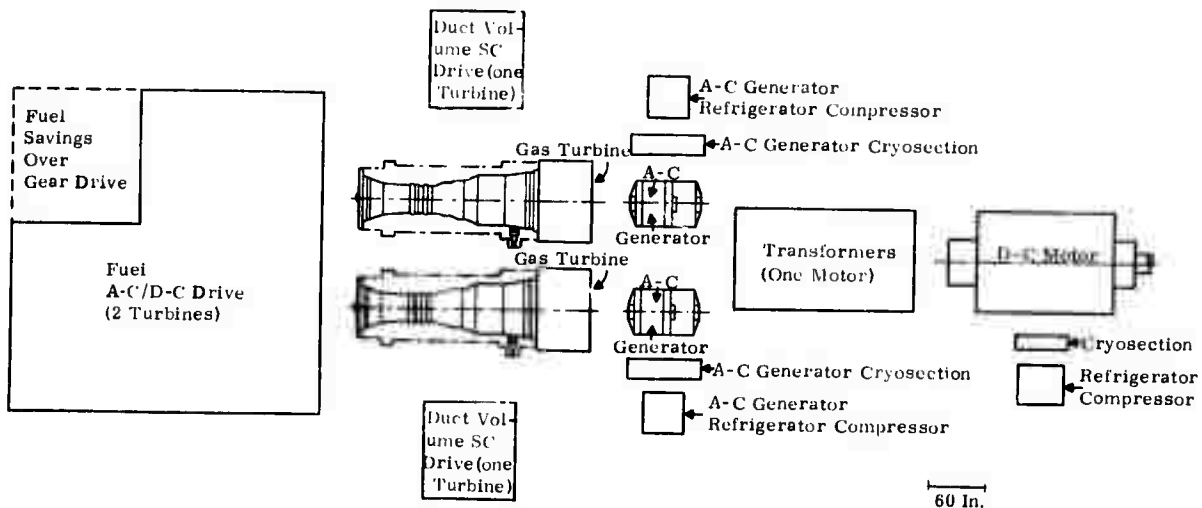


Figure 71. A-C/D-C Propulsion System

Note from Table 25 that the shielding weight of the motor (370,000 lb) is a significant percentage of the total, and if there were any way of reducing this total by relaxing shielding requirements, this means would be significant. Use of aluminum buswork in the d-c/d-c system would reduce total weight by about 33,000 pounds, which, though useful, is a small portion of the total system weight. Control weights have not been estimated. It is believed that there would not be a sufficient enough difference between the systems to affect trade-off considerations.

The most striking feature of Table 26 is that the superconductive systems have a significant reduction in volume compared to the gear drive (about 30%). This difference is due to the combined effects of reduced gas turbine ducting

volume (see Table 28 for a breakdown) and of fuel volume. Of course it should be noted that volume saving in fuel may not be as important as in the other areas, because of possibly greater flexibility in locating the fuel in the ship. Note also from Table 26 that the combined volume of either electrical system is less than the volume of the reduction gear, although the a-c/d-c system is just barely so, due to the large transformer/rectifier volume. Here it should also be recognized, however, that because many items of equipment are involved with the electrical systems, access to them will require space not included in this volume comparison.

Figures 69 through 71, which graphically illustrate the system arrangements and relative sizes of equipments, show more clearly:

- Very large fuel volume compared to other equipment and the significant fuel volume saving for the superconductive systems.
- Large gas turbine duct volume for the conventional gear drive and the corresponding saving in the superconductive systems.
- Relatively small volume of d-c/d-c buswork, compared to other equipments and particularly, for example, compared to gas turbine ducting.
- Rather large volume of the transformers in the a-c/d-c system.

Corresponding to the previous comment on the significant weight attributable to shielding the d-c motor, it can be noted that shielding also occupies a considerable volume. If it were removed, d-c motor diameter and basic length could be reduced approximately 40 percent and 20 percent, respectively -- significant amounts.

**Efficiency.** Efficiency is significant in the final analysis only as it affects size, weight, and cost, and the effect on size and weight have been factored into the results already discussed. For comparison purposes, the best estimates resulting from this study are that the conventional gear drive will have about 3-percent losses between the gas turbine and propeller, while both types of superconducting drive will have about 7-percent losses, as indicated in Table 29. With these efficiencies, the fuel savings are as illustrated in Figures 70 and 71.

Table 29  
SYSTEM LOSSES

Component	D-C/D-C (%)	A-C/D-C (%)
Generator	1	1.2
Motor	2.6	2.6
Bus	1	Negligible
Transformers/rectifiers	--	0.5
Refrigeration equipment	0.4	0.4
Total	7	6.7

The d-c/d-c bus size and losses have been optimized to minimize total weight of the bus and fuel for a copper bus. In both systems, it is assumed that the d-c motor design finally used will be at a lower flux density and higher efficiency than the nominal design detailed herein (as discussed on page 216).

Although the losses in the superconducting system are somewhat higher than those in the conventional gear drive, the advantages of cross coupling for a twin-screw ship more than offset the losses, resulting in a fuel saving (as previously indicated in Table 25).

Cost Effectiveness. No cost effectiveness analysis has been performed. A few cost figures may, however, be of interest. First, with respect to d-c/d-c buswork, the raw material cost for the twin-screw ship would be about \$29,000 and \$10,000, respectively, for copper and for aluminum buses, assuming a basic metal cost of about 50 cents a pound for copper and 25 cents a pound for aluminum. Second, with respect to fuel costs, the fuel savings using the superconducting drive compared to the conventional gear drive would be about \$7500 per mission, assuming a fuel cost of about 2 cents per pound.

It has not been determined whether any of the above figures will have a significant impact on a final cost effectiveness study.

Other Comparison Criteria. Not a great deal can be said at this time regarding the remaining comparison criteria on page 176 as they apply to the three systems studied. Items such as response to speed commands, startup time, field strength external to the machine, reliability, life, maintenance requirements, vulnerability to accident or enemy action, noise, safety, and detection have quantitatively or qualitatively been made part of the system requirements of Appendix II. The assumption is that all systems can perform satisfactorily in these regards. Probably the a-c/d-c system will have more difficulty meeting noise requirements because of transformer noise. The d-c buswork may be somewhat more vulnerable to enemy action because of its larger size. No really striking potential for significant advantages of one superconducting system relative to another in the foregoing categories, however, is foreseen.

The same comment applies with respect to adaptability to various-type ships and missions, as itemized in the list of comparison criteria (page 176). No particular difference is foreseen for the two superconducting systems, with both having a significant advantage over the conventional gear drive with respect to flexibility of component arrangement, especially location of the prime mover.

In the area of development risk, as itemized on page 177, it would appear that the d-c generator has less risk and requires less development time and cost than the a-c machine, because of its having a stationary instead of a rotating field coil; however, no quantitative estimates have been made.

Not listed as comparison criteria, except by implication, is the effect that refrigeration system requirements and performance might have on the choice between the a-c generator and the d-c generator. At the beginning of the study, it was thought that this effect might be highly significant. Results, however, indicate that refrigeration equipment may play a minor role in selection of the preferred superconducting system. Sizes, weights, and power requirements are essentially the same for the two machines, as can be seen under "Summary of System Designs" on page 133 and also in Tables 24 through 28.

The a-c refrigeration system, as currently designed, has one more rotating stage, implying less reliability, but a reasonable adjustment in the thermal radiation shield temperature could reduce this to two stages, with probably minor effect on performance and size.

### RECOMMENDATIONS

From the results of this study, the following recommendations are made for future work:

- Make a study of transformer-rectifier sizes and weights and performance losses in sufficient detail to make a valid comparison with d-c buswork and arrive at a conclusion regarding a-c/d-c systems versus d-c/d-c systems for any particular application.
- Make a system study of superconductive propulsion equipment for SWATH, hydrofoil and surface effects ship applications to determine the incentive for such use.
- Perform the following studies for destroyer-type ships:

Assess the effect of the capability for locating the prime mover at or near deck level for maintenance, overhaul, replacement of units, and manning requirements.

Assess the effect on overall mission life and cost of reduced average operating time of the prime mover when using superconductive propulsion.

Assess the effect of utilizing contrarotating propellers and motors on the potential advantages of superconductive propulsion.

Assess the real advantage of a volume saving when using a superconductive propulsion system, compared to a gear drive.

From the preceding recommendations, make a recommendation as to the incentive for applying superconductive propulsion to conventional destroyer-type ships as well as to swath-type ships.

## ANALYSIS

### Fuel Economy and Operating Time of Prime Movers

Cases Considered. This section reports on the procedures and results of an analysis carried out to obtain quantitative information on the effects of electrical propulsion on fuel economy and prime mover operating time.

Both single-screw and twin-screw ships were considered, with the following cases considered for each:

<u>Ship</u>	<u>Case</u>	<u>Description</u>
Single screw	1	Two 20,000-hp gas turbines and a gear drive, with capability for operating either or both turbines
	2	Same as Case 1, but with electric drive (two 20,000-hp generators and one 40,000-hp motor)
	3	Same as Case 2, but with one 5000-hp turbine-generator for cruise/low power
Twin screw	1	Four 20,000-hp gas turbines and gear drive, two turbines per shaft with capability for operating either or both, and no cross-connect capability between shafts
	2	Same as Case 2, but with electric drive and cross-connect capability between shafts (two 20,000-hp generators and one 40,000-hp motor per shaft)
	3	Same as Case 2, but with two 5000-hp turbine-generators for cruise power and with cross-connect capability

A typical mission profile was assumed. Analytical, but realistic, gas turbine characteristics were used, and the effects of operating the turbine-generator at both rated speed and at variable speed to obtain minimum fuel consumption were determined.

Mission Profile. The mission profile of Table 30 was used. This profile is taken from Reference 9 and is considered typical of a destroyer-type ship.

Gas Turbine Characteristics. Table 12 indicates that all of the detailed ship applications investigated in this study utilize or plan on utilizing a 20,000-hp, 36-rpm gas turbine, which specifically is the General Electric Company Model No. LM2500. It is therefore pertinent to examine the characteristics of this turbine.

Figure 72 gives the horsepower, speed, and specific fuel consumption of this machine at 100°F ambient temperature. It also shows a typical propeller

Table 30  
TYPICAL MISSION PROFILE

Step	Time (hr)	Operation	Power (% rated)	Prop Speed (% rated)
1	0	Dockside	0	0
2	0-0.1	Dockside	0	0
3	0.1-0.11	Dockside maneuver	0.013	5
4	0.11-1.0	Harbor maneuver	1.6	25
5	1.0-1.1	Harbor maneuver	1.6	25
6	1.1-2.0	Cruise/patrol	12.5	50
7	2.0-3.0	Patrol/watching	0	0
8	3.0-300.1	Patrol/alert	0	0
9	300.1-305	Flank speed	100	100
10	305-310	High speed	70	80
11	310-350	High speed cruise	23	61
12	350-352	Harbor maneuver	1.1	22
13	>352	Dockside	0	0

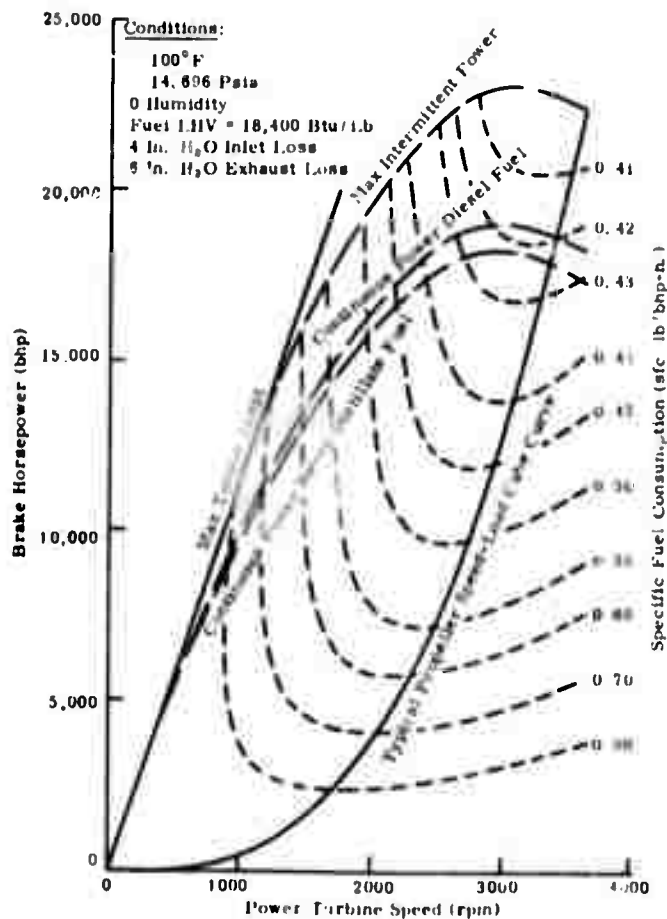


Figure 72. LM2500 Estimated Engine Performance  
(Subject to 5% Production Variation)

speed/horsepower curve, which assumes propeller power is proportional to the cube of the speed. Two items of major interest from this figure are:

- The fact that speed should be reduced as load is reduced, in order to achieve minimum specific fuel consumption.
- The turbine characteristics match very well with propeller characteristics, so the turbine will, over essentially the entire load range, operate near minimum specific fuel consumption when direct-connected to a propeller. This characteristic seems generally typical of gas turbines of this type (with a free power turbine). This observation can be noted from Figures 73 and 74, which give performance of two other actual machines, one in the 20,000 to 30,000-hp range and one in the 5000-hp range.

If the minimum specific fuel consumption points of Figure 72 are plotted versus rated power on a normalized basis, the result is the curve shown in Figure 75. This curve quite graphically shows the penalties that are paid when a gas turbine is run at partial load, even when this is done at the minimum specific fuel consumption points. The advantage, in a multiple-turbine ship, of being able to shut turbines down as load is decreased, is quite apparent.

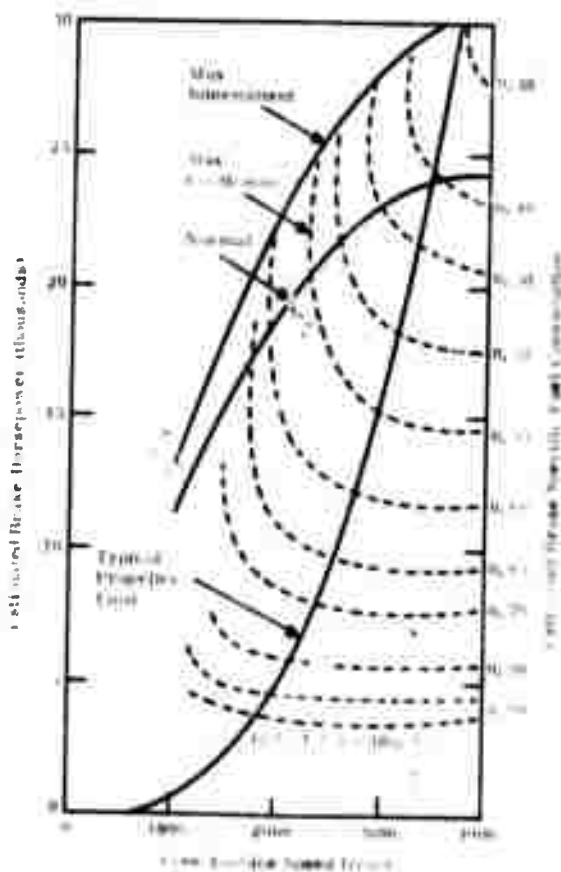


Figure 73. Variation of Fuel Consumption with Horsepower and Speed (59°F Inlet Temperature, Fuel LHV = 18,500 Btu/lb)

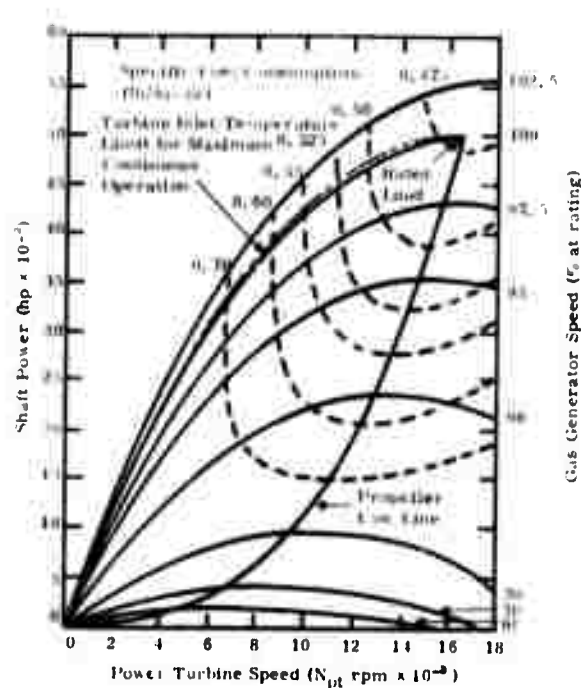


Figure 74. Horsepower SFC Speed Characteristic GTPF990

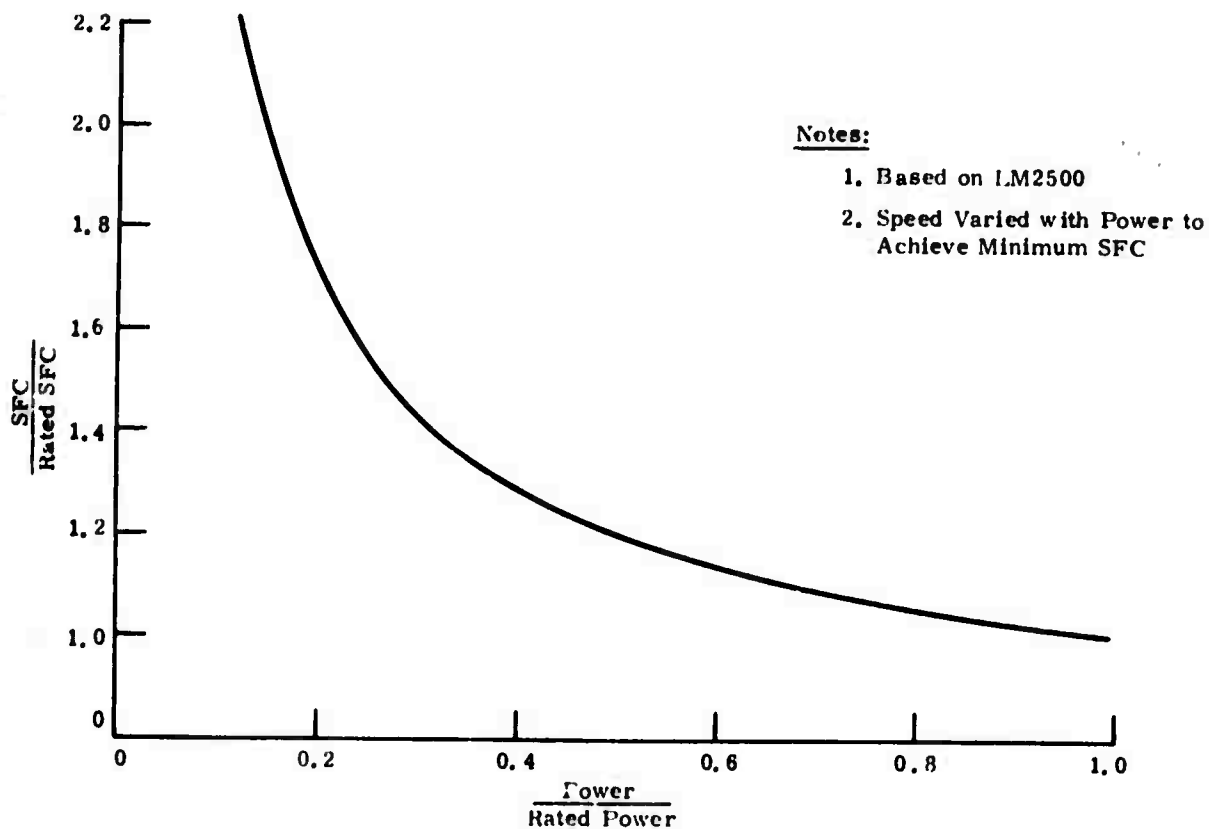


Figure 75. Typical Minimum Specific Fuel Consumption of Marine Gas Turbine (~ 20,000 Hp)

Rather than use the actual characteristics of the LM2500 turbine and those of a smaller 5000-hp turbine, gas turbine performance was assumed to be represented by the analytical expressions given in Reference 9. This assumption has been made in order to make results of this study more comparable with results to be obtained from the forthcoming Navy study, to be based on Reference 9, where these same analytical expressions are to be used.

The relations are:

- 20,000-hp turbine

$$W_f = \frac{Q + 6.6 + 1.05N}{1.143 (8 - N)}$$

where:

$W_f$  = Fuel Rate (1000 lb/hr)

$N$  = Power turbine speed (1000 rpm)

$Q$  = Power turbine torque (1000 lb-ft)

which can be rearranged to give:

$$P = \frac{\frac{6.6 + 1.05 N}{1.143 (8-N)SFC} - \frac{1}{190.2N}}{1000}$$

where:

SFC = Specific fuel consumption (lb/hp-hr)

$P$  = Power turbine horsepower (hp)

- 5000-hp turbine

$$W_f = \frac{Q + 0.66 + 0.042 N}{0.159 (20 - N)}$$

which can be rearranged to give:

$$P = \frac{\frac{0.66 + 0.042N}{0.159 (20-N)SFC} - \frac{1}{190.2N}}{1000}$$

Figures 76 and 77 give the performance resulting from use of these expressions. By comparison with Figure 72 and 74, it is seen that these analytical expressions give quite realistic performance characteristics, compared to actual units, and may therefore be used with considerable confidence in this study.

Similar to Figure 75, Figure 78 gives the specific fuel consumption as a function of propeller power for various numbers and combinations of the 20,000- and 5000-hp units, using the preceding expressions. This is done for the case where speed is adjusted with load, as required to obtain minimum specific fuel consumption and also for the case where speed is maintained constant at the rated value. From this curve, the advantage of switching to fewer units as load is decreased is graphically illustrated.

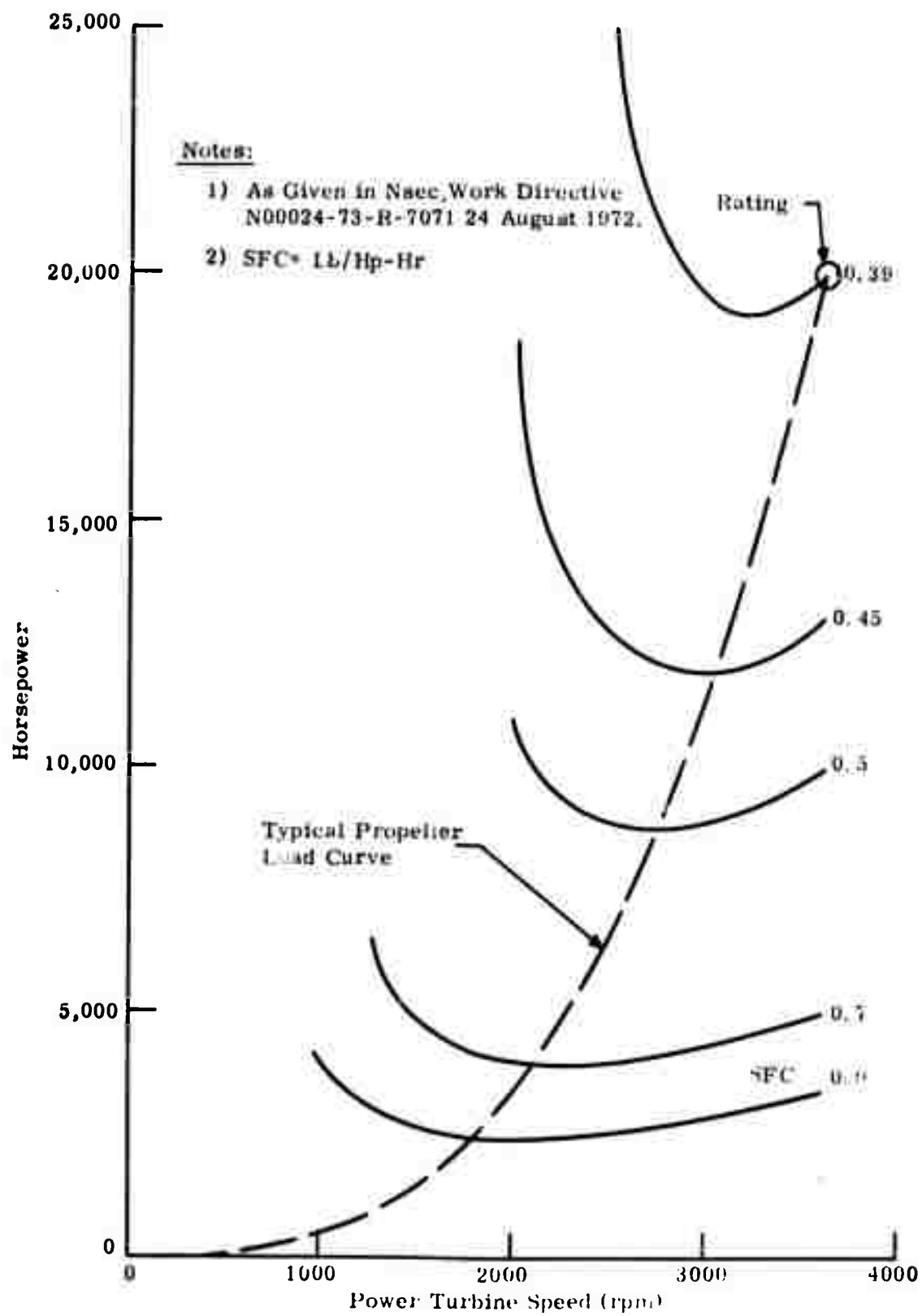


Figure 76. Typical Performance of 20,000-Hp Gas Turbine

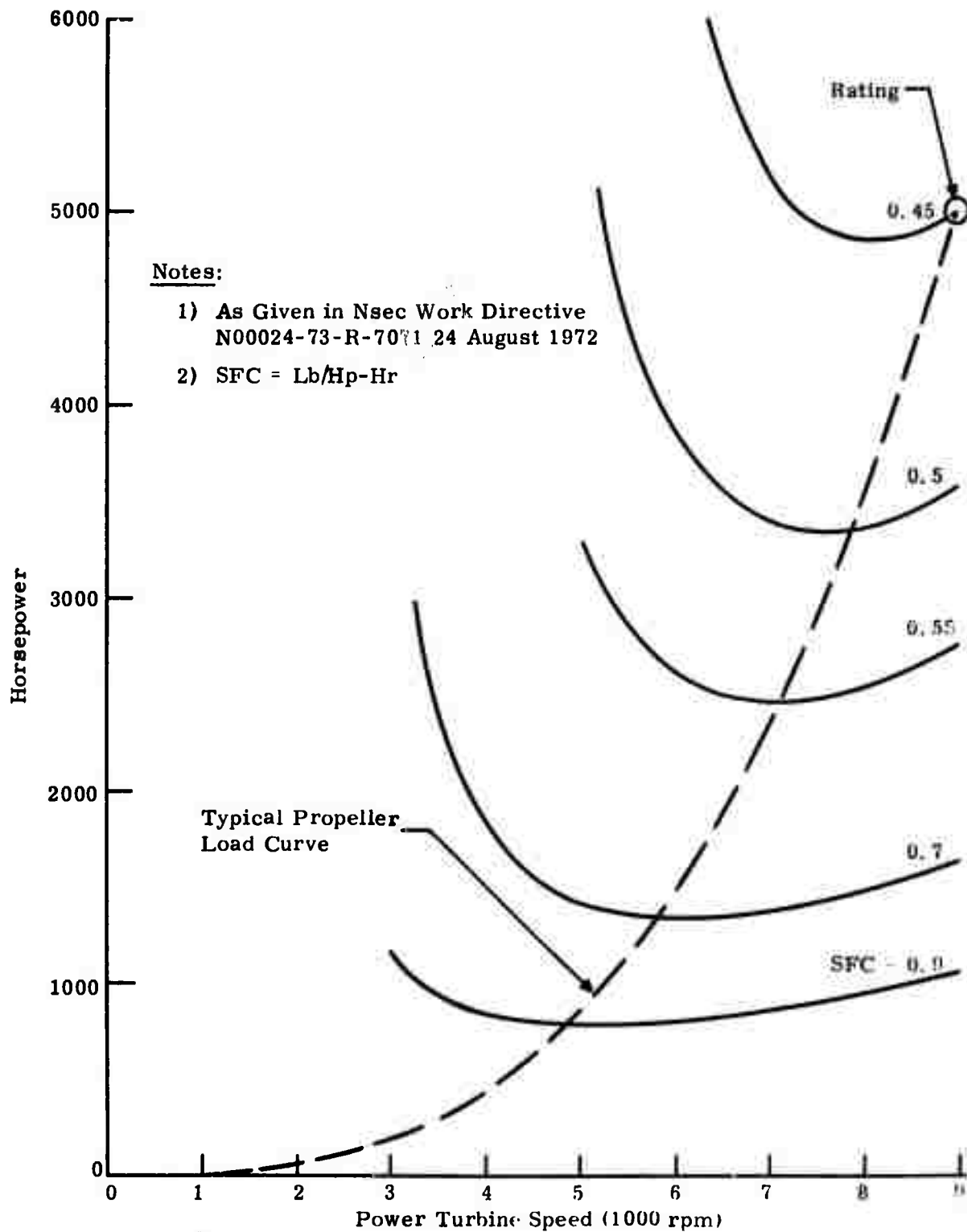


Figure 77. Typical Performance of 5000-Hp Gas Turbine

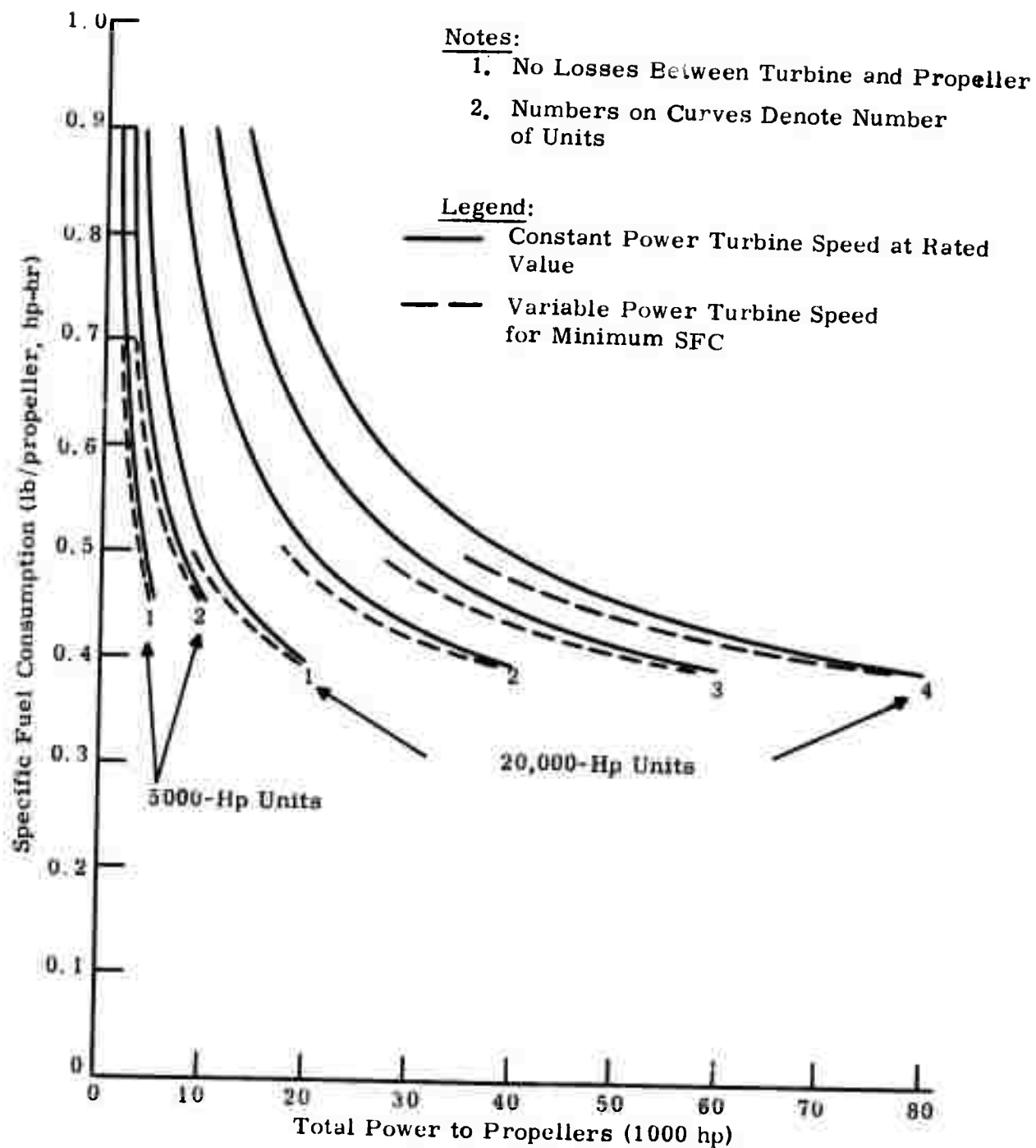


Figure 78. Specific Fuel Consumption for Various Gas Turbine Combinations

Finally, as working curves, Figures 79 and 80 give fuel flow versus turbine horsepower for the 20,000- and 5000-hp units, respectively, for both minimum specific fuel consumption and rated speed.

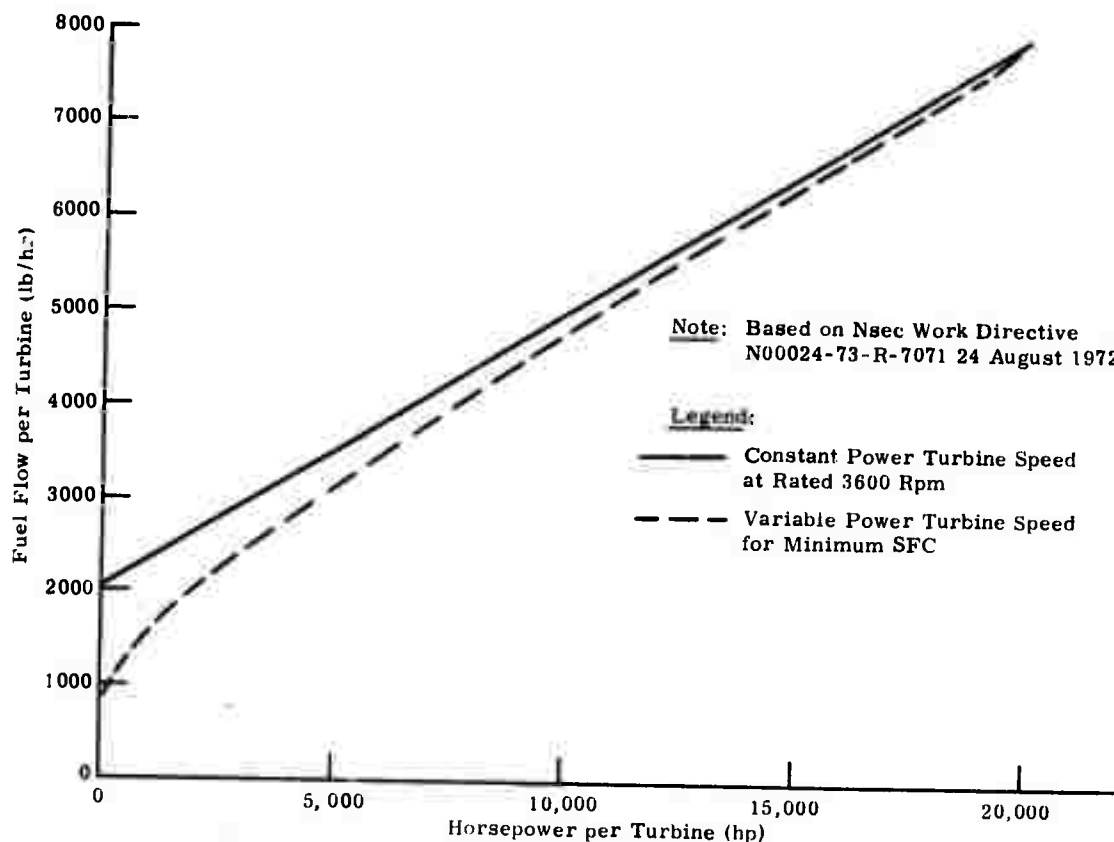


Figure 79. Typical Fuel Flow for 20,000-Hp Gas Turbine

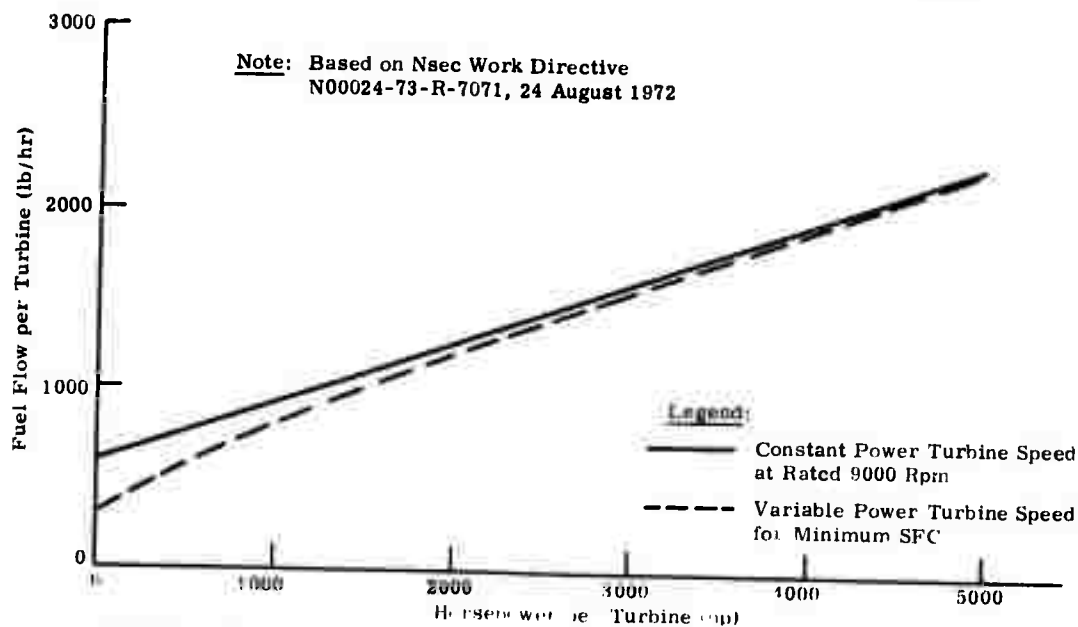


Figure 80. Typical Fuel Flow for 5000-Hp Gas Turbine

**Fuel Consumption.** Based upon the normalized mission profile of Table 30 and actual ratings of the machines used for the cases described on page 191 under "Cases Considered," more detailed mission profiles for the single-screw and twin-screw ship are shown in Tables 31 and 32, respectively. These

**Table 31**  
**MISSION PROFILE, SINGLE-SCREW SHIP**  
**(40,000 Hp)**

Step	Time (hr)	Operation	Propeller Power (% rated)	Propeller Power (hp)	Case 1 (Gear) 20,000 hp			Turbine Status								
								Case 2 (Electric) 20,000 hp			Case 3 (Electric with cruise unit)					
								Off	Idle	Hot	20,000 Hp			5000 Hp		
1	0	Dockside	0	0	2	0	0	2	0	0	2	0	0	1	0	0
2	0-0.1	Dockside startup	0	0	1	1	0	1	1	0	2	0	0	0	1	0
3	0.1-0.11	Dockside maneuver	0.013	5.2	1	0	1	1	0	1	2	0	0	0	0	1
4	0.11-1.0	Harbor maneuver	1.6	640	1	3	1	1	0	1	2	0	0	0	0	1
5	1.0-1.1	Harbor maneuver	1.6	640	1	0	1	1	0	1	2	0	0	0	0	1
6	1.1-200	Cruise/patrol	12.5	5,000	1	0	1	1	0	1	2	0	0	0	0	1
7	200-300	Patrol/watching	0	0	1	1	0	1	1	0	0	0	0	0	1	0
8	300-300.1	Patrol/alert	0	0	0	2	0	0	2	0	0	2	0	1	0	0
9	300.1-305	Flank speed	100	40,000	0	0	2	0	0	2	0	0	2	1	0	0
10	305-311	High speed	70	28,000	0	0	2	0	0	2	0	0	2	1	0	0
11	310-350	High speed cruise	23	9,200	1	0	1	1	0	1	1	0	1	1	0	0
12	350-352	Harbor maneuver	1.1	440	1	0	1	1	0	1	2	0	0	0	0	1
13	>352	Dockside	0	0	2	0	0	2	0	0	2	0	0	1	0	0

\*See page 191 for definition of cases.

**Table 32**  
**MISSION PROFILE FOR TWIN-SCREW SHIP**  
**(80,000 Hp)**

Step	Time (hr)	Operation	Propeller Power (% rated)	Propeller Power (hp)	Case 1 (Gear) 20,000 hp			Turbine Status								
								Case 2 (Electric) 20,000 hp			Case 3 (Electric with cruise unit)					
								Off	Idle	Hot	20,000 Hp			5000 Hp		
1	0	Dockside	0	0	4	0	0	4	0	0	4	0	0	2	0	0
2	0-0.1	Dockside startup	0	0	2	2	0	3	1	0	4	0	0	1	1	0
3	0.1-0.11	Dockside maneuver	0.013	10.4	2	0	2	3	0	1	4	0	0	1	0	1
4	0.11-1.0	Harbor maneuver	1.6	1,280	2	0	2	3	0	1	4	0	0	1	0	1
5	1.0-1.1	Harbor maneuver	1.6	1,280	2	0	2	3	0	1	4	0	0	0	1	1
6	1.1-200	Cruise/patrol	12.5	10,000	2	0	2	3	0	1	4	0	0	0	0	2
7	200-300	Patrol/watching	0	0	2	2	0	3	1	0	4	0	0	1	1	0
8	300-300.1	Patrol/alert	0	0	0	4	0	0	4	0	0	4	0	2	0	0
9	300.1-305	Flank speed	100	80,000	0	0	4	0	0	4	0	0	4	2	0	0
10	305-311	High speed	70	56,000	1	0	3	1	0	3	1	0	3	2	0	0
11	310-350	High-speed cruise	23	18,400	0	0	3	3	0	1	3	0	1	2	0	0
12	350-352	Harbor maneuver	1.1	880	2	0	2	3	0	1	4	0	0	1	0	1
13	>352	Dockside	0	0	4	0	0	4	0	0	4	0	0	2	0	0

\*See page 191 for definition of cases.

tables give not only the actual hp requirements during the mission but also the status of all gas turbine units. Using these tables and the fuel consumption

characteristics given by Figures 80 and 81, the fuel requirements for each phase of the mission, as well as the total fuel requirements, are given in Table 33 and 34, respectively, for the single-screw and twin-screw ships for the various cases for no losses. These tables show which portions of the mis-

Table 33  
FUEL REQUIREMENTS FOR SINGLE-SCREW SHIP  
(No Losses)

Step	Operation	Constant Power Turbine Speed (lb)			Variable Power Turbine Speed (lb)		
		Case 1* (Gear)	Case 2* (Electric)	Case 3* (Electric with Cruise unit)	Case 1* (Gear)	Case 2* (Electric)	Case 3* (Electric with Cruise unit)
1	Dockside	0	0	0	0	0	0
2	Dockside Startup	207	207	59	90	80	32
3	Dockside maneuver	21	21	6	9	8	3
4	Harbor maneuver	1,985	1,985	721	1,200	1,200	579
5	Harbor Maneuver	223	223	81	135	135	65
8	Cruise/patrol	696,000	696,000	447,500	617,500	617,500	447,500
7	Patrol/watching	207,000	207,000	58,300	80,000	80,000	31,700
8	Patrol/alert	414	414	414	160	160	160
9	Flank speed	77,500	77,500	77,500	77,500	77,500	77,500
10	High speed	61,500	61,500	61,500	60,000	60,000	60,000
11	High-speed cruise	189,600	189,600	188,600	180,800	180,800	180,800
12	Harbor maneuver	4,360	4,360	1,480	2,400	2,400	1,100
13	Dockside	0	0	0	0	0	0
	Total	1,238,910	1,238,810	938,161	1,019,783	1,019,783	799,439
	Total fuel ratio	1.22	1.22	0.82	1.00	1.00	0.79

\*See page 191 for definition of cases.

Table 34  
FUEL REQUIREMENTS FOR TWIN-SCREW SHIP  
(No Losses)

Step	Operation	Constant Power Turbine Speed (lb)			Variable Power Turbine Speed (lb)		
		Case 1* (Gear)	Case 2 (Electric)	Case 3* (Electric with Cruise unit)	Case 1* (Gear)	Case 2* (Electric)	Case 3* (Electric with Cruise unit)
1	Dockside	0	0	0	0	0	0
2	Dockside Startup	414	207	59	180	90	32
3	Dockside maneuver	41	21	6	18	8	3
4	Harbor maneuver	3,970	2,150	893	2,400	1,513	919
5	Harbor maneuver	446	242	160	270	170	124
6	Cruise/patrol	1,392,000	980,000	885,000	1,235,000	850,000	895,000
7	Patrol/watching	414,000	207,000	58,300	160,000	80,000	31,700
8	Patrol/alert	828	828	828	320	320	320
9	Flank speed	155,000	155,000	155,000	155,000	155,000	155,000
10	High speed	112,800	112,800	112,600	111,000	111,000	111,000
11	High speed cruise	378,000	297,000	297,000	361,000	294,000	294,000
12	Harbor maneuver	8,720	4,600	1,760	4,800	3,000	1,500
13	Dockside	0	0	0	0	0	0
	Total	2,497,220	1,769,861	1,522,808	2,029,986	1,585,091	1,489,498
	Total fuel ratio	1.22	0.97	0.76	1.00	0.79	0.74

\*See page 191 for definition of cases.

sion require the major portion of the fuel and in which portions of the mission the greatest changes occur between the various cases. Steps 6 and 7, the cruise/patrol and patrol/watching portions of the mission, are seen to affect fuel consumption the most.

In Tables 33 and 34, Case 1, constant turbine speed is of little interest, because there is no reason to run the power turbine at constant speed with the gear drive. It is included, however, for completeness. Case 1, variable speed gear drive, is really the conventional reference case with which the superconducting electric drive should be compared, and the total fuel ratios indicated in these tables are based upon this case.

Tables 35 and 36 summarize the overall results for no losses. Points brought out by these tables are:

Table 35  
COMPARISON OF TOTAL FUEL CONSUMPTION  
FOR VARIOUS PROPULSION COMBINATIONS, SINGLE-SCREW SHIP  
(40,000 Hp, No Losses)

Propulsion Combination	Power Turbine Speed	
	Constant at Rated	Variable for Minimum SFC
Total fuel consumption ( $10^6$ lb)		
Case 1 -- gear drive	1.24	1.02
Case 2 -- electric drive	1.24	1.02
Case 3 -- electric drive with cruise equipment	0.84	0.80
Fuel ratio*		
Case 1 -- gear drive	1.22	1.00
Case 2 -- electric drive	1.22	1.00
Case 3 -- electric drive with cruise equipment	0.82	0.79

\*Defined as ratio of total fuel for case considered to total fuel for Case 1 and variable turbine speed.

Table 36  
COMPARISON OF TOTAL FUEL CONSUMPTION  
FOR VARIOUS PROPULSION COMBINATIONS, TWIN-SCREW SHIP  
(80,000 Hp, No Losses)

Propulsion Combination	Power Turbine Speed	
	Constant at Rated	Variable for Minimum SFC
Total fuel consumption ( $10^6$ lb)		
Case 1 -- gear drive	2.47	2.03
Case 2 -- electric drive	1.77	1.60
Case 3 -- electric drive with cruise equipment	1.53	1.49
Fuel Ratio*		
Case 1 -- gear drive	1.22	1.00
Case 2 -- electric drive	0.87	0.79
Case 3 -- electric drive with cruise equipment	0.78	0.74

\*Defined as ratio of total fuel for case considered to total fuel for Case 1 and variable turbine speed.

- Electric drive for the single-screw ship offers no improvement in fuel consumption unless a small cruise unit is used. This situation exists basically because the gear drive already has the capability for operating one or both large turbines.
- For the twin-screw ship, the addition of electric drive significantly improves fuel consumptions, and the addition of the small cruise units helps only a small amount.
- Operation at variable turbine speed gives a significant improvement over constant speed operation for both gear and electrical drives, but this advantage diminishes considerably if small cruise units are used.

Parenthetically, it is of interest to note that the saving in fuel consumption for the electric drive, compared to the conventional gear drive for the twin-screw ship and variable turbine speed, represents a fuel volume on the order of 7500 cubic feet, a value considerably greater than values of any of the power components.

The effect of inefficiencies on the preceding results has been estimated. Table 37 is a tabulation of typical losses for various components, based upon results of this study. From these losses, it was concluded that a typical effi-

Table 37  
COMPARISON OF TYPICAL LOSSES

Component	% of Rated
A-C generator	1.2
D-C generator	1.0
D-C motor	4.5
A-C/D-C transformers/rectifiers	2
D-C/D-C bus	2
Cryogenic refrigerator power input	
A-C generator	0.19
D-C generator	0.20
D-C motor	0.14
Gear drive (two turbines/ shaft with clutching)	3.0

ciency for the electrical drive is about 92 percent, compared to about 97 percent for a gear drive using two turbines on a single shaft. (See Table 29 for later estimates.) The relative total fuel consumption for variable turbine speed using these values is given in Table 38, where the corresponding values for no losses are also shown. In making these calculations, it was assumed that the effect of inefficiency on turbine specific fuel consumption during each phase of the mission is negligible and that efficiency of the system does not change with load.

Table 38  
RELATIVE FUEL CONSUMPTION

Component	With Losses*		No Losses	
	Twin Screw	Single Screw	Twin Screw	Single Screw
Gear drive**	1.00	1.00	1.00	1.00
Superconducting	0.83	1.05	0.79	1.00
Superconducting with Cruise unit	0.78	0.83	0.74	0.79

\*Gear loss assumed = 3 percent.

\*\*Comparisons must be made vertically. Total fuel for reference gear drive is different for each case.

The effect of losses does not particularly change the nature of the results. It is concluded that for this mission profile, addition of electrical drive compared to conventional gear drive improves fuel consumption about 17 to 22 percent for a twin-screw ship, depending upon whether cruise units are or are not used. Improvement for a single-screw ship requires use of the cruise units, with a resultant fuel saving of about 17 percent.

Operating Time. Using the information of Tables 31 and 32, the operating time of the turbines has been determined for the various cases and is given in Tables 39 and 40, respectively, for the single-screw and twin-screw ships. The relative operating time from these tables is summarized in Table 41. A dramatic reduction in operating time for the large turbines is seen to occur with the addition of the electric drive. Again, however, the single-screw ship requires cruise turbines in order to achieve this reduction.

This reduced operating time should be significant in increasing overall mission life for the large units and in reducing costs.

#### A-C Generator

Detailed design layouts and analyses of the a-c generator used in this study to determine refrigeration requirements were carried out separately

**Table 39**  
**COMPARISON OF TURBINE OPERATING TIMES PER MISSION**  
**FOR SINGLE-SCREW SHIP\***

Description**	Case 1 Gear Drive	Case 2 Electric Drive	Case 3 Electric Drive with Cruise Unit
20,000-hp turbines			
Total time (hr)	362	362	60
Average time per turbine (hr)	181	181	30
Average operating time (%)†	51	51	8.5
5,000-hp turbines			
Total time (hr)	--	--	302
Average time per turbine (hr)	--	--	302
Average operating time (%)†	--	--	86

\*See Table 31 for mission profile.

\*\*See page 191 for definition of cases in detail.

†Defined as ratio of average time per turbine over mission duration of 352 hours.

**Table 40**  
**COMPARISON OF TURBINE OPERATING TIMES PER MISSION**  
**FOR TWIN-SCREW SHIP\***

Description**	Case 1 Gear Drive	Case 2 Electric Drive	Case 3 Electric Drive with Cruise Unit
20,000-hp turbines			
Total time (hr)	719	377	75
Average time per turbine (hr)	180	94	19
Average operating time (%)†	51	27	5.4
5,000-hp turbines			
Total time (hr)	--	--	501
Average time per turbine (hr)	--	--	250
Average operating time (%)†	--	--	71

\*See Table 32 for mission profile.

\*\*See page 191 for definition of cases in detail.

†Defined as ratio of average time per turbine over mission duration of 352 hours.

**Table 41**  
**RELATIVE OPERATING TIME**

Component	Twin Screw (%)	Twin Screw (%)
Gear Drive		
20,000-hp turbine	51	51
Superconducting		
20,000-hp turbine	27	51
Superconducting with Cruise unit		
20,000-hp turbine	5.4	8.5
5000-hp turbine	71	86

and previously using General Electric Company funds. This work includes both rotor and stator studies and applies to a 60-hertz, two-pole machine. Details of this work are contained in a General Electric Company internal report that is available to appropriate persons.

The following comments regarding the design are, however, appropriate here:

- The rotor design is capable of withstanding stresses produced by steady-state loads and transient loads, including 10-percent over-speed, short circuit conditions and 75g steady acceleration (to approximate shockloading, per Appendix II, "System Requirements for Superconducting Naval Ship Propulsion System"). Capability to withstand the 75g steady acceleration was checked as part of this study.
- The rotor design has been checked for stability in both torsion and bending and was found to be adequate. This work was done as part of this study.
- A preliminary assessment was made of the critical speed of the generator rotor, and it has been concluded that the lowest critical speed should be well above the 120 hertz most likely to be the maximum driving frequency for a two-pole, 60-hertz machine. This assessment was also made as a part of this study.
- A complete analysis of torsional natural frequencies requires consideration of the total generator/prime mover system with the inter-connecting shafting. For purposes of this study, it is felt that such an analysis would be premature; however, torsional resonant frequencies in the torque ring and electromagnetic shields themselves were investigated as uncoupled members. It is concluded that the resonant frequencies are well above the most likely maximum driving frequency of 120 hertz.

This work was done as a part of this study. The effect of coupling was not analyzed, but it is believed that it will not change the results significantly.

In connection with the desire to reduce transformer/rectifier volume and weight (see page 182), a preliminary evaluation was made of the effect on generator performance of designing a 180-hertz machine (6-pole at 3600 rpm) as contrasted with the 60-hertz machine just described. The design was not carried out to the detail of the 60-hertz design; it was carried out to the point, however, where it is apparent that the difference between the two cases should not be significant from a system standpoint, although rotor critical speeds, for example, may warrant more careful study due to the higher possible driving frequency.

## D-C Generator

The d-c generator was sized on the basis of being driven at the same shaft speed as the a-c generator, 3600 rpm. The output of two of these generators is combined in series to power a single, 40,000-hp motor at a nominal 100-volt generator terminal voltage. The choice of the system voltage and the series connection of the generators is discussed on pages 218-223. On this basis, the individual generator is required to produce 14.9 megawatts (20,000 hp) plus bus and motor losses; however, to put the generators on a more direct basis of comparison, the d-c generators were sized at the same power as the a-c generator, namely 18 megawatts (24,000 hp).

The type of machine chosen for this study was a multidisk acyclic generator, utilizing a 22-percent sodium, 78-percent potassium eutectic (NaK-78) in a non-flooded collector system. The collector system was modeled after existing machines built by the General Electric Company. In these machines, the sodium potassium is circulated by the inherent pumping action of the collectors. This circulation serves the dual purpose of cooling the generator collector and  $I^2R$  losses and allowing for the cleaning of the sodium potassium. From the standpoint of mechanical simplicity, it is desirable to have the fewest number of disks possible without exceeding peripheral velocities that have been experimentally demonstrated to be practical (25,000 to 30,000 ft/min).

Parametric Study of Generator Designs. To select a suitable nominal design, a computer analysis was performed to yield the parametric size relationships of disk-type acyclic generators. Calculation inputs were power, voltage, and current, and the parametric variables were the number of disks and effective flux density. Details of other assumptions are discussed following the results described below.

The results of the analysis are shown in Figure 81. These results need little interpretation. The parametric variation was not carried beyond four disks, because of the previously mentioned desire to design the generator with a minimum number of disks to minimize the number of sodium potassium external loops. The parametric results show that a two-disk machine can be designed for 100 volts, and other calculations show that a 200-volt generator has acceptable characteristics with three disks. Machine volume is not much improved in going to more disks and machine shape is not of concern, because the generators are relatively small. For the two- and three-disk machines referred to, the losses are acceptable, and the peripheral velocities are below 30,000 rpm, which represents the limit of General Electric operating experience (although not necessarily an absolute limit).

The various assumptions that have gone into the parametric analysis are described below. A constant shaft diameter sized to carry short-circuit torque was used. Disk thickness was set by stress calculations that showed that a total of six inches of axial contact length between the shaft and driven disks

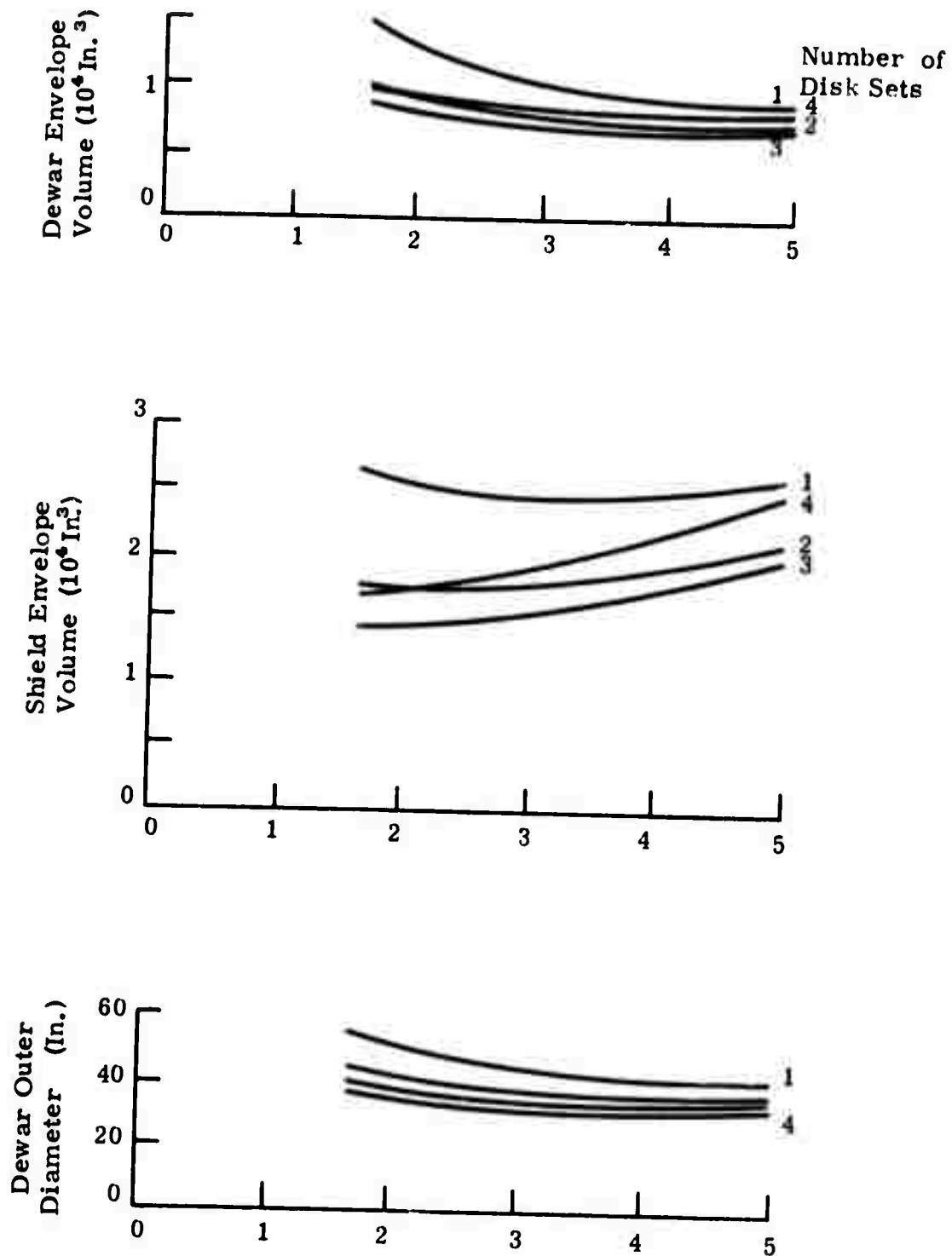


Figure 81. Acyclic Generator Parametric Study  
(24,000 Hp, 3600 Rpm, 100V) (Sheet 1 of 2)

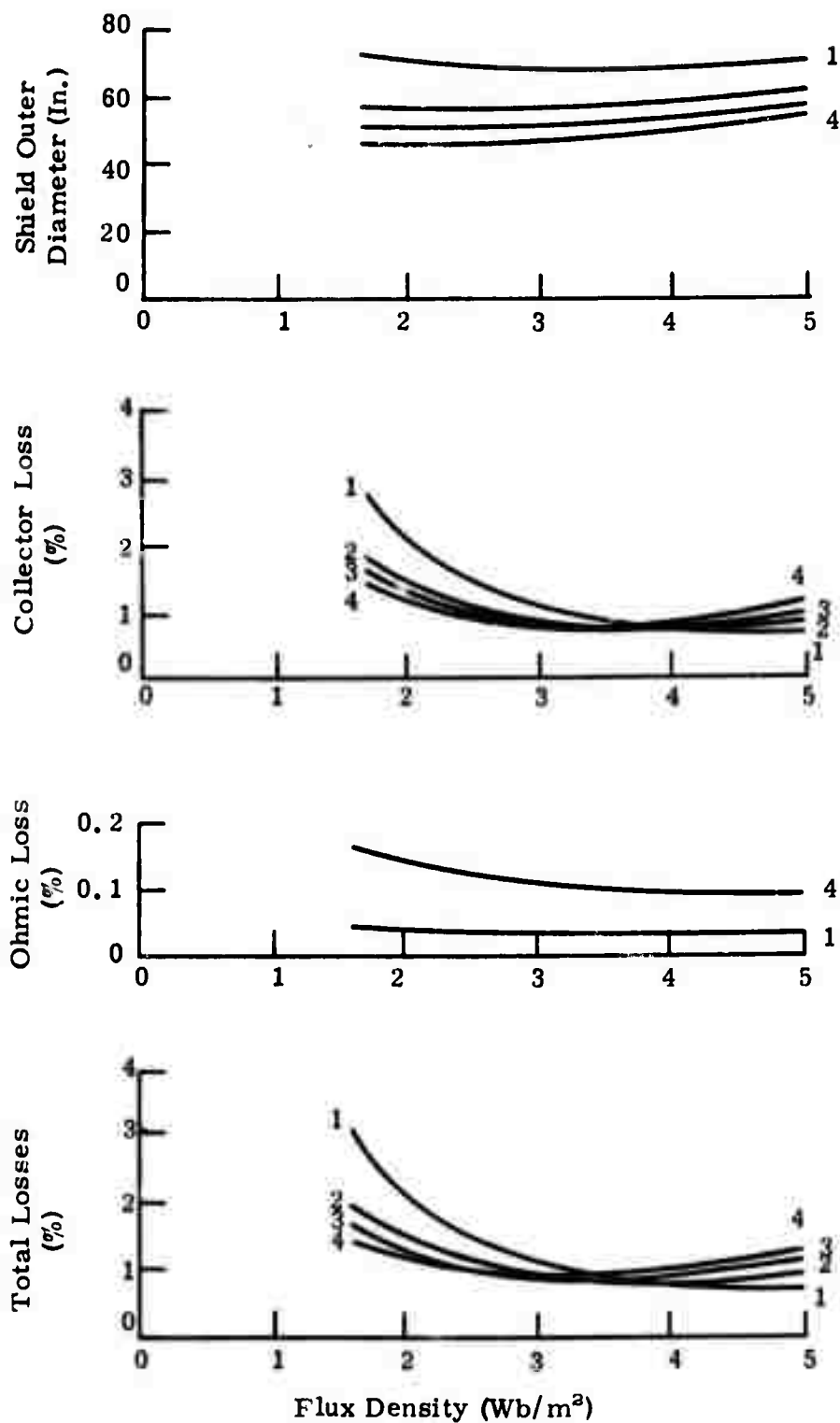


Figure 81. Acyclic Generator Parametric Study  
(24,000 Hp, 3600 Rpm, 100V) (Sheet 2 of 2)

is required to obtain acceptable bending stress in the disk hubs. It was also assumed that the stator and rotor disk thicknesses were equal. For example, in a two-disk machine, each rotor disk is 1.5 inches thick, and each inner collector boss, which is integral with the rotor disk, has 1.5 inches of axial length.

For a larger number of disks, where the above criterion would have led to a disk thickness less than 1 inch, a minimum 1-inch thickness was assumed in order to control the  $I^2R$  losses. In the unflooded generator, the collector losses (primarily mechanical fluid friction) are increased for wider disks, so the wetted collector width of both inner and outer collectors was assumed to be 0.5 inch in all cases, for purposes of loss calculation. The wetted width can be controlled by using an appropriately shaped disk rim.

Magnetic parameters were calculated only to a first approximation. The disk diameter required for a given voltage per disk was calculated by assuming a uniform flux density in the region between collectors; this density is the number that is used as the flux density index in Figure 81. The actual flux density distribution for the generator geometry (assuming coil length equal to machine active length) in which the coil length is much less than its diameter, and incorporating the effects of the iron shield, would require a complicated analysis. For the present purpose, because the generator shield was assumed to include end pieces for guiding the flux into the radial shield, a lumped magnetic circuit was assumed. That is, the flux was assumed to go straight through the bore of the coil, return through the end pieces and the radial shield, and to be uniformly distributed.

This calculation establishes the thickness of the superconducting coil required, based on the assumption for overall current density in the coil. In the present case, the coil overall steady-state current density (total ampere turns per unit of length divided by thickness) was assumed to be 10,000 amperes per square centimeter. This assumption is believed to be conservative by a factor of three, compared to present achievements in fully stable coils of comparable size. With this assumption, coil thicknesses of less than two inches is obtained even at the highest flux densities assumed. Hence conservatism in the assumed current density will cover any inaccuracies introduced by the simplifying analysis assumptions, as well as provide a margin for transient effects.

The iron shield thickness was calculated by:

- Calculating the total flux through the bore of the machine (including the coil and the dewar) with the above assumption of uniform flux density.
- Calculating the iron thickness required to carry this flux at a saturation flux density of 2.0 webers per square meter.

The above assumptions used in calculating the coil and iron thickness are not as approximate as they seem at first glance. First, the generated voltage is proportional to total flux, so the iron must carry this constant number regardless of the distribution. The actual radial (and axial) distribution of the flux density is important, mainly in calculating the unused flux through the shaft and through the outer collector, bus, dewar wall, and coil. The required disk diameter will also be affected if the flux distribution is skewed badly enough. With iron end pieces, it is not unreasonable to assume that the axial and radial distributions are sufficiently uniform to make the approximations valid.

As a check, detailed calculations of the flux density distribution were made for a single machine (the effect of the iron on the bore flux density distribution could not be included) for a coil of appropriate geometry, and the overall result closely matched that obtained using the previously mentioned assumptions. It is therefore felt that this calculation is sufficiently accurate for the sizing estimates needed for this study.

Chosen Generator Design. The generator design chosen for further detailing from the study described in the previous sections was the two-disk machine at a mean flux density of 3.0 webers per square meter. Table 42 shows the results of the expansion of this design to a point where a realistic estimate of the cryogenic refrigeration requirements may be made.

Table 42  
D-C ACYCLIC GENERATOR PARAMETERS

Characteristic	Parameter
Output power	24,000 hp
Output voltage	100v
Output current	179,000 amp
Effective flux density	3.0 Wb/m <sup>2</sup>
Number of rotor disks	2
Rim velocity	25,000 ft/min
Shaft diameter	8.00 in.
Inner collector radius	6.25 in.
Outer collector radius	13.25 in.
Inner dewar radius	15.25 in.
Inner coil radius	16.25 in.
Outer coil radius	17.75 in.
Inner shield radius	19.25 in.
Outer shield radius	31.30 in.
Disk pitch	3.00 in.
Coil length	11.50 in.
Coil thickness	1.50 in.
Losses (fractional)	
Outer collector	$0.731 \times 10^{-2}$
Inner collector	$0.108 \times 10^{-2}$
I <sup>2</sup> R	$0.063 \times 10^{-2}$
Bearings and seals (estimated)	$0.10 \times 10^{-2}$
Total	$1.00 \times 10^{-2}$

Ohmic losses in the generator were calculated on the basis of using Copper Alloy 150 (zirconium copper), which has good strength and electrical conductivity that is 93 percent of copper.

### D-C Motor

The full-power design point of the d-c propulsion motor was chosen as 40,000 hp and 200 rpm at 200 volts, power to be supplied by a pair of generators that are series-connected as described above. The type of motor construction chosen for this study was a multidisk acyclic machine utilizing a sodium-potassium eutectic alloy (NaK-78) in a flooded collector system.

An unflooded collector system, as used in the generator, is not considered desirable on a slow-speed motor, which must be capable of running continuously at any speed, including near zero and through zero, on reversing. Furthermore, separately fed collectors, which cool the machine through external sodium potassium loops, would require a large number of external liquid metal loops, because the motor, due to its low speed, has many more disks than the generator. Therefore the motor is designed to run fully flooded with sodium potassium. Rotor and stator disks are insulated on alternate faces; this configuration produces electromagnetic forces that motor sodium potassium between disks to prevent short circuiting the disk voltage. Some losses (both viscous and electrical) are associated with the presence of the sodium potassium between disks; however, they are tolerable, considering the operational gains.

Because the flooded collector system does not permit collector fluid circulation at a rate high enough to allow that flow to be used in a heat removal system, a separate cooling system must be used in the motor. In the present case, it was verified that the circulation of a low-viscosity silicone fluid in stator passages was a practical method of cooling.

Parametric Study of Motor Configurations. A parametric study of motor size and shape variation was performed. In this case, the power, voltage, and current were held constant, and the parametric variables were the number of disks and operating flux density. The motor voltage was chosen at 200 volts on the grounds that higher voltages would lead to an impractical number of disks. (It is clear that the maximum practicable voltage is desirable from the standpoint of the system interconnection bus size).

The results of the analysis are shown in Figures 82 and 83, which gives machine envelope volumes, diameters, and losses. These figures can be applied with considerable accuracy to both unshielded and shielded machines, by proper interpretation. It is to be noted that calculation of the dewar diameter and volume and all of the losses were made for an unshielded machine. The diameter and volume of an iron shield needed to shield such a machine were then determined, assuming that no change in dewar size would result.

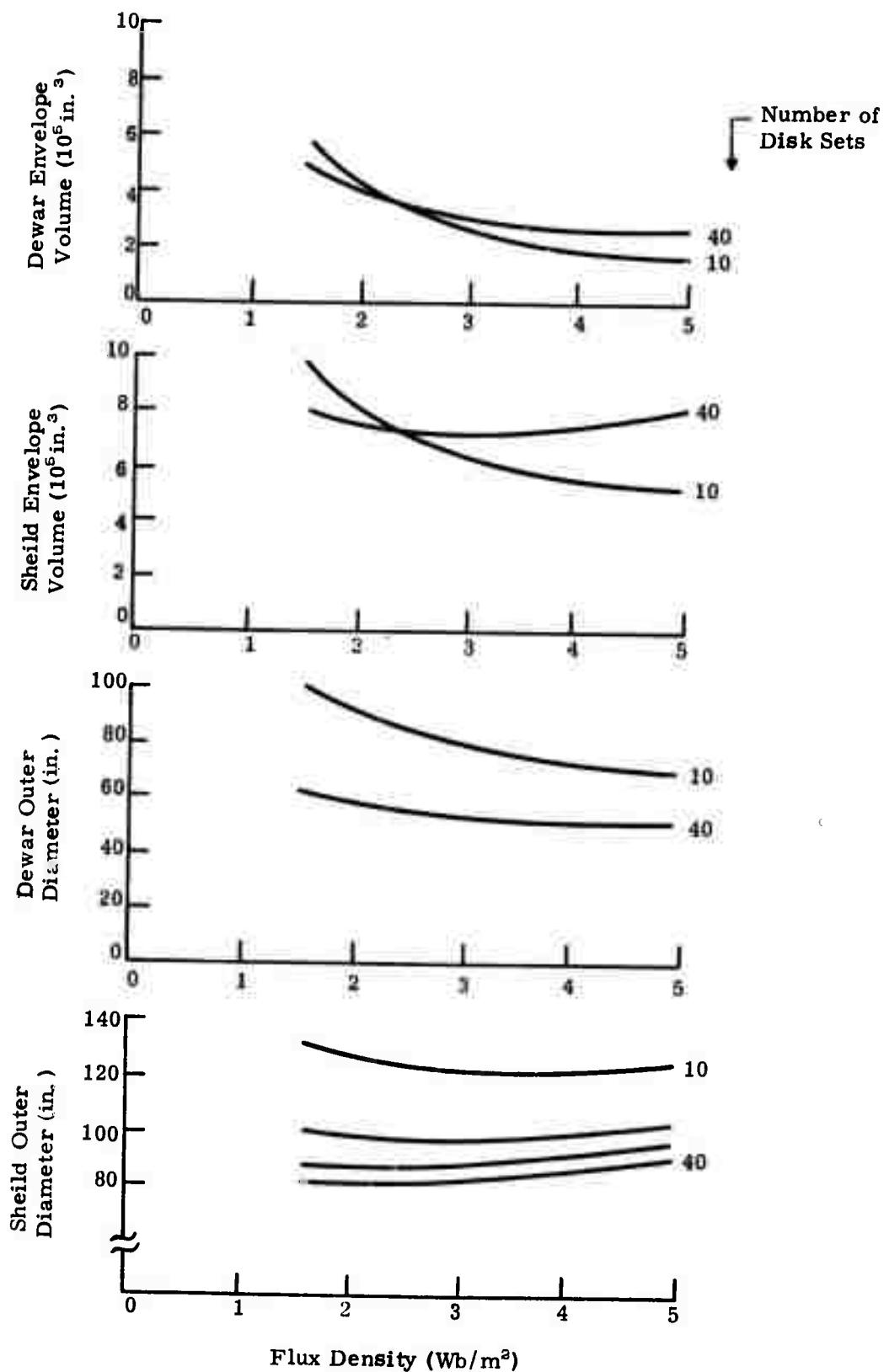


Figure 82. Acyclic Motor Parametric Study, Diameter Versus Flux Density (40,000Hp, 200 Rpm, 200V)

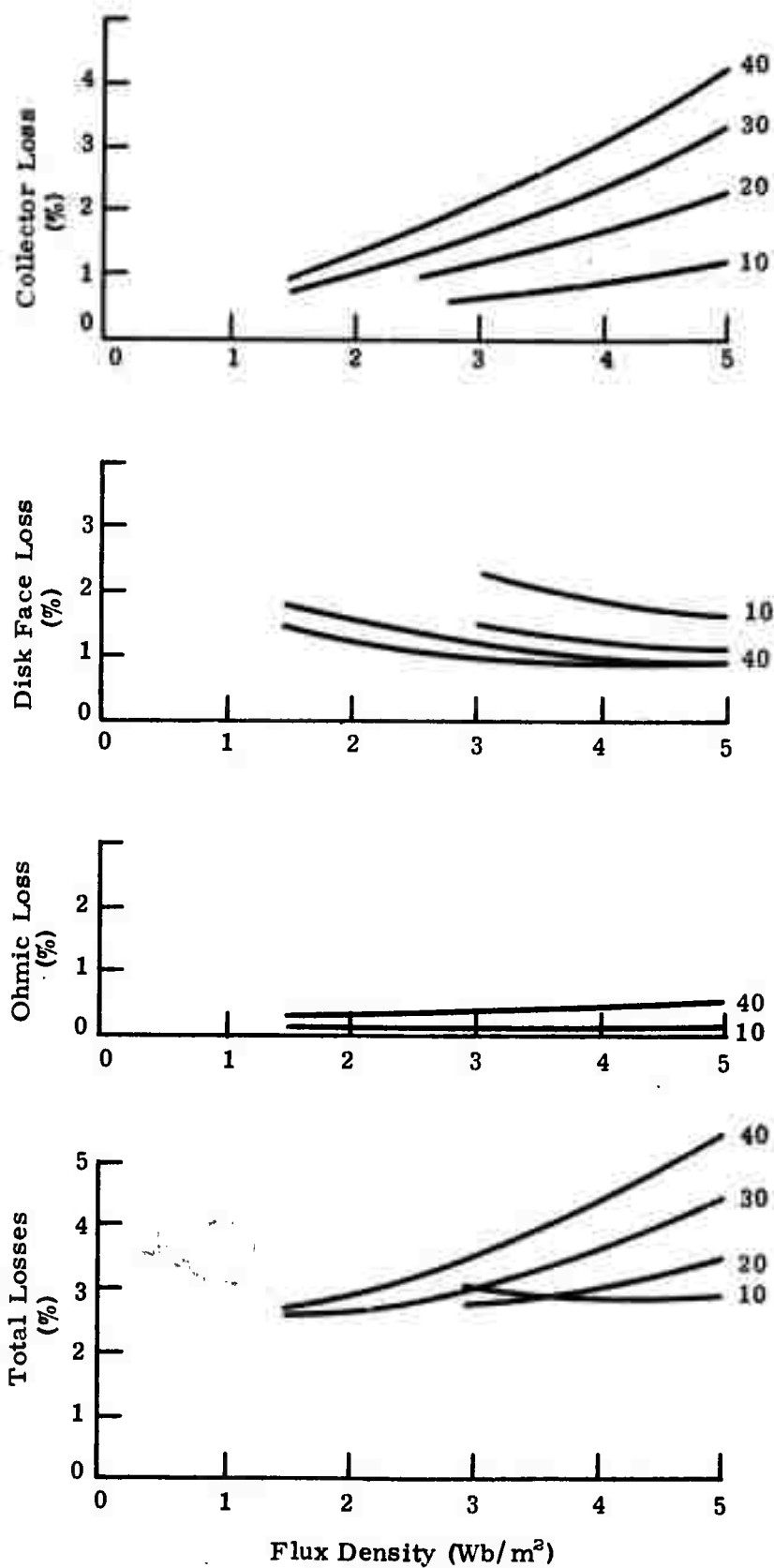


Figure 83. Acyclic Motor Parametric Study, Losses Versus Flux Density (40,000 Hp, 200 Rpm, 200V)

Actually, because of the iron, it would be possible to reduce the dewar size somewhat in the case of the iron machine, but this would only be a small amount. Consequently, with the type of construction postulated, namely a dewar surrounding the rotor and, if shielded, an iron shield outside the dewar, Figure 83 gives envelope diameters and volumes for both unshielded and shielded machines as follows:

- For an unshielded machine, the envelope diameter and dimensions are those of the dewar.
- For a shielded machine, the envelope diameter and dimensions are those of the iron shield and are slightly conservative.

The significant trends from Figure 83 are:

- For unshielded machines, the smallest volume is definitely obtained at the highest operating flux density.
- For shielded machines, this is not the case, as will be clear from the following discussion.

For the unshielded machines, the volume variation with the number of disks is small, even though the machine shape is changing substantially as the disk number is varied.

In the present applications, diameter is probably a more significant characteristic than volume, in itself, because many spaces where the machines would be used may be restricted in diameter but be less restricted in length.

The trend in diameter is monotonic; a large number of small-diameter disks leads to a small overall machine diameter, as expected.

With respect to flux density, the diameter of the unshielded machines using nonferrous disks is smaller for high flux densities as expected although the variation for large numbers of disks is smaller than might be anticipated. One reason for this trend is that the disk active window is so small with large numbers of disks that small variations in outer radius can compensate for substantial variations in flux density. In the case of the shielded machines, with nonferrous disks, the shield outer diameter actually increases with increasing flux density, with large numbers of disks. The reason for this trend is that the generation of voltage requires a constant amount of total flux, which the shield must carry. In addition, the shield must carry the wasted flux -- that which goes through the outer structure of the machine, the coil, and the dewar. For large numbers of disks, the disk window area does not vary fast enough to compensate for the amount of wasted flux, and consequently the shield thickness increases faster with operating flux density than the outer disk diameter decreases.

This trend toward increasing shield thickness and overall diameter with a larger number of disks can be counteracted by using iron disks (both stator

and rotor) at lower flux densities. If such a machine is designed with the disk iron below saturation, there will be substantially no wasted flux outside the active window. Even if designed above the saturation value, only that flux above the saturation value will contribute to the wasted flux that must be carried by the shield.

Figure 83 also shows that the losses (primarily collector losses) also decrease as the design flux density is decreased. Generally speaking, therefore, it appears that if the machine must be completely shielded, an operating flux density in the range of 20 to 30 kilogauss would be best.

Additional benefits from lower flux density accrue from the fact that the superconductive excitation coil is smaller. This leads to: decreased heat leak because of lower weight, decreased excitation voltage for field changing, and decreased superconductor hysteresis losses during field change.

Some of the detailed constraints and assumptions that are included in the motor parametric analysis in addition to a common shaft are:

- The stator disk thickness was held constant at 2.3 inches. Preliminary analysis showed that this thickness was nearly correct for accommodating cooling passages within the stator disk to remove inner collector losses.
- Rotor disk thickness was set by a bending criterion. In the flooded disk machine, alternate layers of liquid metal between the disks are stationary and rotating. This situation produces a pressure rise due to the centrifugal pumping action. The pressure difference due to the centrifugal pumping produces bending forces in the rotor disks. The disk thickness was chosen to limit the deflection due to the above bending forces to approximately 0.015 inch. In most cases, the resulting rotor disk thicknesses were consistent with desirable collector widths and reasonable  $I^2R$  losses.
- In the zeroth approximation, the outer collector width is equal to the rotor disk width. In slow-speed motors, the outer collector loss is the dominant loss. This loss is reduced by increasing the outer collector width. As far as the configuration is concerned, this can be accomplished by providing a recess in the stator disk to accommodate a flange on the rotor disk, which increases the effective collector width. In the present analysis, the outer collector width was assumed to be that given by the previously mentioned disk thickness (set by deflection) plus a constant adder of 0.85 inch (assumed to be the maximum practical recess in the stator disk).
- The motor magnetic circuit was assumed to be comprised of a hollow cylinder to accommodate the disk array plus end pieces to guide the flux at a flux density of 20 kilogauss. The coil thickness was then determined by calculating the required ampere turns to drive the flux

through the reluctance determined by the noniron bore geometry of the motor. An overall current density (ampere turns per unit of length divided by coil thickness) of 10,000 amperes per square centimeter was assumed in calculating the superconductive coil dimensions. This value is conservative compared to today's technology, but allows margin for design uncertainties and transients during operation. The resulting coil thickness are on the order of 2 inches, so this is not a critical assumption.

**Chosen Motor Design.** Scheduling considerations to establish cryogenic refrigeration requirements made it necessary to choose a motor for more detailed design, based on preliminary analyses, and before all of the results of the parametric study just described were complete. The design chosen was a 30-disk machine at a mean flux density of 5.0 webers per square meter. This is a relatively compact machine, particularly if an unshielded application is permissible. However, in the light of the parametric results now available and described in the previous section, for a fully shielded machine, a considerably lower flux density is now preferred. From Figure 83, it appears that by so doing, the overall machine diameter could be decreased on the order of 10 inches for a shielded machine, and efficiency could be improved about 2 percent. However, this would not greatly affect the cryogenic refrigerator requirement.

Table 43 shows results of the development of the 5.0-weber-per-square-meter design to the point where a practical evaluation of the refrigeration load could be made.

Table 43  
D-C ACYCLIC MOTOR PARAMETERS

Characteristic	Parameter
Output power	40,000 hp
Terminal voltage	200v
Design current	150,000 amp
Effective flux density	5.0 Wb/m <sup>2</sup>
Number of rotor disks	30
Shaft diameter	20 in.
Inner collector radius	12.13 in.
Outer collector radius	18.53 in.
Inner dewar radius	23.6 in.
Inner coil radius	24.6 in.
Outer coil radius	26.4 in.
Inner shield radius	27.5 in.
Outer shield radius	48.6 in.
Disk pitch	2.97 in.
Coil length	80 in.
Coil thickness	1.8 in.
Losses (fractional)	
Outer collector	$2.19 \times 10^{-4}$
Inner collector	$1.05 \times 10^{-2}$
Fit	$0.28 \times 10^{-2}$
Bearings and seals	$0.02 \times 10^{-2}$
Total	$3.52 \times 10^{-2}$

The stator disks and the current carrying portion of the rotor disks were assumed to be copper-alloy 150, as in the generator, for calculation of ohmic losses. Critical speed of this motor design was analyzed, and the lowest transverse critical was calculated to be at approximately 4300 rpm, which is well beyond the speed where troublesome vibrations would be induced.

### A-C/D-C Transformers and Rectifiers

If an a-c/d-c system is used, it is necessary to match the d-c motor to the a-c generator in one way or another, in the general case requiring both a transformer and a rectifier. It is conceivable that the a-c generator could be wound to generate the high-current, low-voltage requirements of the motor directly, thus eliminating the transformer. However, this would result in large-size transmission buses, just as in the d-c/d-c system and would still require rectification. It therefore seemed in this study that the preferred approach for the a-c/d-c system would be to generate power at reasonably high voltages to eliminate the need for large-size transmission buses and utilize transformers and rectifiers at the motor end. Other than cost considerations, probably the most significant trade-off consideration between the a-c/d-c system and the d-c/d-c system then becomes the size and weight of transformers and rectifiers for the former, as compared to size and weight of buswork for the latter.

If a transformer is used in the system, the most economical transformer and system weight is expected to occur at a frequency of about 180 hertz on the a-c side. This conclusion is rationalized as follows: increasing frequency will always make the transformer smaller, but will also increase losses. The increased loss may be offset, however, by using thinner punchings in the core and finer strands in the windings. Approximately a 0.005-inch core punching is implied by 180 hertz; thinner punchings can be handled, but are not too practical. Winding strand size will need to be reduced by a third, compared to 60 hertz, using three times as many strands, to limit eddy current losses. Too many strands becomes impractical from the standpoint of transposition. Therefore, 180 hertz seems to represent about an upper limit to frequency beyond which further reductions in transformer size and weight would result in significantly increased losses, which would probably be detrimental to overall system performance.

As indicated above, the size, weight, and performance of the six-pole generator required to produce 180 hertz at 3600 rpm is not expected to be significantly different from values for a 60-hertz machine. However, past studies indicate that power/density falls off above about six poles. Thus, also from the generator standpoint, 180 hertz is indicated as a reasonable selection.

From the above considerations, a limited study was made, in an effort to estimate transformer/rectifier sizes and weights, at a frequency of 180 hertz, to be used in system comparisons. This is not a simple task, because:

- The 180 hertz is a nonstandard frequency.
- Thirty megawatts is well above the rating of present day commercial units, and specific power is not constant at higher ratings.
- The size and weight of the units depends on the cooling; that is, most commercial rectifiers are air-cooled, while water cooling is desirable for high power density. Transformer cooling and acceptable losses also influence size and weight.

It was not possible to devote a significant effort to this task. However, Table 44 contains some numbers obtained in a preliminary manner.

Table 44

TRANSFORMER AND RECTIFIER WEIGHTS AND DIMENSIONS  
 ( System Frequency = 180 Hz  
 ( LV Rating = 200v, 150,000 amp, 30,000 kw )

Weight/Dimension	Transformer	Rectifier
Weight (lb)	115,000	15,000
Height (in.)	150	NE
Width (in.)	230	NE
Depth (in.)	117	NE
Loss (%)	1.5	1.0

The values in Table 44, for transformer dimensions, are scaled values calculated according to commercial practice. They represent an oil-filled transformer cooled by free convection in the windings, with heat rejected to an oil-air radiator. About two thirds of the weight is in the tank and oil. If the transformer were specifically designed for ship installation with forced-cooled windings, the weight might come down by a factor of three and the dimensions by 1.5 (cube root of three).

The rectifier weight is a preliminary estimate obtained by weighing the individual devices and adding an arbitrary factor for cooling, racking, and auxiliaries, assuming forced water cooling. As such, it appears inconsistent with the transformer weight, indicating the need for additional study in this area at some future time. For this reason, rectifier dimensions were not estimated.

#### D-C/D-C System

Circuits and Switches. To provide suitable cross connections, it is necessary to provide interconnection and bypass switches in the d-c power circuits. The present discussion concerns itself with presenting information on a possible approach to show that such switching is within the state of the art with reasonable equipment. It is not presumed that the best procedure will be that outlined here.

Switches. As background, it is necessary that the functions of a switch and a circuit breaker be clearly distinguished. A circuit breaker must function when the system is loaded or during a short circuit. It must both extinguish the resultant arc and withstand reapplication of voltage within a very short time. A switch, on the other hand, operates essentially in an unloaded circuit, and it is designed not by interrupting duty but by steady-state rated current through its already closed contacts. In any case, any breaker must have a current-zero to function. In the case of 60-hertz breakers, reliance is upon the natural current zero. In the case of d-c breakers, a current-zero is imposed, usually by discharging a capacitor through the contacts in the reverse direction. It will be argued below that a current-zero can be produced in the d-c/d-c motor-generator circuit of sufficient duration to allow interconnections to be achieved with switches rather than breakers.

Selection of appropriate switches should be reasonably straightforward, although high-current switches are not a common commercial item. They are available, however, as evidence by material contained in, for example, the Square-D catalog (Ref. 10). The product line referred to is intended for application in electrolytic installations, where heavy current shorting and disconnect switches are required. The basic switch unit is a knife switch, which can be either manually or hydraulically actuated. The point of interest is that a switch of 36,000-ampere rating is offered commercially, which is basically a gang of four 9000-ampere switches. It is not too difficult to conceive, therefore, of constructing a 150,000-ampere switch by ganging 16 of the same knife switches. Thus one can get some idea of the size of a 150,000-ampere switch by taking the catalog dimensions, which are  $23 \times 16\frac{1}{4} \times 3\frac{3}{8}$  inches, for one 9000-ampere module. A 16-switch assembly would, therefore, have dimensions of about  $23 \times 16\frac{1}{4} \times 54$  inches.

Current sharing among contacts must be ensured; this might be done by associating each pair of contacts with its own section of bus, which would serve as a ballast resistor. Other configurations may be more appropriate, including liquid-metal contacts.

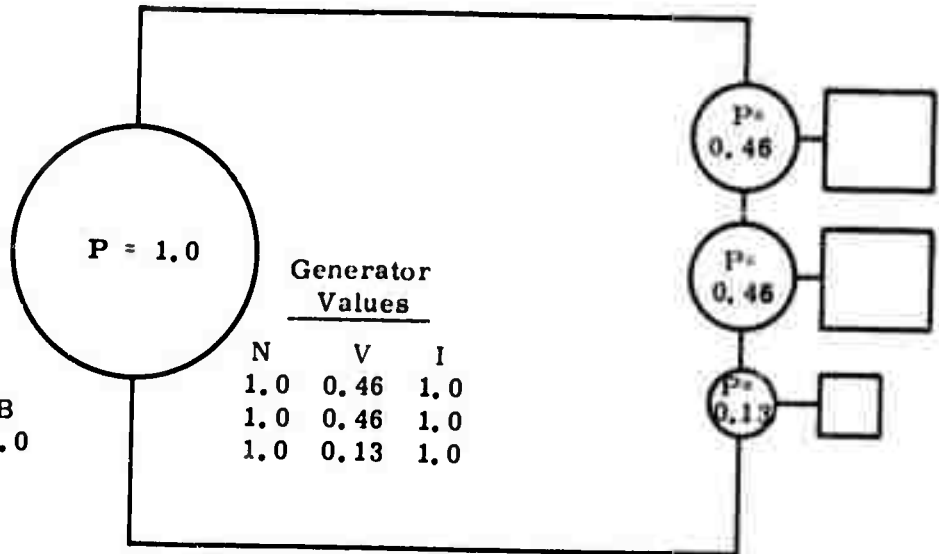
The present discussion is aimed only at establishing that the switch is not a separate research project, but is amenable to engineering solution. Another interesting point from the catalog is that the switches can be used for interrupting duty in circuits, with less than 6-volt capability. Physically, this is because 6 volts is not sufficient to sustain an arc in ambient air. It indicates that precise current-zero should not be necessary.

Circuit Interconnections. Notions of circuit interconnections and switching at zero current are built up by references to Figures 84 through 86. Figure 84 starts with two basic circuits defined by a system that has one motor driven by three generators and three gas turbines in each circuit. Per-unit voltages and currents are used. Base power is 40,000 horsepower, based voltage is 200 volts, and base current is 150,000 amperes. There are two 20,000-hp

40,000 Hp = 1.0  
 200V = 1.0  
 150,000 Arup = 1.0  
 $P \propto N^3$

Motor Values

N	V	I	B
1.0	1.0	1.0	1.0



Legend:

P = Power  
 V = Voltage  
 I = Current  
 B = Flux Density  
 N = Speed

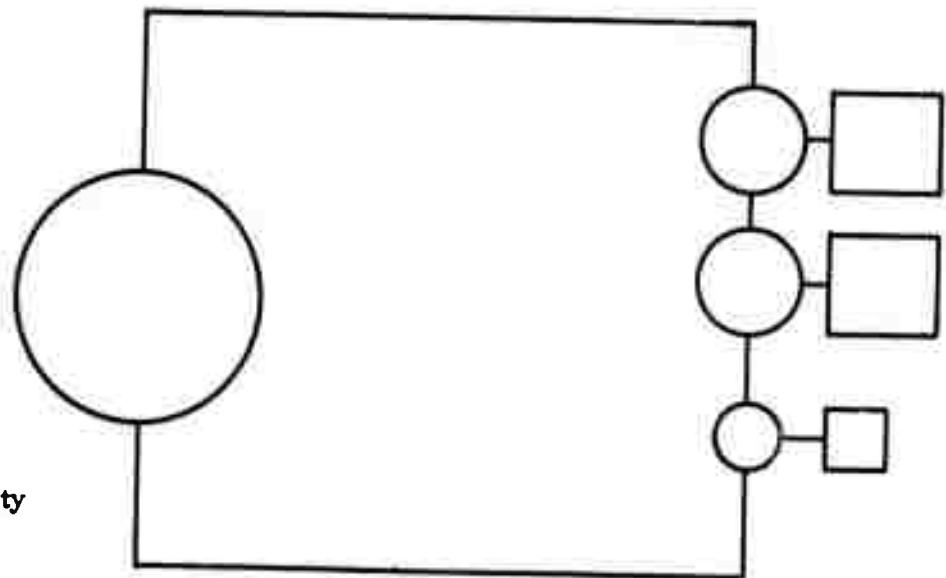


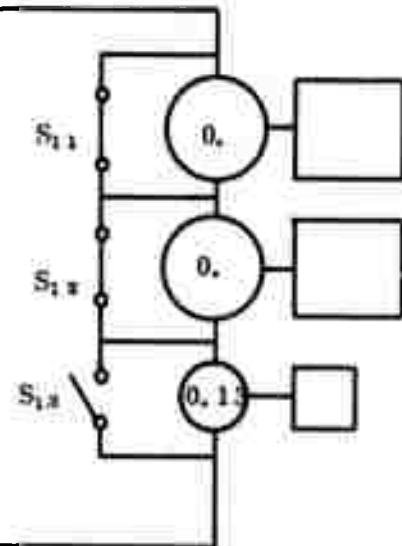
Figure 84. Generator/Motor Connections

2 x 5000-Hp Load  
2 x 5000-Hp Source

<u>Motor Values</u>			
N	V	I	B
0.5	0.13	1.0	0.25
0.5	0.25	0.5	0.5
0.5	0.5	0.25	1.0

$P = 0.13$   
(1/8)

<u>Generator Values</u>			
N	V	I	B
1.0	0.13	1.0	1.0
1.0	0.25	0.5	2.0
1.0	0.5	0.25	4.0



Legend:

P = Power  
V = Voltage  
I = Current  
B = Flux Density  
N = Speed

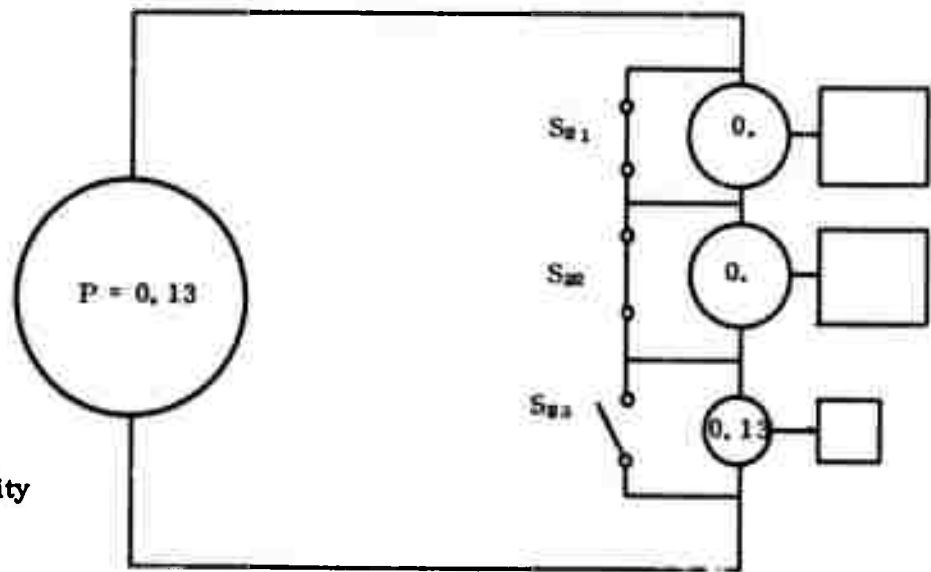


Figure 85. Circuit Interconnections and Switching at Zero Current (Cruise Condition)

2 x 2500-Hp Load  
1 x 5000-Hp Source

Motor Values			
N	V	I	B
0.4	0.13	0.5	0.31
0.4	0.25	0.25	0.60

Generator Values

N	V	I	B
1.0	0.13	1.0	1.0
1.0	0.25	0.5	2.0

**Legend:**

P = Power  
V = Voltage  
I = Current  
B = Flux Density  
N = Speed

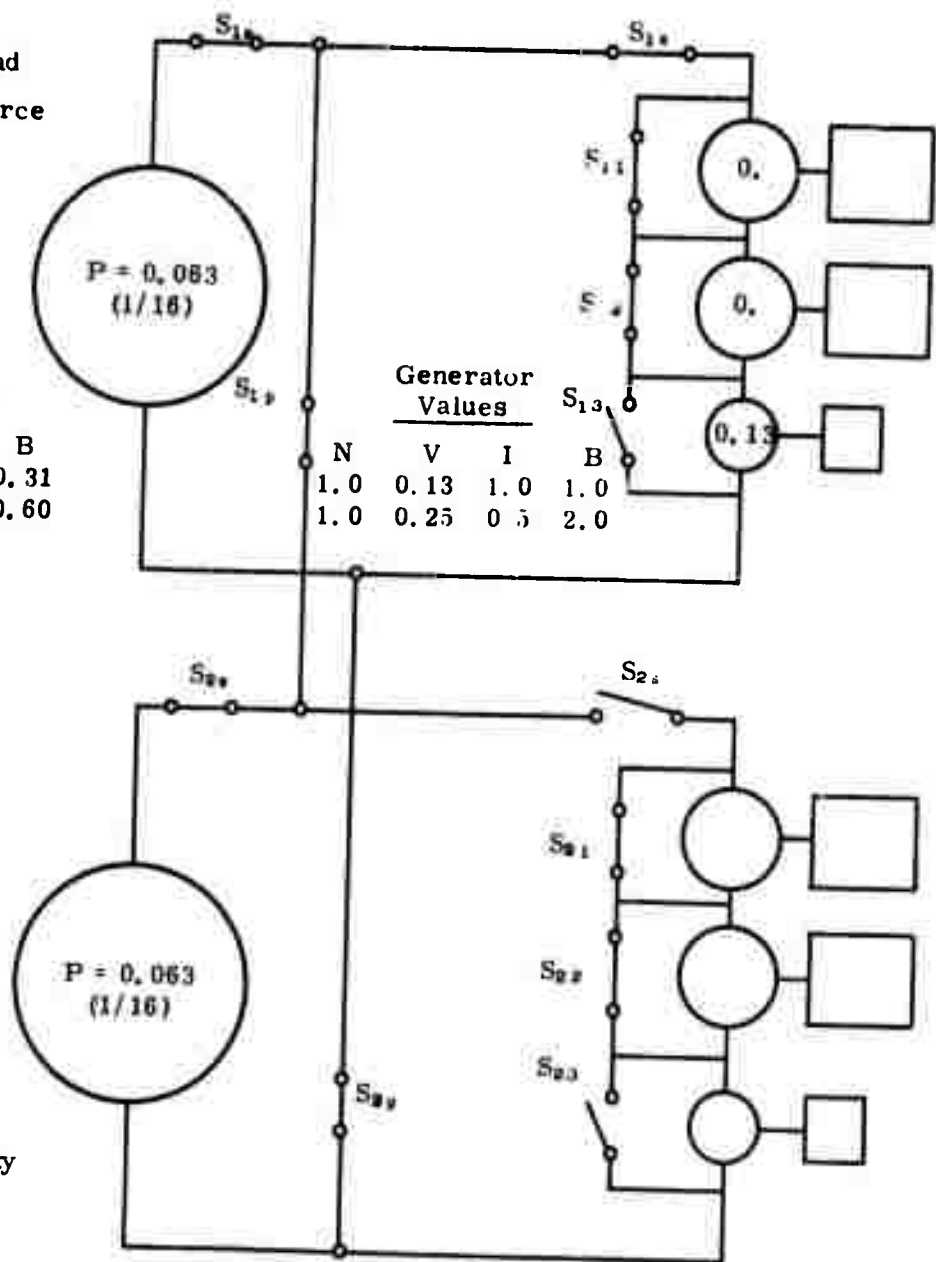


Figure 86. Circuit Interconnections and Switching at Zero Current (One Cruise Generator)

generators and one 5000-hp generator (the powers do not add correctly, but in this discussion round numbers are being dealt with). In these circuits, the generators are assumed to be series-connected. Circuits for parallel-connected generators are equally as obvious.

The series connection is the starting assumption, because this connection requires each generator to put out only 0.5 per-unit voltage. In disk-type machines, this output leads to a small number of disks, which has certain advantages in unflooded generators (see page 207). Interconnection considerations will lead to some reservations regarding this assumption, as discussed below. In the series connection, each generator is required to carry one-per-unit current; however, this is easily accomplished with liquid metal collectors.

Consider Figure 85, in which it is assumed that each motor is driven by its own 5000-hp generator, as might be the case under cruise conditions. Each of the 20,000-hp generators is shown short-circuited by its own shorting switch, (Switches S11, S12, S21, and S22). Also shown in this figure are a set of values for shaft speeds (the power is assumed to be proportional to the cube of speed), voltages, currents, and motor field levels, each of which combines to produce 5000 hp. From this table, it can be seen that if the 5000-hp motor is designed only for its share of voltage under full power, it would be necessary for the circuit to carry one-per-unit current at cruise, in which case the motor field would be reduced to 0.25 rated voltage. The bus losses at one-per-unit current would be the same as the losses at full power, but percentages would be large at cruise and efficiency would suffer.

At the other extreme, if the 5000-hp generator is designed to put out 0.5-per-unit voltage (the generator is assumed to operate at one-per-unit speed throughout), then the circuit current can be reduced to 0.25 per unit if the motor flux is held at one per unit. Therefore it seems obvious that, considering bus losses, it is desirable to operate at a high circuit voltage and at partial power. Full voltage may not be the optimum, however, because face losses in the motor are proportional to flux density, and the option of reducing motor flux (and voltage) may lead to lower total losses. These questions cannot be answered without a detailed study, which has not yet been performed, of all sources of system loss at full and partial power.

Similar considerations apply to the notion of designing the 20,000-hp generators for only half voltage. If the system runs on one 20,000-hp turbine for an extended period, it might be desirable for its generator to be capable of putting out more than the 0.5 per-unit voltage, which is required for series operation at full power.

Partial power operation from one 5000-hp source driving both motors is shown in Figure 86. In this figure, Switches S1s, S2s, S1p, and S2p have been added, because these switches are necessary for this connection. Various combinations of partial power voltages, currents, and fluxes are also shown. In

this case, operation of the motor at low fluxes has an additional advantage in that it would be possible to reverse one motor by reversing its field. This is possible because at a 0.31 field, the stored energy is only one-tenth that at full field, and a relatively low excitation voltage would be required.

Finally, it should be noted that Switches S2m and S1m are required for the conditions in which either motor is operable alone from any generator.

At this point, it is appropriate to discuss the operation of actuating switches at zero current and how this actuation might be carried out. Consider the case of Figure 85, where each motor is operating off its own 5000-hp generator. Assume it is desired to energize one of the 20,000-hp generators, for example, Generator 12. In this case, the procedure is to bring the generator and turbine up to speed with the generator field unexcited. The excitation on the generator is then slowly raised. When the generator excitation is just enough to satisfy the internal IR drop, the current through Switch S12 must be zero, because the IR drop must be equal to the generator terminal voltage, which is zero. At this point, Switch S12 can be opened, and the excitation of Generator 12 can be raised until it assumes whatever share of the load is desired.

Similarly, if it is desired to go from the condition of Figure 86 back to that of Figure 85, Generator 23 can be activated, and its terminal voltage can be raised until it is just equal to that across the motors. Then Switch S2s can be closed. If the voltages of Generators 13 and 23 and of Motors 1 and 2 are balanced, current will cease to flow through Switches S1p and S2p, and they may be opened.

It should be noted that these procedures may not require precise sensing of all voltages and/or precise control of generator fields, because switch actuation at current zero is possible even when there is a finite rate of change of current. In this case, the switch would be programmed so that the condition of an actuation command and current zero through the switch would trigger the actuator. The capability of switches to operate at circuit voltages of 6 volts eliminates the need for precise balancing of voltages.

Finally, it should be observed that although the switches are not gigantic, they are reasonably bulky, and the entire combination shown in Figure 86 may not be required if some modes of operation can be ruled out. Further, if partial power is always accomplished at partial current, then the motor bypass switches and motor paralleling switches need not be designed for full current, thus reducing their size.

Bus Size and Losses. The d-c/d-c system has been conceptually designed with an acyclic motor rated at 40,000 hp (30 megawatts), 200 volts, and 150,000 amperes. Interconnections between the motor and the generators must be made with buswork capable of carrying rated current. To obtain a preliminary notion of the size and weight of the buswork, a bus was sized

for 150,000 amperes, 76 feet in length, and a maximum  $I^2R$  loss equal to 2 percent of the rated motor power at rated current.

The bus configuration was assumed to be water-cooled, rectangular bars, with go and return bars interleaved to minimize stray magnetic fields. The resulting dimensions are shown in Table 45.

Table 45  
COPPER BUS PARAMETERS

Characteristic	Parameter
Current	150,000 amp
Length	76 ft
Loss*	2%
Copper area	112 in. <sup>2</sup>
Copper current density	2700 amp/in. <sup>2</sup>
Total copper weight	32,900 lb
Overall dimension**	12 x 13 in.
Overall area	156 in. <sup>2</sup>
Water flow	600 gpm (at 19 psi)
Water temperature	110/180°F (inlet/outlet)

\*Percent of 30 Mw

\*\*Total for two conductors

Following the preceding calculations, the question of optimizing bus size and losses was investigated. For this purpose, the twin-screw destroyer-type ship of Reference 9 was used, omitting, however, the 5000-hp motor-generator sets. The resulting configuration, then, consists of four 20,000-hp turbine generators driving two 40,000-hp motors, one motor per shaft. General location of the various equipments, based on Reference 9, is indicated in Figure 87. Based on this figure, it is determined that the total length of buswork is about 352 feet.

Maximum conductor operating temperature was assumed to be 50°C (185°F), consistent with the requirements of Appendix II, "System Requirements for Superconducting Naval Ship Propulsion System." For this calculation, the area and weight associated with cooling the conductors was neglected. The procedure was to explore the effect of bus losses on the weight and volume of buswork and fuel, using the fuel consumption results from page 201 for this ship and its specified mission profile. Both copper and aluminum buses were studied, and the effect of doubling system voltage was also determined.

Results are given in Figures 88 through 91. Figure 88 gives the area of each conductor (bus), the total weight of buswork, the incremental weight of fuel,

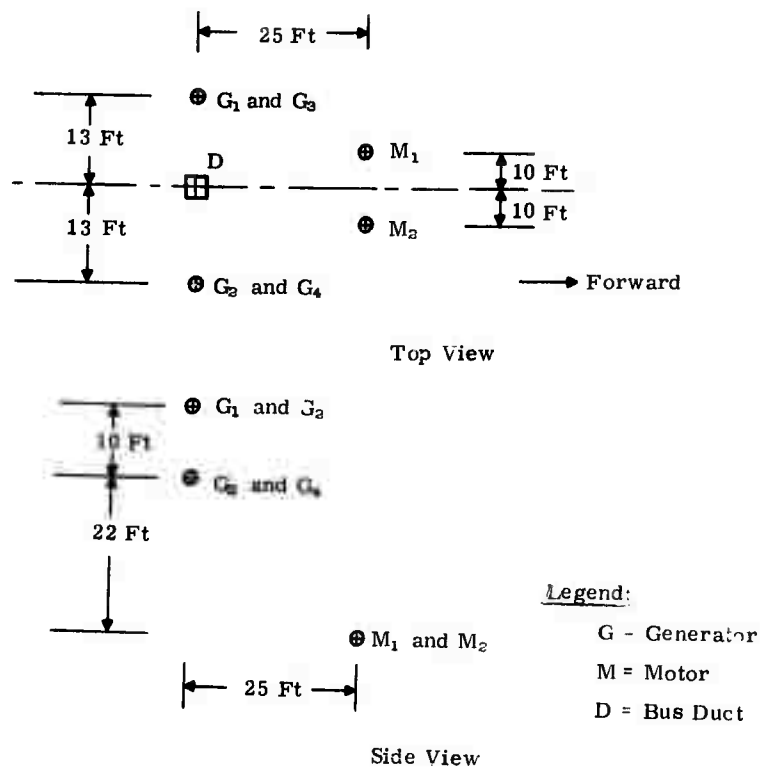


Figure 87. Location of Equipment for Twin-Screw Destroyer (80,000 Hp)

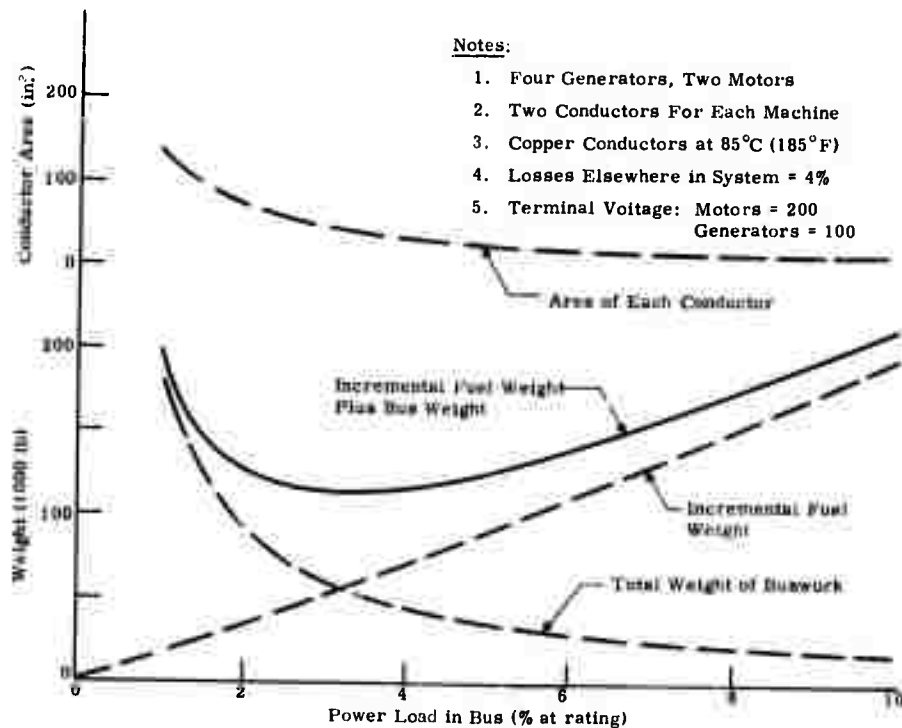


Figure 88. Effect of D-C/D-C Bus Losses on System Weight for Twin-Screw Ship (80,000 Total Hp)

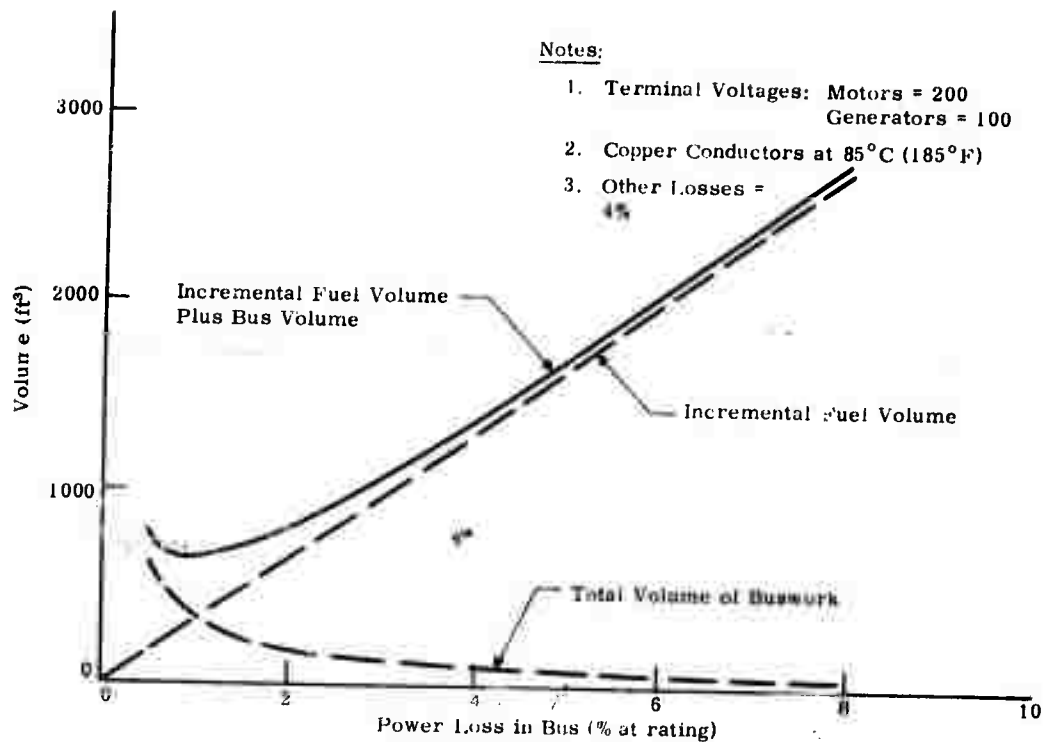


Figure 89. Effect of D-C/D-C Bus Losses on System Volume for Twin-Screw Ship (80,000 Total Hp)

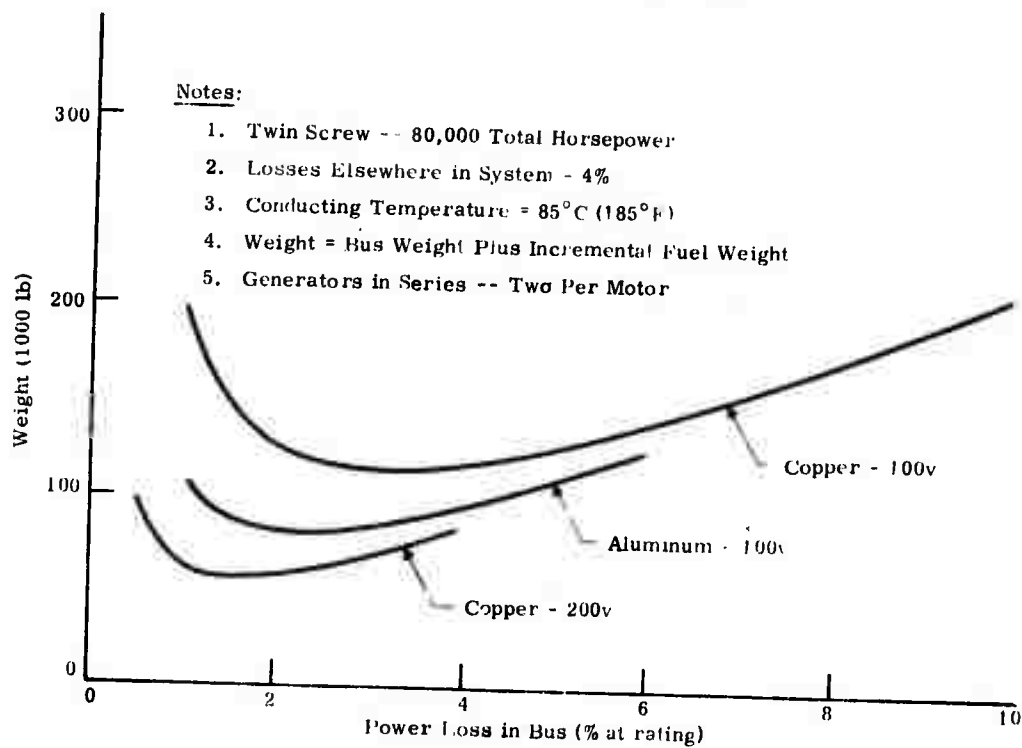


Figure 90. Effect of Bus Material and Generator Voltage on System Weight

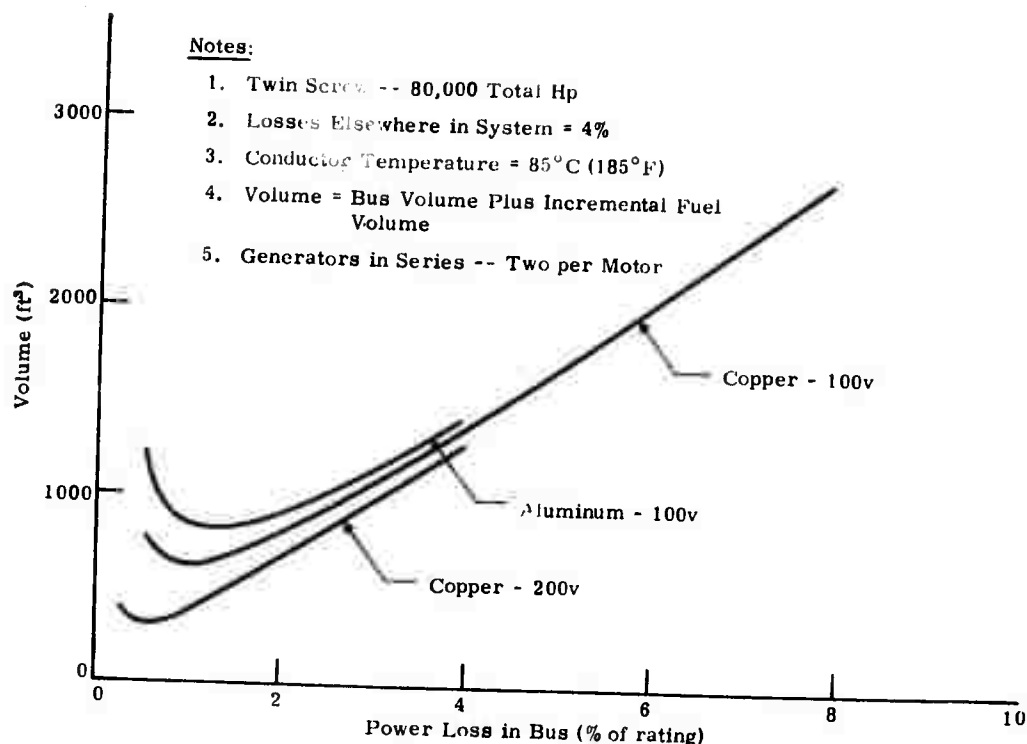


Figure 91. Effect of Bus Material and Generator Voltage on System Volume

and the sum of the bus weight and incremental fuel weight, all as functions of the percent of power loss in the buswork at rating. In this figure, the incremental fuel weight is defined as the added weight of fuel required over what would be required if bus losses were zero. In this connection, losses in the remaining portion of the system (generator and motor losses and refrigeration power requirements) were assumed to be 4 percent. This figure was arrived at by reviewing the values in Table 37 and assuming, per the discussion on page 216, that the motor losses can be reduced to around 2.6 percent by operating at lower flux density than does the present design.

The percent of power loss at rating in the bus is defined as the ratio of the  $I^2R$  loss in the bus to the power being transmitted, both at rating. Loss as a percent of transmitted power was assumed to be a constant over the mission profile, including partial load conditions. Per the discussion on switches and circuit interconnections, the validity of this assumption will depend upon factors yet to be finalized, but it is considered reasonable for present purposes.

Figure 88 shows that the total weight of the bus plus fuel minimizes at a bus loss of about 3 percent and a bus area per conductor of about 45 square inches. (By comparison, for 2% loss, bus area is about 67 in.<sup>2</sup>/conductor, compared to the  $112/2 = 56$  in.<sup>2</sup>/conductor of Table 45, the difference being the longer bus length for each generator and slightly higher temperature used in the calculations for Figure 88.)

Figure 89 gives the volume of buswork and incremental fuel as functions of percent loss, showing minimization at a considerably lower value of loss. Figures 90 and 91 give weight and volume data, respectively, for aluminum conductors and for twice the system voltage. The significant reduction in overall weight for use of either aluminum or of twice the system voltage is to be noted, being about 33,000 pounds for use of aluminum and nearly 60,000 pounds for doubling the voltage. The use of aluminum does increase bus volume; however, as indicated under "Superconductive Power Applications Study," at the beginning of this section, bus volume does not appear, in itself, to be a significant item when the volume of other system components is considered.

In utilizing information from this section, the parametric results just described were modified to allow for cooling area and weight by assuming that the percent increase in area required for cooling is about 35 percent, the value obtained from Table 45.

### Refrigeration

Details of the analysis and design of the refrigeration systems for the a-c and d-c generators and the d-c motor are described under Task R-10 in Section 2, "Cryogenic Turborefrigerator." These analyses are based on the requirements listed in Appendix II, "System Requirements for Superconducting Naval Ship Propulsion System."

### MODEL SYSTEM

As originally proposed, part of the output of Task S-10 of Phase I of this study is a recommendation as to which superconductive approach should be used for a model system, as well as recommendation of the speed and power level of this system. The purpose of Task S-40, to be carried out in Phase II, is to prepare a development plan for the design, construction, and testing of this system.

Subsequent to initiating this study, the Department of the Navy issued a work statement for a superconductive ship propulsion study (Ref 9), and request for quotation for this study, based upon a somewhat revised work statement, is anticipated soon. From this work statement and subsequent communication with Navy personnel, a model system power, speed, and ship application is defined: 3000 hp, 1150 rpm, and the Nasty-class PTF ship.

With the issuance of Reference 9, the position taken in this study with respect to model system recommendations is to concur with the Navy definition, for purposes of this report, unless there is strong reason for disagreement. No such reason has been found, and the foregoing size, speed, and ship application is, therefore, also the recommendation of this report.

A difficulty exists with respect to the type of superconductive approach to be recommended for the model system, however, because results of this study

are not final or conclusive (see page 179). However, because a recommendation is required at this time, the d-c/d-c system is recommended. This recommendation is based on results to date plus the judgment that further analysis will indicate that it is preferable to the a-c/d-c system, largely on the basis of large transformer weights and volumes compared to d-c/d-c buswork.

## **MATERIALS AND PROCESS EVALUATIONS (TASK S-30)**

### **LIQUID-METAL CURRENT COLLECTION**

During the past several years, there has been considerable interest in the use of liquid metals for slipring and current collection applications, with the liquid metal being used to replace conventional brushes. There are a number of advantages of liquid-metal sliprings. These advantages include low-interface, electrical resistance; high current capability; low mechanical losses; extremely low electrical noise; small size; and long life.

Extensive tests directed toward particular applications have previously been made at the General Electric Company, at the Naval Ships Research and Development Laboratories, and elsewhere. The investigations for space systems applications, as discussed in Appendix V, "An Investigation of Gallium Liquid Metal Current Collectors for Space Applications," are illustrative of the work. The particular materials, finishes, rotational speeds, physical shapes and configurations, liquid-metal supply methods, seals, and cover gas or fluid, and the presence of traces of elements such as oxygen or water vapor are all specific to the successful operation of such collectors. In superconductive machinery, the liquid metal is an electrical and physical part of the active (torque producing) portion of the rotor. As such, forces are generated, in the liquid metal itself, that will cause it to move with different velocity components with respect to the collector surfaces than would be the case at the same rotational speeds without the presence of the high magnetic field and armature currents.

Thus it is intended that the unflooded collector and seal configuration concepts for superconductive machines that have been studied in Phase I of this program will have preliminary tests made during Phase II, without electrical currents and magnetic fields, and that successful tests will then be followed with high currents and superconductive fields during Phase III.

Generally, the liquid metals considered for sliprings and current collectors have been mercury, sodium potassium (sodium and potassium alloys), and gallium. For space applications, gallium is currently used because of its low vapor pressure, high surface tension, and good electrical characteristics. For power applications, sodium potassium and mercury have had the widest usage. Mercury has the disadvantage of being highly toxic.

While the properties and behavior of sodium potassium are well enough understood to allow design work to proceed with confidence, additional ex-

perimental verification is necessary before development and production drawings should be made for those designs that involve departures from previously demonstrated collector geometry and operating conditions.

During Phase I of this contract, a study of the literature has been conducted. This study has included proprietary company sources as well as published sources and has had as its objectives:

- Reexamination of available information with respect to sodium potassium, including their eutectic solutions.
- Inquiry into gallium and its eutectics.
- Examination of various other liquid metals in both the open literature and in unpublished proprietary work done within the General Electric Company, to assure that the best possible recommendations are provided to determine the metal and method of current collection to be used in superconductive, acyclic, d-c motor and generator design.

It is significant to note that liquid-metal current collectors using mercury and those using sodium potassium have been used successfully by the General Electric Company for many years. Collectors using sodium potassium have been provided and are currently offered for commercial, nonsuperconductive, acyclic, d-c generators by General Electric's Large D-C Motor Section.

Recently, in developmental tests on a 10-inch-diameter experimental collector at 3600 rpm, liquid gallium has been successfully operated for more than 150 hours. This operation was made possible by the proprietary development and application of a cleaning and reclamation circuit for the liquid gallium.

### Sodium Potassium Metals and Alloys

In the work previously done at the General Electric Company in the use of liquid-metal collectors for superconductive machines, the sodium potassium eutectic, NaK-78 (22% Na, 78% K), was selected as the collector fluid. This choice was made because of the previous company investigations and particularly because of the successful use of NaK-78 in nonsuperconductive, acyclic generators produced at General Electric.

Sodium potassium metal alloys (e. g. , NaK-78 and NaKCs) are characterized by low density and high chemical activity. The low density of these alloys and their low absolute viscosity and good electrical and heat conductivities make them very desirable in high-speed collector configurations (e. g. , generators). These characteristics are of less importance in low-speed applications (e. g. , motors).

Most important for the development of d-c acyclic machines and for current collectors of very high current density, sodium potassium is fully compatible with a great many of the materials commonly used in such equipment. This compatibility includes magnetic and high-electrical-conductivity materials (e. g. , iron and copper alloys), although it does not include aluminum.

Sodium potassium can be used with a wider range of materials than any other liquid metal considered. It is not toxic, and the ability of sodium potassium metals to wet other materials, such as copper, is particularly valuable in assuring good electrical contacts and low contact resistance.

Each of the liquid metals has high rates of chemical activity with certain other materials and material combinations, and each of them (just as is the case for fuels) must be handled carefully, to assure that uninformed personnel are excluded and that material or environmental combinations that involve potential hazards are eliminated.

It should equally be noted that, as in the case of fuels, completely satisfactory procedures are available and, correspondingly, that when these procedures are employed, the potential hazards are effectively eliminated. Over the years, a considerable amount of development work has been done using the liquid metals in heat transfer applications. While thorough instruction of the involved personnel is essential, and consistent attention must be given to following proper procedures (using suitable materials combinations in handling these liquid metals), experience has shown that they can be safely used in properly designed and operated installations.

The General Electric Company has published a 35-page document (Ref. 11) that covers the information needed to develop a safe operational environment for a sodium potassium liquid-metal facility.

Some references have been made to the potential hazards of superoxides in sodium potassium liquid-metal systems. These references have been vague and undefinitive and have had a tendency to disturb rather than inform the reader. This subject received further research and thermodynamic analysis during Phase I of this program, and its principal findings are that:

- The only significant oxide in equilibrium with excess metal in a sodium potassium liquid-alloy system is  $\text{Na}_2\text{O}$ . The superoxides of sodium and potassium and the  $\text{K}_2\text{O}$  oxide are all reduced by the liquid sodium metal.
- Because of its limited solubility in liquid-sodium-potassium alloy,  $\text{Na}_2\text{O}$  could only marginally affect the physical properties of the alloy.
- Accumulation of the  $\text{Na}_2\text{O}$  should be avoided to ensure that the chemical properties of the oxide will not adversely affect the machine components. Mating materials, particularly insulating and sealing materials, need to be so selected as to eliminate any long-term effects.

Thus, the equipment design practices employed by the General Electric Company under its development contract (N00024-68-C-5415) for the Department of the Navy, in which the liquid metal continues to be circulated, filtered to remove any oxide that may have been formed, cooled, and returned to the collectors of the active (torque-producing) elements of the machine are confirmed by the independent study conducted under Phase I of this Program.

In an analytical study prepared during Phase I, standard enthalpies and free energies of formation for each of the various oxides (e. g. ,  $\text{Na}_2\text{O}$ ,  $\text{Na}_2\text{O}_2$ ,  $\text{NaO}_2$ ,  $\text{K}_2\text{O}$ ,  $\text{K}_2\text{O}_2$ , and  $\text{KO}_2$ ) were compiled, the equilibrium equations were examined, the equilibrium constants were determined as a function of temperature, and the conclusion was reached that other reactions could be considered. However, the conclusion was clear that the only oxide favored in the system is  $\text{Na}_2\text{O}$ . In the case of those reactions in which  $\text{K}_2\text{O}$  is shown to be a favored product, it should be recalled that the  $\text{K}_2\text{O}$  would be removed via reaction ( $\text{K}_2\text{O} + 2\text{Na} = \text{Na}_2\text{O} + 2\text{K}$ ) in a system containing excess sodium. This result is in complete agreement with the statements of D. D. Williams that the equilibrium oxide in a sodium potassium alloy is  $\text{Na}_2\text{O}$ .

It is also worth noting that in the General Electric work for the Navy, after the six-week liquid-metal assembly and test period, plus a six-week nonoperating period, not only the active portion of the d-c superconductive generator itself but also the filter system was clean and free of any accumulation of oxides. This result served to emphasize both the value of effective seals (to exclude oxygen) and the practicability of applying liquid-metal collectors to superconductive d-c machines for specific applications, including marine environments. The development work involved for long-life testing and for changes of scale (in building much larger machines) must, of course, be conducted to assure the future success of such machine applications.

### Gallium Metal and Alloys

The information on these metals, which is necessary for their successful application to liquid-metal current collection in high-powered machinery is much less readily available. Much of the key data, both in this country and abroad, appears in proprietary publications or is unpublished. For this reason, more inquiry was made into the work that has been done on gallium. A more detailed discussion is provided in Appendix V.

General Observations. Gallium has not found any extensive use in current collectors, mainly because of the very unfavorable experiences with it when applied to electrical machines. It had been found that gallium turns into a paste after only a few seconds of high-speed operation. Efforts to identify the paste and the cause of its formation had not been successful; however, based on work done by the General Electric Company, this problem has been overcome. The paste-like substance, generally called contamination, has been identified, and methods of preventing its formation and techniques for cleaning

it have been delineated. This work has been done on internal company research and development funds over the past two years and is considered proprietary.

Specifically, the contamination has been identified as gallium oxide, principally  $\text{Ga}_2\text{O}_3$ . Its formation can be prevented by operation in an oxygen-free and moisture-free environment. To the degree that a completely oxygen-free and moisture-free environment is not attainable in applications using rotating seals, gallium oxide may form, and it is necessary to provide a means for removing these oxides from the gallium. Both filtering and electrolytic procedures that will clean gallium for a current collector have been developed and demonstrated.

In view of these findings, the application of gallium to current collectors has been reconsidered, and considerable development work has been completed. When properly applied, and with provision for cleaning, gallium can be used for current collection in electrical machines.

Whether sodium potassium or gallium is used in power applications, the requirements for successful equipment are essentially the same:

- High-quality, properly designed rotating seals must be provided.
- The use of a controlled environment (cover gas or liquid) is necessary inside these sealed liquid-metal areas, to assure that both oxygen and moisture vapor are limited to very few parts per million.
- Equipment and procedures, preferably automatic, must be provided for the removal of the oxides that are formed.

Characteristics of Gallium. Gallium is a silvery white metal that lies in Group IIIa of the periodic table, between aluminum and indium. It has a number of unusual properties: it melts at near-room temperature ( $29.3^\circ\text{C}$ ), it has very low vapor pressure and a high surface tension, it expands on freezing, and it is nontoxic. Gallium is available in purities of 99.9 to 99.9999 percent. A summary of the physical properties of gallium is given in Table 46.

Gallium is very reactive when in the liquid state and will alloy readily with many metals, so care must be exercised to select materials that are compatible with it. Materials such as aluminum, copper, gold, magnesium, tin, and zinc should not be used with gallium. On the other hand, tungsten, tantalum, molybdenum, nickel, graphite, 300-series stainless steel, Kapton, Delrin, Noryl, Mylar, Teflon, and epoxy-filled fiberglass can be used with gallium.

Liquid gallium oxidizes very readily in the presence of air or oxygen. The oxide forms over the surface of gallium in a film of monomolecular thickness. The film displays very cohesive characteristics and has the property of being able to entrap gallium. Once the film is formed, there is little

Table 46  
PHYSICAL PROPERTIES OF GALLIUM

Property	Value		
Atomic number	31		
Atomic weight	69.7		
Melting point	29.8°C (85.6°F)		
Boiling point	2403°C		
Specific gravity (g/ml)			
Solid	5.904 (29.6°C)		
Liquid	6.095 (29.8°C)		
	5.095 (301°C)		
Expansion of solidification	3.2%		
Volume coefficient of thermal expansion			
Solid (0 to 30°C)	$5.8 \times 10^{-6}$		
Liquid (100°C)	$12.0 \times 10^{-6}$		
Vapor pressure (mmHg)			
30°C	$\approx 10^{-36}$		
600°C	$4.4 \times 10^{-9}$		
800°C	$5.9 \times 10^{-8}$		
Viscosity (centipoises)	1.6 (97.7°C)		
Surface tension (dynes/cm)	735		
Volume resistivity ( $\mu\Omega\text{-cm}$ )			
Liquid	25.2 (0°C)		
	25.6 (20°C)		
	26.0 (40°C)		
Solid	<u>C Axis</u>	<u>A Axis</u>	<u>B Axis</u>
0°C	48.0	15.4	7.2
29.7°C	54.3	17.4	8.1
Crystal structure	Orthohombic		
Specific heat (cal/g°C)			
0 to 24°C (solid)	0.089		
12.5 to 200°C (liquid)	0.095		
Heat of fusion (cal/g)	19.2		
Gallium purity available	99.9 to 99.9999%		
Toxicity	Nontoxic		

further oxidation. Oxidation of liquid gallium can be prevented by maintaining it in an inert environment, such as nitrogen or argon. There is no evidence that solid gallium oxidizes beyond a monolayer in the presence of oxygen.

In addition to pure gallium, considerations have been given to using alloys of gallium. By alloying gallium with indium, tin, or zinc, it is possible to reduce the melting temperature. Depending upon the alloying elements, the melting temperature can be reduced to 3°C. There does not appear to be any great advantages to using alloys of gallium in either slipring or current collector applications. The problem of oxidation would not be lessened, the alloy would have a more complex metallurgy, and there would be additional problems of preparation and handling.

Available information indicates that indium (and the indium of the gallium indium eutectic) surfaces oxidize slowly, even under a protective atmosphere containing less than one part per million of oxygen. The oxide formations of the eutectic are very similar to those of gallium alone. The presence of water vapor has a definite influence in increasing the rates of formation of indium oxides.

Procedures for reclaiming the metals from the oxides are more complex as the number of elements involved is increased. While the methods developed at the General Electric Company for reclaiming the gallium would be expected to be satisfactory for the eutectic, the experimental testing is presently planned only for gallium itself. For additional details of prior work, see Appendix V.

### Other Liquid Metals and Alloys

Experimental and analytical research work has extended over many years, and a large literature is available with respect to the use of mercury as a liquid metal electrical connecting fluid. No attempt is made in this report to provide a bibliography for mercury, because it is readily available and because mercury is toxic and is not recommended for use in superconductive machinery. Many successful applications have been made using mercury; the best of these being those that involve complete hermetic seals of glass or metal, with no possibility for operators to have any occasion for contact with the fluid.

More recent investigations of mercury, mercury amalgams, bismuth eutectic alloys, and so forth under a purified gas atmosphere containing no oxygen and low moisture contents (e.g., 0.25 ppm and above) have been made. These tests have been separately initiated and conducted using General Electric Company funds, and the data is considered proprietary.

In each of these instances, the formation of black or gray powders and scums was found to be present at various moisture levels (e.g., ppm) and to be strongly influenced by the moisture content. The bismuth alloys with melting points of between 100°F and 200°F would require heating mantles to

be maintained in most applications. Metal reclamation developments would also be required for the application of the bismuth alloys.

### SUPERCONDUCTIVE COIL TECHNOLOGY

The principal activities in the superconductive coil technology area will be carried out during Phase II of this contract. These activities will include confirming the application of the Culham Laboratories technology to superconductive coils at the General Electric Company and at the Intermagnetics General Corporation. During Phase I, the documentation of this technology was formally completed in a separate activity, under General Electric Company funding.

Superconductive coils built at Culham Laboratories, using this technology, have been able to produce an effectively monolithic character and structure, so there is no movement of any individual conductor relative to the other conductors in the individual superconductive coil. At the same time, this technology produced coils that have been able to attain full, short-sample, current-carrying capabilities in the completed coil.

This technology, though of a proprietary nature, is believed to be the best technology presently available. The work during Phase II is expected to confirm the results obtained in England at Culham Laboratories and provide data for comparison with other processes. Work in this area is being conducted at the Naval Ships Research and Development Laboratories and whatever data are available at the end of Phase II will be compared with that obtained at the General Electric Company.

## Appendix I

### IDEAL HEAT EXCHANGER MODEL

As noted in Section 2, in the discussion of the overall refrigeration system model, the key element presently requiring modeling attention is the heat exchanger. For purposes of a performance model (as contrasted with a design model), what is desired is a transfer function that will provide a direct input-output relationship in terms of primary system variables. It is not necessary that the mechanical details of construction be treated explicitly, but only that the model behave in a sufficiently realistic manner with respect to these system variables. The calculated and/or measured figures of merit for the actual design can ultimately be inserted into the simplified model by direct empirical calibration of its constant parameters.

Specifically, for an unbalanced counterflow heat exchanger, for given temperature ( $T$ ), and for mass flow rate ( $m$ ) inputs, the output temperatures as functions of  $T$  and  $m$  are expressed as indicated symbolically in Figure 92.

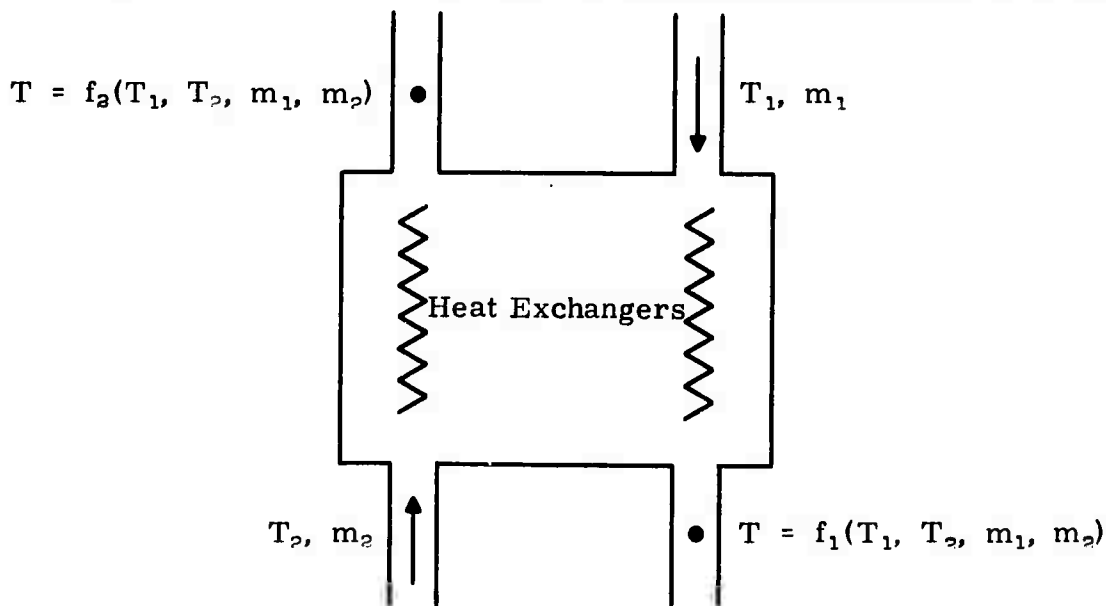


Figure 92. Output Temperatures as Functions of  $T$  and  $m$

### ASSUMPTIONS

The following basic assumptions are made:

- Steady-state operation
- No axial heat transfer
- Constant surface heat transfer coefficient
- Constant specific heat

In general, an arrangement whereby the two streams are separated by a large-area, thin conducting wall is implied (Figure 93).

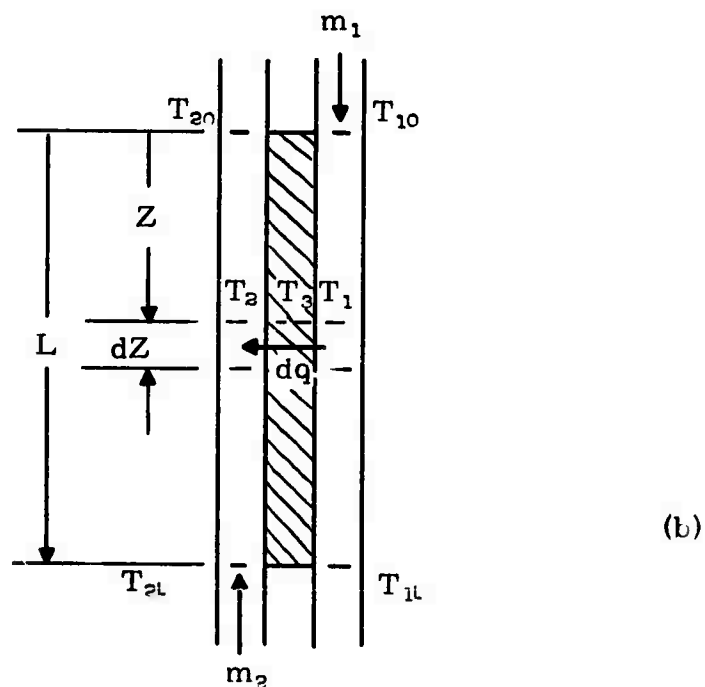
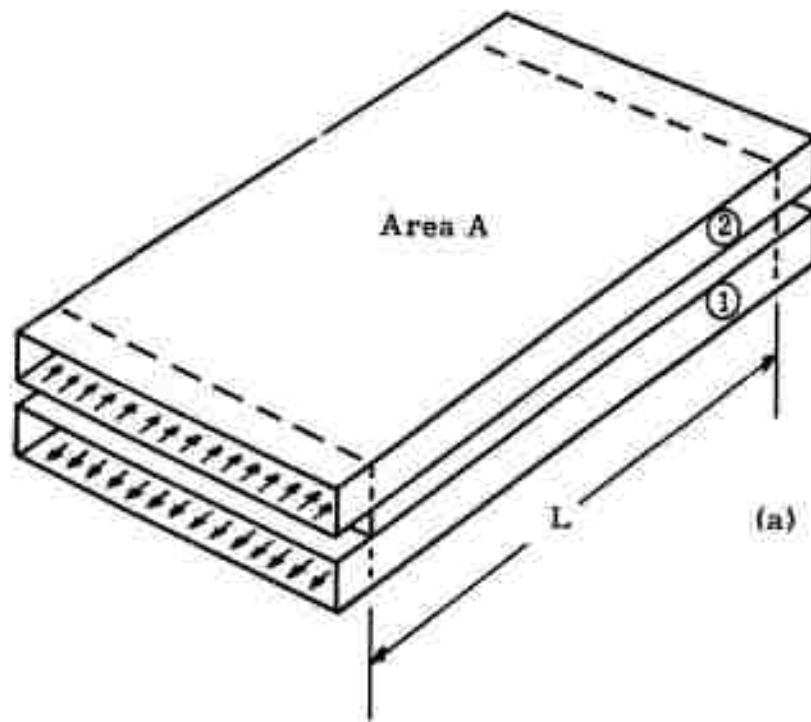


Figure 93. Two Streams Separated by Large-Area, Thin Conducting Wall

## ANALYSIS

Under the assumptions, this problem is one-dimensional, in which temperature is a function of the axial distance,  $z$ . The rate of heat transfer from the fluid (1) to the wall material (3) over axial distance  $dz$  is:

$$dq_{13} = h_1 (T_1 - T_3) \frac{A_1}{L_1} dz$$

where:

$h$  = Surface heat transfer coefficient

$A$  = Effective total area

$L$  = Effective total length

$T$  = Temperature

$q$  = Heat flow

$z$  = Axial distance

Similarly, the rate of heat transfer from the wall material (3) to the fluid (2) is:

$$dq_{32} = h_2 (T_3 - T_2) \frac{A_2}{L_2} dz$$

Under the assumptions, no change in heat storage takes place, and axial heat transfer is negligible. Therefore:

$$dq_{13} = dq_{32} = dq$$

and

$$\frac{h_1 A_1}{L_1} (T_1 - T_3) = \frac{h_2 A_2}{L_2} (T_3 - T_2)$$

Eliminating  $T_3$  from this relationship:

$$dq = \frac{\frac{h_1 A_1}{L_1} \frac{h_2 A_2}{L_2}}{\frac{h_1 A_1}{L_1} + \frac{h_2 A_2}{L_2}} (T_1 - T_2) dz$$

The combination of constants can be treated as a single equivalent parameter of the design:

$$\frac{\frac{h_1 A_1}{L_1} \frac{h_2 A_2}{L_2}}{\frac{h_1 A_1}{L_1} + \frac{h_2 A_2}{L_2}} = \left( \frac{hA}{L} \right)$$

$$dq = \frac{hA}{L} (T_1 - T_2) dz \quad (5)$$

The heat extracted from the fluid (1) will lower its temperature:

$$dq = C_p m_1 (-dT_1) \quad (6)$$

where:

$C_p$  = Fluid specific heat

$m$  = Mass flow rate

Similarly, the heat added to the counterflowing fluid (2) will raise its temperature:

$$dq = C_p (-m_2) dT_2 \quad (7)$$

From these two expressions, assuming  $C_p$  and  $m$  are constant:

$$d(m_1 T_1) = d(m_2 T_2)$$

and because  $T_1$  and  $T_2$  are functions only of the single variable,  $z$ :

$$m_1 T_1 = m_2 T_2 + D \quad (8)$$

where  $D$  is a constant (difference).

Substituting Equation 8 into Equation 5, and equating the result to Equation 6:

$$\frac{dT_1}{\frac{D}{m_1 - m_2} - T_1} = \frac{m_1 - m_2}{m_1 m_2} \frac{hA}{C_p L} dz \quad (9)$$

Integrating from  $z = 0$  to some general point  $z$ :

$$\begin{aligned} \int_{T_{10}}^{T_1} \frac{dT_1}{\frac{D}{m_1 - m_2} - T_1} &= \frac{m_1 - m_2}{m_1 m_2} \frac{hA}{C_p L} \int_0^z dz \\ \ln \left| \frac{\frac{D}{m_1 - m_2} - T_1}{\frac{D}{m_1 - m_2} - T_{10}} \right| &= \frac{m_1 - m_2}{m_1 m_2} \frac{hA}{C_p L} z \\ -T_1 &= \left( \frac{D}{m_1 - m_2} - T_{10} \right) e^{\frac{m_1 - m_2}{m_1 m_2} \frac{hA}{C_p L} z} - \frac{D}{m_1 - m_2} \end{aligned}$$

$$T_1 = T_{10} e^{\frac{m_1 - m_2}{m_1 m_2} \frac{hA}{CpL} z} + \frac{D}{m_1 - m_2} \left( 1 - e^{\frac{m_1 - m_2}{m_1 m_2} \frac{hA}{CpL} z} \right) \quad (10)$$

Substituting in Equation 8 and solving for  $T_2$ :

$$T_2 = \frac{m_1}{m_2} T_{10} e^{\frac{m_1 - m_2}{m_1 m_2} \frac{hA}{CpL} z} + \frac{D}{m_1 - m_2} \left( 1 - \frac{m_1}{m_2} e^{\frac{m_1 - m_2}{m_1 m_2} \frac{hA}{CpL} z} \right) \quad (11)$$

To solve for  $D$ , it is noted that at  $z = L$ ,  $T_2 = T_{2L}$ , one of the inputs:

$$T_{2L} = \frac{m_1}{m_2} T_{10} e^{\frac{m_1 - m_2}{m_1 m_2} \frac{hA}{Cp} L} + \frac{D}{m_1 - m_2} \left( 1 - \frac{m_1}{m_2} e^{\frac{m_1 - m_2}{m_1 m_2} \frac{hA}{Cp} L} \right)$$

$$D = \frac{\frac{m_1 - m_2}{m_1 m_2} \frac{hA}{Cp}}{\frac{m_1}{m_2} e^{\frac{m_1 - m_2}{m_1 m_2} \frac{hA}{Cp} L} - 1} \left( \frac{m_1}{m_2} T_{10} e^{\frac{m_1 - m_2}{m_1 m_2} \frac{hA}{Cp} L} - T_{2L} \right) \quad (12)$$

Substituting for  $D$  in Equations 10 and 11:

$$T_1 = \frac{\left( \frac{m_1}{m_2} e^{\frac{m_1 - m_2}{m_1 m_2} \frac{hA}{Cp} L} - e^{\frac{m_1 - m_2}{m_1 m_2} \frac{hA}{Cp} \frac{z}{L}} \right) T_{10} - \left( 1 - e^{\frac{m_1 - m_2}{m_1 m_2} \frac{hA}{Cp} \frac{z}{L}} \right) T_{2L}}{\frac{m_1}{m_2} e^{\frac{m_1 - m_2}{m_1 m_2} \frac{hA}{Cp} L} - 1} \quad (13)$$

$$T_2 = \frac{\frac{m_1}{m_2} \left( e^{\frac{m_1 - m_2}{m_1 m_2} \frac{hA}{Cp} L} - e^{\frac{m_1 - m_2}{m_1 m_2} \frac{hA}{Cp} \frac{z}{L}} \right) T_{10} + \left( \frac{m_1}{m_2} e^{\frac{m_1 - m_2}{m_1 m_2} \frac{hA}{Cp} \frac{z}{L}} - 1 \right) T_{2L}}{\frac{m_1}{m_2} e^{\frac{m_1 - m_2}{m_1 m_2} \frac{hA}{Cp} L} - 1} \quad (14)$$

Finally, the desired values for  $T_1$  and  $T_2$  are those at the outputs:

$$T_1 = T_{1L} \text{ at } z = L$$

$$T_2 = T_{20} \text{ at } z = 0$$

$$T_{1L} = \frac{\left(\frac{m_1}{m_2} - 1\right) e^{\frac{m_1 - m_2}{m_1 m_2} \frac{hA}{Cp}} T_{10} - \left(1 - e^{\frac{m_1 - m_2}{m_1 m_2} \frac{hA}{Cp}}\right) T_{2L}}{\frac{m_1}{m_2} e^{\frac{m_1 - m_2}{m_1 m_2} \frac{hA}{Cp}} - 1} \quad (15)$$

$$T_{20} = \frac{\frac{m_1}{m_2} \left( e^{\frac{m_1 - m_2}{m_1 m_2} \frac{hA}{Cp}} - 1 \right) T_{10} + \left( \frac{m_1}{m_2} - 1 \right) T_{2L}}{\frac{m_1}{m_2} e^{\frac{m_1 - m_2}{m_1 m_2} \frac{hA}{Cp}} - 1} \quad (16)$$

## Appendix II

### SYSTEM REQUIREMENTS FOR SUPERCONDUCTING NAVAL SHIP PROPULSION SYSTEM

#### SCOPE

These requirements define the system and give the performance requirements, operational requirements, and environmental requirements applicable to a superconducting naval ship propulsion system. This document is applicable to all elements of the system unless stated otherwise. These elements include the generator, the motor, the refrigeration system, the transmission system, the power conditioning equipment, and controls. Unique requirements of the refrigeration system are given on pages 168 and 169 of this report.

#### APPLICABLE DOCUMENTS

The following documents are applicable to the extent listed herein:

<u>Document</u>	<u>Title</u>
MIL-STD-785A	Reliability Program for Systems and Equipment
MIL-STD-470	Maintainability Program Requirements
MIL-STD-461A	Electromagnetic Interference Characteristics, Requirements for Equipment
MIL-S-901C	Shock Test, H.I. (High Impact); Shipboard Machinery, Equipment and Systems, Requirements for
MIL-STD-167B	Mechanical Vibrations of Shipboard Equipment
MIL-G-18473A	Generators and Motors, Direct Current, Naval Ship Propulsion
MIL-G-18474	Generators and Motors, Alternating Current, Naval Ship Propulsion
MIL-G-18475	Switchboards, Power, Naval Surface Ship, Propulsion Control

#### SYSTEM DEFINITION

The basic superconducting naval ship propulsion system is as indicated in Figure 94. This system is applicable to a destroyer-class ship and shows the equipment associated with each propeller shaft. For each shaft, the system consists of two generators, each directly coupled to a gas turbine, driv-

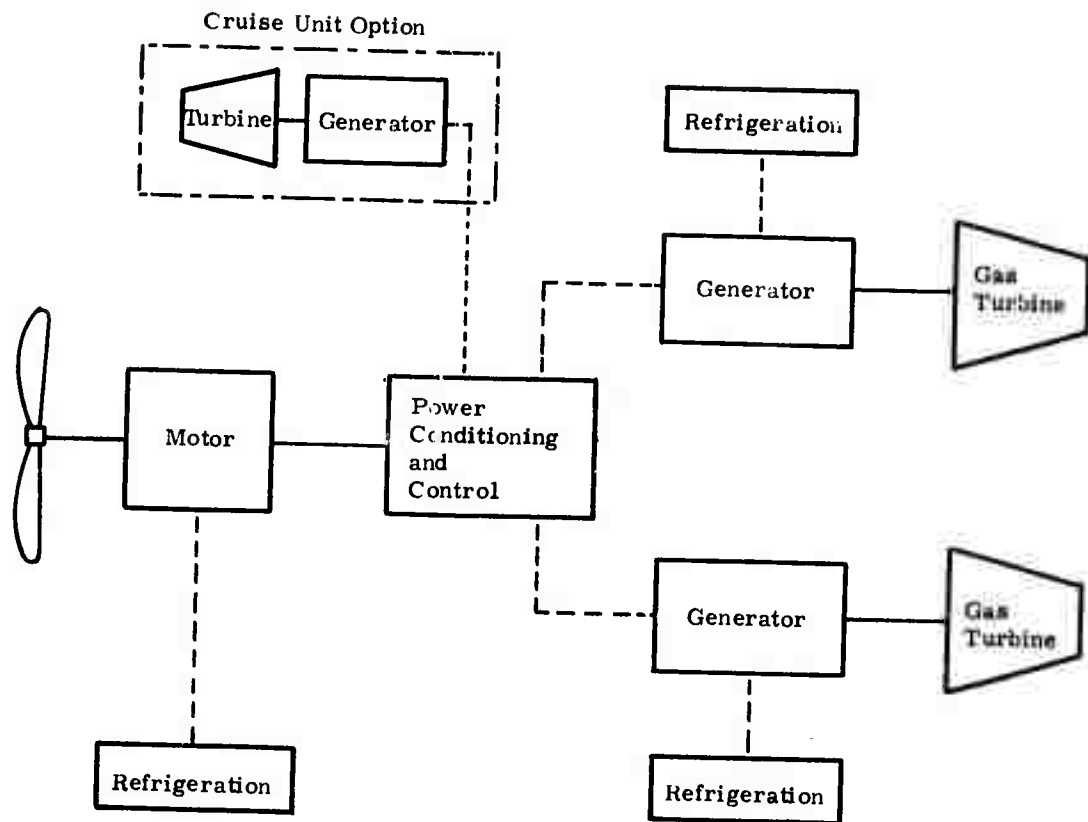


Figure 94. Basic System Schematic

ing a single motor through suitable power conditioning and control. Refrigeration equipment is provided to maintain superconducting fields in the generators and the motor. For a double-shaft system, this basic building block is simply repeated, except that all generators and motors are coupled electrically through the power conditioning and control.

A system option shown by the dotted line in Figure 94, is a single, smaller gas turbine/generator unit for each shaft, for low-power operation. This latter unit may or may not be superconducting. This smaller unit has not been sized, and no layouts have been made of it.

## PERFORMANCE REQUIREMENTS

### MOTOR RATING

Nominal output shall be 40,000 hp and 200 rpm.

### MAIN GENERATOR RATING

Nominal output shall be 18,000 kw (24,100 hp) at 3600 rpm for sizing and layout studies. Output shall be consistent with motor rating and system efficiencies for fuel consumption studies.

## MAIN GAS TURBINE RATING

This rating is nominally in the 20,000-hp range, but shall be adjusted, as required, in fuel consumption studies, to be consistent with the motor rating and system efficiencies.

## CRUISE TURBINE/GENERATOR UNIT

Nominal rating shall be 5000 hp but shall be adjusted, as required, in fuel consumption studies, to account for system efficiencies.

## EFFICIENCY

The overall system shall have the highest efficiency possible, consistent with reasonable size, weight, and complexity.

As a design goal, the product of generator efficiency, transmission efficiency between the generator and the motor, and motor efficiency, including power required for the cryogenic refrigeration system, shall exceed 90 percent.

## WEIGHT

Weight shall be minimized to the extent practicable, consistent with maintaining high efficiency.

## SIZE

Maximum envelope dimensions shall be as given in Table 47.

Table 47

### MAXIMUM ENVELOPE DIMENSIONS

Component	Requirement (in.)	Goal (in.)
Generator		
Width	86	< 62
Height	84	< 62
Length	No requirement	< 105
Motor		
Width	168	< 108
Height	168	< 108
Length	No requirement	< 180
Refrigeration equipment for generator (unit)		
Width	86	< 62
Height	84	< 62
Length	No requirement	< 105
Refrigeration equipment for motor		
Width	168	< 108
Height	168	< 108
Length	No requirement	< 180

## CROSS-CONNECT CAPABILITY

Capability shall exist to connect generators and motors in all possible combinations with independent motor speed control.

## CROSS-CONNECT SWITCHING TIME

This time is defined as the time required to switch from one set of generator/motor connections to any other set and be transmitting power in the second mode. This time shall be as short as practicable with a goal of 1 minute or less.

## COOLDOWN

The cooldown time from room temperature to superconducting and operating temperatures shall not exceed 72 hours for both the generator and the motor.

Cooldown capability at sea is required.

Superconductive elements shall be maintained continuously at superconducting temperatures, except for:

- Extended periods at dockside (greater than 1 week).
- Shutdown due to malfunction or maintenance.

## GENERATOR STARTING TIME

As a goal, it shall be possible to bring the generator from zero speed (but with the field at superconducting temperatures) to idle speed and no load in less than 75 seconds.

As a goal, the generator shall be capable of going from idle speed, no load, to full load and rated speed in less than 30 seconds.

## MOTOR STARTING TIME

As a goal, the time from zero speed (but with the field at superconducting temperatures) to a condition where the motor can accept the load shall be less than 75 seconds.

As a goal, the motor shall be capable of going from no load to full load in less than 30 seconds.

## CRASH REVERSAL

The maximum time from the issuance of a reversing command to the time when the electrical system is fully reversed and ready to apply reversing power shall be 15 seconds.

## WARMUP

As a goal, the maximum warmup time from superconducting temperatures to room temperature shall be 6 hours, for both the generator and the motor.

## OVERSPEED

The motor shall be designed to safely withstand an overspeed of 25 percent, with no permanent damage.

The generator shall be designed to safely withstand an overspeed of 10 percent, with no permanent damage.

## SHORT CIRCUIT

The generator, if a-c, shall be designed to safely withstand an external short circuit, with no permanent damage, for as long a time period as the short circuit can be expected to persist, consistent with the performance of circuit protective devices. The field shall remain superconducting during this time, and capability shall exist to reapply the load as soon as the fault is cleared.

The generator, if a-c, shall be designed to withstand an internal short circuit without incurring structural damage that would constitute a hazard. The field need not remain superconducting during this time.

Systems involving d-c generators and/or motors shall be designed so no permanent damage shall result, in the event of a short circuit, including a short circuit arising from the loss of field of either a motor or a generator.

## LOSS OF SUPERCONDUCTIVITY

All motor and generator designs shall be such that no permanent structural damage shall occur and no safety hazard shall exist in the event that a coil goes normal for any reason whatsoever.

## RESONANT FREQUENCIES

No resonant frequencies in either torsion or bending shall lie within the operating speed ranges of any generator, motor, or refrigeration equipment.

## OPERATIONAL REQUIREMENTS

### DUTY CYCLE

The duty cycle of Table 48 shall be considered typical and shall be used for estimates of fuel consumption and definition of appropriate operational procedures and control requirements.

Table 48  
TYPICAL MISSION PROFILE

Step	Time (hr)	Operation	Power (% rated)	Prop Speed (% rated)
1	0	Dockside	0	0
2	0 - 0.1	Dockside	0	0
3	0.1 - 0.11	Dockside Maneuver	0.013	5
4	0.11- 1.0	Harbor Maneuver	1.6	25
5	1.0 - 1.1	Harbor Maneuver	1.6	25
6	1.1 -200	Cruise/Patrol	12.5	50
7	200 -300	Patrol/Watching	0	0
8	300 -300.1	Patrol/Alert	0	0
9	300.1 -305	Flank Speed	100	100
10	305 -310	High Speed	70	89
11	310 -350	High-Speed Cruise	23	61
12	350 -352	Harbor Maneuver	1.1	22
13	>352	Dockside	0	0

#### LIFE

The goal is for a design life of 100,000 hours for all system equipment.

#### RELIABILITY

Each generator and each motor shall have its own refrigeration system.

Capability shall exist to connect any generator to any generator refrigeration system and any motor to any motor refrigeration system.

MIL-STD 785 shall be used as a design guide, where applicable.

As a design goal, the mean time between failure (MTBF) for any major equipment (e.g., the generator, motor, power conditioning system, or refrigeration system) shall be greater than 140,000 hours.

The preliminary design process shall include identification of principal items inhibiting reliability and of possible improvements that can be made.

#### MAINTAINABILITY

Good maintainability design features shall be emphasized using MIL-STD 470 as a guide, especially paragraph 5.4.

The goal is that major inspections or overhauling shall occur no more frequently than every 45,000 hours.

### NOISE AND ELECTROMAGNETIC INTERFERENCE

The objective is to minimize noise and electromagnetic interference to the maximum extent practicable.

MIL-STD 461A shall be used as a guide.

The preliminary design process shall include identification of potentially high values and shall indicate possibilities for reducing them.

### SAFETY

The preliminary design process shall include identification of major safety hazards and approaches for minimizing them.

### VULNERABILITY TO ACCIDENT OR ENEMY ACTION

The goal shall be, through good design practice, to minimize vulnerability to accident or enemy action.

### ENVIRONMENTAL REQUIREMENTS

#### SHOCK

All equipment shall be designed to meet the shock test requirements of MIL-S-901C for grade A -- Essential, hull-mounted, Class I -- no-resilient mounting.

If necessary, equipment may be shock-mounted to a rigid subbase, with the equipment and subbase then, for testing purposes, considered as a unit.

Section 6.2 of MIL-S-901C and the documents listed in Section 4.2.8 of MIL-S-901C shall be used for design guidance.

The design for shock, especially if shock mounts are used, must make adequate allowance for relative motion between major elements, especially the gas turbine/generator and the motor/propeller shaft.

As a design guide, but not superseding test requirements of MIL-S-901C, experience has been that design for steady-state accelerations has been found satisfactory for meeting shock test requirements for heavy equipment such as gears, as follows:

- Vertical: 75g
- Lateral: 45g
- Longitudinal: 20g

## VIBRATION

All equipment shall be designed to meet the requirements of MIL-STD-167B.

The use of resilient mounts shall be minimized.

The preliminary design process shall delineate the sources of any unusual internally generated vibration.

## MAGNETIC FIELD STRENGTH

Magnetic field strength shall be no greater than 100 gauss at 6 inches from the surface of the equipment.

## INCLINATION

Maximum values are (any installation angles must be added to these limits):

<u>Value</u>	<u>Pitch</u>	<u>Roll</u>
Maximum bias (deg)	±5	±10
Maximum total deg (bias plus transient) (10-sec duration)	±10	±45

## SURFACE TEMPERATURE

The temperature of all exposed surfaces exposed to personnel shall be between 32°F and 140°F.

## TEMPERATURE RISE

Nonsuperconducting elements of generators, motors, and power conditioning shall not exceed values given in MIL-G-18473, MIL-G-18374, and MIL-G-18475.

## AMBIENT TEMPERATURE

Design shall allow the capability of operating continuously in an ambient temperature between 32°F and 122°F.

## COOLANT

Seawater shall be used as the coolant for equipment operating at temperatures greater than 85°F, unless it can be demonstrated that another approach is better and is acceptable from total system considerations.

Seawater supply temperature shall be a maximum of 85°F.

Double-tube heat exchangers shall be used to reduce the chance of seawater entering the equipment being cooled. For example, the seawater shall pass through a tube that is inside of and concentric with another tube.

### HUMIDITY

Design shall allow capability of operating continuously at 0 to 95 percent relative humidity.

### SALT

Design shall allow capability of continuous operation in an atmosphere with five parts per million of salt content.

### GROUNDING

All electrical equipment shall be ungrounded.

## Appendix III

### CALCULATION OF D-C GENERATOR CONDUCTION AND RADIATION HEAT LEAKS TO SUPERCONDUCTING FIELD COIL

#### COIL WEIGHT

At a gross coil current density of  $10^4$  amperes per square centimeter and an effective flux density of 3.0 webers per square meter, magnetic calculations show the coil cross section to be:

- Inner radius: 16.25 inch
- Thickness: 1.50 inch
- Length: 11.5 inch

Therefore, the total current in the sheet is:

$$NI = (11.5)1.5(10^4) 6.45 = 1.113 \times 10^6 \text{ (amp turn)}$$

For the coil conductor, select the Niomax-FM C361/142, made by Imperial Metal Industries, Ltd. For an effective flux density of 3.0 webers per square meter, the estimated maximum flux density at the coil surface is 4.6 webers per square meter, at which the above conductor has a critical current of 900 amperes. The coil current is chosen at 700 amperes, which makes the number of turns in the coil,  $N$ , equal to:

$$N = 1.113 \times 10^6 / 700 = 1590 \text{ turns}$$

Because the wire diameter is 1.42 millimeters ( $A = 2.46 \times 10^{-3} \text{ in.}^2$ ) and the density is 0.32 pound per cubic inch, the coil weight is approximately:

$$W_c = 1590 (34) \pi (2.46)10^{-3} (0.32) = 134 \text{ lb}$$

#### COIL ENCLOSURE WEIGHT

The inner cylinder of the coil enclosure must support the maximum helium pressure on the outside against a vacuum on the inside. This support requires a thickness of 1/8 inch of stainless steel. Taking the enclosure ends at 3/8 inch thick yields an enclosure weight of 115 pounds.

#### THICKNESS OF SUPPORT TUBES

The weight to be supported is 249 pounds. To meet the requirements for shock (see Appendix II), the support structure was designed for 60g loading. The failure mode is the buckling of the thin-walled stainless steel tube, which was determined to have a thickness of 0.025 inch (24 ga).

## HEAT TRANSFER BY CONDUCTION

The details of the coil support structure are shown in Figure 68. For this analysis, the support material is assumed to be an A286 stainless steel sheet, which is taken to have a thermal conductivity expressed by the curve fits:

$$k = \frac{T}{a + bT} \quad (\text{w/cm } ^\circ\text{K})$$

where:

$$25^\circ\text{K} < T < 300^\circ\text{K}$$

$$T = \text{Temperature } (^\circ\text{K})$$

$$a = 1082.04$$

$$b = 4.05743$$

and also, at lower temperature:

$$k = cT^d \quad (\text{w/cm } ^\circ\text{K})$$

where:

$$5.5^\circ\text{K} < T < 25^\circ\text{K}$$

$$c = 3.18558 \times 10^{-4}$$

$$d = 1.31389$$

Heat transfer by radiation is assumed to be independent of heat transfer by conduction; this situation is conservative for this configuration.

To determine the amount of heat conducted from the ambient temperature mounting point to the support shell joint held at  $80^\circ\text{K}$ , and from the  $80^\circ\text{K}$  point to the coil enclosure, it is necessary to integrate the basic equation of conductivity:

$$q = -kA \frac{dT}{dx}$$

with the appropriate expression for the thermal conductivity. The following expressions result:

$$300 < T < 25: \quad q = \frac{A}{L} \left[ \frac{T_2 - T_1}{b} - \frac{a}{b^2} \ln \left( \frac{a + bT_2}{a + bT_1} \right) \right]$$

$$25 < T < 5.5: \quad q = \frac{A}{L} \frac{c}{(1+d)} \left[ T_2^{(1+d)} - T_1^{(1+d)} \right]$$

In the case where the  $25^\circ\text{K}$  point lies along the member being analyzed, both of the above equations must be satisfied in their respective regions of applicability. This is most readily done by equating the two conduction equations and solving for the length of the member from one end to the  $25^\circ\text{K}$  point. Once this length is found, either of the two above equations can be used to determine the heat flow.

If  $L$  is the distance between the high-temperature end of the member and the point where  $T = 25^\circ\text{K}$  (Figure 95), then:

$$\left(\frac{L}{L_1} - 1\right) = \frac{c}{(1+d)} \frac{[T_1(1+d) - T_c(1+d)]}{\left[\frac{(T_H - T_1)}{b} - \frac{a}{b^2} \ln \frac{a + b T_H}{a + b T_1}\right]}$$

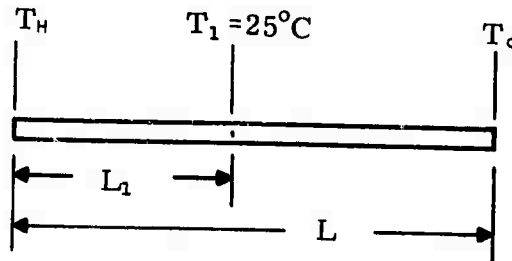


Figure 95. Distance from High-Temperature End of Member to Point Where  $T = 25^\circ\text{K}$

### HEAT TRANSFER BY RADIATION

Radiation heat transfer between parallel surfaces is described by:

$$q = A \bar{\epsilon} \sigma [T_1^4 - T_2^4]$$

where:

$\bar{\epsilon}$  = Effective emissivity

$\sigma = 0.533 \times 10^{-8} \text{ (w/ft}^2 \text{ } ^\circ\text{K}^4 \text{)}$

For parallel surfaces with  $n$  radiation shields interposed, and all surfaces having equal emissivity:

$$\bar{\epsilon} = \frac{1}{\left(\frac{2}{\epsilon} - 1\right)(n+1)}$$

## Appendix IV

### TRANSIENT REFRIGERATION LOADS DUE TO RAMPING

#### LOSSES DUE TO INDUCED CURRENTS IN SUPPORT STRUCTURE

A circumferential conducting member in the immediate vicinity of the field coil will have an induced voltage,  $E$ :

$$E = \pi r^2 \frac{dB}{dt} \quad (v)$$

where:

$r$  = Coil radius (m)

$B$  = Average flux density (Wb/m<sup>2</sup>)

$t$  = Time (sec)

Assuming a uniform cross section, the resistance of the structural member is:

$$R = \frac{2\pi r \rho}{A} \quad (\text{ohm})$$

where:

$\rho$  = Resistivity (ohm m)

$A$  = Cross-sectional area (m<sup>2</sup>)

The power dissipated in the member during slow ramps, where inductance is unimportant, is:

$$P = \frac{E^2}{R} = \frac{\pi A r^3}{2 \rho} \left( \frac{dB}{dt} \right)^2 \quad (w)$$

For a linear ramp between the levels of flux density,  $B_1$  and  $B_2$ , in time  $T$ , the dissipated energy is:

$$Q_L = \frac{\pi A r^3 (B_1 - B_2)^2}{2 \rho T} \quad (j)$$

which becomes, for a field reversal:

$$Q_L = \frac{2\pi A r^3 B^2}{\rho T} \quad (j)$$

For stainless steel at coil temperature, resistivity is approximately:

$$\rho = 0.37 \times 10^{-6} \quad (\text{ohm m})$$

**Preceding page blank**

Using this value of  $\rho$ , and expressing the cross-sectional area in square inches,  $A_1$ , and the radius in inches,  $r_1$ , the loss for a field reversal becomes:

$$Q_L = 0.180 \frac{A_1 r_1^3 B^2}{T} \quad (j)$$

The loss in a 0.010-inch-thick can with a cross-section periphery of 32 inches and a mean radius of 17 inches, if subjected to a 3.0-weber-per-square-meter field reversal in 15 seconds, is therefore 170 joules.

### RAMPING LOSS IN SUPERCONDUCTOR

An approximate evaluation of the hysteretic superconductor losses during a linear ramping from full to zero field is presented in Reference 12 as:

$$Q_L = \frac{VdJ_0H_0}{4(10^8)} \left[ \ln \frac{H_m + H_0}{H_1 + H_0} \right] \text{ average over coil} \quad (j)$$

where:

- $V$  = Volume of superconductor ( $\text{cm}^3$ )
- $d$  = Superconductor filament diameter (cm)
- $J_0$  = Characteristic current density ( $\text{amp}/\text{cm}^2$ )
- $H_0$  = Characteristic field strength (G)
- $H_m$  = Mean field strength in SC (G)
- $H_1$  = Empirical limiting field strength  
evaluated at 1000G

In the composite chosen for the present machine:

- $J_0 = 6.48 \times 10^5 \text{ (amp}/\text{cm}^2\text{)}$
- $H_0 = 15,700 \text{ (G)}$
- $d = 0.0043 \text{ (cm)}$
- $V = 2230 \text{ (cm}^3\text{)}$

The mean field strength in the coil can be obtained from the following approximate field strength on the inside coil surface. As the field strength drops off approximately linearly to zero at the outside coil surface, the mean field,  $H_m$ , is half the value at the inner surface (Figure 96). On this basis, the calculated loss for a 15-second reversal is 350 joules.

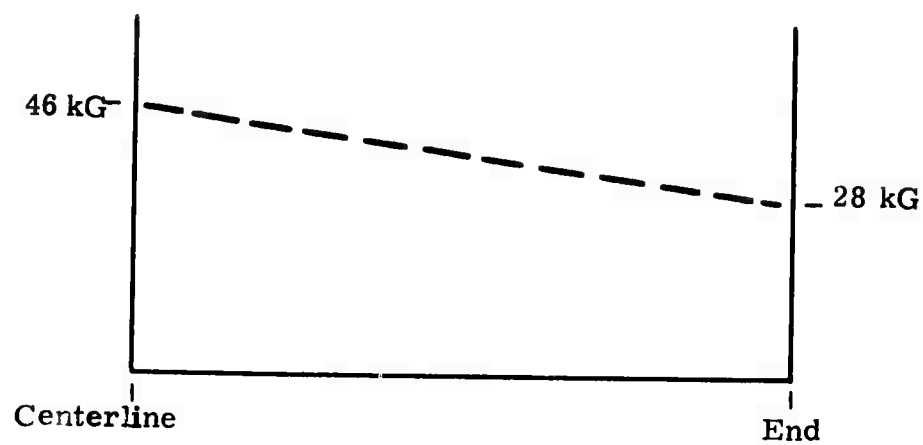


Figure 96. Field Strength on Inner Coil Surface

## Appendix V

# AN INVESTIGATION OF GALLIUM LIQUID METAL CURRENT COLLECTORS FOR SPACE APPLICATIONS

### INTRODUCTION

The General Electric Space Systems Products Department has been involved in the development of liquid metal sliprings for space applications since late 1968. These liquid metal sliprings have been developed for use on future, high-power, synchronous, orbit satellites that have large sun-oriented solar arrays that rotate slowly relative to the earth-oriented satellite centerbody. The sliprings will be used to transfer electrical power and signals from the solar arrays to the satellite body. Up to this time, power and signal transfer have been accomplished using conventional brushes and sliprings. These devices have a number of critical disadvantages:

- High mechanical drive torque.
- Brush wear-out and debris.
- High electrical noise and large electrical power losses.

The liquid metal slipring reduces many of the problem areas and eliminates others. There is no wear-out or debris, the drive torque is small, the electrical losses are very low, and there is no electrical noise. The sliprings used gallium as the liquid metal, because of its favorable melting temperature, vapor pressure, surface tension, and fluid and electrical characteristics.

The slipring work done at the General Electric Company has been accomplished both under internal research and development funds and under contract. The work done with Company research and development funds is proprietary, covering basic studies of liquid metals, the solution to the gallium contamination problem, and the development of cleaning techniques. There were two contracts with the National Aeronautics and Space Administration Lewis Research Center. The first contract culminated in the successful demonstration of a high-current gallium slipring capable of carrying currents up to 200 amperes d-c and voltages up to 3000 volts d-c.

This program consisted of three major tasks:

- Material selection and experiments.
- Engineering test model design.
- Fabrication, testing, and evaluation.

During the material selection and experiment phase, candidate liquid metals, electrodes, and insulation materials were selected and tested. Gallium was selected as the liquid metal; tungsten, tantalum, molybdenum, and graphite

**Preceding page blank**

were selected as the electrode materials; Noryl, Teflon, and Delrin were chosen as the insulation materials.

Selection was based on the functional requirements of the slipring, the inherent properties of the materials, their compatibility with each other, and their suitability for ground and space operation. An experimental program was run to evaluate the materials and their compatibility with each other. There was no gallium attack upon the electrodes, as determined by metallographic and spectrographic analyses. Delrin and Teflon insulations showed no attack by gallium. An engineering test model slipring was designed, fabricated, and tested. It was operated at 100 amperes d-c, at up to 3000 volts between rings, at rotational speeds of one revolution per day in air and vacuum environments. In the engineering test model, the electrodes were fabricated from tungsten, tantalum, and molybdenum, and the liquid metal was gallium. A gallium contamination was observed in the slipring, and efforts were made to identify it by means of spectrographic, x-ray diffraction and infrared analysis.

The second contract with the National Aeronautics and Space Administration Lewis Research Center was for the development of a liquid metal slipring/solar array orientation mechanism (LMSR/SAOM). This mechanism serves to continuously rotate a solar array with respect to the main body of a satellite and provide a means of transferring electrical power and signals across the rotating interface.

The basic requirements for the LMSR/SAOM were for a slipring using gallium, having 116 rings capable of carrying currents ranging from 0.2 to 30 amperes at up to 15,000 volts. The orientation mechanism had torque motors to provide rotary motion at the rate of one revolution per day and a position sensor to indicate shaft location. The entire assembly was less than 10 inches diameter and 24 inches long, and it weighed less than 40 pounds.

The overall program consisted of three major tasks:

- Preliminary design
- Design verification
- Detail design

In the preliminary design task, a design study was made in which a number of design concepts for the LMSR/SAOM evolved and were investigated in detail by means of design and engineering studies. Based on these studies, recommendations were made and a design concept was selected. The selected approach was the probe design concept. A verification model of the probe concept was designed, fabricated, and tested, in order to verify the integrity of the approach. The verification model was designed to carry currents up to 30 amperes per ring at up to 15,000 volts, in a six-ring configuration. The model was successfully tested for dielectric strength at 15,000 volts, launch

and orbital vibration, acceleration, shock, and operation. The cause of debris formation and ejection from gallium liquid metal sliprings has been identified, and the problem has been successfully solved.

As a result of the success with the gallium liquid metal slipring and the identification and solution of the contamination problem, Company funds were allocated for the development of a Company proprietary gallium liquid metal current collector. This current collector was developed for use in industrial power generation equipment as a replacement for conventional brushes and as an alternative to mercury and sodium potassium. It has the capability of carrying several thousand amperes of direct current. The gallium current collector has now been successfully demonstrated by personnel of the General Electric Company.

## **CONTAMINATION**

### **BACKGROUND**

During the development of the first liquid metal slipring for the National Aeronautics and Space Administration Lewis Research Center, a contamination was observed on top of the gallium, in the electrode cavity. This contamination was quite thin and had a mottled appearance (light and dark grey). When one electrode was turned relative to the other, the contamination showed a tendency to ball up and be ejected from the electrode cavity. Upon disassembly of the slipring, another contamination was found at the bottom of the electrode cavity. Its appearance was quite different from that observed previously; it was very dark grey and appeared powdery.

Efforts were undertaken to identify the contamination. Samples of the contamination as well as the gallium were examined by emission spectroscopy to determine whether they contained any electrode material. There was no indication of electrode material in the contamination or in the gallium. X-ray diffraction tests were run on the contamination to check for the presence of oxides, hydrated oxides, or hydroxides of gallium. All samples showed a diffraction pattern indicative of amorphous materials.

There are two possible reasons for the appearance of this pattern:

- To obtain a diffraction pattern, it is necessary to have a crystal at least 100 angstroms in size. Because the surface oxidation of gallium has been estimated to be of the order of 10 angstroms thick, it is possible that the crystal size of the oxidation was not sufficient to produce a diffraction pattern.
- There is not a sufficient quantity of oxide present in the test sample to produce the pattern.

An infrared absorption test was run on a contamination sample, because gallium oxide,  $\text{Ga}_2\text{O}_3$ , shows two characteristic absorption bands: one at 13.5

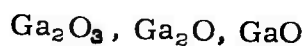
microns and the other at 14.35 microns. The infrared test showed no absorption up to 16 microns. The lack of results from this test has now been ascribed to the small quantity of oxide in the test sample.

Although the sample appeared to be highly contaminated, a microscopic examination of the powdery contamination indicated that the sample was mostly gallium, perhaps 95 to 99 percent by volume. The sample consisted of droplets of gallium covered with small, dark grey particles. The sample of contamination was centrifuged in an attempt to separate the powder from the gallium. Separation was not successful, because of the small difference in density between the powder (5.88) and the gallium (6.0), and because of the effects of the high gallium surface tension.

It was possible, from these tests, to postulate the probable composition of the contamination. It was known by testing that the gallium did not react with the electrode materials. It was also known that liquid gallium reacts very rapidly (e. g., in microseconds) with oxygen to form an oxide. This oxide layer is monomolecular, at least at temperatures up to several hundred degrees centigrade. The degree to which water vapor might enter into the reaction of gallium and oxygen was not known.

It was postulated that the contamination was either an oxide, a hydrated oxide, or hydroxide of gallium. The probable compositions are:

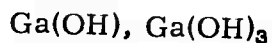
- Oxides of gallium



- Hydrates of gallium oxide



- Gallium hydroxides



Because gallium does not readily react with nitrogen, even at temperatures up to 1000°C, it was felt that the contamination did not contain compounds of nitrogen and gallium.

In addition to this experience with gallium in low-speed, liquid metal sliprings, the very rapid formation of a pastelike contamination was observed in high-speed current collectors operated in air. This formation caused a very rapid failure of the current collector. Based on more recent work, it is now known that the pastelike mass produced in the current collector is the same as that observed in the slipring.

#### GALLIUM CONTAMINATION STUDIES

A Company-sponsored program was undertaken to determine the possible composition of gallium contamination. Although the previous efforts to define

the composition of the contamination had been inconclusive, it was fairly certain that the contamination was either an oxide, a hydrated oxide, or a hydroxide of gallium. A number of approaches were considered for determining the contamination composition. A direct approach to determine the effects of oxygen and water vapor upon gallium was undertaken, rather than attempting further analysis of the contamination itself. This approach was to bubble various gases of known purity and composition through gallium and determine the effects. The gases used were oxygen, nitrogen, and hydrogen.

The nitrogen was selected as a control, because gallium does not react with it at normal temperatures. Hydrogen was selected because it is normally used for cooling large electrical machines. The oxygen and nitrogen were used both dry and saturated with water vapor.

Using this combination of gases, the effects of oxygen, water vapor, oxygen and water vapor, and hydrogen upon gallium could be ascertained. Tests were run both at 35°C and 125°C. In all tests, 12 grams of gallium were used and the gas flow rate was 70 cubic centimeters per minute. The gases used were:

- Oxygen -- research purity grade

Oxygen	99.99% (min)
Nitrogen	20 ppm
Argon	20 ppm
Carbon dioxide	10 ppm
Hydrocarbons	20 ppm
Dew point	-85°F

- Nitrogen -- prepurified grade

Nitrogen	99.998% (min)
----------	---------------

- Hydrogen -- ultrahigh-purity grade

Hydrogen	99.999% (min)
Impurities	Mostly helium

- Hydrogen -- industrial grade

Hydrogen	99.995% (min)
Oxygen	1 ppm
Water	3 ppm

The weight change of the gallium was monitored to provide an indication of whether a chemical reaction with the gas had taken place.

When dry oxygen was passed through the gallium, a rapid change in the gallium was observed. A contamination was formed that was white in color. After 15 minutes of bubbling, the gallium became very pastelike, losing its liquid characteristics. This condition was called channeling and was used as

the indication of failure. The resulting mixture was weighed, and the weight change was found to be about 0.02 percent.

These findings were considered to be very important. As expected, there was a reaction between the gallium and the oxygen, indicating that an oxide of gallium was formed. The rate of oxidation was somewhat more rapid than expected. What was very important and completely unexpected was the very small quantity of reaction product, 0.02 percent or 0.0024 grams in 12 grams, sufficient to completely immobilize the gallium. Thus only a small amount of gallium oxide contamination can change the physical characteristics of the gallium from a liquid, having a viscosity approximately equal to that of water (1.6 centipoise at 98°C), into a pastelike mass.

The bubbling test was then repeated using saturated oxygen. The results were practically identical to the results of the dry oxygen test: the gallium channeled in 15 minutes and had a net weight change of 0.02 percent. This change was a preliminary indication that the oxide is not of the hydrated form. Next, dry and saturated nitrogen were bubbled through the column of gallium. The time required to channel with the dry nitrogen was 9.5 hours and the weight change was 0.056 percent. With saturated nitrogen, there was no evidence of channeling after two hours. These tests indicated water vapor itself does not react rapidly with gallium. The time required to channel with the nitrogen with up to 20 ppm of oxygen was approximately 40 times as long as the time required with pure oxygen.

Pure and industrial-grade hydrogen were bubbled through the gallium. Pure hydrogen (up to 10 ppm of oxygen and other gases) was bubbled for 13 hours, and the commercial grade (up to 50 ppm) was bubbled for 23 hours before the gallium channeled.

In addition to the significant difference in time to failure between oxygen, nitrogen, and hydrogen, there was a significant difference in the failure characteristics of the gallium. When oxygen was bubbled through, the gallium became pastelike at failure. When nitrogen and hydrogen were used, the gallium became extremely viscous but still displayed liquid characteristics. This difference has been attributed to the physical form in which the contamination develops. In an oxygen-rich environment, the gallium is formed as a large, monolayer film covering the entire exposed surface. When agitated, this monolayer is churned into the bulk material, retaining its filmlike characteristics. By comparison, in an oxygen-poor environment, the monolayer is smaller, covering only portions of the exposed surface. This monolayer has more of the characteristics of particulate material, rather than being filmlike. The effects of particulate matter on a liquid is to make the liquid more viscous, without its becoming an immobile paste.

It is felt that there is no significance in the differences in time to failure between nitrogen and hydrogen. These differences are probably the results

of small differences in parts per million of oxygen, oxygen leakages, or outgassing in the test apparatus.

A number of important conclusions can be reached as a result of the contamination studies:

- Contamination is probably gallium oxide.
- The contamination is not a hydrated form of gallium oxide.
- The presence of less than 0.1 percent of filmlike oxide contamination immobilizes gallium.
- Very few parts per million of oxygen produce significant contamination.
- Pure, dry, inert gases will not contaminate gallium.
- Contamination formed in an oxygen-rich environment is pastelike. Contamination formed in an oxygen-poor environment is a viscous fluid.

## IMMOBILIZATION

### Analysis

One of the important results of the gallium contamination studies was the finding that small amounts of gallium oxide can effectively immobilize large quantities of liquid gallium.

There appears to be a very basic and fundamental difference in the two liquid metals, gallium and mercury, with regard to their oxidation and immobilization characteristics. Mercury can be stirred in an oxygen environment for hundreds of hours without failure, whereas gallium under similar conditions will be immobilized in the matter of seconds or minutes. The rates of formation of a surface oxide on clean mercury or gallium surfaces are in nanoseconds and are the same to within less than an order of magnitude. However, the oxide that formed on gallium surfaces has a high-strength, filmlike characteristics, which apparently does not exist on the mercury surfaces to the same degree.

An analysis was made to relate the immobilization of gallium to the surface physics of the gallium-gallium oxide interface, involving surface energy, contact angle, and work of adhesion. In addition, a number of low-melting-temperature pure metals and a soft solder were examined experimentally to determine the characteristics of their oxidized surfaces.

The physical characteristics of a number of common pure metals that have low melting temperatures were examined in order to identify any unusual parameters associated with gallium (Table 49). Examination of these param-

Table 49

## CHARACTERISTICS OF LOW-MELTING-TEMPERATURE METALS

Element	Melting Point (°C)	Boiling Point (°C)	Surface Energy (ergs/cm <sup>2</sup> )	Vapor Pressure (mm Hg)	Viscosity (Centipoise)
Gallium	30	2400	735	10 <sup>-36</sup> (30°C) 10 <sup>-12</sup> (400°C)	1.6 (98°C) 0.6 (1100°C)
Mercury	-39	357	442	10 <sup>-8</sup> (25°C)	1.5 (20°C)
Cadmium	321	767	608	10 <sup>-1</sup> (320°C)	1.4 (350°C)
Sodium	98	880	190	10 <sup>-7</sup> (100°C)	0.71 (100°C)
Potassium	62	760	119	10 <sup>-6</sup> (65°C)	0.52 (70°C)
Bismuth	271	1560	376	10 <sup>-10</sup> (270°C)	1.6 (300°C)
Lead	327	1620	442	10 <sup>-8</sup> (320°C)	2.5 (350°C)
Tin	231	2260	526	10 <sup>-2</sup> (500°C)	2.1 (240°C)
Zinc	419	907	735	10 <sup>-1</sup> (425°C)	3.2 (450°C)

eters shows that gallium is an extremely unique material. It has one of the highest surface energies and highest boiling points, one of the lowest melting points, and the lowest vapor pressure. Because gallium has been commonly utilized at temperatures close to room temperature, it actually would be operating very close to its melting temperature and very far from its boiling temperature. Perhaps these factors are involved in giving gallium its unique immobilization characteristics.

An attempt was made to determine some of the parameters that entered into the immobilization phenomenon and to correlate this information with experimental results. The first approach was from the aspect of the adhesion characteristics between the gallium and gallium oxide.

The work of adhesion between a solid and liquid is given by:

$$W_{SL} = \gamma_{SA} + \gamma_A - \gamma_{SL}$$

where:

$W_{SL}$  = Work of adhesion (ergs/cm<sup>2</sup>)

$\gamma_{SA}$  = Surface energy between solid and air (ergs/cm<sup>2</sup>)

$\gamma_{LA}$  = Surface energy between liquid and air (ergs/cm<sup>2</sup>)

$\gamma_{SL}$  = Surface energy between solid and liquid (ergs/cm<sup>2</sup>)

From the Young-Dupre equation:

$$\gamma_{SA} - \gamma_{SL} - \gamma_{LA} \cos \theta = 0$$

where  $\theta$  equals the contact angle between liquid and solid. Combining these equations:

$$W_{SL} = \gamma_{LA} (1 + \cos \theta)$$

Examination of this equation shows there may be a finite work of adhesion between solids and liquids, even if nonwetting, provided the contact angle is less than 180 degrees. As a comparison, the work of cohesion of a liquid is:

$$W_c = 2\gamma_{LA}$$

If it is assumed that the oxide film acts as a solid and if it has an area,  $A$ , the total work of adhesion  $W_{SLT}$ , between the liquid and solid is:

$$W_{SLT} = W_{SL} A$$

$$W_{SLT} = \gamma_{LA} (1 - \cos \theta) A$$

The total adhesive force between the liquid and its oxide is:

$$f_T = \frac{W_{SLT}}{s} \text{ dynes}$$

or:

$$f = \frac{W_{SL}}{s} \text{ dynes/cm}^2$$

where  $s$  = distance (cm). To use this equation, it is necessary to define a distance,  $s$ , and an area,  $A$ .

Because the adhesion forces are intermolecular in nature, the distance,  $s$ , will be quite small, in the magnitude of angstroms. An estimated value would be 10 angstroms, which is on the order of magnitude of the thickness of a molecule. The elemental oxide area was assumed to be quite large for gallium, because the oxide film has been observed to be large and tenacious.

As a comparison, mercury has completely disparate oxide characteristics, no film is observed, and it does not agglomerate. It was therefore assumed that the elemental oxide area of the mercury film is quite small. Representative oxide diameters were assumed to be in the following range:

- Gallium --  $10^{-2}$  to 1 centimeter
- Mercury --  $10^{-7}$  to  $10^{-3}$  centimeters

Taking: 
$$f_T = \frac{\gamma_{LA} A(1 + \cos \theta)}{s}$$

Element	$\gamma_{LA}$ (ergs/cm <sup>2</sup> )	$\theta$	$\gamma_{LA} (1 + \cos \theta)$
Gallium	735	135°	215
Mercury	476	135°	140

$$s = 10\text{\AA} = 10 \times 10^{-8} \text{ cm}$$

$$A = 0.785 d^2$$

Where  $d$  = the diameter of the oxide particle:

$$\text{Gallium} \quad f_r = 21.5 \times 10^{-8} A = 16.8 \times 10^8 d^2$$

$$\text{Mercury} \quad f_r = 14.0 \times 10^{-8} A = 11.0 \times 10^8 d^2$$

	$f_r$ (dynes)	
<u>Cm</u>	<u>Ga</u>	<u>Hg</u>
$10^{-7}$	--	$11.0 \times 10^{-6}$
$10^{-6}$	--	$11.0 \times 10^{-4}$
$10^{-5}$	--	$11.0 \times 10^{-2}$
$10^{-4}$	--	11.0
$10^{-3}$	--	$11.0 \times 10^2$
$10^{-2}$	$16.8 \times 10^4$	--
$10^{-1}$	$16.8 \times 10^6$	--
1	$16.8 \times 10^8$	--

Based on these assumptions of possible oxide diameters, it can be seen that the adhesive forces between gallium and its oxide would be very much higher than those between mercury and its oxide. Thus, the immobilization characteristics of gallium are considered to be directly related to the presence of the large, tenacious, oxide film elements that are associated with gallium.

### Oxide Characteristics of Liquid Metals

The film and oxide characteristics of a number of metals in the liquid state were examined and compared with gallium. The metals were mercury, cadmium and soft solder (60% tin, 40% lead). The cadmium and soft solder were tested above their melting points, the mercury was at room temperature, and the gallium was at room temperature and also at 400°C. Three film and oxide characteristics were monitored:

- Presence of visible oxide
- Mechanical removability of oxide
- Tendency to immobilize

The observations of this investigation are summarized in Table 50.

An unexpected result of the test was the change in the immobilization nature of the gallium oxide at an elevated temperature. Although the oxide was present at the high temperature, it showed none of the immobilization characteristics that are so evident at room temperature.

Table 50  
INVESTIGATION OBSERVATIONS

Material	Presence of Visible Oxide	Mechanical Removability of Oxide	Tendency to Immobilize
Mercury	No	No	No
Cadmium	Yes	Yes	No
Soft solder	Yes	Yes	No
Gallium 30°C	Yes	Yes	Yes
400°C	Yes	Yes	No

The physical parameters of gallium were examined to determine which had changed markedly between room temperature and 400°C. The vapor pressure shows the most significant change being  $10^{-36}$  torr at 30°C and  $10^{-12}$  torr at 400°C. However, the vapor pressure of gallium at 400°C is still substantially lower than that of mercury at 25°C,  $10^{-3}$  torr, and cadmium at 320°C,  $10^{-1}$  torr. The viscosity change was not considered to be significant between 30°C and 400°C, because it is 1.6 centipoises at 98°C and 0.6 centipoises at 1100°C. The surface energy of gallium is only slightly reduced (e. g., 6%) at 400°C. It therefore appears that the change in immobilization of the gallium oxide upon gallium cannot be ascribed to any major changes in these properties of the gallium.

## GALLIUM CLEANING

### GENERAL COMMENTS

Because of the oxidation and immobilization characteristics of gallium, it is necessary to clean the gallium oxide, or ultimately there will be a failure in the current collector. There are a number of possible ways of cleaning the oxide: electrolytically, by filtering, by thermodynamic reduction, and by microtoming. These various techniques have been studied and it appears that cleaning by electrolysis or filtering are the most promising approaches. Microtoming, a physical cleaning technique, appears feasible in certain application, but offers no particular advantage over filtering. Thermodynamic reduction of gallium oxide is not considered to be a viable approach because of the extreme stability of the oxide and the high temperatures required.

### ELECTROLYTIC CLEANING

Contaminated gallium has been successfully cleaned using a proprietary electrolytic cell technique developed by the General Electric Space Systems Products Department, using internal research and development funds. This

electrolytic technique was successfully used to clean gallium through which oxygen was bubbled at a rate that would normally completely contaminate it within 15 minutes. The test cell operated satisfactorily with no failure or indications of incipient failure for 100 hours, at which time the test was deliberately terminated. More recently, the cell design has been modified and used at Schenectady in a rotating electrical machine that had a gallium liquid metal current collector. This machine has been operated successfully for 150 hours, until the test was terminated as planned. The feasibility of electrolytic cleaning of gallium has now been established both on a theoretical basis and on an actual machine.

The electrolytic cell consists of an electrolyte and two electrodes placed in a reaction vessel. One electrode is gallium and the other is platinum; both are placed in the electrolyte. The electrolytic cell works as follows; the electrolyte dissolves the gallium oxide present in the cell. When a voltage is applied between the electrodes, pure gallium (and hydrogen) are formed at the negative (gallium) electrode.

In practice, gallium would be cleaned by pumping it from the current collector into the electrolytic cell and pumping the cleaned gallium back into the current collector. The pumping of the contaminated gallium must be at a sufficient rate so that the gallium is cleaned long before it has any tendency to be immobilized in the current collector. Tests at Schenectady have demonstrated that this situation poses no problem. Based on calculations for the current collector, a pumping rate of 16 cubic inches per hour should be adequate to maintain a very low concentration of gallium oxide in the collector gap.

In situ gallium cleaning is a legitimate technique, and there does not appear to be any theoretical reasons to keep it from working. However, no electrolyte has been found that will dissolve gallium oxide at a high boiling point and a low melting point.

## FILTERING

Regardless of the exact physical parameters of the contamination, it is a mixture of some proportion of solid gallium oxide(s) in liquid gallium. It has been demonstrated that the gallium oxide can be removed by a filtering process. In the selection of a filter, such variables as pore size, filter capacity, filter material, pressure drop, and flow characteristics must be considered.

There are two general types of filters available: sheet type and cartridge type. The sheet-type filter is basically a sheet of porous material that is most familiar in the form of filter paper; other materials also are available such as fiberglass and polymeric materials. Fritted glass and screening would be considered as a sheet-type filter. The major advantage of sheet filters is the avail-

ability of extremely small pore sizes. Sheet filters are available with pore diameters from 0.025 to 100 microns. The major disadvantages of sheet filters are their small retention capability and the fact that they are relatively easily clogged by particles that approximate the pore size or by gels.

Cartridge-type filters have a much greater retention capability and generally are not as easily clogged. The minimum pore sizes are much larger than for the sheet filters, being approximately 1 micron in diameter. Cartridge filters have a media that consists of wound filaments, agglomerations of fibers, woven mesh, or porous plates.

In the consideration of pore size, especially in sheet filters, the bubble point or starting pressure is an extremely important parameter. The starting pressure is the pressure required to initiate flow through the filter. Once continuous flow is established through the filter, the operating pressure drops off considerably. The starting pressure is given by:

$$p = \frac{2 \cos \theta}{r}$$

where:

- p = Starting pressure
- = Surface tension of liquid
- $\theta$  = Contact angle
- r = Radius of pore

For a filter application using mercury, the starting pressure was approximately 300 psi, while the operating pressure was 5 to 10 psi. For gallium, taking:

$$= 735 \text{ dynes/cm}$$

$$\theta = 135^\circ$$

The starting pressure as a function of pore radius is:

<u>r</u> <u>(cm)</u>	<u>Starting Pressure (p)</u>	
	<u>(dynes/cm<sup>2</sup>)</u>	<u>(psi)</u>
10 <sup>-6</sup>	1.04 x 10 <sup>9</sup>	1.51 x 10 <sup>4</sup>
10 <sup>-3</sup>	1.04 x 10 <sup>6</sup>	15.1
10 <sup>-1</sup>	1.04 x 10 <sup>4</sup>	0.151

The pore size is a critical parameter for the specification of the filter. If a small pore is used, it will necessitate a high starting pressure to initiate the flow; if a large pore is used, it may be ineffective in retaining the solids in the contamination. It is therefore necessary to attempt to define the probable lower and upper limits of pore diameter.

surface as a monomolecular film. The thickness of this monolayer is probably on the order of 10 angstroms,  $10^{-3}$  microns. However, because the oxide film is very cohesive, its basic dimension must be several orders of magnitude greater than this. It was assumed that the smallest possible diameter of the gallium oxide is  $1000 \times 10$  angstroms, 1 micron. For reference, it can be noted that 1 micron is approximately five times the size of the smallest bacteria and the lower limit of the range of an optical microscope, so that in all probability the gallium oxide is larger in size than 1 micron. Also, it is known that mercury can be satisfactorily filtered through a 60-micron filter. An upper limit of pore diameter would be in the magnitude of 1000 microns, for heavily contaminated gallium, to 100 microns for lightly contaminated gallium.

To determine whether contaminated gallium could be successfully filtered, a 1.2-micron sheet filter was obtained and fitted, with an adapter, to the end of a hypodermic syringe. The syringe was filled with heavily contaminated gallium. However, no gallium could be forced through the filter with the application of thumb pressure to the syringe. The reason for this is apparent from Equation 17. For gallium, the starting pressure is:

$$\begin{aligned} p &= \frac{2(735) \cos 135^\circ}{1.2 \times 10^{-4}} \\ &= 8.70 \times 10^5 \text{ dynes/cm}^2 \\ &= 126.5 \text{ psi} \end{aligned}$$

The adapter and filter were then removed, exposing a 0.050-inch- or 0.127-centimeter- (1270 microns) diameter hole in the end of the syringe. The test was then repeated to determine whether this larger diameter hole would act as a filter to clean the gallium in the syringe. With a small amount of thumb pressure, clean gallium was expelled into a watch glass from the syringe, leaving a small pellet of gallium oxide remaining in the syringe. A close microscopic examination of the gallium indicated no evidence of contamination; its surface was perfectly shiny; and when the gallium was removed from the watch glass, no residual film remained. The starting pressure for the 0.050-inch-diameter hole is:

$$\begin{aligned} p &= \frac{2(735) \cos 135^\circ}{0.127} \\ &= 8.21 \times 10^3 \text{ dynes/cm}^2 \\ &= 0.119 \text{ psi} \end{aligned}$$

This test, although simple in concept, has demonstrated the feasibility of cleaning gallium by filtration techniques.

## REFERENCES

1. W. M. Kays and A. L. London, Compact Heat Exchangers, McGraw-Hill Book Company, New York, New York, 1964, p. 15.
2. R. B. Fleming, Fabrication and Evaluation of Advanced High-Effectiveness Cryogenic Heat Exchangers, Report No. AFFDL-TR-70-7, Prepared for Air Force Flight Dynamics Laboratory, General Electric Company, Schenectady, New York, 10 February 1970.
3. R. B. Fleming, "A Compact Perforated-Plate Heat Exchanger," Advances in Cryogenic Engineering, Vol. 14, 1969, pp. 197-204
4. R. L. Gessner, Computer Programs for the Design of Miniature Turbo-machinery Cryogenic Refrigerators, Report No. 69-C-243, General Electric Company, Schenectady, New York, July 1969.
5. R. B. Fleming, Miniature Cryogenic Refrigerator, Bimonthly Progress Report No. 5, Prepared for U.S. Army Mobility Equipment Research and Development Center, Contract No. DAAK02-71-C-0026, General Electric Company, Schenectady, New York, 30 November 1971.
6. D. B. Colyer, et al, Design and Development of Cryogenic Turbo Refrigerator Systems, Report No. AFFDL-TR-72-154, Prepared for Air Force Flight Dynamics Laboratory, Contract No. F33615-71-C-1003, General Electric Company, Schenectady, New York, December 1972 (in publication).
7. Z. J. J. Stekly, et al, Inductive Energy Storage System Study, Report No. AFAPL-TR-69-101, Prepared for U.S. Air Force Aero Propulsion Laboratory, Magnetic Corporation of America, Cambridge, Massachusetts, December 1969.
8. Study of Development of an Inductive Energy Storage System, Report No. AFAPL-TR-69-102, Prepared for U.S. Air Force Aero Propulsion Laboratory, AVCO Everett Research Laboratory, Everett, Massachusetts, January 1970.
9. Work Directive for Superconducting Machinery Development Program, Publication No. N00024-73-R-7071, Department of the Navy, 24 August 1972.
10. "Type DB Double Break Heavy Duty Manual and Pneumatically Operated Class 9840," Square D Catalog, Square D Company, Park Ridge, Illinois, January 1971.

11. P. W. Woodbury, Developing a Safe Operational Environment for a Liquid Metal Facility, Technical Information Series Report No. 69APJ17, General Electric Company, Schenectady, New York, June 1970.
12. M. N. Wilson, et al, "Experimental and Theoretical Studies of Filamentary Superconducting Composites," British Journal of Applied Physics, Vol. 3, 1970.
13. P. Thullen, A New Criterion for the Design of Gas Cooled Cryogenic Current Leads, Paper No. J-6, Presented at the 1970 Cryogenic Engineering Conference, 1970.